Heat Integrated Distillation: the Impact of Heat Transfer on Murphree Tray Efficiency

Michael Kaeser

Institute for Energy Systems

School of Engineering and Electronics

Doctor of Philosophy

University of Edinburgh

2004

Declaration

The work described in this thesis is the original work of the author and was carried out without the assistance of others, except when explicit credit was given in the text. It has not been submitted, in whole or in part, for any other degree at any University.

Michael Kaeser

Edinburgh

June, 2004

Acknowledgements

Despite my being not taught the touch system of type writing, this thesis came into existence. It was a heavy burden; but the collection of knowledge, which led to this product, has been quite an experience, and it would not have prevailed without the help and assistance of many people. Sometimes, the support was a little bit far from leaving nothing to be desired; but hey, when in Rome, do as the Romans do. The following deserve special mention for their donations of advice, aid, comfort and encouragement through those years:

- *Dr. Colin Pritchard,* for the guidance and priceless advice through the project.
- *Dr. Heide Niesalla,* for keeping me going, bullying me into finishing and making life worth living.
- *My parents,* for all their kindness and understanding.
- *Dr. Khelil Sefiane,* standing in when Colin was trotting around the globe.
- *Rab Kilgour and Bobby Hogg,* for implementing my outlandish designs and for immediate support when it was needed most.
- *Alistair Fitchie,* for his electronic magic.
- *Miguel Jorge, Andreas Schuster, Aimee Martin, Christian Schumacher, Christophe Guillaume and many other postgraduates,* for their provision of wisdom and companionship.
- *Dr. Henri Hoffmann, Dr. Christian Doehring and Urs Marolf from Hoffmann La-Roche,* for their financial support, which facilitated this bold adventure.
- *The Carbon Trust,* for their financial support of the project, which rescued me in my direst hour.

Abstract

This thesis describes research carried out by the author between 2000 and 2004 at the Institute for Energy Systems (IES), University of Edinburgh, under the supervision of Dr Colin Pritchard and Dr Khellil Sefiane. The aim of the research was to devise and conduct experiments with a novel heat transfer distillation tray focussing on the impact of heat transfer onto Murphree tray efficiency. The project is a part of research considering heat integration in distillation. Inspired by previous work conducted in packed columns, the recent research focuses on trayed distillation columns. Heat integration and heat exchange is established by applying a pressure difference between the rectifying and stripping sections. This can be achieved by compressing vapour from a low-pressure stripping section to a higher-pressure rectifying section through heat transfer devices mounted or within the plates of a tray column. Potentially high energy savings can be achieved by retro-fitting existing adiabatic distillation columns.

The design of a heat transfer sieve tray and its operation in an adiabatic 150 mm diameter distillation column is described. The capability to transfer a significant amount of heat is pivotal; hence altering the vapour and liquid composition in a traceable way. The design philosophy of the heat transfer sieve tray and appropriate sampling devices are explained in detail. A review of heat integration technology is included. Numerous experiments with a binary mixture of methanol-water have been conducted in the cooling and heating mode respectively. The influence on Murhree tray efficiency of key variables like vapour flow rate, reflux ratio and heat flux were investigated. Simultaneously, overall heat transfer coefficients and plate-to-froth heat transfer coefficients were measured.

Prediction methods for Murphree tray efficiency and stage models are reviewed. Based on the review, a model for simulating a diabatic tray is proposed. The model is a modified nonequilibrium model including material and energy balances, rate equations and equilibrium relations. A set of equations for modelling a binary mixture is presented.

Prediction methods for the overall and plate-to-froth heat transfer coefficients are presented. The prediction methods correlate heat flux, plate temperature, heat transfer medium temperature and froth temperature profile data. The experimental heat transfer coefficients were correlated with the plate-to-froth temperature difference in the heating mode, in which nucleate boiling is promoted and with the vapour velocity in the cooling mode, where convective cooling / condensation takes place along the vapour path. The experimentally obtained heat transfer coefficients and heat transfer correlations might be useful as contributor of real data in the modelling of diabatic distillation columns. The heat transfer tray developed is a purely experimental device for fundamental research and by no means a prototype for an applicable tray design.

Contents

List of Figures

List of Tables

Chapter 1

Introduction

1.1 Distillation

1.1.1 Significance of distillation as a separation technology for obtaining pure products

Distillation is a dominant technology in chemical process industries. World-wide, about 95% of all separations are made with it (Humphrey and Keller 1997) [1]. The separation process has been around almost as long as the dawn of human technology. Those first applications of distillation "technology" can mostly be linked to alcoholic beverage production. Forbes (1948) found relevant evidence of distillation going back to the first century A.D. [2]. Distillation remained a batch-based and single stage separation process until the 16th century. By then, it was acknowledged that the extent of separation could be improved by providing multiple liquid-vapour contacts (stages) in so called Rectificatorium. The first vertical columnar continuous distillation still was developed by Cellier-Blumenthal in France 1813. Perrier introduced an early version of the bubble-cap tray in England in 1822. Packings followed in the 1820s and sieve trays had their first appearance in 1830.

During the first quarter of the 20th century, distillation technology evolved from a tool in the alcohol beverage industry into the prime separation technology in the chemical industry. This process was accelerated by the recognition of distillation as an effective means of separating crude oil into various products. The petroleum industry is still the largest user of distillation technology nowadays.

Distillation is a process of physically separating a mixture into two or more products that have different boiling points, by preferentially boiling the more volatile components out of the mixture. Apart from different component volatilities, two conditions more have to be fulfilled for a successful separation.

- A second phase has to be formed so that both liquid and vapour phases are present and can contact each other on appropriate devices.
- The two phases can be separated by gravity or other mechanical means.

The pre-eminence of distillation for the separation of fluid mixtures is not accidental, but fundamental, and therefore unlikely to be dispatched. The reasons are both kinetic and thermodynamic. Additionally, distillation had a long time to mature. Keller (1987) illustrated the state of development of several separation processes [3]. The degree of development (i.e., technological maturity[1]) and the extent of application (user maturity) for separation processes are shown in Figure 1.1.

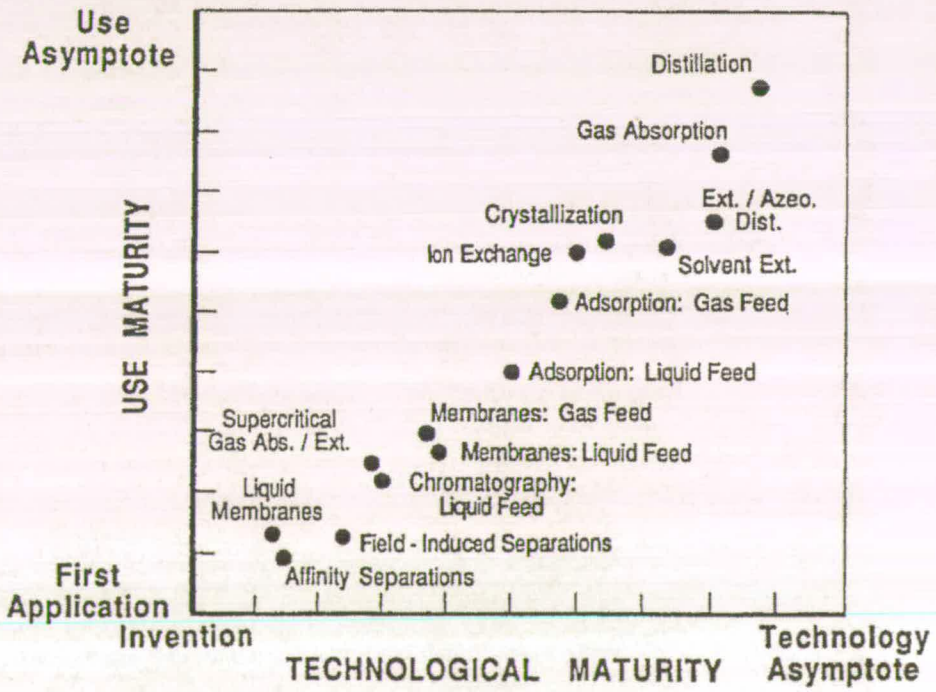

Figure 1.1: State of development of separation processes.

(Source: Keller 1987 [2])

[1] The development is only considered in terms of product purity.

From a kinetic standpoint, (Haselden (1981) [4] showed that, with no inert present, mass transfer per unit volume in distillation is limited only by the diffusional resistance in either side of the vapour-liquid interface in the turbulent phases. In almost any other separation process, there are either inert solvents or solid matrices present, and these lower the mass fluxes. Distillation therefore has the potential for high mass transfer rates, leading to low capital costs.

From the thermodynamic viewpoint, a typical thermodynamic efficiency of a distillation system is about 10%. That does not sound impressive, but not many other processes are more effective [3]. The thermodynamic aspect will be addressed more thoroughly in Chapter 2.

Ellis (1974) [5], Rush (1979) [6], Zuiderweg (1988) [7] and Fair (1990) [8] concluded that distillation provides the cheapest and best method for separating a liquid mixture to its components except when:

1. The difference of volatility between the components is small.
2. A small quantity of the low-volatile component is to be recovered from the feed. Distillation requires that the whole feed be vaporised in order to recover this small quantity.
3. A compound is thermally unstable even under vacuum conditions.
4. The mixture is extremely corrosive or highly fouling.

The relative volatility is a vapour-liquid equilibrium parameter and, together with the reflux ratio it determines the number of stages required for a particular separation. The relative volatility is the ratio of vapour-liquid equilibrium ratios of two components.

(1.1)

A big α value represents an easier separation between the two components. Therefore, fewer stages in a distillation tower are required. This is illustrated in Table 1.2.

Binary Mixture	Average Relative Volitility	Number of Trays	Typical Operating Pressure, psia	Reflux-to-Minimum-Reflux Ratio
1,3-Butadiene/vinyl acetylene	1.16	130	75	1.70
Vinyl acetate/ethyl acetate	1.16	90	15	1.15
o-Xylene/*m*-xylene	1.17	130	15	1.12
Isopentane/*n*-pentane	1.30	120	30	1.20
Isobutane/*n*-butane	1.35	100	100	1.15
Ethylbenzene/styrene	1.38	34	1	1.71
Propylene/propane	1.40	138	280	1.06
Methanol/ethanol	1.44	75	15	1.20
Water/acetic acid	1.83	40	15	1.35
Ethylene/ethane	1.87	73	230	1.07
Acetic acid/acetic anhydride	2.02	50	15	1.13
Toluene/ethylbenzene	2.15	28	15	1.20
Propyne/1,3-butadiene	2.18	40	120	1.13
Ethanol azeotrope/water	2.21	60	15	1.35
Isopropanol/water	2.23	12	15	1.28
Benzene/toluene	3.09	34	15	1.15
Methanol/water	3.27	60	45	1.31
Cumene/phenol	3.76	38	1	1.21
Benzene/ethylbenzene	6.79	20	15	1.14
HCN/water	11.20	15	50	1.36
Ethylene oxide/water	12.68	50	50	1.19
Formaldehyde/methanol	16.70	23	50	1.17
Water/ethylene glycol	81.20	16	4	1.20

Table 1.1: Representative commercial binary distillation operations.

(Source: Mix *et al.* 1978 [9])

1.1.2 A brief review of adiabatic distillation

Distillation is a manifold field in regard to equipment used, operation type and mixtures separated in columns. Figure 1.2 gives an impression of the variety of the field. Chemical engineers have to take several factors into account to achieve their major design and operation goal; the separation quality demanded in its most economic way. The following section describes briefly the aspects mentioned in Figure 1.2.

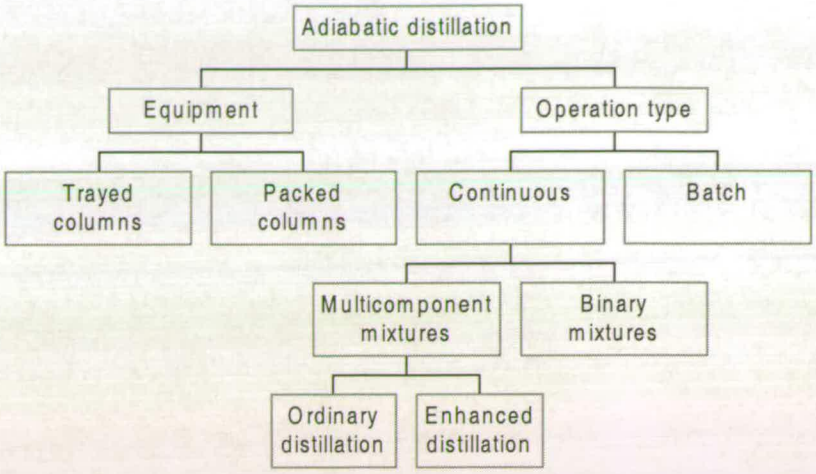

Figure 1.2: Design aspects in adiabatic distillation.

1.1.2.1 Binary mixture separation and equipment

The separation of binary mixtures has been investigated for centuries and it's usually performed in trayed columns. Each tray serves as independent separation stage. A typical configuration is given in Figure 1.3. All design calculations are dependent on the availability of vapour-liquid equilibrium VLE data and other physical properties.

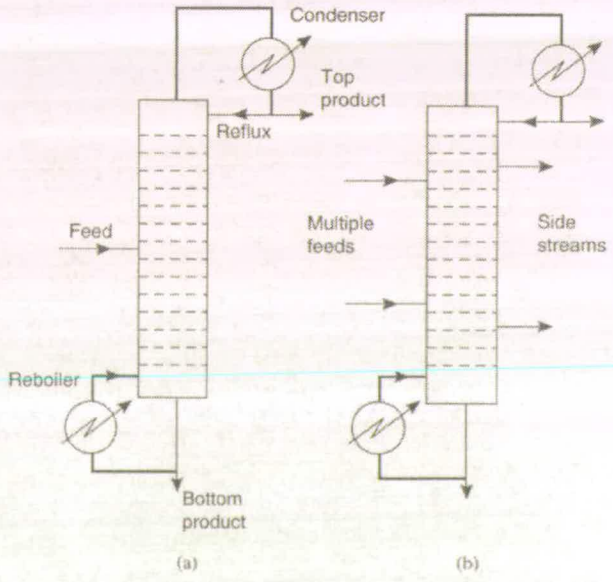

Figure 1.3: Trayed distillation column. (a) Basic column, (b) multiple feeds and side streams. (Source: Seader 1998 [10])

Alternatively, trays can be replaced by packed beds transforming the apparatus into a continuous separation device. One distinguishes between random and structured packing. Packed columns have certain advantages over trayed columns:

- Packed columns can cope better with foaming systems.
- Due to a lower liquid hold-up, they are more preferable in handling toxic or flammable liquids.
- Low pressure drop.
- More suitable in small diameter columns ($< 0.6m$)[2].

On the other hand, packed columns feature certain disadvantages.

- Cleaning is more expensive if fouling occurs.
- Provision for side streams is more complicated.
- Packed columns are not suitable for low liquid rate systems.
- Packed columns are less flexible in handling a range of liquid and vapour flow-rates.

Nowadays, trayed columns are often modified by retrofitting, thus combining the advantages of efficient packings with the advantages of trays. This leads to an improved performance of separation systems. The problem of packed columns is addressed in Stringle (1994) and Billet (1995) [11, 12]. The insights gained from binary mixture separation research formed the basis for the development of multicomponent design concepts.

1.1.2.2 Multicomponent separation

The design of multicomponent separators is more complicated and laborious than in the case of binary systems. Bottom and top product compositions cannot be specified independently. This problem has been circumvented by the determination of so-called key components, between which it is desired to make a separation. In the

[2] Plates are more difficult to install in small columns, and expensive.

simplest case, where the concentration of the non-key components is smaller than 10%, the system may be regarded as a binary system for which the number of stages can be obtained by using a McCabe-Thiele diagram. Hengstebeck (1946) proposed a method for systems with non-key component concentrations > 10% in which the system is reduced to an equivalent binary system (pseudo-binary system) [13].

An overall treatment method without considering detailed changes in individual stages was developed by Kremser (1930) [14]. His group method had been improved by Souders and Brown (1932) [15], Horton and Franklin (1940) [16] and Edmister (1943) [17] over the following years. More popular are two empirical approaches considering all components. The oldest approach is the combined equations of the Fenske-Underwood-Gilliland method developed in the 30's of the 20th century. Fenske (1932) proposed an equation for the minimum equilibrium stages [18]. Underwood (1932) developed an equation for minimum reflux [19]. Gilliland's correlation (1940) calculates actual reflux ratios and theoretical stages [20]. Erbar and Maddox (1961) correlated a similar method, which delivers more precise and reliable predictions [21].

With the rise of computers, more rigorous methods for multicomponent separations became available and are standard today. The methods are mostly based on stage-by-stage calculations taking equilibrium stages into account. On each stage a set of MESH (Material balance, phase Equilibrium equation, Summation equation, Heat balance) equations has to be solved. The computing process goes through a cycle of iterations until the system converges. The output delivers product distributions, flow rates and temperature profiles across a distillation column. Those methods are integrated in commercial software packages like ASPEN PLUS and HYSYS. A description of the short-cut and the more rigorous methods can be found in relevant textbooks (King 1980 , Kister 1992, Seader 1998, Coulson 1999) [22 , 23, 10 & 24]

1.1.2.3 Enhanced distillation methods

The above mentioned methods are used for designing columns to deliver products of specific purity. They are straightforward and economic for ideal systems with high relative volatility. However, if a system has a relative volatility of less than 1.1 and

forms a nonideal liquid solution, distillation may be uneconomic, and if an azeotrope forms even impossible. Both systems are illustrated in Figure 1.3.

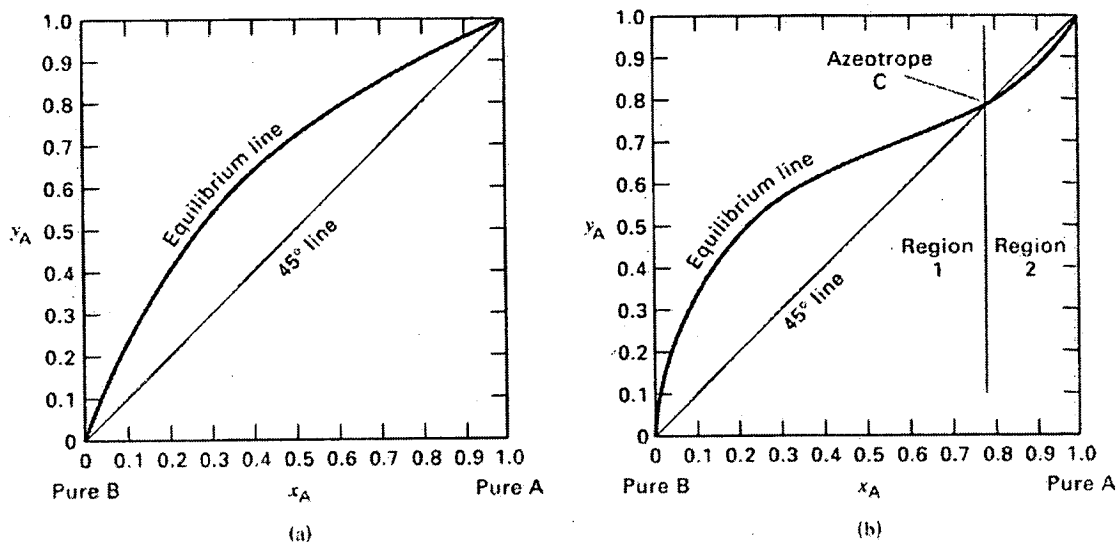

Figure 1.4: Vapour-liquid equilibrium for binary systems. (a) Ideal system, (b) Azeotropic system. (Source: Kister 1992 [22])

Other separation techniques have to be considered in this case. Stichlmair, Fair and Bravo grouped appropriate trouble-shooter methods (1989) [25]. Depending on the separation problem, the following methods may be applied.

Extractive distillation

A large amount of relatively high-boiling solvent alters the liquid-phase activity coefficients of the mixture, so that the relative volatility of key components becomes more favourable. The solvent enters the column above the feed entry and exits from the bottom without causing an azeotrope to be formed. If the feed to the column is an azeotrope, the solvent breaks it. Also, the solvent may reverse volatilities.

Salt distillation

Dissolving a soluble, ionic salt in the top reflux alters the relative volatility of the key components. The resulting effect is similar to extractive distillation. Because of the salt's involatility, it remains in the liquid phase as it passes down the column.

Pressure swing distillation

A pressure-sensitive azeotrope can be broken by utilising two columns operated in sequence at two different pressures.

Homogeneous azeotropic distillation

The addition of an entrainer forms a homogeneous minimum- or maximum-boiling azeotrope with one or more feed components. The entrainer is added near the top of the column, to the feed, or near the bottom of the column, depending upon whether the azeotrope is removed from the top or bottom.

Heterogeneous azeotropic distillation

An entrainer forms a minimum-boiling heterogeneous azeotrope. The azeotrope spits into two liquid phases in the overhead condensing system. One liquid phase is sent back to the column as reflux, while the other liquid phase is sent to another separation step or is the product. This method is particularly prevents thermal decomposition of the product by forming a minimum-boiling azeotrope.

Reactive distillation

A separating agent is added to the system to react selectively and reversibly with one or more of the constituents of the feed. The reaction product is subsequently distilled from the nonreacting components. The reaction is then reversed to recover the separating agent and the other reacting components. Reactive distillation also refers to the case where a chemical reaction and a multistage distillation are conducted simultaneously in the same apparatus to produce another chemical. This combined operation commonly uses heterogeneous or homogeneous catalysts. It is especially suited to chemical reactions limited by equilibrium constraints like ketale synthesis, since one or more products of the reaction are continuously separated from the reactants shifting the equilibrium in favour of the products.

In the case of ordinary distillation of multicomponent mixtures, the design and optimisation of columns is tedious, but relatively straightforward. This is not valid for enhanced distillation. In particular, rigorous calculations of such systems fail because of liquid-solution nonidealities and/or the difficulty of specifying feasible separation. To significantly reduce the chances of failure, graphical techniques

developed by Doherty (1978), Stichlmair (1988) and Partin (1993) [26, 27, & 28] provide valuable guidance for the design of feasible enhanced distillation sequences.

1.1.2.4 Batch distillation

Batch distillation columns are usually much simpler in design than their continuous distillation counterparts. A feed mixture is charged to a still pot, retort or flask and heated to boiling. The vapour formed is continuously removed and condensed to produce a distillate. Unlike in continuous distillations, the composition of the initial charge and distillate change with time. Batch distillation should be considered when the quantity to be distilled is small; when it is produced at irregular intervals; when a range of products has to be produced; or when the feed composition is likely to vary considerably. It is the dominant distillation type in the pharmaceutical and speciality chemistry industry. The practical design of batch distillation has been described in depth by Hengstebeck (1961), Ellerbe (1979) and Billet (1979) [29, 30 & 31].

1.1.3 Energy consumption in distillation

Although distillation can deliver high purity products, it is a very energy –intensive technique. A mixture, with its highest boiling point at the bottom of the column, has to be constantly evaporated by a reboiler. Due to the separation effect on each stage, the high volatile component gets enriched in the vapour on its path to the top of the column; hence lowering the dew point of the rising vapour. Then the top product has to be totally condensed. Additionally, heat losses occurring across the column (despite modern insulation techniques) demand additional energy input. To make things even worse, the separation process demands that part of the condensed head product must be returned to the column as reflux. The result is additional energy input for the multiple evaporation. With a given number of stages, the reflux ratio is a commanding factor for achieving a desired product quality.

Due to its dominant character, there are thousands of distillation columns in the world; over 40 000 continuous distillation columns in the United States alone. The US columns represent a capital investment of $8 billion and use the energy

equivalent to 136000 tonnes per day of crude oil – some 15% of all United States industrial energy consumption (Zanetti, 1997) [32], or about 2% of the national energy consumption (BP, 2003) [33]. The development of the primary energy use world-wide, of Europe and chosen countries (China, UK &USA) over a period of 10 years are given in Figures 1.5 & 1.6.

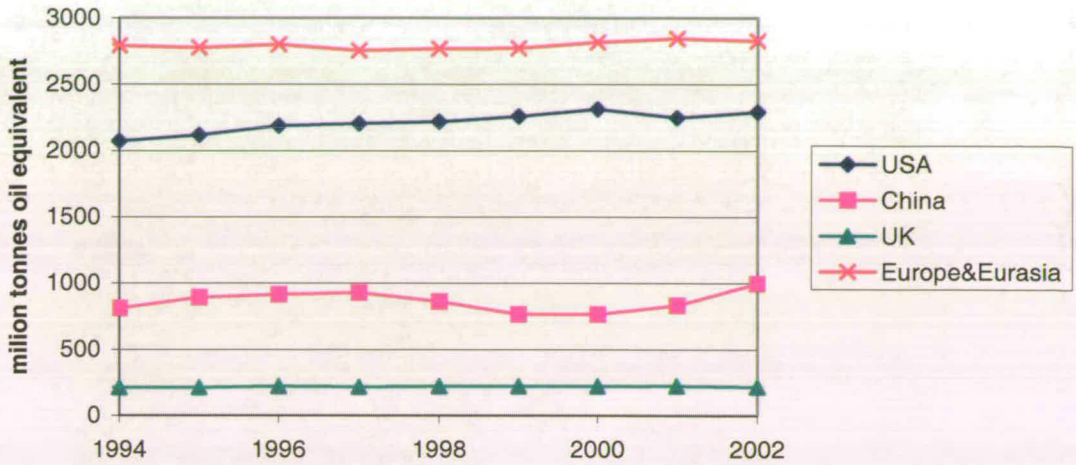

Figure 1.5: Primary energy consumption development 1993-2002 of chosen countries / zones.
(Source: BP 2003 [33])

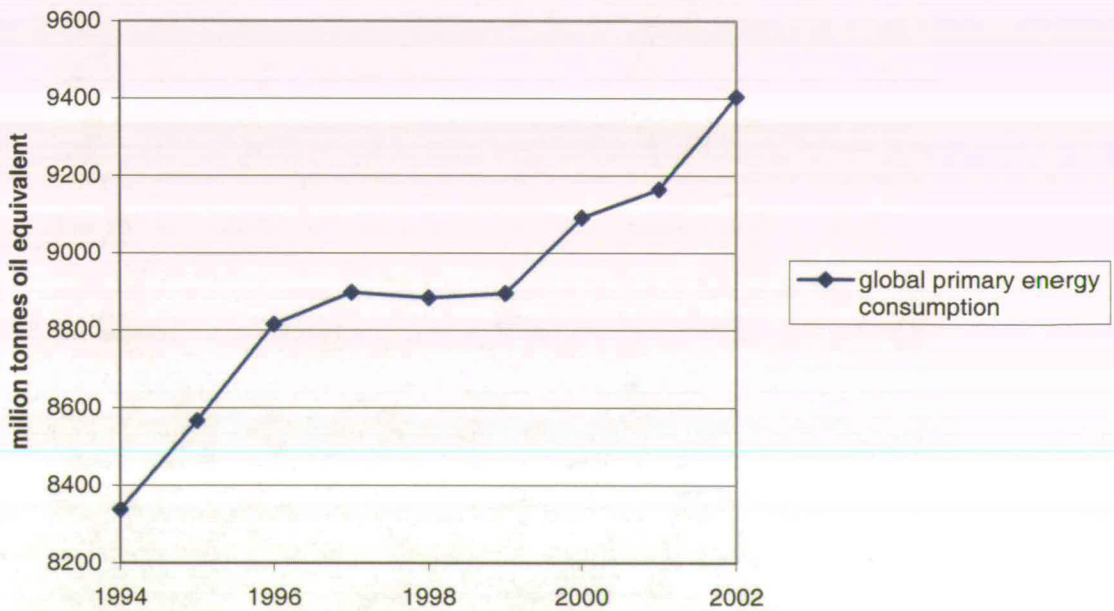

Figure 1.6: Global primary energy consumption development 1993-2002.
(Source: BP 2003 [33])

The world consumption of primary energy increased by 2.6% between 2001 and 2002. Contributors to this increase were the Asia-Pacific zone, China in particular. The continuing industrialisation of China will also lead to the creation of further distillation capacities. Europe's and the UK's primary energy consumption remained fairly constant; indicating a move to renewable energy sources.

The petroleum industry with its tall and big diameter columns claims most of the energy consumption in the distillation sector. The capacity development in refinery columns over the last 10 years is given in Figure 1.7 (BP 2003 [34]). The tendencies are similar to the aforementioned ones in primary energy consumption. In 2002, the total capacity equalled 4.3 billion tonnes of crude oil per year.

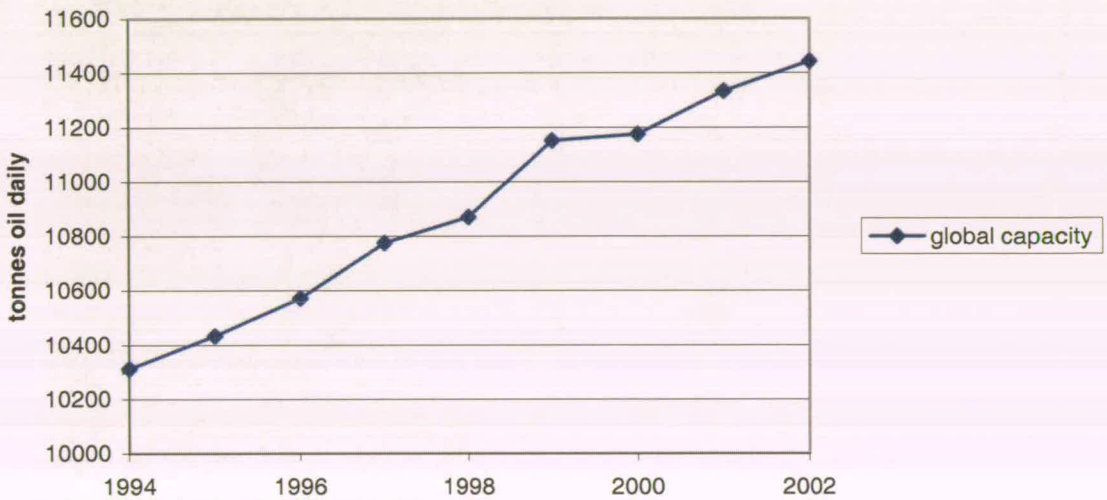

Figure 1.7: Global distillation column capacity development 1994-2002.
(Source: BP 2003 [34])

Due to a continuing growth in the distillation capacity sector, new columns will be implemented, most likely according to proven design experience. This indicates that the most used type of distillation column, the trayed column, will prosper. The next section gives an insight to sieve tray technology.

1.1.4 Sieve trays in distillation applications

Most of the large-scale absorption and distillation processes are performed in trayed columns. Amongst a variety of tray designs sieve and valve trays are illustrated in Figure 1.8. Their non-proprietary nature, simplicity of design, retrofit capability, and effectiveness of contacting are some of the factors that make sieve trays particularly interesting in commercial distillation.

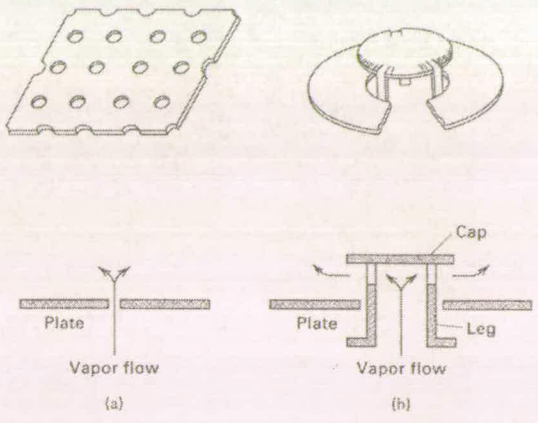

Figure 1.8: Tray opening types. (a) Sieve, (b) valve cap.
(Source: Seader 1998 [9])

In a trayed column, vapour and liquid flow counter-currently and are contacted on a series of trays; an example is shown in Figure 1.9. Liquid flows across each tray, over an outlet weir, and into a downcomer, which takes the liquid by gravity to the tray below. Vapour flows upward through holes in the tray. It prevents liquid flowing down through the holes. Additionally, it creates a turbulent, bubbling two-phase zone (active area) in which interface mass transfer takes place. The downcomer regulates the liquid inventory on the tray.

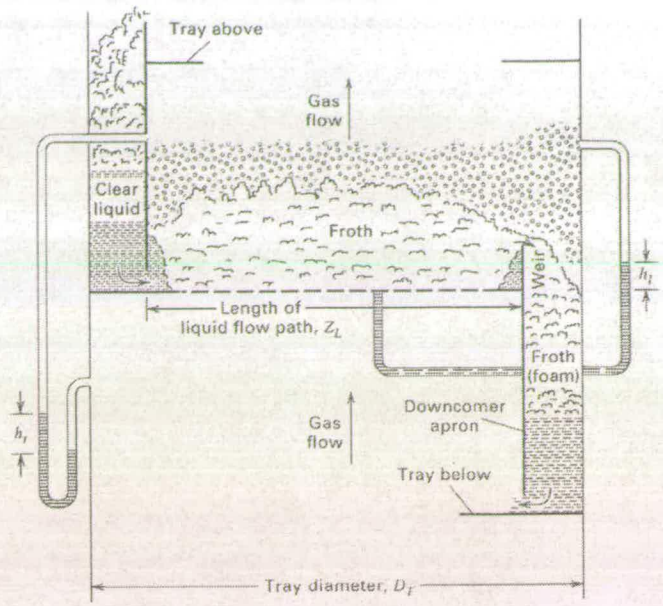

Figure 1.9: Details of a contacting sieve tray in a trayed column.

(Source: Smith 1963 [35])

Depending on liquid and vapour flow rates, any of the five two-phase flow regimes shown in Figure 1.10, and considered in detail by Lockett (1986) [36], may occur. The froth regime is the most common and favoured regime, in which the liquid phase is continuous and the vapour passes through in the form of jets or a series of bubbles. The spray regime differs from the froth regime by having a continuous vapour phase. It occurs for low weir heights[3] and at high vapour flow rates. For low vapour flow rates, the bubble regime can occur, in which the liquid is fairly quiescent and bubbles rise in swarms. At high liquid flow rates, small vapour bubbles may be undesirably emulsified. If the bubble coalescence is hindered, an undesirable foam forms.

[3] Causing low liquid depths.

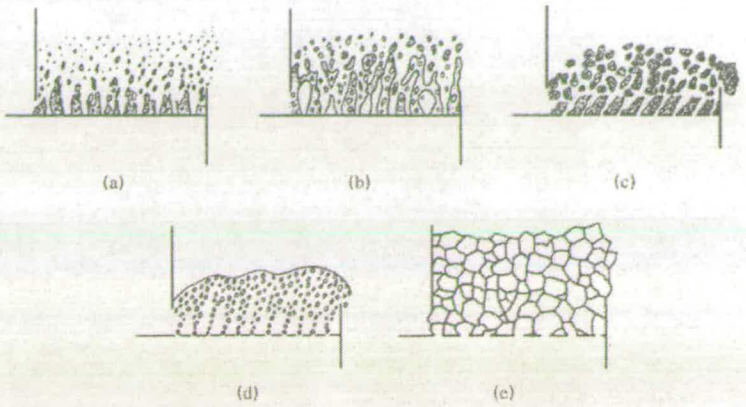

Figure 1.10: Possible vapour-liquid flow regimes for contacting tray.
(a) Spray, (b) froth, (c) emulsion, (d) bubble, (e) cellular foam.
(Source: Lockett 1986 [36])

For a satisfying separation the tray must work in a stable area. Liquid and vapour flow rates influence the tray performance significantly. This is illustrated as tray stability diagram in Figure 1.11. The area of satisfactory operation (shaded) is bounded by the tray stability limits. The upper capacity limit is the onset of flooding. At moderate and high liquid flow rates, the entrainment (jet) flooding limit is normally reached when vapour flow is raised, while the downcomer flooding limit is normally reached when the liquid flow is raised. At very low liquid rates, as the vapour rate is raised, the limit of excessive entrainment is often reached. As the vapour flow is lowered, the limit of excessive weeping is reached. Closing in to those borders or exceeding them lead to significant decrease of the sieve tray separation performance (tray efficiency).

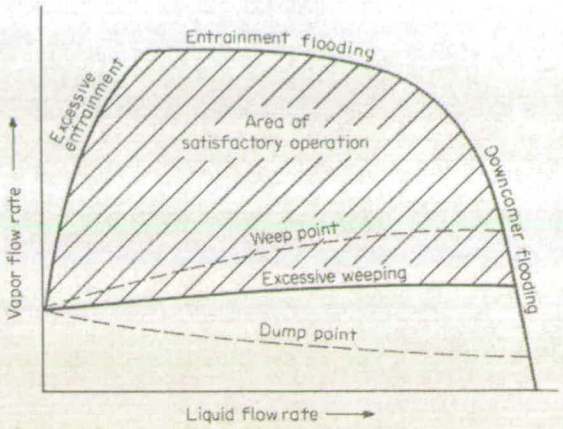

Figure 1.11: Sieve tray performance diagram.
(Source: Kister 1992 [23])

Souders and Stichlmayr proposed the use of the F-factor as a major design parameter for the determination of upper capacity limit and column diameters [37 & 27].

$$F = w_s * \sqrt{\rho_v} \tag{1.2}$$

1.2 Summary

Due to its massive scale of operation, even small improvements in distillation can have a significant impact. This is particularly valid for close boiling mixture separations featuring high reflux ratios and a high number of stages. Those improvements can be achieved by developing better separation quality column internals, more precise efficiency prediction methods, applying heat integration in distillation columns (diabatic distillation) and enhanced distillation methods. Zuiderweg (1973) has estimated that two billion dollars in column investment cost alone were saved between 1950 and 1970 by research and development [38]. A literature review focussing on diabatic distillation and sieve tray improvement research ought to reveal the potential for energy savings in distillation. Enhanced distillation and other tray internals are omitted from this study because they are less favourable for retrofit approaches.

Chapter 2

Literature Review

This Chapter features heat integration in distillation columns and the research covering improvements in sieve tray design. It starts by emphasising the importance of the second law analysis in distillation, followed by a review addressing various heat integration approaches. Based on this review, the HIDiC technology is explained in greater depth. In the second part of the Chapter, the focus is directed towards tray efficiency and the development of sieve trays to improve tray efficiency. This line is continued to the proposed heat integration on sieve tray.

Information demonstrated from this review leads to the research proposal.

2.1 Heat integration in distillation

Distillation is an energy intensive separation process. Energy savings became important after the oil crisis of the 1970s. On the one hand, increased competition demanded more and more economic processes. On the other hand, fuel shortages accompanied by rising energy prices transformed energy to a more and more valuable commodity. Broad interest in the field led to interdisciplinary R&D groups, which contribute to the development of economic distillation solutions. Figure 2.1 shows a network, in which such a group could work.

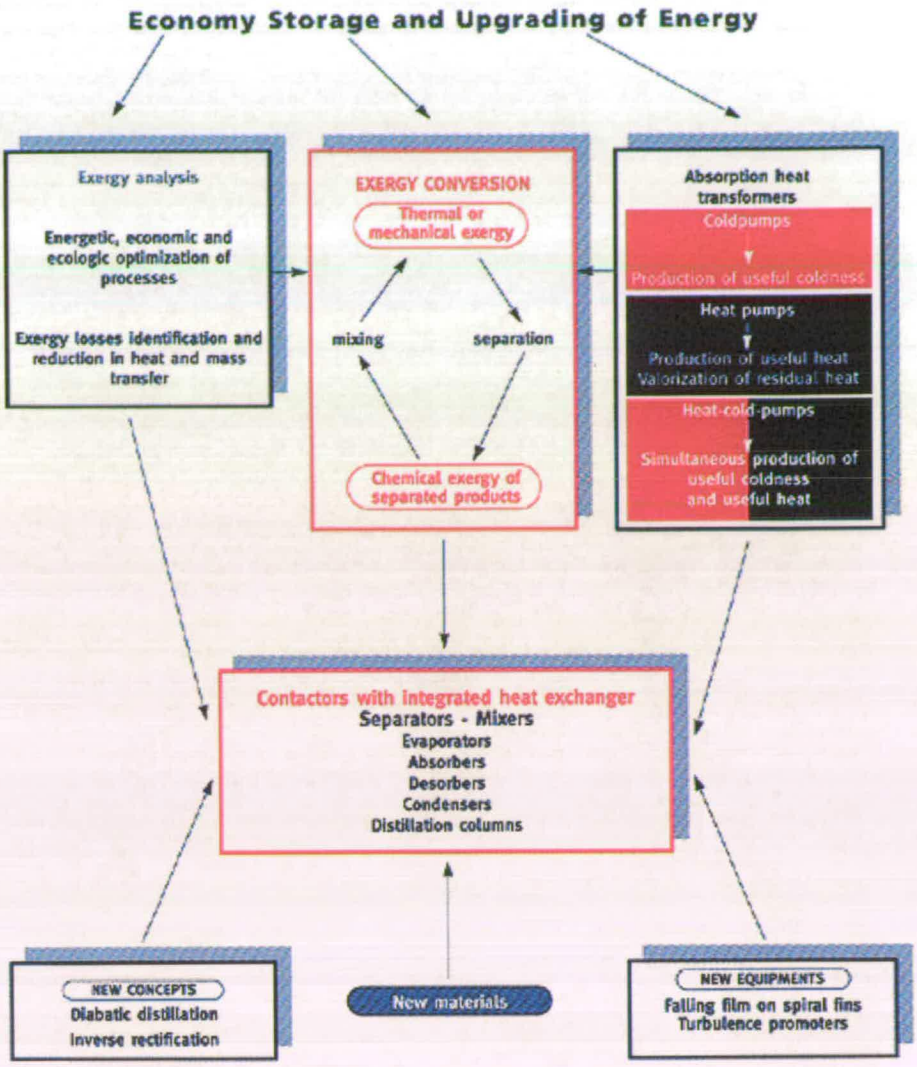

Figure 2.1: Example of a research network and its interactions.

(Source: Le Goff 2002 [39])

Energy savings in distillation are closely linked with how efficiently energy is used and the performance of the mass transfer devices involved. The former aspect is addressed in section 2.1.1.

2.1.1 Thermodynamic aspects

Energy saving concepts are derived from thermodynamics. Efficiency definitions are a way to measure how favourable, or how energy efficient processes are. The first law of thermodynamics is well known in the non-engineering world but often misused or misunderstood. According to the first law, energy cannot be created nor

be destroyed but only be transformed from one form into another. Considering the case of a heat engine and applying the first law the thermal efficiency is defined as

$$\eta = \frac{W_{out}}{Q_{in}} \tag{2.1}$$

But the first law only considers the quantity of energy and not the quality. In all real processes the quality of energy is degraded. This is expressed by the second law of thermodynamics, which assesses the quality of energy. The 2nd law efficiency definition for a work generating process would be

$$\eta = \frac{W_{out,real}}{W_{out,reversible}} \tag{2.2}$$

whereby the divisor is the work output of an ideal, reversible process. Another efficiency-like figure expressing the second law is the Coefficient Of Performance (COP) of refrigerators or heat pumps. The COP refers to the upgrading of the quality of heat at the expense of work. A powerful tool for the measure of the work potential of a process is exergy and the destruction of exergy in real processes. The exergy change can be generally defined as

$$Ex = (H - H_0) - T_0(S - S_0) \tag{2.3}$$

where the subscript 0 stresses the link to and importance of the environment. The next following paragraphs describe the history of exergy combined with entropy analysis, its connections to second law efficiencies and its rise in importance.

Gouy (1889) and Stodola (1910) made the first statement connecting entropy creation caused by irreversible processes with the amount of work lost (destroyed exergy) [40 & 41]. The law of Gouy-Stodola is given in eqn. 2.4

$$W_{rev} - W_{irrev} = T_o S_{gen} = D \tag{2.4}$$

where D is the exergy lost as a result of the irreversibility. The law did not gain as much attention as it deserved, and it needed a particular event such as the oil crisis to bring it back on stage. Nevertheless, the same principle had been restated by Darrieus (1930) and Keenan (1940) who in the process clarified its implications and made it more accessible to engineering practice. [42 & 43].

In 1951, Freshwater considered the thermal economy of distillation [44]. He describes a "reversible distillation", in which the only work required is the equivalent to the entropy change during the "unmixing" process, which can be calculated by

$$W_{rev} = -RT_D[x_F \ln x_F + (1-x_F)\ln(1-x_F)]F \qquad (2.5)$$

The main feature of the reversible distillation concept is the absence of entropy generation by temperature gradients in heat transfer. But inefficiencies in the separation process and heat losses add further work input for the separation. Freshwater defined a thermodynamic efficiency by converting the reversible work for separation into steam consumption, and compared those values with the minimum steam consumption based on minimum reflux of distillation columns. The data were taken from a phenol-cresol mixture. He investigated the influence of product purity and feed composition on thermodynamic efficiency. Table 2.1 shows the result for the former parameter.

Product purity wt. %	Min reflux ratio	Steam for R min lb/lb product	Steam equivalent of separation work lb/lb product	Thermodynamic efficiency %
90	1.34	0.575	0.0545	9.5
94	1.55	0.62	0.0624	11.5
96	1.67	0.65	0.0731	13.0
98	1.77	0.675	0.0858	14.7

Table 2.1: Comparison of thermodynamic efficiency between reversible separation and min reflux steam consumption. (Source: Freshwater 1951 [44])

The efficiency increase with higher product purity can be explained by higher unmixing work input while the irreversibilities remain constant. Those values do not look impressive, but the reality is worse. With the steam consumption of a real column of 4.5 lb./lb.; producing phenol of 85% purity, the thermodynamic efficiency is as small as 1.5%. Freshwater proposes several methods of heat integration (i.e. heat pumps) for increasing thermodynamic efficiency.

Denbigh published a valuable contribution to the exergy field in 1956 applying the second law efficiency to chemical processes [45]. He describes the concept of "waste

work" and proposes its minimisation for increasing efficiencies. He defines the work in/output for a reversible (eqn. 2.6a) and an irreversible process (eqn. 2.6b).

$$w_{t\,\min} = \Delta U + P_0 \Delta V - T_0 \Delta S \tag{2.6a}$$

$$w_t = T_0 S_{gen} + \Delta U + P_0 \Delta V - T_0 \Delta S \tag{2.6b}$$

The difference between the two is the product of environment temperature and created entropy, which has been named "wasted work" or "dissipated energy" by Denbigh. The term on the right hand side of the reversible work required is nothing else than change in exergy, but is not explicitly identified as such. Keenean [43] addressed the right side of eqn. 2.6a as "increase of availability" (ΔB). Denbigh calculated the waste work of the ammonia oxidation process. This yielded an *absolute efficiency* of 6%, taking the irreversibility of the chemical reaction into account. Realising that he could not influence the irreversibility of the chemical reaction and probably not much impressed by low efficiency numbers either, Denbigh also defined a *practical efficiency* by removing the chemical reaction from the list of reversible processes. The departure of this 100% efficiency was calculated by computing the amount of wasted work, which led to a 11% efficiency of the process. Denibgh concluded that it is essential to minimise the entropy production proposing :

- Heat transfer taking place over the lowest possible temperature difference
- Keeping pressure drop and other form of friction to a minimum

Also in 1956, Rant coined the expression "exergy" in a short paper [46]. Fonyo specifically considered rectification in 1974 [47]. Exergy was used as a thermodynamic measure of column efficiency. His thermodynamic second law analysis coupled with capital and operating costs led to the proposal of the reversible distillation concept. Earlier attempts are difficult to track down. Fonyo cited Flower's work (1963) [48] and it is our believe that Le Goff published related work in the 1960s, but unfortunately not available in English. Bruzustowski and Golem made the concept of exergy more public to American engineers in 1976 [49]. The authors give an introduction to exergy and its importance in energy conservation. This is nicely expressed in a statement, featured in Bruzustowski and Golem's paper [49]:

> "An important, but often overlooked, element of energy conservation is the matching of the quality of energy required in a given application with the quality of the energy supplied for that application."

This statement gained more weight when it became more and more obvious that the world had grown entirely dependent on non-renewable energy sources, which were not available in infinite amounts. The paper suggests that the energy crises ought to be renamed entropy crisis or, even more appropriate, exergy crisis. The authors give an example of the difference between the effectiveness of a process, given in eqn. 2.7, and the ordinary thermal efficiency.

$$\varepsilon = \frac{Ex_{in}}{Ex_{out}} \tag{2.7}$$

Obviously, there is no significant difference between those two efficiencies, if the energy inputs and outputs are of high quality (i.e. storage batteries, fuel cells); but it can cause a bad surprise if the energy qualities are different. A steam generation plant for instance has a overall thermal efficiency of 0.36 compared with a effectiveness of 0.31. To make things even worse, the boiler, supposedly having a thermal efficiency of 0.9, only has an effectiveness of 0.49. As this example shows, exergy analysis can be a powerful tool for revealing irreversibilities in processes.

Bejan (1979) performed a second law analysis on convective heat transfer, focusing on the irreversibilities due to heat transfer along finite temperature gradients and viscous effects [50]. He investigated four fundamental flow configurations and stressed the usefulness of entropy generation profiles and maps. He proposed appropriate selection of flow geometric parameters for minimising entropy generation. Bejan continued his work considering second law analysis in heat transfer and published a comprehensive paper, taking thermal design into account, in 1982 [51]. He summarised the trend in the mid 1980's in heat transfer design; represented by the infusion of the second law of thermodynamics and its design-related concept of entropy generation minimisation. He underlined that from the engineering standpoint, it is recommended to first identify the irreversibilities associated in a process and, secondly, to design for lower irreversibilities in order to avoid the loss of available energy. He stated that the irreversibility analysis is a

useful approach for deciding if a process is efficient or inefficient. Like Fonyo, Bejan characterised the interplay between irreversibility design and profitability. A minimisation of irreversibility is likely to lead to a decrease in operating cost. On the other hand, this effect is often accompanied by a corresponding increase in capital cost. Additionally, he clarifies the confusion of the public between energy and exergy. This confusion was mainly caused by various names for work potential like *availability* (Keenan [52]), *"die groesste Nutzbarkeit"* (maximum useful work, Clausius [53]) and *energie utilisable* (useful energy, Darrieus [54]). They all mean available work or exergy. This is nicely illustrated in Figure 2.2.

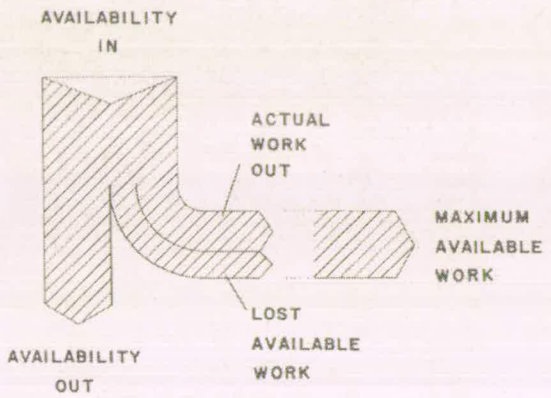

Figure 2.2: Schematic representation of availability analysis of a thermodynamic system. (Source: Bejan 1982 [51])

Ray and Sengupta developed a second law analysis for sieve trays in distillation in 1993 [55]. They evaluated the entropy generation rate associated with heat, mass and momentum transfer for bubble movement through a liquid pool. This paper demonstrates the computation of entropy generation as a result of energy dissipation in tray internals. They used a 0.75 m diameter sieve tray and a benzene-toluene system for their simulations. Weir height and sieve hole diameter were altered. They distinguished entropy generation rates before and after bubble detachment. Results for a variety of sieve tray diameter are given in Table 2.2.

Orifice radius in m	0.0015	0.0020	0.0030	0.0040
Entropy generation per unit mass of bubble	$JK^{-1}s^{-1}kg^{-1}$	$JK^{-1}s^{-1}kg^{-1}$	$JK^{-1}s^{-1}kg^{-1}$	$JK^{-1}s^{-1}kg^{-1}$
Orifice flow loss	0.025	0.020	0.012	0.007
Bubble liquid heat transfer	0.002	0.002	0.002	0.003
Bubble-liquid mass transfer	0.427	0.444	0.469	0.495
Viscous drag on bubble	0.354	0.342	0.321	0.305
Dissipation as liquid momentum	0.302	0.385	0.449	0.426
Work against static head	0.320	0.307	0.281	0.254
Work against surface tension	0.018	0.014	0.010	0.008
Bubble bursting	0.025	0.020	0.016	0.013
Total	1.473	1.534	1.560	1.511

Table 2.2: Effect of sieve hole diameter variation on entropy generation on tray. (Source: Ray & Sengupta 1996 [55])

Ray and Sengputa observed an increase in entropy generation with increasing weir height and sieve tray diameter respectively. The increased irreversibility caused by increased weir height is caused by additional work done against the static head. Bigger holes cause a faster rate of change from the initial thermodynamic state as the life time of the bubble is lower for bigger holes. The authors proved that the major contributor to irreversibility on sieve trays is the bubble-liquid interaction on the tray, with mass transfer as largest single contributor. The effect of interaction of the flowing liquid with the tray internals is negligible.

Le Goff *et al.* performed exergy analysis of distillation processes in 1996 [56]. The authors describe a distillation column as an exergy converter, which transforms thermal exergy into chemical exergy. They define exergy for the separation process as

$$\Delta Ex_{sep} = \Delta Ex_{chem} + \Delta Ex_{thermal} \tag{2.8}$$

whereby the chemical exergy ΔEx_{chem} is given by

$$Ex_{chem} = RT_o \sum N_j X_j \ln \gamma_j X_j \tag{2.9a}$$

and the thermal exergy $\Delta Ex_{thermal}$ is given by

$$\Delta Ex_{thermal} = \Delta H\theta = \Delta H\left(1 - \frac{T_0}{T}\right) \tag{2.9b}$$

Chemical and separation effectiveness can be defined as

$$\varepsilon_{chem} = \frac{\Delta Ex_{chem}}{Q_r\theta_r - Q_c\theta_c} \tag{2.10a}$$

$$\varepsilon_{sep} = \frac{\Delta Ex_{sep}}{Q_r\theta_r - Q_c\theta_c} \tag{2.10b}$$

where Q_r and Q_c are the heat load supplied to the reboiler and the heat load removed from the condenser.

Le Goff *et al.* simulated the exergy losses of ethanol/water rectification with a mass fraction of ethanol of $X_f = 0.35$ to obtain a top product with $X_d = 0.90$ in adiabatic and diabatic columns respectively. The results are given in Table 2.3. In the adiabatic column, irreversible exergy losses inside the column (96.8 kJ/s) are associated with irreversibility of the separation process alone, since no heat is extracted from the column. The irreversible exergy losses in the diabatic column are the sum of irreversibility of the separation process and the heat transfer process. The overall effect is a reduction of the exergy losses by 40% by using diabatic distillation columns. On the other hand, diabatic distillation needs more theoretical stages to achieve the same separation quality than its adiabatic equivalent. As one can see, the chemical effectiveness is poor in both cases, only the thermal effectiveness is significantly increased by applying reversible distillation principles (decreasing the temperature gradients between the plates i.e. by using intermediate heat exchangers).

	Adiabatic column		Diabatic column	
Location of exergy losses	kJ/s	%	kJ/s	%
Exergy losses in the reboiler	43.7	10	43.7	17
Exergy losses in the condenser	290.1	67	53.3	21
Exergy losses in the column	96.8	23	157.2	62
Total exergy losses	431	100	254	100
Exergy extracted by the cooling medium	15.5	-	192.8	-
Exergy supplied by the heating medium	491	-	491	-
Separation exergy change	44.8	-	44.8	-
Chemical exergy change	9.8	-	9.8	-
Separation effectiveness	-	9.4	-	15.0
Chemical effectiveness	-	2.1	-	3.3

Table 2.3: Exergy comparison of adiabatic and diabatic columns.
(Source: Le Goff *et al.* 1996 [56])

The authors also introduced a graphical representation of exergy losses. An example is given in Figure 2.3. A part of the thermal exergy loss is converted into chemical exergy, and the other fraction is destroyed. This plot is a useful tool for the assessment of exergy losses.

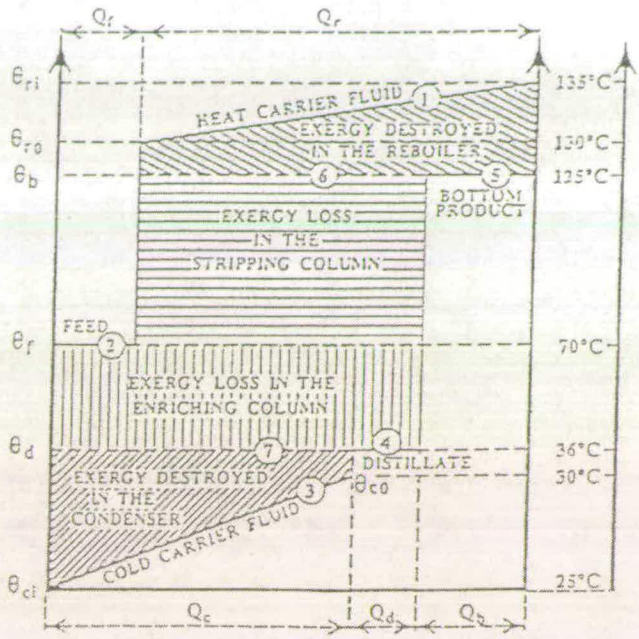

Figure 2.3: Enthalpy/Carnot factor diagram for distillation.

(Source: Le Goff 1996 [56])

Diabatic distillation systems continued to raise the interests of engineers and mathematicians, who deal with entropy and exergy analysis. Andresen and Salamon tried to optimise reversible distillation systems in 2000 [57]. The authors honour previous diabatic distillation approaches but criticise their optimality claims. According to them, the previous claims are flawed by fixing the tray temperatures to those of an adiabatic column. They proposed the application of equipartition of entropy production. By using equal thermodynamic distance values, they achieve thermodynamically optimal tray temperature distribution. The concepts of thermodynamic geometry and thermodynamic length are described by Weinhold (1975, 1978) and Salomon (1980) [58, 59 & 60]. Andresen and Salamon considered the temperature profile of an adiabtic column separating benzene-toluene first. The composition profile, given in Figure 2.4, implies that the major part of the entropy production occurs near the end of the column and is not uniformly distributed. Even more importantly, an increase of the number of trays would only extend the flat middle section. This means that dissipation does never approach zero as the number of trays go infinity. A different picture can be drawn for the diabatic distillation. The principle of equal thermodynamic distance leads to an even distribution of the

entropy production along the column, causing an even composition profile (see Figure 2.4). The total entropy production approaches zero as the number of trays go infinity. It is evident that non-chemical engineers were working on this problem. The curve for the conventional column in Figure 2.4 is everything but a reflection of a practical separation. The profile is theoretically correct, but for such a low top product quality (x_D = 0.9) one would never use 70 stages. A more realistic separation aim would be x_D =0.99. What is nicely, but unintentionally illustrated is the consequence of a highly overtrayed column with approximately 60 wasted stages. If those stages are cut out, one will obtain the real profile with steep gradients in the middle sections and flat ends at either side.

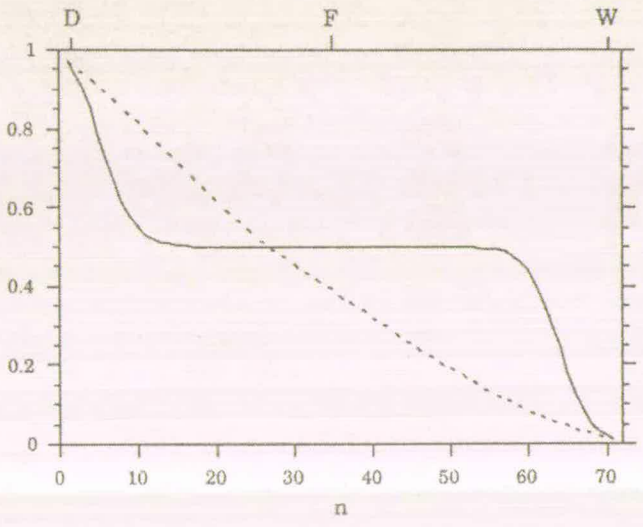

Figure 2.4: Liquid concentration profile vs. tray number. Conventional column (solid), ideal diabatic column (dashed). (Source: Andresen & Salamon 2000 [57])

A calculation example using a benzene feed of x_F = 0.5 and a product quality of x_D=0.99 led to an exergy requirement of 191 J/mol for the fully optimised equal thermodynamic distance column. In comparison, the diabatic column had an exergy requirement of 842 J/mol. Even the addition of just two intermediate heat exchanger results in an exergy requirement of 423 J/mol, still half of the requirements of a diabatic column.

Schaller *et al.* (2001) continued the research in the concept of Equal Thermodynamic Distance in distillation (ETD) [61]. They programmed a fully numerical,

multidimensional optimisation routine to determine the minimum entropy production. The performance of EDT was compared with numerical optimisation by varying the number of trays and purity requirements. An important role was played by the temperature dependence of the "total constant pressure heat coexistence heat capacity", defined by Rowlinson in 1969 [62]. The agreement between the two methods is good for columns with high number of trays; some deviations occur for short columns as illustrated in Figure 2.5.

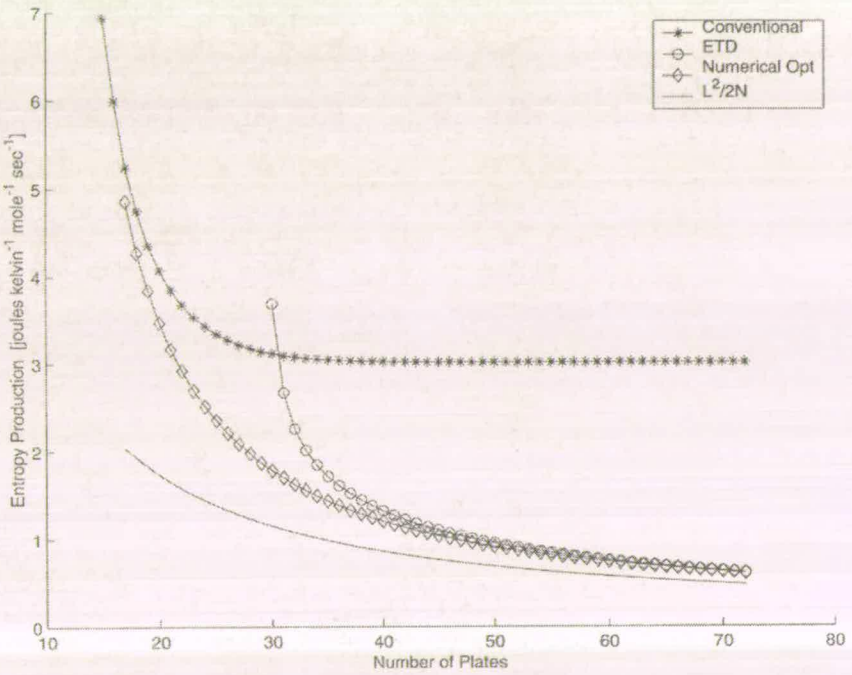

Figure 2.5: Comparison of entropy production for purity requirement x_D=0.99. (Source: Schaller *et al.* 2001 [60])

The heating requirements per stage were almost constant to achieve the proposed optimal temperature profile. This works well with Rivero's implementation of diabatic columns dating from 1993 [63]. From the chemical engineer's viewpoint, it is a shame that the group put efforts in the calculations of meaningless separations like $x_D = 0.9$ or 0.95.

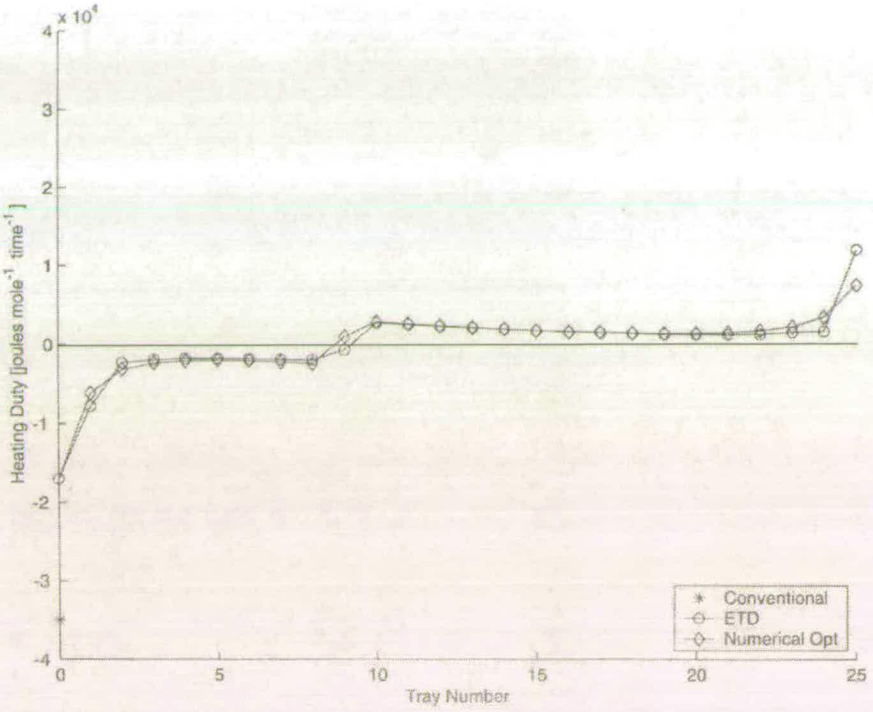

Figure 2.6: Comparison of corresponding heating requirements for a 25 tray column; purity requirement xD=0.95. (Source: Schaller *et al.* 2001 [61])

In 2002, Rivero published a review of the exergy-related research conducted by the Mexican Petroleum Institute (IMP) [64]. IMP is dedicated to the application of the second law of thermodynamics by the exergy concept. The research is channelled into two directions. First, a methodological direction, which is focused on the development of simulations, analysis and optimisation programs. Second, a technological direction, which leads to improved systems and processes. Similar to Bejan, Rivero looks for energy degradation (product of irreversibility) first, and tries to reduce them in a second step. Rivero uses exergy to solve problems coming from the connections of Energy, Ecology and Economy[4], illustrated in Figure 2.7. This led to two new approaches, namely exergoeconomic and exergoecologic analysis respectively. An early application, dating from 1985 led to improved combustion

[4] Called the three E model.

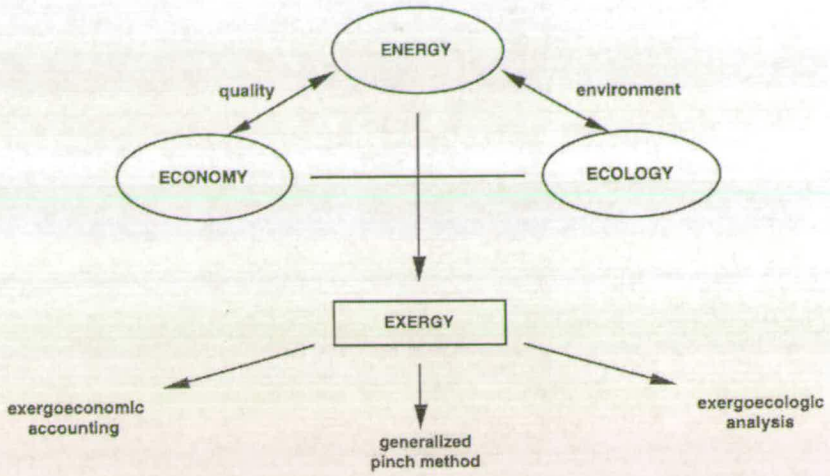

Figure 2.7: The energy-economy-ecology connection.

(Source: Rivero 2002 [64])

equipment by using the exergy concept. In 1987-88, a project optimised a 150,000 barrel per day refinery in Tula, Mexico by reducing the exergy losses in various plant units [65]. The result is given in Table 2.4.

Reduction in energy degradation of an existing refinery (Tula project)

Unit	Exergy losses (%)	
	Original	After optimization
Combined distillation unit	20.4	17.2
Naphtha HDS unit	3.2	2.7
Naphtha reforming unit	10.9	7.9
Intermediate distillates HDS unit	3.4	2.8
Catalytic cracking unit	19.5	12.7
Visbreaking unit	2.9	3.7
Utilities plant	39.8	36.7
Total	100.0	84.3

Table 2.4: Reduction in exergy degradation of an existing refinery in Tula, Mexico.

(Source: Rivero 2002 [64])

Research on the methodological side led the enthalpy-Carnot temperature diagram, invented by Le Goff and to three-dimensional exergy diagrams [63 & 66]. Such an enthalpy-Carnot temperature for ethanol-water is given in Figure 2.8. Present studies at IMP deal with exergoeconomic analysis of a 270,000 barrel per day refinery, reactive distillation optimisation and the set-up of integrated fuel cells in crude oil refineries.

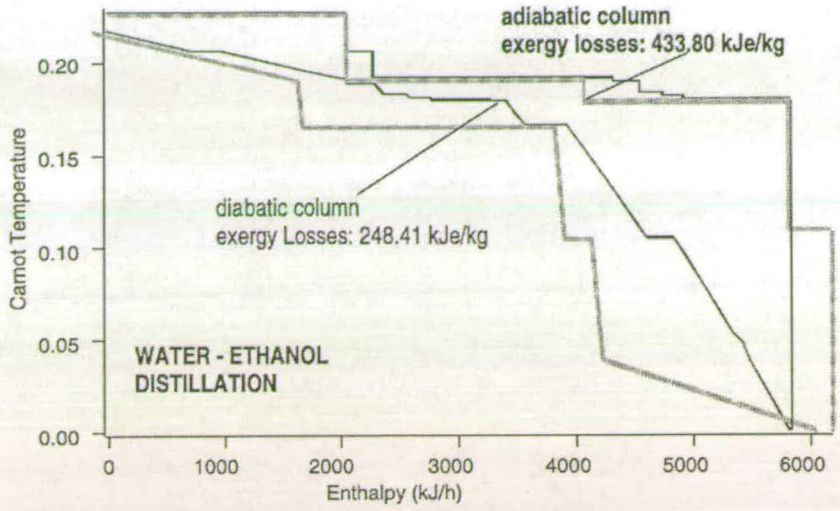

Figure 2.8: Enthalpy/Carnot temperature diagram for ethanol-water separation.

(Source: Rivero 2002 [64])

2.1.2 Overview of heat integration techniques

Heat integration in distillation can be achieved in various ways. Principally, all the methods can be classified into either inter- or intracolumn heat transfer methods. Inside this groups further divisions are possible, as shown in Figure 2.9. Other classifications of heat integration are possible as for example given by Freshwater (1951) [44].

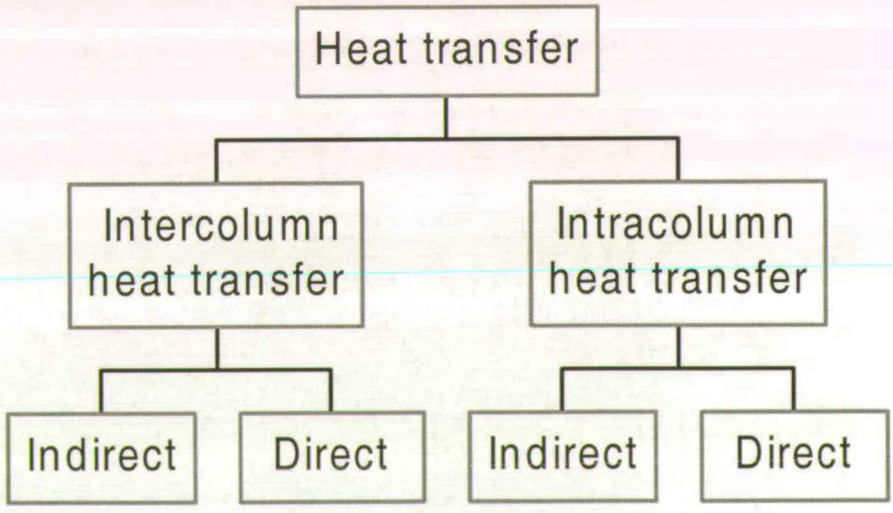

Figure 2.9: General heat integration scheme.

In general, intercolumn heat integration is applied first in a complex plant. Additional intracolumn heat transfer lead to further process efficiency gains. Intracolumn heat transfer is the first choice option in stand-alone plants (i.e. single distillation column). Inter- / intracolumn heat and their methods of implementation are addressed in the following sections.

2.1.2.1 Intercolumn heat transfer

Intercolumn heat transfer can principally be achieved by indirect or direct methods. Possible schemes are given in Figure 2.10 and are discussed below.

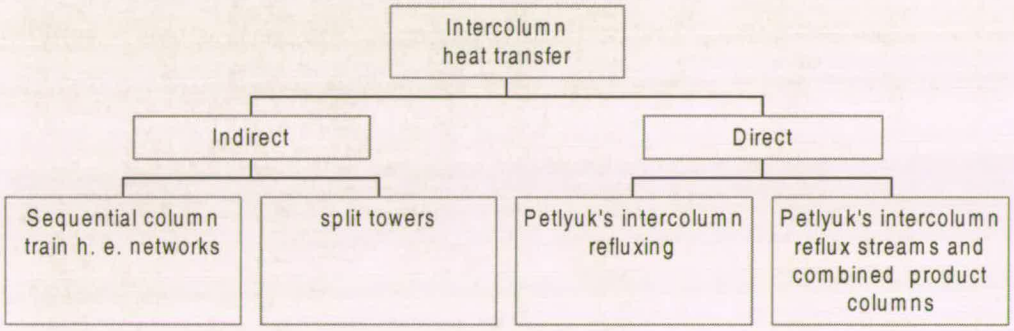

Figure 2.10: Intercolumn heat transfer scheme.

2.1.2.1.1 Sequential column train, heat exchanger networks & split towers

Column trains and heat exchanger networks come into play if several high pressure or high temperature streams can be specified. Process integration can lead to a substantial reduction in energy requirements. Gundersen and Naess (1988) published a review covering various analysis and design methods for heat integration [67]. One of the most successful and by now well-established techniques is pinch technology. The heat recovery pinch was discovered by Huang and Elshout (1976) and Umeda *et al.* (1978) [68 & 69]. Linnhoff *et al.* (1982) developed systematic methods for the pinch point analysis [70]. The thermodynamic break described by the pinch point sets the boundary of useful heat transfer. Fonyo (1991) developed the diverse pinch concept, which can deal with unequal heat transfer coefficients [71]. Heat recovery and process integration are essential parts of general chemical engineering [24] and process design books today [72]. They are also embedded in process simulation

programs like ASPEN PLUS and HYSYS. As an example, a column train for a five-component separation is given in Figure 2.11.

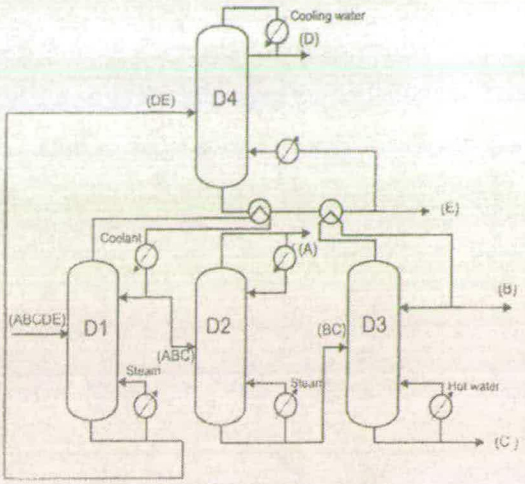

Figure 2.11: Column train for a C3-C5 splitter ($P_{D1} > P_{D2} > P_{D3} > P_{D4}$).
(Source: Sobočan 2000 [73])

2.1.2.1.2 Petlyuk columns

Petlyuk columns embody a particular arrangement of towers, which are able to separate ternary mixtures or, arranged in a sequence, capable of separating multicomponent mixtures in a thermally more efficient way. The standard direct sequence arrangement and the equivalent Petlyuk column are given in Figure 2.12.

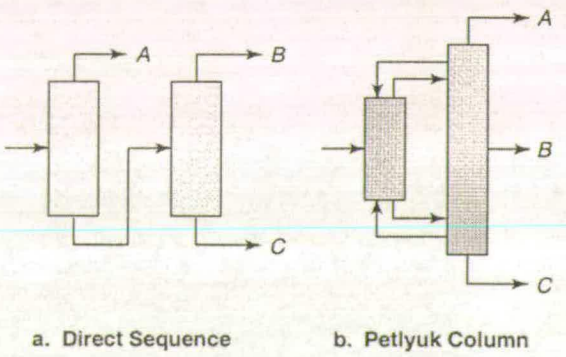

Figure 2.12: Column arrangement for ternary mixture separation.

Petluyk (1965) used a prefractionator to perform a sharp split between A and C, while allowing B to distribute between those two streams [74]. All of A and some of

B are removed in the overhead of the smaller prefractionation column, while all of C and the remaining B are removed in the bottom. The upper portion of the second column then performs an A/B separation, while the lower portion separates B and C. By preventing B from being remixed as it is in the direct sequence, the thermal inefficiency is removed; leading to significant energy savings of about 30% for typical designs [74]. Becker (2001) and Triantafyllou (1992) show that fully thermally coupled distillation columns (Petlyuk column) can achieve up to 60% energy savings by using unconventional design approaches [75 & 76}. Various Petlyuk column arrangements can also be found in Stupin's (1972) and Tedder's (1978) work [77 & 78].

Research concerning Petlyuk columns is still a lively field, as recent publications prove. Kim (2002) proposed a rigorous design method for Fully Thermally Coupled Distillation Columns (FTCDC), focusing on thermodynamic efficiency [79]. In 2003, Kim published results comparing the performance of an extended FTCDC applied to a naphta reforming plant with a conventional system; and Jimenez compared the performance of proposed alternative schemes of FTCDC [80 & 81].

The next improvement in the field of FTCDC led to divided wall columns, illustrated in Figure 2.13. Although Wright patented the divided wall column in 1949, the lack of reliable design methods together with concerns about the operation and control of such columns prevented their widespread application. The divided wall column features the same advantages as the Petlyuk column. Additionally, it reduces the capital costs significantly by investing in one fewer column. Schultz (2002) provides a survey of divided wall columns [82].

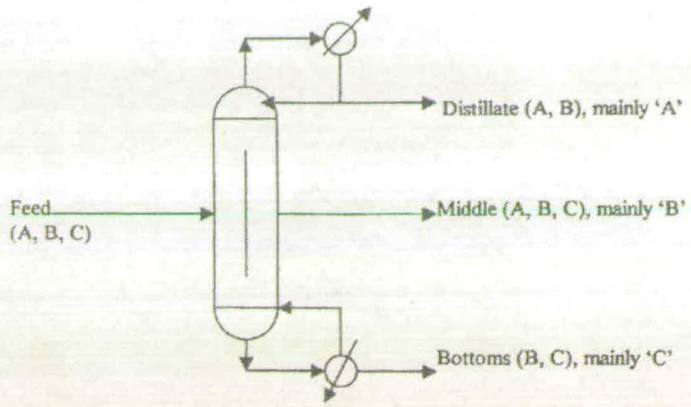

Figure 2.13: Dividing wall column.

(Source: Muralikrishna 2002 [83])

Additional energy savings in FTCDC can be achieved by applying reversible distillation principles. Halvorsen (2001) investigated the advantages of internal heat integration in FTCDC in respect of the minimum energy and entropy requirements [84]. His examples of heat integrated FTCDC are given in Figure 2.14 and the results can be found in Table 2.5 (cases 3a–3d). Methods for heat integration within columns are explained in the next section.

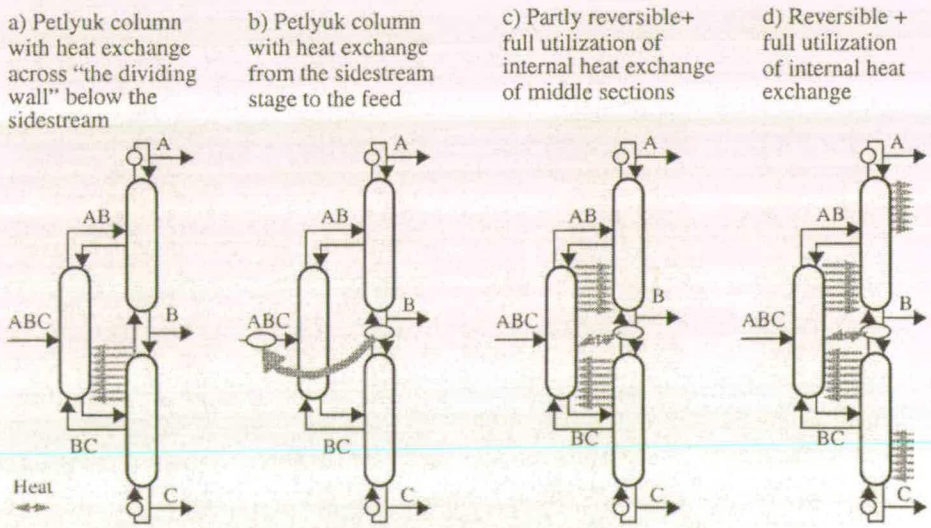

Figure 2.14: Internal heat integration in Petlyuk columns.

(Source: Halvorsen 2001 [84])

Figure	Configuration (Ad: Adiabatic Non: Non-ad.)		Energy (V_{min})	Entropy (S_r)
1a	Direct Split (conventional)	Ad	2.072	0.59
1b	Indirect Split (conventional)	Ad	2.032	1.21
1c	Side Rectifier (directly coupled)	Ad	1.882	0.86
1d	Side Stripper (directly coupled)	Ad	1.882	1.05
2a	**Reversible Petlyuk Column**	Non	1.667	**0.00**
2b	Separate prefractionator arrangement	Ad	1.556	0.63
2c	**Petlyuk Column** (minimum energy without internal heat exchange)	Ad	**1.366**	0.72
2d	Petlyuk Column with heat removal or supply at sidestream stage	Ad	1.366	0.54
3a	Petlyuk column with heat exchange across the dividing wall	Ad+Non	1.222	0.54
3b	Petlyuk column with heat exchange from sidestream to feed	Ad	1.181	0.49
3c	Petlyuk with total heat exchange in middle sections	Ad+Non	1.000	0.26
3d	Reversible Petlyuk column with internal heat exchange	Non	1.000	0.05
-	Reversible process with only two temperature levels (The theoretical minimum energy process)	Non	**0.793**	**0.00**

Table 2.5: Comparison of minimum energy and relative entropy production for a set of column arrangements for a given feed. (Source: Halvorsen 2001 [84])

2.1.2.2 Intracolumn heat transfer

Methods belonging to intracolumn heat transfer class are given in Figure 2.15 and are addressed in the following paragraphs.

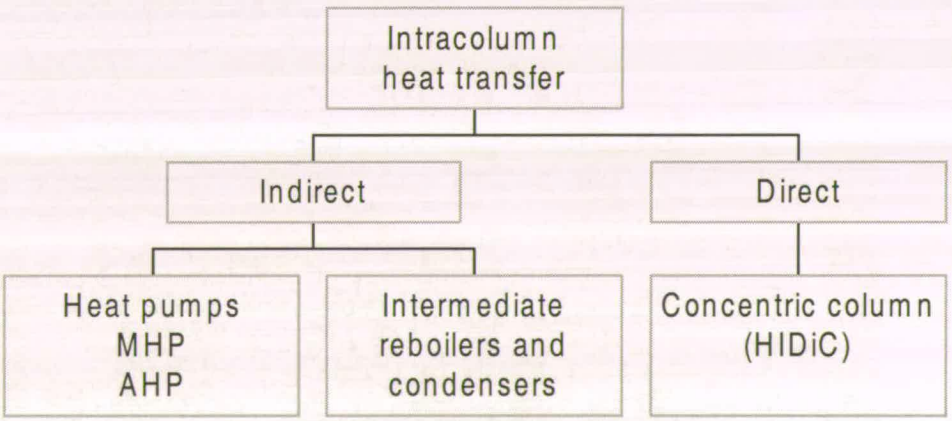

Figure 2.15: Intracolumn heat transfer scheme.

2.1.2.2.1 Heat pumps

Heat pumps have been around since the late 18th century, although they were not used for energy saving matters in the first place (Stephan 1974) [85]. In the 20th century, simultaneously to the technical development, the thermodynamic basis for heat pump theory made considerable progress by the work of Merkel and

Bosnjakowic (1929) [86]. They introduced the enthalpy-concentration diagrams and thus made it possible to evaluate absorption heat pump cycles, just as the heat engine could be analysed with the aid of the enthalpy-entropy diagram.

Basically, heat pumps can be regarded simply as heat engine in reverse, illustrated in Figure 2.16. In the heat engine, heat is extracted from a high temperature source, power is produced and heat is discharged to a sink. On the other hand, the heat pump (HP) requires either work input or external driving thermal energy to remove heat from a low temperature source and to transform it to a high temperature level.

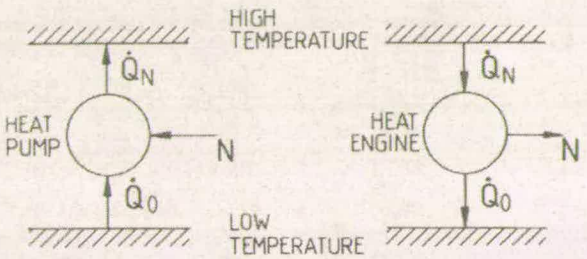

Figure 2.16: Thermodynamic model of heat engine and heat pump.
(Source: Moser 1985 [91])

Mechanical heat pumps (MHP) are electrically driven vapour compression types. They work on the principle that a liquid boils at a higher temperature if its pressure is increased, as illustrated in Figure 2.17. A low-pressure vapour is passed to the compressor where it is compressed by the device to a higher pressure. The resulting high-pressure vapour flows to the condenser where it condenses, giving up its latent heat at high temperature, before expanding back to a low-pressure liquid.

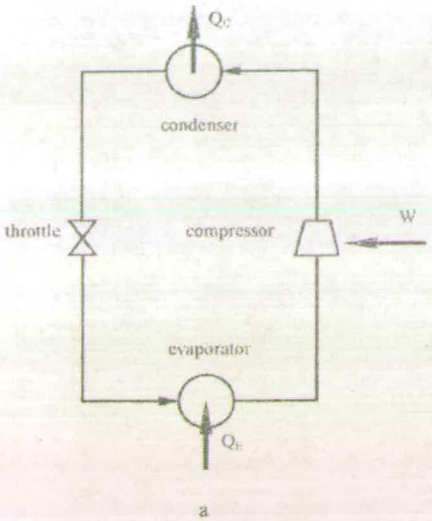

Figure 2.17: Mechanical heat pump arrangement.

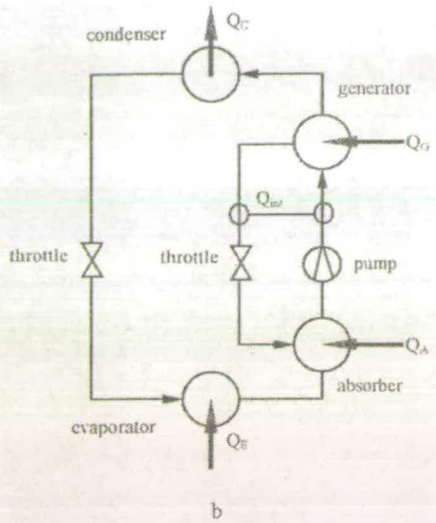

Figure 2.18: Absorption heat pump arrangement.

In some industrial applications like distillation, useful variants may be implemented. The system can be run as a closed heat pump cycle, given in Figure 2.19. The heat pump replaces the steam heating of the reboiler by a condensing refrigerant at a relatively high pressure and the coolant by an evaporating refrigerant at a relatively low pressure. The column itself is not changed from the conventional system, but the heat exchangers will be quite different.

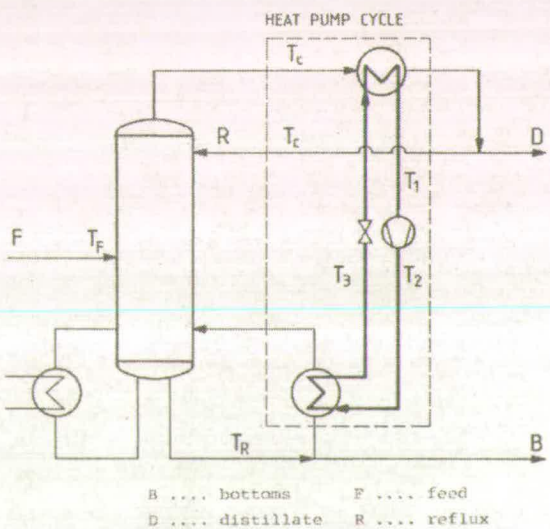

Figure 2.19: Distillation column with closed cycle heat pump.
(Source: Moser 1985 [91])

If the fluid in the column exhibits refrigerant properties, it is possible to improve heat pump performance by utilising this fluid as the heat pump working fluid. The two possible configurations of this open heat pump cycle are given in Figure 2.20. In the vapour recompression case, the condenser is eliminated by feeding the overhead vapour or fluid to the compressor, from which the vapour passes to the column reboiler. The condensed refrigerant is throttled and the liquid fraction is fed back to the column as reflux or tapped off as product. In the bottom flash case, the reboiler is eliminated by flashing liquid across the expansion valve. The liquid is cooled below the temperature of the overhead vapour by this process and can be used as the cooling medium in the distillate condenser. After evaporation, the vapour is compressed, by which the temperature and pressure of the column bottom are regained and the vapour enters the column again.

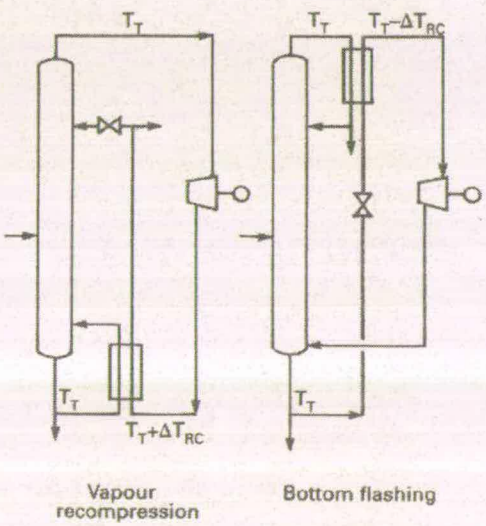

Figure 2.20: MHP arrangements; open cycle.
(Source: Fonyo 1994 [87])

The alternative to MHP are absorption heat pumps (AHP). An absorber, a desorber[5] and an additional fluid loop between these units effect the pressure elevation and the corresponding higher boiling point of the fluid. This additional fluid loop[6] is driven by thermal energy and the whole absorber/generator system replaces the compressor

[5] Usually called generator.
[6] Also called absorbent loop.

found in the literature [91 & 92]. The COP can be improved by using heat pumps that operate with non-azeotropic binary refrigerant mixtures. The gliding temperature profile of the mixture in the evaporator and condenser leads to additional energy savings (Rojey 1980) [93]. Additionally, this behaviour can be exploited in self-regulating heat pumps (Low 1990) [94]. Despite these advantages, there are drawbacks in using non-azeotropic mixtures. Due to the characteristics of mixtures each fluid must be examined individually for each type of heat pump application, which is cumbersome and time-consuming. Nevertheless, research in this field continues e.g. Sami's work (1991) [95].

System-external criteria are useful in comparing different HP systems. The primary energy ratio (PER) is the ratio of primary energy demand to the required output. It considers the COP as well as the efficiency of conversion of the primary fuel (e.g. oil, gas or coal).

$$PER = \frac{1}{COP * \eta_f} \tag{2.12}$$

Additionally, an energy cost factor (ECF) can be defined[7]

$$ECF = COP_{actual} * UER \tag{2.13}$$

where UER is the ratio of the unit cost of steam (c_s) and the unit cost of electrical energy[8] (c_e).

$$UER = \frac{c_s}{c_e} \tag{2.14}$$

2.1.2.2.2 Examples of the implementation of heat pumps in distillation processes

Numerous researchers have investigated the benefits of heat pumps in distillation processes. Kreuter (1973) proposed an optimisation in the Ethane-Ethylene separation [96]; Schultze-Trautmann (1976) and Quadri (1981) considered the

[7] Mostly used for the evaluation of MHP.
[8] Locally derived electricity costs.

implementation of heat pumps in propane-propylene splitters (p-p-splitters)[9] [97 & 98]; Finelt (1979) analysed the impact of HP on C_3 distillation [99]. Fonyo's interdisciplinary work, conducted in the 1990s and published in a series of papers is addressed more properly. In 1994, Mizsey and Fonyo published a parametric study of the use of HPs in energy integrated distillation [87]. They proposed a design strategy for the application of HP in distillation systems. This approach was evaluated with three case studies considering the separation of light hydrocarbons (C3-C5). Several AHP and MHP configurations were taken into account. The next study featured the application of various HP schemes to C4 splitters (1995) [90]. A standard column was compared with three MHP and three AHP configurations. The two most favourable configurations are illustrated in Figures 2.22 & 2.23.

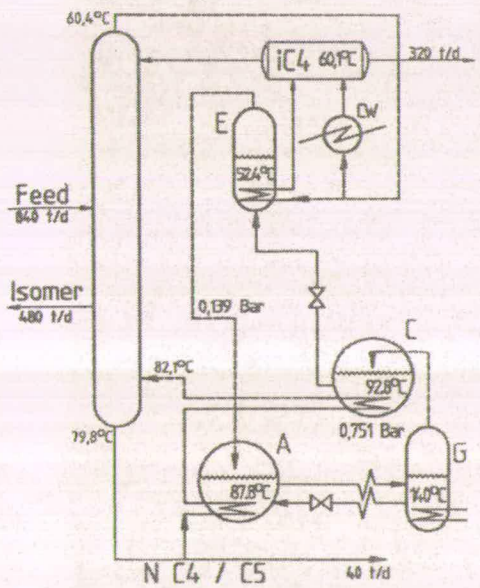

Figure 2.22: Single stage absorption heat pump; sequential operation. (Source: Fonyo 1995 [90])

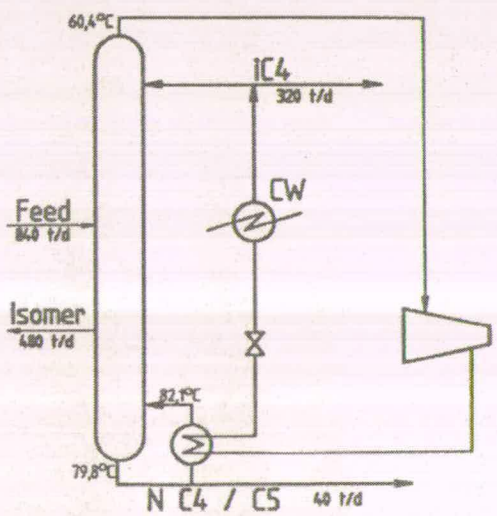

Figure 2.23: Vapour recompression HP. (Source: Fonyo 1995 [90])

[9] p-p-splitters proved to be very popular for case studies in close boiling systems.

From the economic standpoint, the different AHP configurations proved to be the process of choice for C4 separations; but from the water management aspects the three MHP configurations became more favourable. The results are summarised in Table 2.6. Total costs are given in MM$.

			utility cost [MM$/a]				capital cost [MM$]			Total
Type	COP	PER	Water	Steam	Electr.	Σ	Compr.	HX/AHP	Σ	cost
BASE			0.24	10.31	0.00	10.55				10.55
MHPBF	2.45	0.41	0.00	1.68	6.06	7.74	1.71	0.66	2.37	7.98
MHPCC	4.60	0.22	0.06	0.00	6.08	6.14	1.83	1.06	2.89	6.48
MHPVR	4.78	0.21	0.04	0.00	5.85	5.89	1.82	0.51	2.33	6.12
AHPSP	1.89	0.40	0.13	5.15	0.00	5.28		3.72	3.72	5.65
AHPSS	1.87	0.41	0.13	5.22	0.00	5.38		3.72	3.72	5.75
AHPDE	2.48	0.28	0.10	4.21	0.00	4.31		5.58	5.58	4.87

Table 2.6: Cost comparison of various HP arrangements.

(Source: Fonyo 1995 [90])

In 1998, Fonyo and Benkö presented the results of simulations of HPs application in distillation, considering C4 splitters and acetic acid recovery [100]. Their rigorous investigation proved that:

- Larger heat load and smaller process temperature difference provide shorter pay back time for HPs.
- AHPs have an even chance for implementation at larger process ΔT, if the other configurations are to be discarded.

2.1.2.2.3 Intermediate condenser and reboiler

The use of intermediate condensers and reboilers led to an improvement of the thermodynamic efficiency of distillation processes. Such a set-up, based on a heat pump cycle, is given in Figure 2.24.

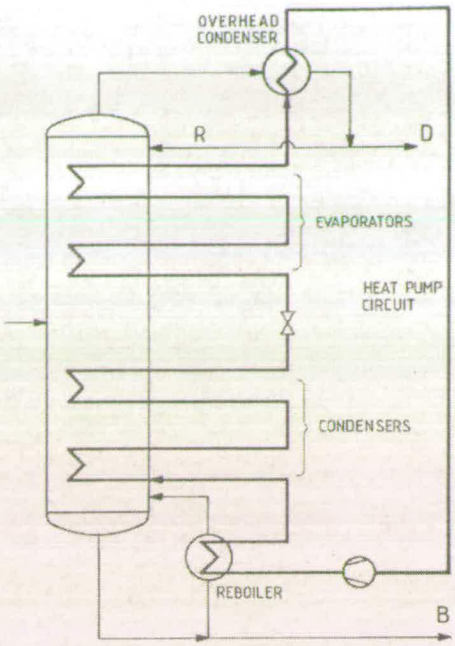

Figure 2.24: Distillation process with intermediate heat exchange.
(Source: Moser 1985 [91])

The implementation of the intermediate reboilers and condensers led to variation of the ratio of the vapour to the liquid flows. The operating line in a McCabe-Thiele diagram becomes buckled, as illustrated in Figure 2.25. Consequently, if the original vapour-liquid ratio is used, the number of plates can be significantly reduced. Alternatively, when the same number of plates is used, the reflux ratio can be lowered. The theoretically most energy saving configuration would be a "reversible" distillation column with an infinite number of intermediate heat exchangers.

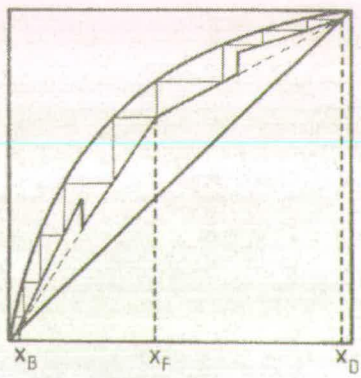

Figure 2.25: McCabe-Thiele diagram for a distillation process with intermediate heat exchange.
(Source: Moser 1985 [91])

Knowledge gained from intensified exergy-related research was applied to the analysis of distillation columns separating binary mixtures. Fonyo (1974) performed a thermodynamic analysis of rectification leading to an intermediate heat exchange model [47]. Fitzmorris and Mah (1980) used thermodynamic availability analysis to improve distillation column design [101]. In 1982, Franklin gave some thought to the application of reversible distillation to multicomponent mixtures [102]. Koehler (1991) expanded the use of reversible distillation theory to nonideal and azeotropic systems [103]. Le Goff et al (1996) published a rigorous exergy analysis for a distillation column containing ethanol-water mixture [56]. The exergy losses could be minimised by the implementation of an intermediate condenser and reboiler in the column. Furthermore, they claimed that diabatic column could lead to reductions of capital costs.

Binary mixtures proved to be more useful improving the understanding of intermediate heat exchangers, due to their less complicated behaviour in comparison to multicomponent mixtures. Therefore, all the pioneering work in this field was performed with simulations using binary mixtures. Pradubsripetch (1994) performed an early attempt at analysing ternary systems [104]. One has to be even more cautious in placing intermediate heat exchangers in multicomponent separation columns. The changes in composition, thereby induced, can lead to severe problems in a system in which the composition profile is paramount for the separation quality. Pradubsripetch [104] identified heating and cooling zones and terminated them by setting upper and lower hypothetical pinch zones.

The work of two further research groups is significant. The first group gathered around Rivero, who started research in this field in 1993 with a thesis [63] covering exergy analysis in distillation. This group focused on binary mixtures and refined their work continuously. In 1997, Sauar and Rivero simulated the optimisation of the separation (ethanol/water) of a diabatic column [105]. They showed that the separation work obtained in an adiabatic stripping column could not be achieved in a diabatic column without adding either a distributed condenser in the upper section of the column, or more plates. In 2001, Rivero amended this work covering the same system [106]. Rivero (2002) applied the insights of the previous work to petroleum

refining and petrochemical industry [64]. Additionally, Schaller and Rivero investigated the influence of heat transfer irreversibilities on the optimal performance of diabatic distillation columns [107]. In 2003, Koeijer and Rivero presented results from an experimental study considering an ethanol/water mixture [108]. First of its kind in terms of accessibility in English, it was able to confirm the theory of diabatic distillation. The heat flux, temperature and concentration profiles are given in Figure 2.26. The diabatic column lost 39% less exergy than the adiabatic column. Additionally, it became transparent that heat and mass transfer on the trays and in the heat exchangers are the major contributors to the entropy production rate. Rivero analysed the potential of diabatic distillation in a large-scale *tertiary* amyl methyl ether (TAME) unit in 2004 [109].

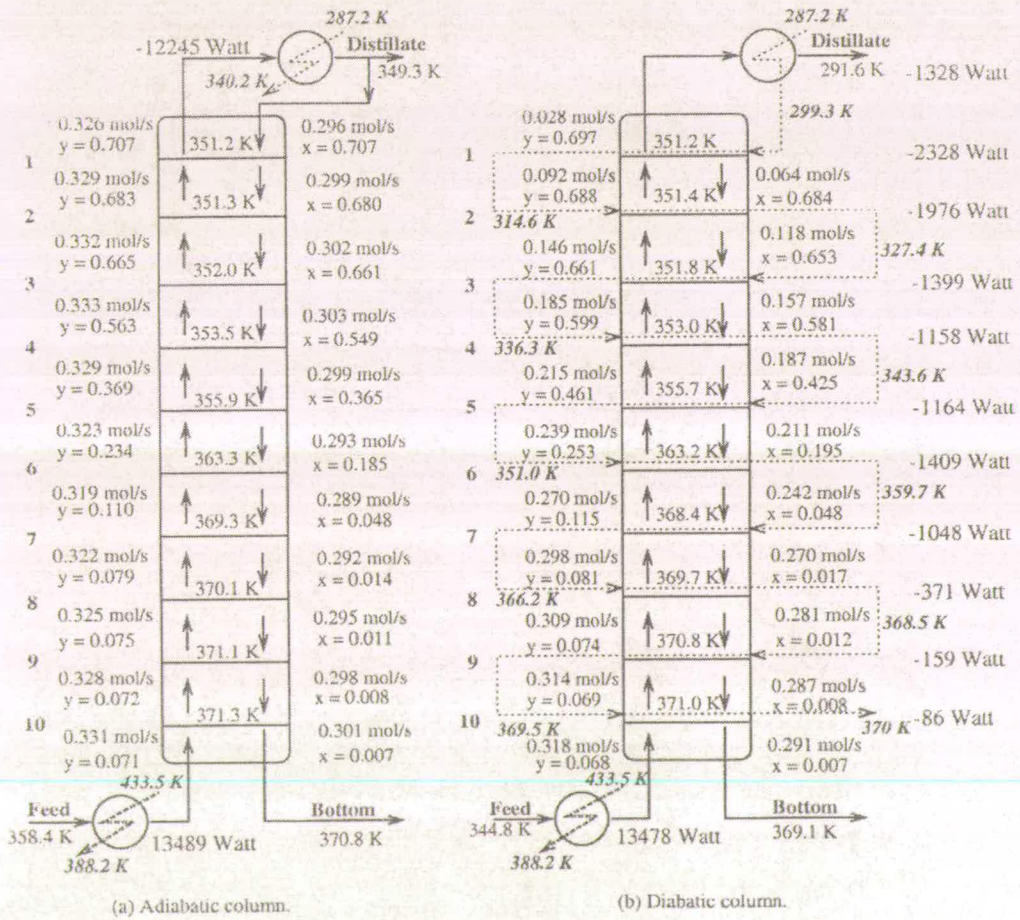

Figure 2.26: Results per tray of adiabatic and diabatic rectifier.
(Source: de Koeijer, Rivero 2003 [108])

The other group formed around Agrawal, who published several papers in the second half of the 1990s. They focused on the placement of intermediate heat exchangers in the stripping and rectifying section of the column. In 1996, Agrawal showed the energy saving benefits of a prefractionator without changing the utility temperatures [110]. Energy integration was established by condensing vapour overhead from the prefractionator in an intermediate reboiler in the stripping section or by boiling bottoms liquid from the prefractionator in an intermediate condenser placed in the rectifying section. This is illustrated in Figure 2.27. The analysis performed concentrated on the minimisation of the vapour flow. A simulation containing a benzene-toluene separation led to a reduction of 33% in energy requirement.

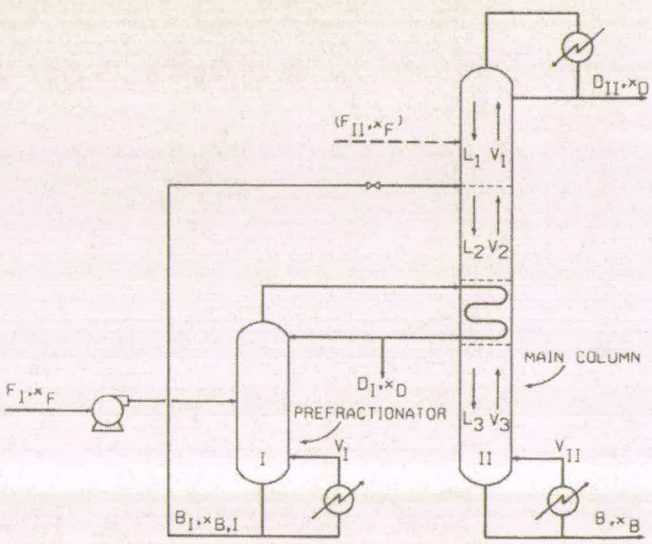

Figure 2.27: Prefractionator configuration with an intermediate reboiler.
(Source: Agrawal 1996 [110])

Furthermore, Agrawal applied a new approach to the use of intermediate heat exchangers by placing intermediate reboilers in the rectifying section and intermediate condensers in the stripping section in columns separating highly non-ideal systems [111]. This seemingly counterintuitive approach enables the partial replacement of the more expensive heating utility in the bottom reboiler by a less expensive heating medium[10] in the intermediate reboiler. The same principle can be

[10] At a lower temperature.

applied to the condenser. It was also proposed that this arrangement could reduce the total number of stages in the column with a lower level of utility. In 1998, Agrawal presented a method for finding the optimal placement of intermediate heat exchangers, purely determined by the feed composition [112]. Additionally, Agrawal proposed heuristics for the assessment of using intermediate heat exchangers in binary distillation [113]. According to his method, intermediate heat exchangers become particularly beneficial when relatively pure feed[11] streams are distilled. The extremely low efficiencies of distillation in this region can be remarkably improved by using intermediate heat exchangers. Finally, Agrawal applied his insights previously gained to ternary mixtures by proposing thermodynamically efficient systems [114].

2.1.3 HIDiC project

Heat integrated distillation columns (HIDiC) belong to a group of distillation columns, in which direct heat transfer is achieved by a concentric configuration. The term was coined by the Japanese research group . The career of HIDiC is described in the following paragraphs due to its big influence and inspiration on our project.

As an alternative to intermediate heat exchangers a new column arrangement was presented by Gunther (1974) and Mah *et al.* (1977) [115 & 116]. Both approaches suggested splitting a column into separate stripping and rectifying sections, heat transfer is enabled by operating the rectifying section under a higher pressure than the stripping section. Heat transfer takes place from the high-pressure column to the low-pressure column, causing condensation in the former and evaporation in the latter column. Thus the system resembles a "reversible distillation." Gunther described his system as a diabatic "heat-transferring fractionator" and became very excited about the topic as it can be noticed from his quote [115]:

> "We have developed a new system of fractional distillation that we believe constitutes the only fundamentally new contribution to this art that has been made since the last century."

---

[11] Concentration of either component > 90%.

Heat transfer occurs through a plate-fin heat exchanger, which serves as heat-transferring fractionator. Narrow vertical passages are designed so that rectifier passages alter with stripper passages. Simulations of cryogenic air separation producing 99.5% pure oxygen led to energy consumption of 180 kWh/ton for the diabatic system vs. 280 kWh/ton for the conventional system. Additionally, tests showed that the countercurrent capacity of the plate-fin heat exchanger is well over twice that of a conventional packed conventional tower.

Mah called his scheme "distillation with Secondary Reflux and Vaporisation" (SRV). Heat transfer also occurs between the separated rectifying section; working under higher pressure, and the stripping section. The pressure difference is achieved by vapour compression from stripping to rectifying section. Mah's scheme for the diabatic column is given in Figure 2.28. This created a distillation pattern approaching the reversible distillation scheme. The liquid reflux rate steadily increases as one proceeds down the rectifying section as a result of the heat exchange between the two sections, and the vapour flow steadily increases as one proceeds up the stripping section. Unfortunately, they drew a dangerous conclusion stating that fewer stages are needed for accomplishing the same separation. This is only true if one takes the reduced overhead stream from the SRV distillation as benchmark.

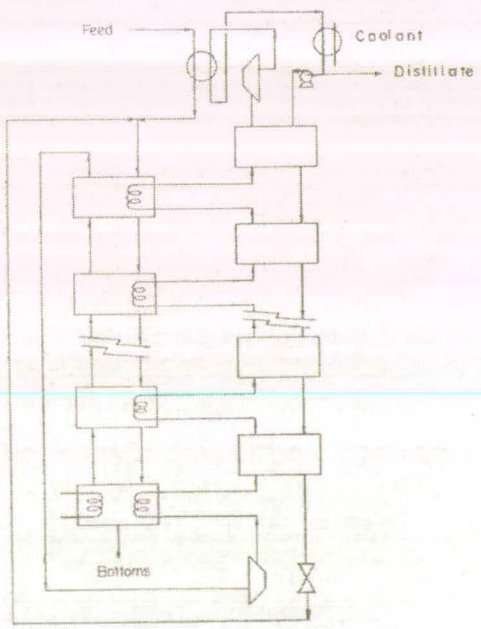

Figure 2.28: Distillation scheme with secondary reflux and vaporisation.
(Source: Mah 1977 [116])

They scrutinised three binary mixtures (butene isomers, propylene/propane, ethylene/ethene) for their potential in energy savings using a modified Wang-Henke method for the simulations. Compression work was transformed into equivalent steam and cooling water consumptions. The pressure difference was set to fit a ΔT of about 27K for the first two cases and 11K in the third case. Utility requirements for the three cases are given in Table 2.7.

	Conventional distillation			SRV distillation		
Refrigerant mixture	Trans-2-/ cis-2-butene	Propylene/ propane	Ethylene/e thane	Trans-2-/ cis-2-butene	Propylene/ propane	Ethylene/ ethane
R 22						
cooling water	860.57	235.24	19.42	558.42	91.98	8.46
steam kg/s	31.75	7.67	132.19	26.96	13.10	32.62
Re 170						
cooling water	860.57	235.24	33.92	558.42	91.98	11.12
steam kg/s	46.92	11.46	184.84	28.90	14.27	42.27

Table 2.7: Utility requirements for cases 1-3.

(Source: Mah 1977 [116])

The butene mixture required 15% less steam and 35% less cooling water in the SRV mode than the conventional column. Another outcome was obtained in the propylene/propane case. Although the cooling water consumption was 61% less, the steam consumption increased by 71%. The SRV distillation performed notably better in the ethylene/ethane case than the conventional column by using 54% less steam and 77% less cooling water. Mah delineated 3 circumstances, which favour SRV distillation.

- Process conditions that make compression work less expensive in comparison with thermal energy. For example, cryogenic distillation that requires refrigeration in the condenser; leading to a higher significance in the case of a reduction of the condenser duty.
- Close boiling mixtures featuring a low temperature range between the two column ends. Therefore less compression is needed to reverse the temperature differences between the two sections. Additionally, mixtures whose bubble points increase rapidly with pressure also require less compression.

- Difficult separations that have their operating lines close to the equilibrium line (close boiling mixtures again).

Mah promised an extension of his work to multicomponent mixtures. Sadly, he couldn't realise this promise. Glenchur and Govind picked up Mah's idea in 1987 and developed a "concentric column" configuration illustrated in Figure 2.29 [117]. Heat transfer again occurs from the high pressure rectifying section in the centre to the surrounding stripping section through the dividing wall. Again, vapour leaving the top of the stripping section is compressed and liquid leaving the bottom of the rectifying section is throttled.

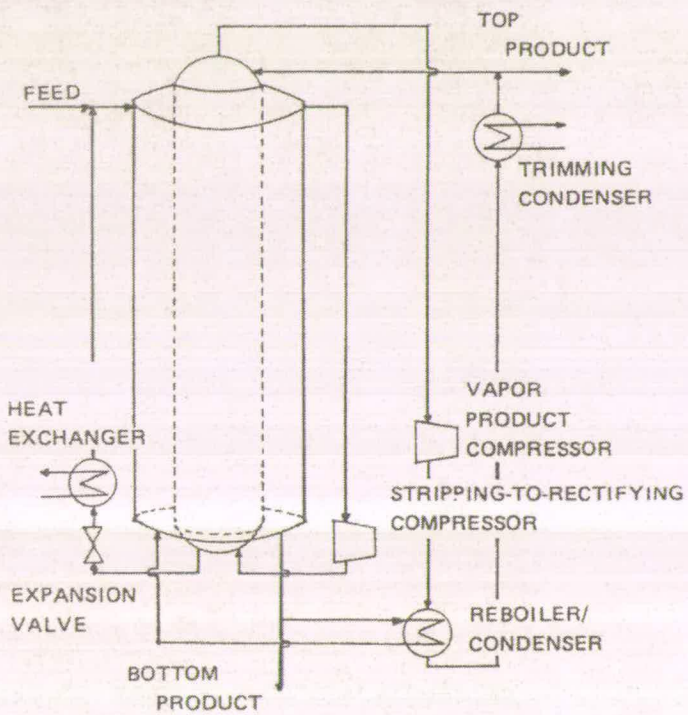

Figure 2.29: Scheme of a continuous heat integrated or concentric column.
(Source: Glenchur & Govind 1987 [117])

Furthermore, Glenchur and Govind proposed several multicolumn configurations for the application of the concentric column concept. Additional thoughts were given to possible designs for heat integrated trays in concentric columns, illustrated in Figure 2.30. An exergy analysis comparing the proposed configuration with ordinary distillation proved the superiority of the former.

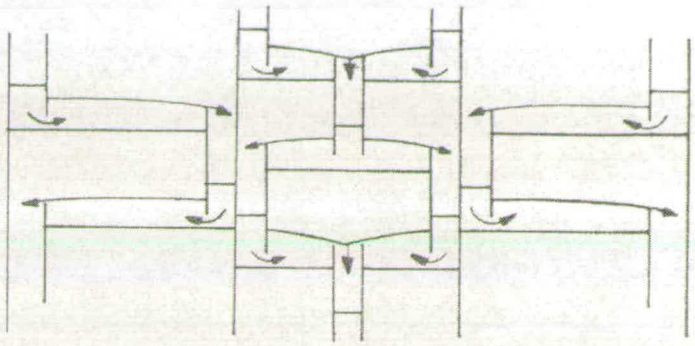

Figure 2.30: Scheme of a possible design for heat integrated trays in a concentric column. (Source: Glenchur and Govind 1987 [117])

The well-known ethylene/ethane system was chosen for their simulations, which are based on MESH equations. The MESH equations were solved by using a modified Boston and Sullivan (1972) algorithm [118]. Plots of the number of stages vs. an interstage heat transfer coefficient area (UA) revealed – one is given in Figure 2.31. – that with a sufficient UA value, separations can be achieved with much smaller reflux ratios than with conventional columns. In the extreme case, the separation is impossible with a limited reflux ratio (< 2.0) for the conventional column. Adiabatic distillation is represented in the plot along the UA = 0 ordinate. The spacing between the reflux ratio decreases with larger pressure ratios between the columns. On the other hand, the minimum reflux ratio is more sensitive in the case of larger pressure ratios.

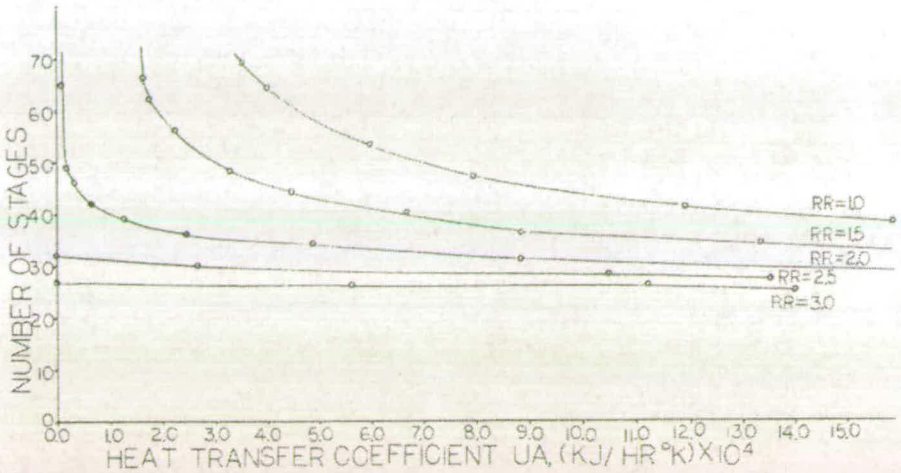

Figure 2.31: Number of stages vs. interstage heat transfer coefficient area at changing reflux ratio (RR). Distillate purity > 0.995 ethylene. Bottoms purity > 0.995 ethane. P rectifying = 3.03 bar. P stripping = 1.52 bar. (Source: Glenchur and Govind 1987 [117])

A comparative study of the ethylene/ethane case involved the use of vapour recompression, leading to particular savings in cooling water. Table 2.8 features 7 schemes for adiabatic two pressure columns and concentric columns (cases 6 & 7) where Q_{SRC} represents the duty of the stripping-rectifying compressor and Q_{VCR} the duty of the vapour recompression compressor respectively. The column "Steam equivalent" represents the equivalent steam consumption of the unit.

Case[b]	Reflux ratio	Q_R, (kJ/h) $\times 10^7$	Q_C, (kJ/h) $\times 10^7$	Q_{SRC}, (kJ/h) $\times 10^6$	Q_{VRC}, (kJ/h) $\times 10^6$	Steam equivalent, (kJ/h) $\times 10^5$	Cooling water, (kJ/h) $\times 10^5$
1	2.67	−2.225	2.264	0.000	−1.529	0.5066	0.2075
2	2.67	−2.087	2.264	−3.889	0.000	2.735	12.04
3	2.67	−2.087	2.264	−3.889	−1.921	0.4374	0.9416
4	2.67	−2.077	2.264	−4.480	0.000	2.763	12.04
5	2.67	−2.077	2.264	−4.480	−1.921	0.4773	0.9948
6	1.80	−1.554	1.727	−3.736	0.000	2.109	9.187
7	1.80	−1.554	1.727	−3.736	−1.464	0.3999	0.9203

1 Adiabatic one-pressure column with vapor recompression
2 Adiabatic two-pressure column without vapor recompression
3 Adiabatic two-pressure column with vapor recompression
4 Concentric column without vapor recompression
5 Concentric column with vapor recompression
6 Concentric column without vapor recompression
7 Concentric column with vapor recompression

Table 2.8: Comparison case studies of adiabatic two-column operation with concentric column operation. (Source: Glenchur and Govind 1987 [117])

Nakaiwa *et al.* picked up the idea of concentric columns in the mid 1990s. His group published several papers covering concepts, control, energy efficiency and experimental studies. This work will be reflected in the following lines.

Inspired by and partly involved in publications of Takamatsu (1988, 1994, 1996), Nakaiwa started to peruse a way for efficient heat integration in packed columns [119, 120 & 121]. In 1996, the Nakaiwa's group published two conference papers describing design methods [122] and fundamental experimental research in HIDiC [123]. Both studies were conducted with a benzene-toluene mixture. The simulation study features a modified McCabe-Thiele method, taking the changing vapour and liquid flows into account. This approach will be explained in greater depth in Chapter 3. The HIDiC column is compared with a conventional column that has 30 stages. Product quality was set as 99.5% benzene for the overhead product and 0.5% benzene for the bottoms. The pressure ratio between the rectifying and stripping section was set as two. The investigation led to plots describing the behaviour of UA and the energy consumption vs. the number of plates; given in Figure 2.32. It is noticeable that the energy consumption drops significantly between 30 and 50 stages, before reaching a plateau stage. Furthermore, the authors stated that the HIDiC always requires more stages than a conventional column.

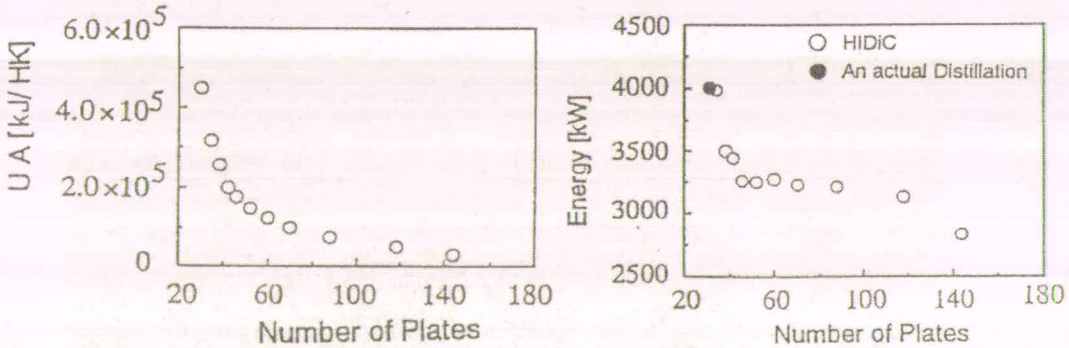

Figure 2.32: UA vs. number of plates (left), energy consumption vs. number of plates (right). (Source: Nakanishi 1996 [122])

The experimental paper features a 315.5 mm diameter shell column, containing three 114.3 mm diameter tubes and Sulzer packing. The arrangement is given in Figure 2.33. Mutual heat transfer was achieved by changing the benzene-toluene composition. No pressure difference was applied. Overall heat transfer coefficients

between 300 – 500 W/m^{2}K could be obtained. The aim of the study was to proof the feasibility of the HIDiC heat transfer concept.

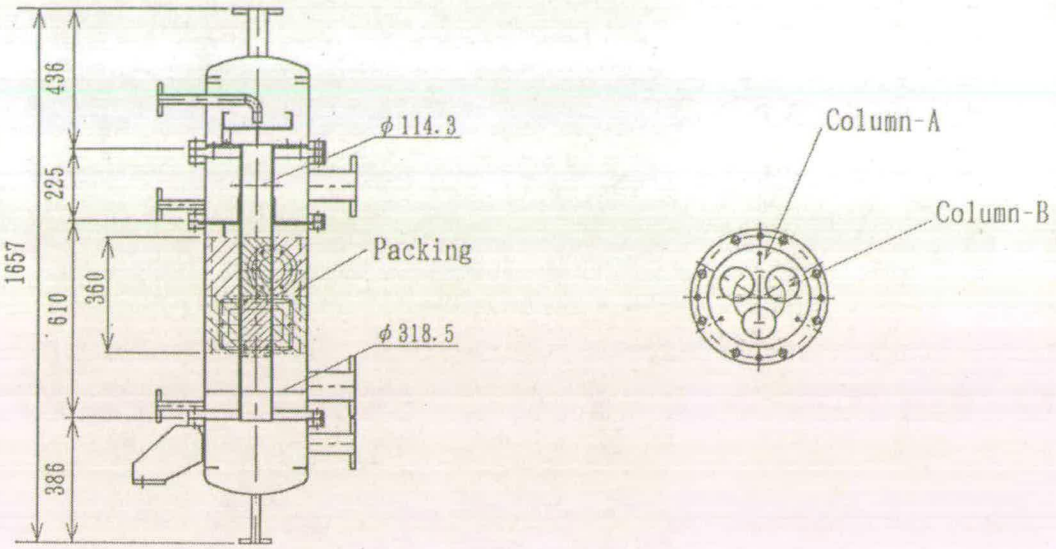

Figure 2.33: Test column for HIDiC system (left), cross sectional view (right). (Source: Noda 1996 [123])

HIDiC caused some problems in terms of controllability, particularly if the system was optimised; leading to a scheme without the need of a reboiler or condenser[12]. A scheme of the ideal HIDiC is given in Figure 2.34. The dynamics of the process were investigated by Huang and Nakaiwa in 1996 [124]. They found - by using non-linear and linearised models – that thermal interactions were stronger at low pressure differences. The system did not become unstable though. Huang and Nakaiwa (1996) proposed a control mechanism for the aforementioned problem in 1996 [125]. They proved that ideal HIDiC could be efficiently regulated by manipulating either the thermal feed condition, or the pressure of either rectifying or stripping section. 1997 saw the intensification of the controllability investigation. Huang and Nakaiwa investigated the influence of the thermal feed condition more exactly with three specified cases ($q<0.5$, $q=0.5$ and $q>0.5$) in a first paper [126]. This was followed by a proposal of alternative configurations for ideal HIDiC [127], shown in Figure 2.35. It could be shown that the control loop interactions were strongest for $q = 0.5$.

[12] Called ideal HIDiC.

Nevertheless, the system could be operated smoothly. Additionally, the feed location strongly affected the dynamic performance of the system. The configuration study proved that the symmetrical configuration contributed substantially to the interaction between top and bottom control loops. This could be solved by adding additional stages to one of the two sections. The scheme with more stages in the rectifying section appeared to be most promising. However, those additional stages do not contribute to heat integration. The gain of better controllability at the price of higher capital costs ought to assessed carefully.

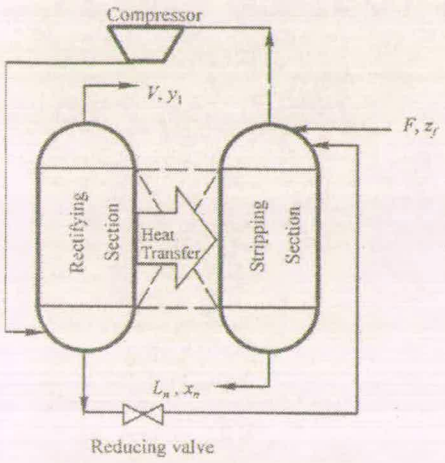

Figure 2.34: Scheme of an ideal HIDiC. (Source: Huang 1996 [124])

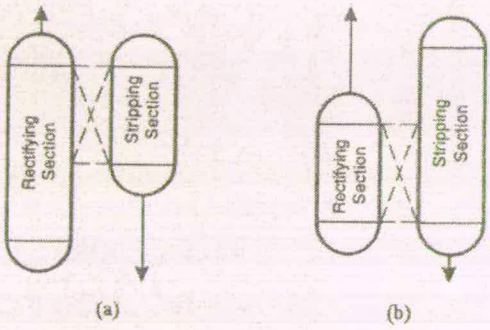

Figure 2.35: Alternative configurations of ideal HIDiC. (Source: Huang 1997 [127])

Nakaiwa and Huang also published a study considering the energy saving potential of HIDiC[13] and ideal HIDIC in 1997 [128]. The simulation features the benzene-toluene system and a pressure ratio between the sections of two[14]. Three cases were investigated, of which the best led to overall energy savings of 60%. However, the number of stages needed is increased. 1998 brought further amendments in the field of process control. Nakaiwa and Huang addressed five control algorithms for ideal

[13] With trim-reboiler and condenser.
[14] The stripping section was operating under atmospheric pressure.

HIDiC [129] and designed a multivariable internal model control system for the improvement of ideal HIDiC [130]. Another study (Nakaiwa *et al.* 1998) focussed on exergy analysis of the HIDiC process [131]. The benefits were displayed in a T-Q diagram and on several exergy plots. A chosen plot can be seen in Figure 2.36. The exergy loss for conventional columns and ideal HIDiC are given in eqn. 2.15 & 2.16.

$$\Delta e_c \equiv P(1+r)\lambda T_0\left(\frac{1}{T_{distillate}}-\frac{1}{T_{bottoms}}\right)-F(1-q)\lambda T_0\left(\frac{1}{T_{feed}}-\frac{1}{T_{bottoms}}\right) \qquad (2.15)$$

$$\Delta e_h \equiv \Pr\lambda T_0\left(\frac{1}{T_{feed}}-\frac{1}{T_{rect}}\right)-F\lambda T_0\left(\frac{1}{T_{distiilate}}-\frac{1}{T_{rect}}\right) \qquad (2.16)$$

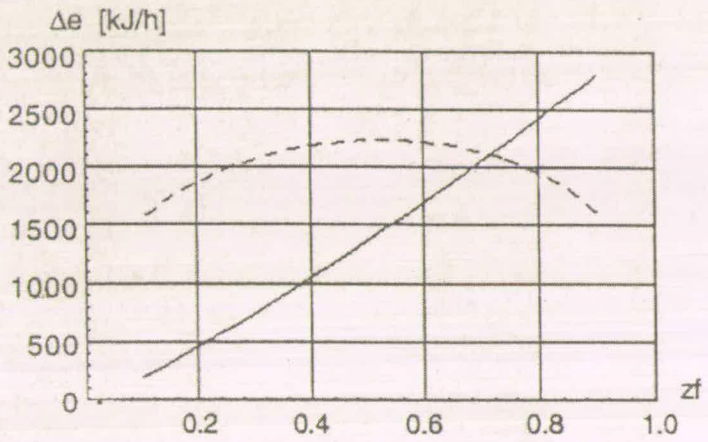

Figure 2.36: Comparison of the exergy loss for distillation of the ideal HIDiC with that of a conventional column. Full curve: the ideal HIDiC, dotted curve: conventional column. (Source: Nakaiwa 1998 [131])

It is evident from eqn. 2.16 that the exergy loss is significantly lower for low feed compositions.

Huang went to China and founded a satellite group. This group published a paper in 1999 covering the modelling aspect and a paper in 2000 containing an assessment of control configurations in HIDiC [132 & 133]. This work was conducted in co-operation with Nakaiwa. The modelling paper features a new test mixture (ethanol-water). The system was chosen due to is non-ideal character requiring a highly energy intensive separation process. HIDiC proved to be an energy saving alternative.

After solving the controllability problem Huang and Nakaiwa turned their attention to the start-up problem of HIDiC (1998) [134]. The paper suggested the use of a trim-condenser and trim-reboiler. According to the authors, a smooth start-up is also feasible without the presence of a trim-condenser. Additional information is given in form of appropriate start-up control system proposals. HIDiC evolved a stage further in 2000. Nakaiwa *et al.* proposed a new ideal HIDiC by implementing additional heat integration between the overhead product and the feed, given in Figure 2.37 (controller positions are given by C1 and C2)[135]. This additional heat integration has the advantage of being self-regulating, which is not the case for the heat transfer between the sections in HIDiC.

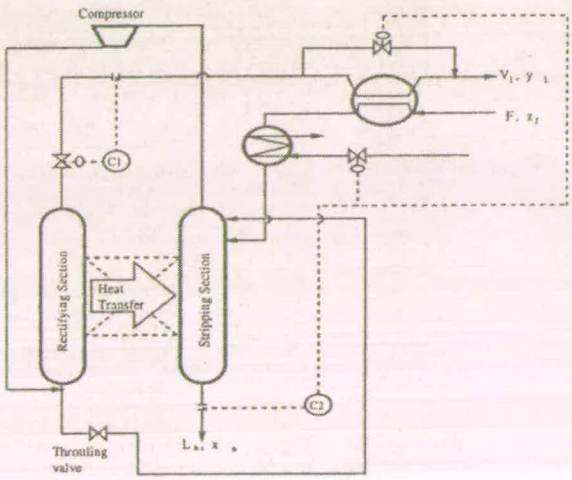

Figure 2.37: Scheme of a new HIDiC.
(Source: Nakaiwa 2000 [135])

A milestone was achieved by publishing an experimental study conducted in bench-scale plant (Nato and Nakaiwa 2000) [136]. A layout of the bench scale plant is given in Figure 2.38. The experiments were performed with a benzene-toluene mixture in an impressive, 20 m high column with a 254 mm diameter stripping section (displayed in Figure 2.39). The rectifying and stripping sections were filled with structured packings from Sulzer. A cone-shaped rectifying section had been proposed in the first place to suit the changing vapour flow rates. This was rejected due to manufacturing problems. A cascaded column was chosen instead, given as dark central column in Figure 2.30.

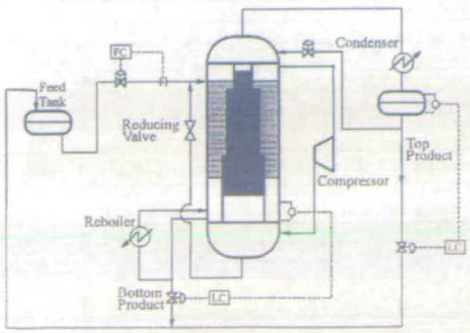

Figure 2.38: Layout for the bench-scale HIDiC plant. (Source: Naito 2000 [136])

Figure 2.39: Bench-scale HIDiC in Japan.

The experimental series gave precious insights into start-up time and energy saving potential. Steady state was usually achieved after 10 h. Additionally, the temperature data was used for the calculation of overall heat transfer coefficients by us. This will be addressed in Chapter 5. The stripping section was run under atmospheric pressure and the rectifying section was pressurised up to 2 bar. With a feed flow rate of 3.2 kmol/h, an overhead product quality of >99.9% benzene and bottoms of >99.5% toluene could be achieved. An energy consumption for a conventional column, a HIDiC and an ideal HIDiC are given in Table 2.9. The study showed that smooth reflux and reboil-free operation can be achieved by the ideal HIDiC.

Items	Energy consumption (kW)	Comparison (%)
Conventional (R=7.0)	73.9	100
Ideal HIDiC (R=0.0)	44.1	60
HIDiC (R=0.3)	45.7	62

Table 2.9: Comparison between the ideal HIDiC and a conventional distillation column. (Source: Naito & Nakaiwa 2000 [136])

Noda *et al.* conducted experiments with three different internal tube configurations in 2000, given in Figure 2.40 [137]. A benzene-toluene mixture was used in the 318.5 mm diameter shell. As in Nakaiwa's conference paper [123], the experiments were conducted under the absence of pressure difference. Noda determined overall heat transfer coefficients and number of transfer stages per meter. All three configuration performed equally well, giving an overall heat transfer of 500 W/m^2K. and producing NTSM (number of theoretical stages per meter)values of 3.8.

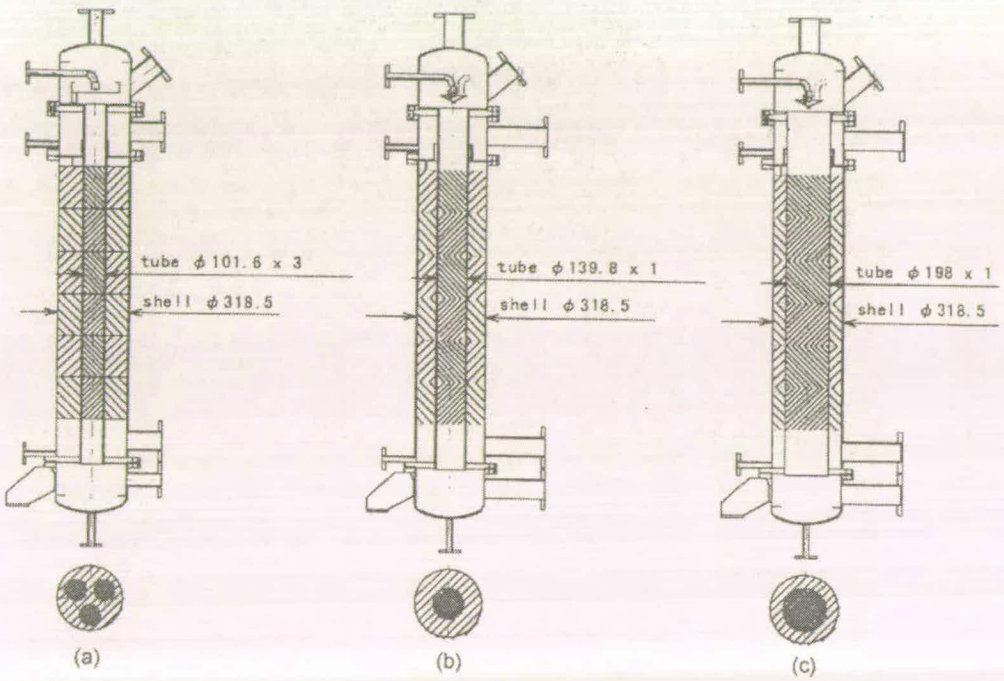

Figure 2.40: A multi-tube column, b + c coaxial column.
(Source: Noda *et al.* 2000 [137])

Nakaiwa rounded up his work with a review first presented at the International Conference on Absorption and Distillation in 2002 and subsequently published in 2003 [138]. This review provides a good starting point for familiarisation with HIDiC. The group implies future development heading for multicomponent separation investigation and the application of the system to binary system with large relative volatilities using partial heat integration. The multicomponent separation will demand very complicated configurations, according to the authors.

The HIDiC project has raised interest in the world. Several groups formed around the world and published their first results emphasising process design (Niang *et al.* 1995

& Rivera-Ortega *et al.* 1999), process operations (Liu and Qiang 2000), internal heat/mass transfer mechanism and internal structure arrangements (Pritchard *et al.* 2002 & Jansens *et al.* 2001) [139, 140, 141, 142 & 143]. Pritchard and Beggs (2002) presented potential configurations for a trayed HIDiC such as using heat pipes as heat transfer devices between the sections (Figure 2.41) or a pumparound configuration as illustrated in Figure 2.42 [144]. Beggs (2002) performed simulations with the aforementioned systems revealing energy-saving potential for both [145]. The pumparound configuration was further refined by Pritchard's proposal (2004) of using binary refrigerants as HEM [146]. This approach allows the establishment of a constant temperature glide from tray to tray in a diabatic column. Watson (2004) investigated and assessed some binary refrigerant mixtures in his project [147]. Cameron and Mottram (2004) measured overall heat transfer coefficients of copper coils in cooling and heating modes [148]. Copper coils are potential candidates as a part of the proposed pumparound system. Olujic *et al.* (2004) chose another path and implemented heating panels in a pilot plant column [149, 150 & 151].

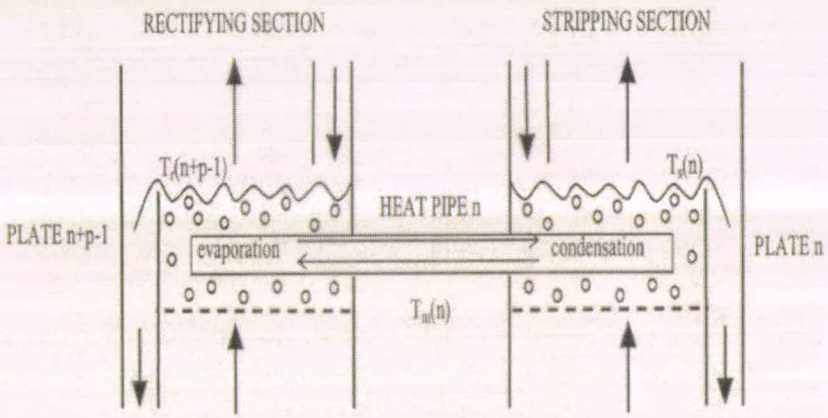

Figure 2.41: Heat pipe configuration of a trayed HIDiC.
(Source: Beggs 2002 [145])

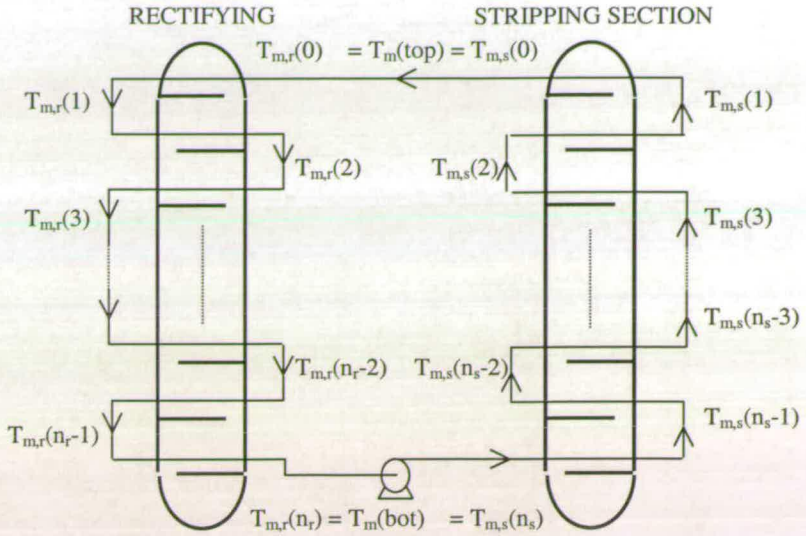

Figure 2.42 Pumparound configuration of a trayed HIDiC.
(Source: Beggs 2002 [145])

2.1.4 Summary

The second law of thermodynamics, applied in exergy analysis, has become well known in engineering applications and is present in thermodynamic textbooks. Separation processes are optimised by analysing the system for irreversibilities first, followed by the removal of such exergy loss sources. Exergy analysis developed powerful tools like Enthalpy / Carnot temperature diagram and "tridimensional" Exergy plots for the assessment of exergy losses. Second law-related research led to the proposal of the reversible (diabatic) distillation. Efficiency in energy conservation ought to be replaced by various effectiveness definitions.

Heat integration in distillation can be applied by either linking individual columns (intercolumn heat transfer) or using streams from the same column (intracolumn heat transfer). Intercolumn heat transfer is well established in production plants and ought to be applied first before moving towards intracolumn methods. Intracolumn methods may amplify the benefits gained from intercolumn methods. Heat pumps are most popular and widespread amongst internal heat integration applications. Better from the exergy viewpoint are intermediate heat exchangers in columns. Efforts in this field have been mostly simulation-based with the exception of Rivero's diabatic

column [63 & 108]. Closest to a reversible distillation is the ideal Heat Integrated Distillation column (HIDiC), developed by Nakaiwa *et al.* HIDiC splits a packed tower and rearranges the rectifying and stripping section concentrically. Heat transfer occurs between the central rectifying section, which operates under higher pressure, and the surrounding stripping section. The system can operate without reboiler and condenser. Thoughts have been given to the application of the HIDiC concept, but fundamental, experimentally obtained data are still missing.

2.2 Sieve Trays

Sieve trays are the workhorses in distillation. Their popularity is unbroken and R & D in this field still continues. Better understanding of the mechanism, which define the quality of separation (efficiency) and improvements in the design can lead to reduced capital and operating costs. Due to the simplicity of sieve tray towers, new improvements can be relatively easily implemented by retrofitting. The next sections give brief review in the fields of efficiency investigation and prediction as well as design improvements.

2.2.1 Efficiency related research

Most of the design methods rely on the determination of the number of theoretical stages required for a particular separation. After such a calculation, the result is usually multiplied by a "safety factor" recommended by the tray manufacturer or taken from a database. This reflects the separation performance of the plates. There are many definitions for efficiencies in distillation, which will be properly addressed in Chapter 3, but the so-called Murphree tray efficiency became closest to a standard (eqn. 2.7).

$$E_{MV} = \frac{\overline{y}_n - \overline{y}_{n-1}}{y_n^* - \overline{y}_{n-1}} \tag{2.7}$$

It represents the ratio of the difference of the vapour concentration between a real tray and an ideal tray. Standart and Kastanek (1966) addressed the problems caused

by carryover[15] [152]. They developed reduced flow rates and concentrations for the calculation of Murphree efficiencies taking entrainment into account. With the knowledge of the complete concentration profile on the plate it is possible to calculate entrainment and efficiency values by using general balance relations. The same authors presented a comprehensive paper in 1967 covering the experimental determination of Murphree tray efficiencies and their comparison with existing prediction methods [153]. They conducted experiments in a large-scale column (976 mm diameter) to obtain nonuniformities in tray hydraulics. Methanol-water served as a text mixture. They carried out measurements of the efficiencies of the following plates: bubble cap, sieve, Uniflux, APV-West of the downcomer type, and Ripple and Turbogrid of the type without downcomer. The resulting efficiency values lay between 80-90% with a deviation of +/- 5%. The Murphree efficiency values obtained were compared with the AIChE model and with various models originating from Eastern Europe [154, 155 & 156]. Even in the cases where entrainment was absent, the agreement with the experimental data was only fair to good. The authors partly blame a combination of sampling errors and equilibrium data uncertainties for this phenomenon. Additionally, they give a thorough insight to liquid and in particular, vapour sampling. A cyclone-based system is recommended for obtaining dry[16] vapour samples. It is also shown that the measurement of entrainment influenced samples is in vain due to the random character of the entrainment stream.

Lockett and Ahmed conducted Murphree tray efficiency experiments with Methanol-water mixtures in a 0.6 m diameter column in 1983 [157]. Vapour samples were withdrawn according to Standart's recommendations. Additionally, the liquid profile across the plate was investigated by sampling across the central line of the sieve tray. The composition profile is given in Figure 2.43. The aim of the work was to transform measured plate efficiencies (given in Figure 2.44) into point efficiencies and from there a calculation of the number of transfer units – explained in Chapter 3 – was possible. The values for the transfer units in each phase were compared with

[15] Also called entrainment.
[16] Entrainment-free.

the AIChE model (1958) [158], proving that several assumptions in the model were wrong. The tray efficiency values obtained ranged from 80 – 90%.

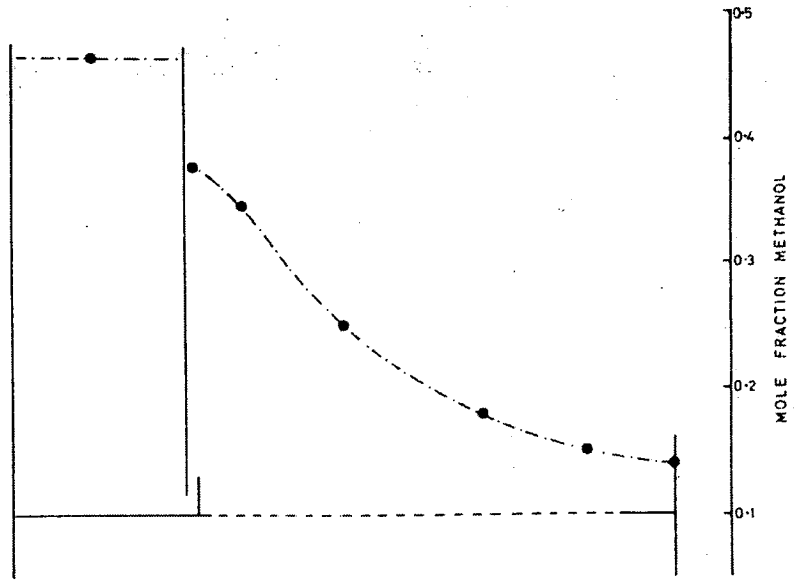

Figure 2.43: Typical liquid concentration profile on the 0.6 m diameter column. (source: Lockett & Ahmed 1983 [157])

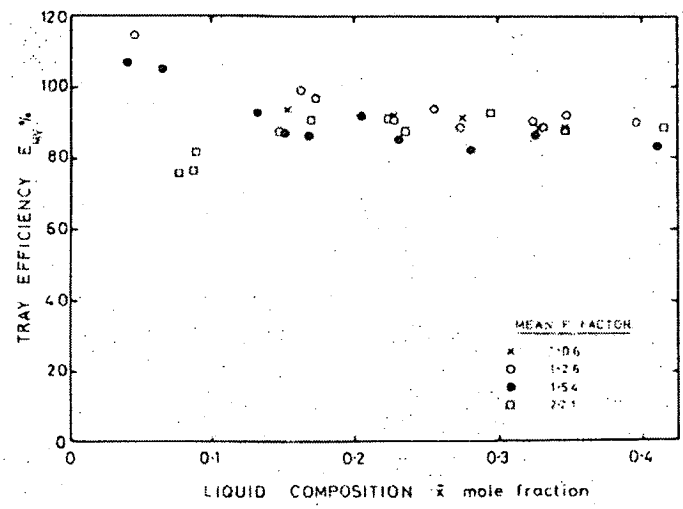

Figure 2.44: Murphree tray efficiencies for methanol-water system; 0.6 m diameter column. (Source: Lockett & Ahmed 1983 [157])

Chan and Fair (1984) improved the prediction of point efficiencies in the vapour phase, cutting the absolute deviation from 22.9% in the AIChE model down to 6.3% [159]. The new correlation was obtained from data plots based on an extensive data

base containing various hydrocarbons and non-hydrocarbons. Additionally, the same authors investigated the prediction of point efficiencies of ternary mixtures on sieve trays (1984) [160]. They developed a rigorous matrix method and a pseudo-binary model. After validation with experimental data obtained from a 25 mm diameter Oldershaw column, Chan and Fair showed that the pseudo-binary approach was reliable enough for producing reasonable results.

Krishnamurthy and Taylor published a new rate-based multicomponent stage model in 1985[161]. They criticised the approach of equilibrium models and its adaptation to reality by using Murphree tray efficiencies. A second paper validated their results in binary and multicomponent distillation mixtures 1985 [162]. The model proved to be groundbreaking and was further improved by Taylor in 1994 and Mueller in 2000 [163 & 164].

In 1989, Plaka *et al.* used the same 0.6 m diameter column mentioned in Locket's work to predict Murphree point efficiencies and number of transfer units using a methylcyclohexane-toluene mixture [165]. The diameter of the column is large enough to avoid potentially large wall, tray liquid entry and exit effects, but not as large as to encounter liquid channelling effects – all of which make data interpretation difficult. The authors linked the number of transfer units with the bubble size and velocity distribution in the froth, and compared the results with the AIChE model. They pointed out that the AIChE model was not reliable unless the resistance in the separation was purely caused by one phase. This was not the case for their test system, finding a contribution to the mass transfer resistance of 55 – 70% for the liquid phase.

Prado and Fair (1990) elucidated the connection between mass transfer and hydraulics by proposing a mechanistic model for the prediction of sieve tray efficiencies [166]. They divided the tray into different zones by applying horizontal cuts. Appropriate equations were developed for each zone, derived from comparisons with a big database. The experiments were conducted in a mechanically agitated vessel containing air-water mixtures. This model was further refined by Garcia and Fair (2000) and made applicable for non-aqueous systems [167 & 168]. The

predicted efficiency values were found to be within +/- 25% of the measured or deduced values.

Chen and Chuang published a semiempirical model for the prediction of sieve tray efficiency in 1993 [169]. The model takes into account the effect of physical properties on mass transfer coefficients and interfacial area. Fits with experimental data were achieved by implementing experimentally obtained constants. In 1994, the same authors compared their model with three existing models, given below [170].

- The slope and intercept method [171].
- Penetration theory base model [172].
- "Two bubble size" interfacial area model [173].

The authors give a brief overview on the disadvantages of the aforementioned models. Their own model fares better than the other models in a comparison of six different binary mixtures. The results obtained from this work were also used for the assessment of the liquid phase mass transfer contribution. The resistance was particularly high for hydrocarbon mixtures (i.e. C_6 / C_7) claiming 50%; and particularly low for aqueous systems (methanol-water) claiming 10% (Chen and Chuang 1995) [174]. The authors stress that the AIChE model greatly overpredicts the number of liquid transfer units.

Korchinski *et al.* turned their attention back to the 0.6 m diameter column in 1994 [175]. They investigated three binary systems (methanol-water, isopropanol-water and methylcyclohexane-toluene) to obtain experimental point efficiency data. These data were compared using five point efficiency and transfer unit prediction methods. Stichlmair's [176] and Chan and Fair's [159] methods delivered the best agreements with the experimental data. The expected accuracy of prediction was about +/- 10% absolute. The same experimental set was used for the calculation of eddy diffusion coefficient (Korchinsky 1994) [177]. The comparison with various available diffusion prediction methods led to the conclusion that Zuiderweg's approach [171] was the most useful.

Xu *et al.* measured tray efficiency values in six different systems in 1996 [178]. One of the investigated systems was methanol-water. Murphree tray efficiency values

obtained in 150 mm and 300 mm diameter columns are given in Figure 2.45. The objective of their program was to investigate the impact of packings on sieve trays on tray efficiency. Liquid samples were withdrawn from the inlet and outlet of the test tray and analysed by a gas chromatograph. Furthermore, they developed a model, which can predict point efficiencies for packed sieve trays with an average error of 3.9%. The model takes the change of bubble size distribution into account (shown in Figure 2.46) and it combines parts of existing point efficiency models with correlations for liquid mixing for packed sieve trays.

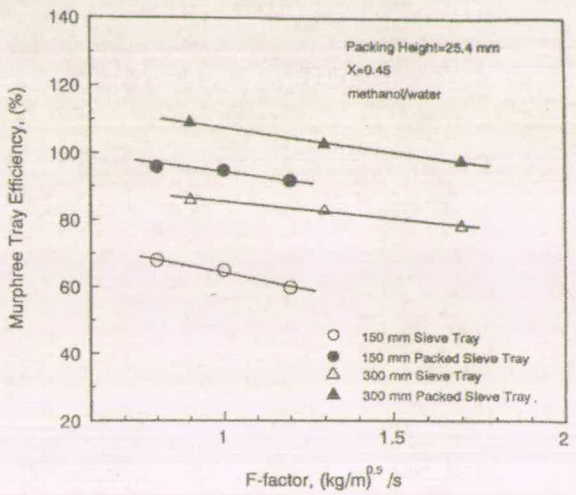

Figure 2.45: Murphree tray efficiencies for methanol-water system. Standard and packed sieve trays. (Source: Xu *et al.* 1996 [178])

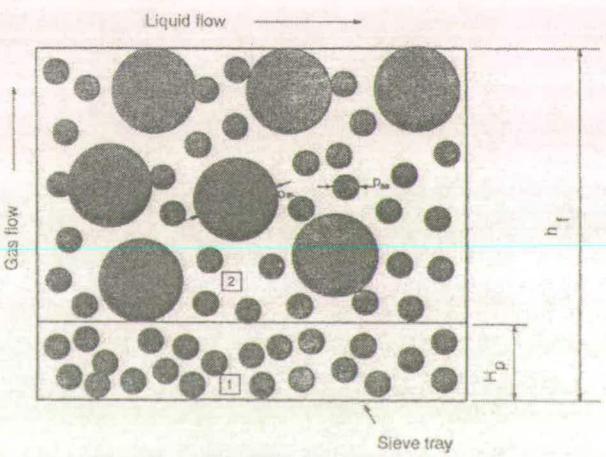

Figure 2.46: Hydraulic model of dispersion above a packed sieve tray. (Source: Xu *et al.* 1996 [178])

Bennet *et al.* developed a new point efficiency model in 1997 [179]. Their correlation is based on the division of the froth into liquid-continuous and vapour-continuous regions. The best results were achieved with their liquid-continuous-only model. Jaćimović (1999) presented a tray efficiency model with a better consideration of entrainment effects [180]. It features a one-parameter model, corrected for entrainment based on the slope and intercept method.

2.2.2 Sieve tray research and design improvements

The next few paragraphs give a brief account of research, committed to the improvement of sieve tray based distillation systems, conducted in the last 15 years. Stevens and Furzer (1989) tried to obtain a better understanding in multi-phase distillation [181]. They monitored the composition profile of an incipient three phase[17] distillation and its impact on tray efficiency. A 610 mm diameter column was used as experimental tray. Bakr and Salem (1993) drastically improved the tray efficiency of a sieve tray by disks of wire mesh pad on the trays [182]. They used a 78 mm diameter column with acetone-methanol as test mixture. The Murphree efficiency without mesh was 38%, a rather low value. This could be improved up to 90% by placing 3 disks of wire mesh pad on the plates. The efficiency boost was accompanied by an increase of the pressure drop of 33%. These results seem rather too good to be true. Nevertheless the adding of mesh can improve the performance of sieve trays. Sidyagin and Chekow (1994) investigated the influence of vapour by-passing[18] on Murphree tray efficiency [183]. They conducted their experiments in a 500 * 800 mm rectangle, using multiple channels for the creation of the bypassing vapour. The Murphree tray efficiency fell with the increase of vapour bypassing. The authors believed that the fall in efficiency could be compensated by higher liquid load in the column caused by using the bypass system.

[17] A hydrocarbon-water mixture was kept in the single liquid phase on a tray by adjusting the ethanol content.
[18] Vapour makes no contact with the liquid when flowing through the sieve tray

Zhang and Yu simulated the liquid two-dimensional phase flow on distillation trays in 1994 using computational fluid dynamics (CFD) [184]. They believed that this approach would lead to more precise results than the flow pattern results from experiments, due to the imperfection of experimental work. Their model regarded the rising vapour as resisting force. They computed velocity profiles across a 1.2 m diameter tray. CFD has become a powerful tool in the hands of engineers. A pioneering CFD work was presented by Krinshna *et al.* at the International Conference on Absorption and Distillation in 2002 [185]. They modelled the hydraulics on a 0.3 and 0.9 m diameter sieve tray describing the system in 3 dimensions. The fully 3D transient simulation revealed the chaotic character of the system with liquid circulation cells in both vertical and horizontal directions. Although their model is restricted to the bubbly flow regime, it provided correct looking trends for superficial clear liquid height and liquid hold-up. The simulation results deny the existence of dead zones. The next threshold would be the expansion of the model to the froth regime.

In 1995, Xu *et al.* picked up again the idea of packing on sieve trays [186]. They measured the influence of the packing on mixing on the plate – expressed by monitoring the eddy diffusivity – and the amount of entrainment created. The experiments were conducted in a 300 mm air-water column. Samples were withdrawn across the central line of the plate, measuring the concentration of an added tracer. They found that the eddy diffusivity could be reduced significantly by adding a shallow bed of mesh packing on the trays and that the diffusivity decreased with greater packing heights. According to the results found by Spagnolo (1984), this enhances the tray efficiency. [187]. Additionally, the packing reduced the amount of entrainment. Xu *et al.* expanded their work in 1996 by measuring the influence of packing on Murphree point and tray efficiencies in six systems [178]. Experiments were conducted in a 153 mm and a 300 mm distillation column. The efficiency values could be increased up to 20% by adding packing with a height of 25.4 mm.

Wijn (1996) focussed on the problems of liquid mixing problem on large trays [188]. The problem can be solved by using multiple downcomers, which eliminate the potentially detrimental effect of stagnant zones. A possible downcomer configuration

is given in Figure 2.47. Wijn developed a model that predicts tray efficiencies in multi-downcomer / multi-cell systems. The simulation results showed efficiency improvements for such systems. The model lacked validation, leading the author to recommend experimental work for efficiency and flow distribution pattern tests in multiple downcomer systems.

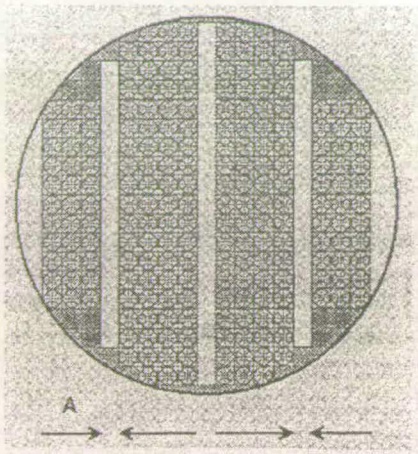

Figure 2.47: 4-pass downcomer layout.
(Source: Wijn 1996 [188])

Billet tested a new design for systems without downcomers in 1997 [189]. Trays without downcomers[19] can be designed with a higher percentage of open area, thus allowing a greater throughput than traditional cross flow trays. On the other hand, the simple dualflow[20] tray can only deliver a decent separation quality in a narrow operation zone. Outside of this zone, the contact time of the phases is too short or tray weeping becomes dominant. A solution can be offered by Dualflex trays firstly reported in 1994 [190]. The design of this tray creates better contact of the phases and reduces weeping by using a movable valve plate in the middle of the construction, illustrated in Figure 2.48. Results from an ammonia-air-water proved the superiority of valve trays in achieving higher tray efficiencies and larger operating ranges.

[19] Also called Dualflow trays.
[20] A sieve tray with larger perforation.

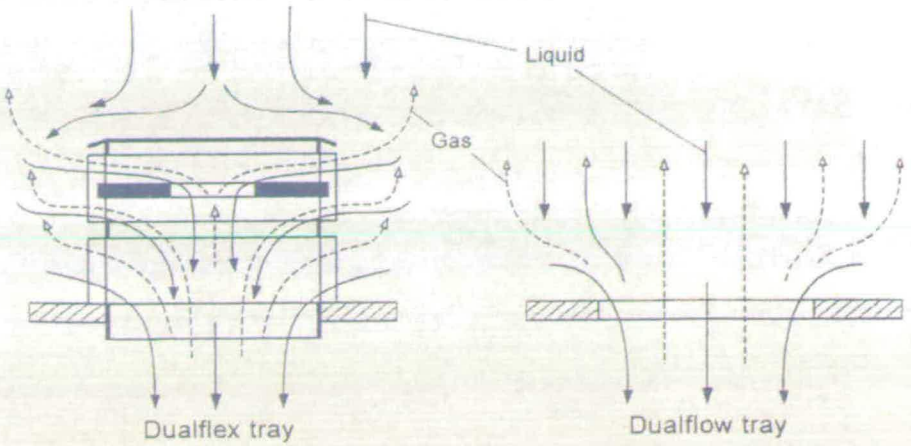

Figure 2.48: Schematic representation of the fluid dynamics of the Dualflex and the Dualflow trays showing flow lines for vapour and liquid. (Source: Billet 1997 [189])

Recently, Noda patented a so called lift tray given in Figure 2.49 [191]. The lift tray falls into the category of trays without downcomer and is able to adapt the fractional free area to vapour flows encountered, thus offering a broader operating range. The lift tray might be useful in diabatic distillation columns.

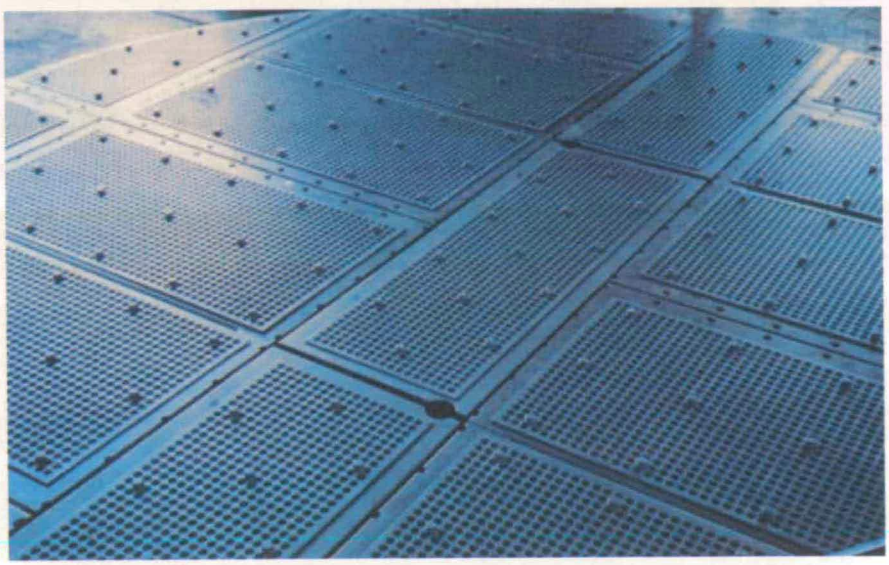

Figure 2.49: Picture of a lift tray.
(Source: Noda 2003 [191])

Lopez and Castells investigated the influence of the hole diameters in sieve trays on tray efficiency in 1999 [192]. The experiments were conducted in a 75 mm diameter test column using 2 binary mixtures. As part of their project, they tested the influence

of tray spacing and the composition change on tray efficiency. Samples of the inlet and outlet vapour, liquid tray and reflux were collected simultaneously in precooled bottles and analysed by gas chromatography. The results obtained were used for scaling up tray efficiency. The authors found that small hole diameters lead to significant reduction in tray efficiency. Tray spacing didn't influence the efficiency directly, but influenced entrainment.

Gouvêa *et al.* simulated the concept of "parastillation" to three binary systems in 2000 [193]. In parastillation, the vapour phase is divided in two or more equal parts at the bottom of the column and the whole amount of the falling liquid is stage-by-stage alternately contacted with the two vapour streams as illustrated in Figure 2.50. Heuke (1987) proposed that the division of the phases could lead to better separation [194].

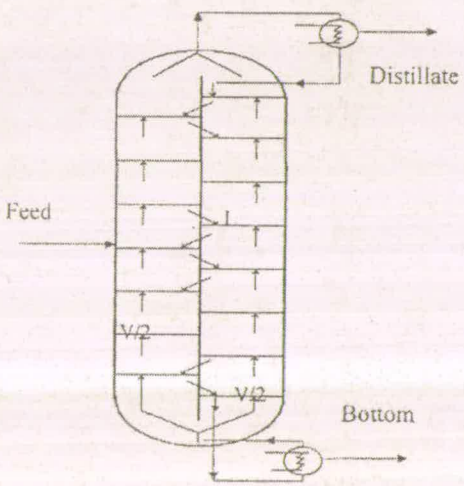

Figure 2.50: Scheme of a parastillation column.
(Source: Gouvêa *et al.* 2000 [193])

One of the systems investigated was methanol-water. For obtaining a product purity of 99% methanol, 50% more stages are required in the case of the parastillation. On the other hand, the parastillation system reduces the column height required by 20% and the tray area required by 44% respectively. A pressure drop decrease of 22% results from the reduction of the aforementioned parameters. By maintaining the same column height, parastillation leads to significant energy savings in reboiler (-20%) and condenser duty (-30%). Due to its geometric configuration, the

parastillation column has a smaller diameter and contains more stages than its conventional equivalent, which allows a smaller reflux ratio to achieve the degree of separation. Gouvêa also investigated the tray efficiency in parastillation. Figure 2.51 shows the comparison of Murphree tray efficiencies between a conventional column and parastillation. Although smaller in the case of parastillation, the efficiency values are still in the same order of magnitude.

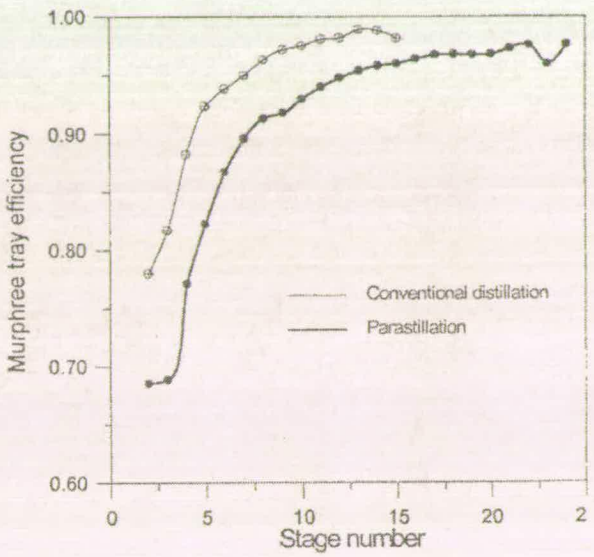

Figure 2.51: Comparison of Murphree tray efficiency values for methanol-water. (Source: Gouvêa *et al.* 2000 [193])

Yang *et al.* (2003) analysed the methanol-water system in a 0.3 m diameter standard distillation column in over a wide concentration range (0.1-99.9% methanol) [195]. They measured the efficiency of valve trays obtaining particularly low efficiencies at both high and low methanol concentrations, as illustrated in Figure 2.52. The effect occurred in bigger columns as well as in Oldershaw columns (Syeda 2003) [196].

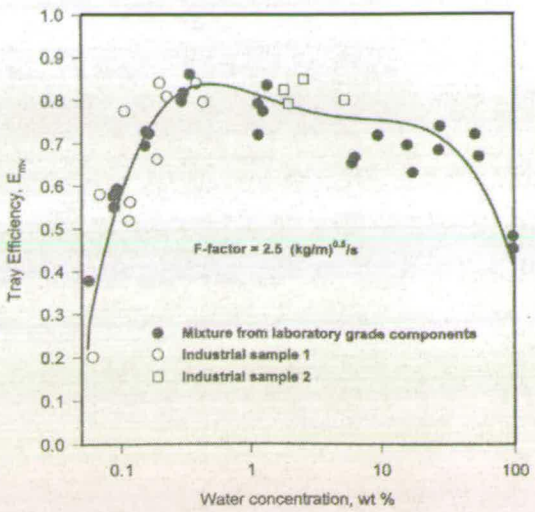

Figure 2.52: Murhpree tray efficiency as a function of water concentration.
(Source: Yang *et al.* 2003 [195])

This phenomenon was linked with surface tension. In methanol-water systems the surface tension increases as the liquid proceeds down the column (see Figure 2.53). The surface tension gradient is quite flat near the bottom and the top of the column. Another situation is encountered near the feed, where the gradient is extreme and invites Marangoni effects. Previous publications (Ellis *et al.* 1961 & Brian *et al.* 1971) hint that the Marangoni effect increases the mass transfer coefficient of gas-liquid interface and possibly increasing the interfacial mass transfer area by inhibiting bubble coalescence [197 & 198]. This effect is missing at low and high methanol concentrations causing low efficiencies.

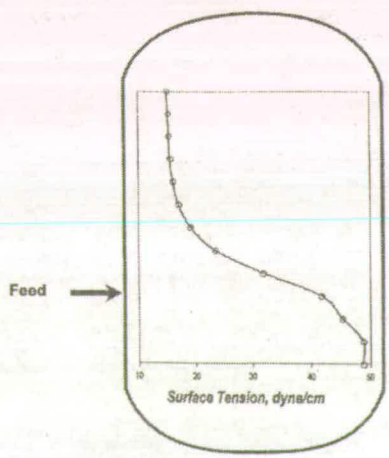

Figure 2.53: Surface tension profile of methanol-water in a industrial column.
(Source: Yang *et al.* 2003 [195])

The low efficiencies raised suspicion of inaccuracies in the VLE model of the methanol-water system. The doubts were dispelled by comparing the VLE model with experimental data illustrated in Figure 2.54. The same VLE print out was obtained by us using ASPEN PLUS and the WILSON VLE model. Another aspect of the paper investigated the influence of impurities – often found in industrial methanol – on separation quality. Impurities like methyl acetate in small concentration, < 0.004%, cause a slight drop of the efficiency at low vapour rates. Another picture is drawn at high vapour loads, where impurities cause premature flooding, and thus entrainment, leading to a significant drop in tray efficiency. The Marangoni effect is also related to this foaming problem. Yang *et al.* countered this problem by using structured packing as de-entrainment device (DED), thereby enhancing the capacity substantially. They also found that DED reduced the pressure drop of the valve trays as a result of entrainment suppression.

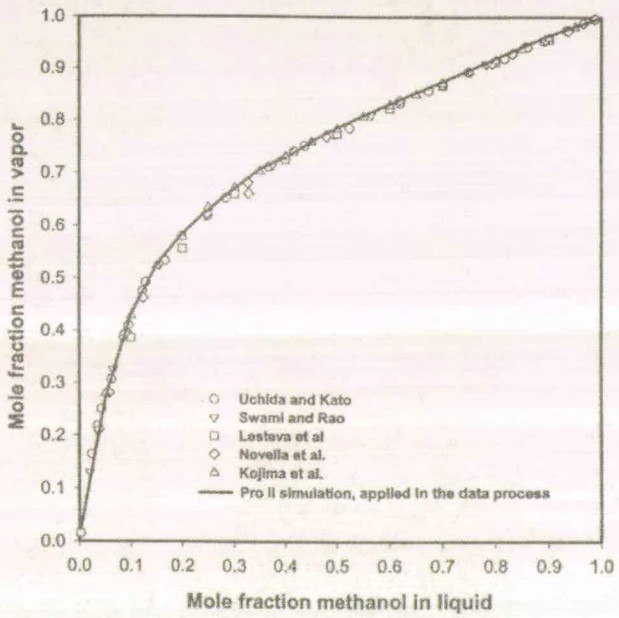

Figure 2.54: VLE experimental data and model prediction.

(Source: Yang *et al.* 2003 [195])

2.2.3 Heat transfer on sieve trays

Heat transfer is not common on sieve trays. Sieve trays usually serve as mass transfer devices in separation processes under adiabatic conditions. Even in the case of heat integration, the trays are seldom targeted. Spagnolo *et al.* (1988) defined a so-called heat transfer efficiency [199].

$$E_{OH} = \frac{\bar{t}_{Vout} - \bar{t}_{Vin}}{\bar{t}_{Lout} - \bar{t}_{Vin}} \tag{2.18}$$

Overall heat transfer coefficients for trays were in a way similar to the transfer unit concept:

$$U = \frac{h_V h_L}{h_V + h_L} \tag{2.19}$$

where h_V and h_L are given by

$$h_V = \rho_V \overline{C}_{p(V)} k_V \sqrt{Le_V} \tag{2.20}$$

$$h_L = \rho_L \overline{C}_{p(L)} k_L \sqrt{Le_L} \tag{2.21}$$

Their model was developed for the Gridler Sulfide process (Galley and Bankroft 1981) [200]. This chemical reaction causes temperature gradients across the column and plates. The predicted temperature profile was in good agreement with experimental data obtained from a 311 mm diameter column. The model has not been applied to distillation systems.

Rivero conducted diabatic distillation runs in a 150 mm diameter distillation column, as an experimental part of his exergy analysis published in 1993 [63]. His heat transfer plate approach consisted of a standard sieve tray with a serpentine heat exchanger at the top of it, delivering heat to or removing heat from the froth. A sketch of the system is given in Figures 2.55 & 2.56. Ethanol-water was used as binary test mixture. Samples were withdrawn from a capillary tube placed near the exit weirs.

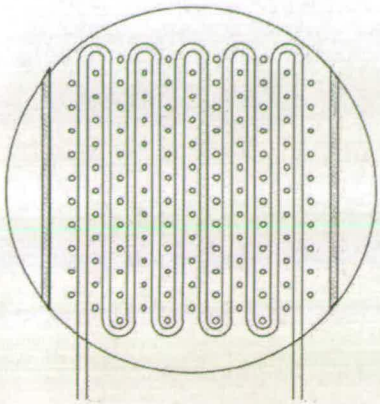

Figure 2.55: Diabatic distillation tray. (Source: Rivero 2002 [64])

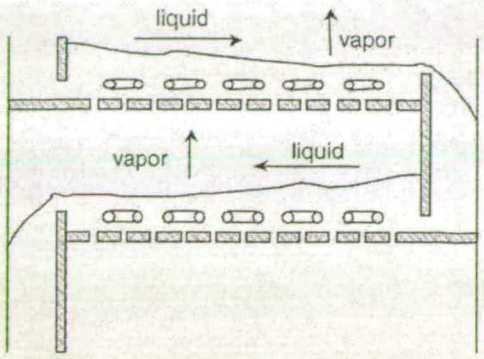

Figure 2.56: Column cross section showing diabatic trays. (Source: Rivero 2002 [64])

The system contained 10 heat transfer trays. Rivero performed various runs. The impact of a cooling run on Murphree tray efficiency, achieving an overall heat transfer coefficient of 3800 W/m^{2}K, is given in Figure 2.57. The efficiency values are particularly low and alter massively along the column. Presumably, lower vapour flow rates inflicted by condensation led to this efficiency reduction. From the experimentalist viewpoint, the project demands attention due to its revolutionary approach.

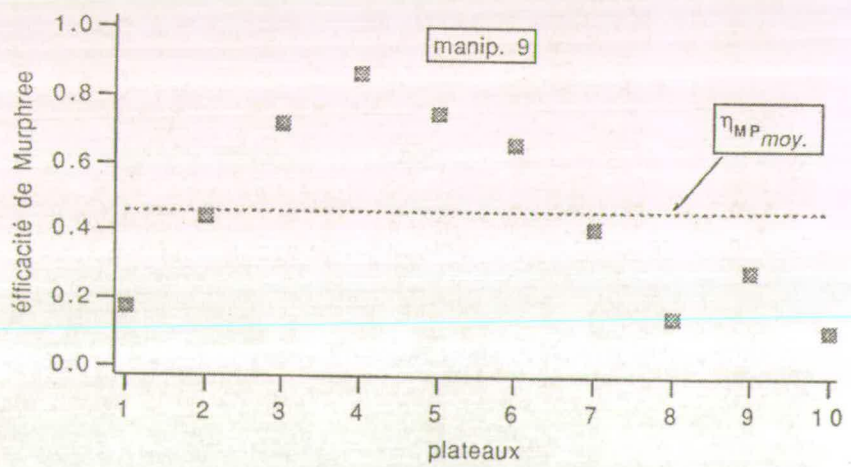

Figure 2.57: Murphree tray effieciencies in ethanol-water; diabatic run. (Source: Rivero 1993: [63])

Björn and Grén (2001) simulated diabatic distillation in the rectifying section by withdrawing vapour sidestreams, which were cooled by water [201]. Their system contained a 200 mm diameter column with 12 plates. Ethanol-propanol served as a binary test mixture. Although not performing direct heat transfer on plates, the impact of the vapour stream manipulation on Murphree tray efficiency is interesting. The Murhpree tray efficiency drops seriously for the trays below the tray to which the partly condensed vapour is returned. On the trays right above the liquid extraction the efficiency is increased. Additionally, they performed an entropy analysis and tried to simulate the diabatic simulation in MATHCAD, using Chan and Fair's model [160].

2.2.4 Summary

The proper measurement and prediction of tray efficiencies is paramount for the economic design of distillation columns. Murhpree tray efficiency has become closest to a standard and is by far the most widely reported efficiency in distillation databases. Various prediction methods, becoming more rigorous with more powerful computers, and efficiency measurement techniques, have been developed in the last decades. Computational Fluid Dynamics (CFD) has gained a reputation for being a powerful tool in fundamental distillation tray research.

Research targeting the improvement of sieve trays has concentrated on either gaining a better understanding of the fluid dynamics on the tray and the regimes (i.e. bubble, froth regime), or on the modification of trays such as using packing on trays. Modifications of downcomers, the use of modified, downcomerless trays and the split of vapour streams (parastillation) also led to improved distillation applications. The proposed use of lift trays could be the key for the handling of changing liquid and vapour flow rates in diabatic distillation columns.

Research in heat transfer is scarce due to the fact that trays do not work as heat exchangers in distillation columns. Attempts have been made to define a heat transfer efficiency in columns with chemical reactions taking place on trays [199]. Rivero established heat transfer to the froth on several trays by using coils sitting slightly above the trays [63]. Such a configuration is common in exoergic absorption.

2.3 Scope of research

The literature review revealed that plenty of work has been put into energy effective distillation. The HIDiC concept was regarded as most promising. An adaptation of this concept to trayed columns promises big benefits. This is based on the information that most of the existing columns are trayed columns and retrofitting is more likely for such columns. The accessible research work is mostly concerned with simulations of diabatic distillation system. Additional experimental data would be extremely useful for validating such approaches.

It was decided to conduct experiments on fundamental research in diabatic distillation. This contains:

- The design of a novel heat transfer sieve tray with integrated heat exchanger and the integration of such a single diabatic plate in an adiabatic lab-scale column with a binary test mixture. The heat exchanger sieve tray has to be regarded as purely experimental device for obtaining data. It is by no means a prototype for a real plate design.
- The measurement of overall heat transfer coefficients and plate-to-fluid heat transfer coefficients.
- The measurement of Murphree tray efficiencies in diabatic columns. This contains the development of reliable sampling and analytic methods.

The influence of parameters like vapour flow rate and reflux ratio (altered by direct heat transfer on a plate) on tray efficiency and heat transfer coefficients will be investigated. The heat transfer from the plate to the highly turbulent froth will be modelled in a simple approach, based on experimental data obtained.

Additionally, existing separation models will be surveyed for their use in diabatic distillation and the most promising candidate will be modified for such a purpose. The model will be set-up, ready for programming. Programming itself has not been undertaken due to its time-consuming nature and this was essentially an experimental investigation.

Chapter 3

Theory

3.1 Tray efficiencies in distillation

3.1.1 Definitions

Modern commercially available simulation packages are capable of calculating the number of theoretical stages required for a particular separation. However, for a real separation it is necessary to determine the number of actual trays. Several definitions for tray efficiency have been proposed over the years, but the more rigorous and acceptable the definition, the more difficult it is to use practically. For example, the overall column efficiency E_O is easy to use but meaningless for multicomponent mixtures, whereas the Standart efficiencies are the soundest fundamentally but have seldom been used in actual design. Additionally, it is very common to interchange wrongly the different efficiency terms. The most common definitions and the conversions between each are given below.

Overall column efficiency, E_O

The overall efficiency is most commonly used for quick and rough calculations. It is defined as the ratio of the number of theoretical stages for a specific separation, at a specific reflux ratio, to the actual number of trays required for the same reflux ratio:

$$E_O = \frac{N_{theoretical}}{N_{actual}} \tag{3.1}$$

This efficiency does not have a fundamental basis.

Murphree tray efficiencies

Murphree (1925) [202] defined tray efficiencies for the liquid and vapour phase by comparing a real tray shown in Figures 3.1 with an ideal trays shown in Figures 3.2 & 3.3[21].

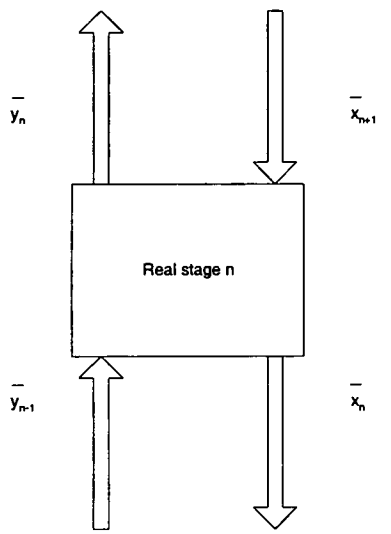

Figure 3.1: Real tray.

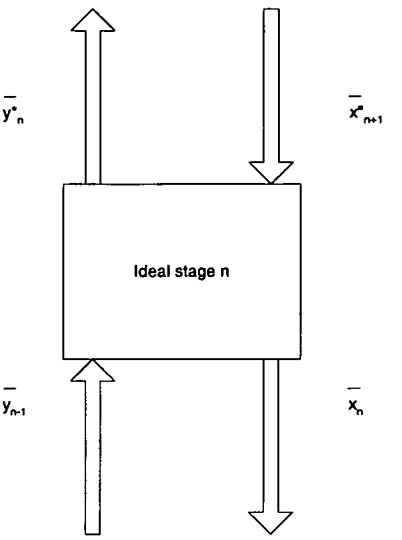

Figure 3.3: Ideal tray for definition of E_{MV}.

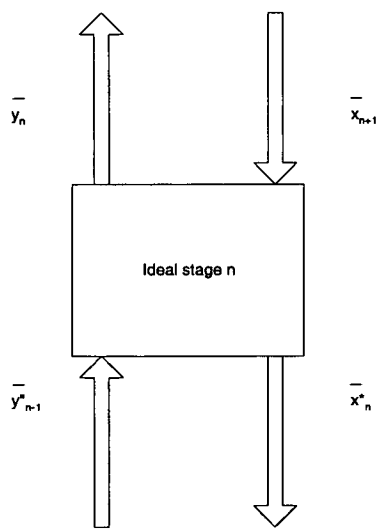

Figure 3.2: Ideal tray for definition of E_{ML}.

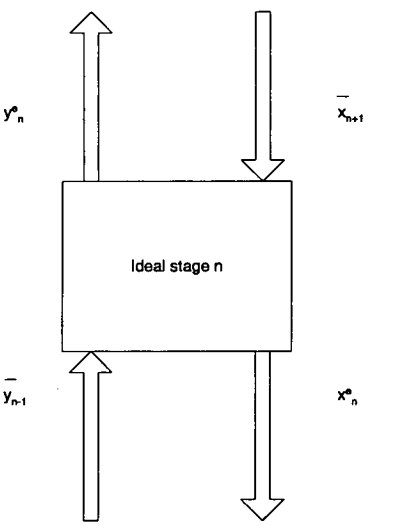

Figure 3.4: Ideal tray for definition of E_H.

[21] In each case one of the entering streams differs in composition between the real tray and the ideal tray denoted by superscript".

The Murphree vapour and liquid phase efficiencies are defined as

$$E_{MV} = \frac{\bar{y}_n - \bar{y}_{n-1}}{y_n^* - \bar{y}_{n-1}} \tag{3.2a}$$

$$E_{ML} = \frac{\bar{x}_n - \bar{x}_{n+1}}{x_n^* - \bar{x}_{n+1}} \tag{3.2b}$$

where x* and y* are the liquid and vapour compositions in equilibrium with the corresponding vapour ($\bar{y}_n$) and liquid ($\bar{x}_n$) streams **leaving** the tray, not the average liquid/vapour concentration.. Thus E_{MV}, E_{ML} values can exceed 1 (100%), depending on the liquid/vapour concentration gradients across/above the tray. Those equilibrium compositions can be obtained by using appropriate vapour-liquid equilibrium models like Wilson. In the case of straight operating line as in the case of adiabatic distillation, and the equilibrium line is also straight within the considered composition range, E_{ML} can be converted into E_{MV} over that composition range.

$$E_{MV} = \frac{E_{ML}}{E_{ML} + \lambda(1 - E_{ML})} \tag{3.3}$$

Where λ is a function of the molar flow rates V & L and the slope of the equilibrium line m.

$$\lambda = \frac{mV}{L} \tag{3.4a}$$

$$m = \frac{\alpha}{[1 + (\alpha - 1)x]} \tag{3.4b}$$

Murphree tray efficiencies are very convenient for tray-to-tray calculations involving a binary mixture. E_{MV} is used when moving up the column and E_{ML} when moving down. Lockett (1986) [36] recommended approaches for dealing with multi-component mixtures considering them as pseudo-binary mixtures.

Murphree point efficiency

The point efficiency is the ratio of the change of vapour/liquid composition at the point, to the change that would occur if equilibrium was reached. The Murphree vapour point efficiency is given below.

$$E_{OV} = \left(\frac{y_n - y_{n-1}}{y_n^* - \bar{y}_{n-1}} \right)_{point} \tag{3.5}$$

Depending on the fluid dynamics on the tray, E_{OV} can be linked with E_{MV}. Lewis (1936) defined three mixing cases, assuming no horizontal liquid mixing (plug flow) in all of them [203]. The three cases considered by Lewis and shown in Figure 3.5 are

Lewis Case 1: Vapour is completely mixed between the trays. The direction of the liquid flow on successive trays is immaterial.

Lewis Case 2: Vapour is unmixed between the trays. Liquid flows in the same direction on successive trays.

Lewis Case 3: Vapour is unmixed between the trays. Liquid flows in alternate directions on successive trays.

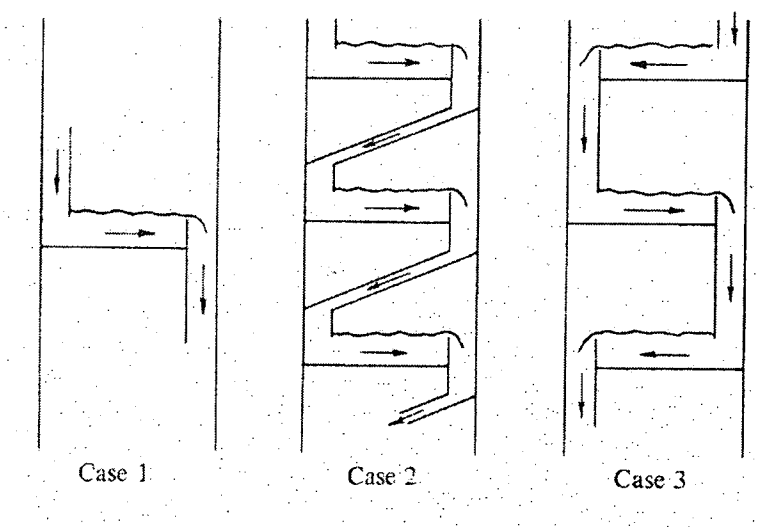

Figure 3.5: Representation of Lewis's three cases.

The majority of the tray efficiency models are based on Lewis Case 1, which states that vapour is completely mixed between the trays. Lewis differentiated between

three relationships in Case 1. The other two Cases are described in Lockett's textbook [36]. Lewis honed his approach to Case 1 by distinguishing between liquid plug flow and complete liquid mixing. For any degree of liquid mixing on the tray he defined

$$\frac{E_{MV}}{E_{OV}} = \frac{\left[1 - e^{(\eta + Pe_L)}\right]}{(\eta + Pe_L)\left\{1 + \left[\frac{(\eta + Pe_L)}{\eta}\right]\right\}} + \frac{\left[e^{n} - 1\right]}{\eta\left\{1 + \left[\frac{\eta}{(\eta + Pe_L)}\right]\right\}} \tag{3.6a}$$

$$\eta = \frac{Pe}{2}\left[\left(1 + \frac{4\lambda E_{OV}}{Pe}\right)^{0.5} - 1\right] \tag{3.6b}$$

The dimensionless Pecelet number is an indicator for the degree of mixing onto the tray and is defined as

$$Pe_L = \frac{L_T^2}{De * t_L} \tag{3.7}$$

The calculation of the eddy diffusion coefficient gained greater attention by being mentioned in the AIChE bubble tray design manual (1958) [158] and has been subject of constant refinement performed by Foss *et al.* (1958) [204], Gilbert (1959) [205], Barker *et al.* (1962) [206], Shore et al. (1969) [207], Yu *et al.* (1990) [208] and Bennet *et al.* (1991) [209.

If the path length is very long (large diameter column) and the eddy diffusional characteristics in the liquid are very slow, Pe_L approaches infinity. Thus, plug flow of liquid is approached and equation 3.6 is transformed to

$$E_{MV} = \frac{e^{\lambda E_{OV}} - 1}{\lambda} \tag{3.8}$$

On the other extreme, if the liquid flow path is very short (small diameter column or multi-downcomer trays) and the diffusional characteristics of the liquid are very high (as for convective transport of liquid in a vacuum distillation column) Pe_L approaches very low values. This leads to complete mixing of the phases such that tray efficiency is essentially the same as point efficiency.

$$E_{MV} = E_{OV} \tag{3.9}$$

Hausen tray efficiency, E_H

One objection to the Murphree efficiency is that the entering streams differ for the real and ideal trays. Hausen's approach (1953) (see Figure 3.6) is based on the variation of the vapour compositions of both exit streams if the entering streams are held constant [210]:

$$E_{HV} = \frac{\bar{y}_n - \bar{y}_{n-1}}{\bar{y}_e - \bar{y}_{n-1}} \tag{3.10}$$

In the case of the Hausen efficiency E_{HV} equals E_{HL}. Thus,

$$E_{HV} = E_{HL} = E_H \tag{3.11}$$

The expression that relates E_H and E_{MV} may be obtained from a geometrical analysis using a x-y diagram (see Figure 3.6). Each of the efficiencies is represented together with the operating and equilibrium lines. The procedure leads to

$$E_H = \frac{E_{MV}(1+\lambda)}{1+\lambda E_{MV}} \tag{3.12}$$

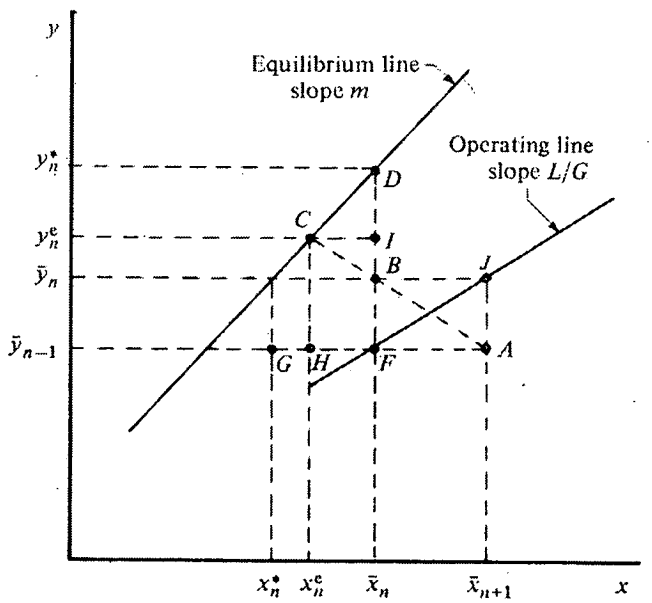

Figure 3.6: Representation of E_H, E_{MV} and E_{ML} for a binary mixture.
(Source: Lockett 1986 [36])

Holland's vaporisation efficiency

Holland (1963) chose another approach for the definition of efficiency [211]. His efficiency is based on fugacities

$$E_{ni}^{V} = \frac{\overline{f}_{ni}^{V}}{\overline{f}_{ni}^{L}} \tag{3.13}$$

were $\overline{f}_{ni}^{V}$ and $\overline{f}_{ni}^{L}$ are the fugacity of component i in the vapour and liquid stream leaving tray n, evaluated at the conditions of this vapour and liquid streams. The vaporisation efficiency is rather difficult to apply in computer calculations.

Standart efficiency

Standart (1965) developed a very general term, which is not subject to constant vapour and liquid molar rates over the tray [212]. The Standard efficiency based on an overall material balance is defined as follows

$$E_S = \frac{V_n - V_{n-1}}{V_n^e - V_{n-1}} \tag{3.14}$$

Likewise, a component efficiency can be defined

$$E_S = \frac{V_n y_n - V_{n-1} y_{n-1}}{V_n^e y_n^e - V_{n-1} y_{n-1}} \tag{3.15}$$

For equimolar flow, equation 3.15 is reduced to the Hausen efficiency given by equation 3.10. The biggest obstacle in using the Standart efficiency is that a flash calculation must be performed on each tray to determine the exit streams from the ideal tray. Murphree efficiencies are much more convenient, although they are not as rigorous.

3.1.2 Models for the prediction of tray efficiency

Rigorous testing of a plant column is generally the most reliable method of obtaining tray efficiency data. However, there may be no access to plant equipment for test work. Over the years many procedures have been proposed for estimating tray efficiencies, using empirical methods. In addition, theoretical prediction methods have been derived based on the two-film theory. For convenience, these two approaches will be termed empirical and fundamental.

3.1.2.1 Empirical methods

One of the earliest attempts to correlate empirically plant overall column efficiencies was made by Drickamer and Bradford (1943) [213]. By measuring the column efficiency of 54 refinery columns containing hydrocarbon systems they found that the values could be related to the average molar viscosity of the liquid feed[22]. O'Connell (1946) modified the Drickamer/Bradford correlation to include nonhydrocarbon and high-relative-volatiliy systems [214]. The O'Connell correlation has been the standard of industry for several decades. He modified the correlating parameter of Dickamer and Bradford to the product of the molar average viscosity and the relative volatility of the key components, with both parameters evaluated at the arithmetic mean of the top and bottom temperatures. Lockett (1986) expressed the O'Connell plot for bubble cap trays in equation form [36]:

$$E_O = 9.06(\mu_L \alpha)^{-0.245} \tag{3.16}$$

where E_O is the overall column efficiency in percent, μ_L is the liquid viscosity in (Pa*s) and α is the relative volatility. This method has been considered as a reasonable option for estimating distillation tray efficiency, particularly for conceptual process designs. Kister (1992) recommended it for this purpose because of its reasonable accuracy (+/- 15%), good reliability and simplicity [23].

MacFarland *et al.* (1972) developed a correlation for predicting Murphree tray efficiency based on binary data systems for bubble-cap and sieve trays [215].

[22] An equilibrium liquid composition was used if the feed contained vapour.

Efficiency is expressed in terms of dimensionless groups, which include liquid and vapour properties,

$$E_{MV} = 7.0\left(\frac{\sigma}{\mu_L w_b}\right)^{0.14}\left(\frac{\mu_L}{\rho_L D_L}\right)^{0.25}\left(\frac{h_w w_h \rho_V}{\mu_L}\right)^{0.08} \quad (3.17a)$$

or

$$E_{MV} = 6.8\left(\frac{\sigma}{\mu_L w_b}\right)^{0.115}\left(\frac{\mu_L}{\rho_L D_L}\right)^{0.215}\left(\frac{h_w w_h \rho_V}{\mu_L}\right)^{0.1} \quad (3.17b)$$

where μ_L is the liquid viscosity, ρ_L and ρ_V equal the densities of the vapour and liquid mixtures, σ equals the surface tension of the liquid, h_w equals the weir height, w_b equals the bubble rise velocity and w_s is the superficial vapour velocity based on the active area A_b.

3.1.2.2 Theoretical or semi-empirical models

Theoretical prediction methods for point efficiency are based on the two-resistance theory and the use of a sequence of steps to convert phase resistances into a tray efficiency. Almost all theoretical models have been evolved from the AIChE modelling of bubble-cap trays developed [158]. In 1952, the Research Committee of the American Institute of Chemical Engineers initiated a fundamental research project to study bubble-cap tray efficiencies in distillation and absorption. The objective was to study the main factors that affect the efficiency under conditions where entrainment is negligible. After a period of five years filled with experimental work and one year correlation development and testing, the following significant factors were evaluated:

- Rate of mass transfer in the vapour phase.
- Rate of mass transfer in the liquid phase.
- Degree of liquid and vapour mixing on the tray.

The variables affecting these factors were found to fall into 3 main categories:

- Operating.
- Tray design.
- System properties.

Unfortunately, each of the main factors governing efficiency responded differently to a given change in operating, design and system variables, and it was not possible to relate tray efficiency to these variables in a single correlation. The AIChE recommended procedure for predicting efficiency follows:

1. Prediction of the number of vapour-phase mass transfer units N_V by

$$N_V = \frac{0.776 + 4.57h_w - 0.238F + 104.8L_F}{(Sc_V)^{0.5}} \tag{3.18}$$

2. Calculation of the liquid holdup on the tray h_L (in inches) by

$$h_L = 0.0419 + 0.189h_W - 0.0135F + 2.45L_F \tag{3.19}$$

3. Calculations of the average liquid contact time t_L on the tray (in seconds) by

$$t_L = \frac{h_L L_T}{L_F} \tag{3.20}$$

4. Prediction of the number of liquid-phase mass transfer units N_L[23] by

$$N_L = 1.97 * 10^4 D_L^{0.5} t_L (0.403F + 0.17) \tag{3.21}$$

5. Calculation of the overall vapour-phase transfer units N_{OV} and conversion to point efficiency using

$$\frac{1}{N_{OV}} = \frac{1}{N_V} + \frac{\lambda}{N_L} \tag{3.22}$$

$$E_{OV} = 1 - e^{-N_{OV}} \tag{3.23}$$

[23] Note that the use of diffusivities in equation 3.18 & 3.21 indicate the use of penetration theory instead of two-resistance theory.

Where F is the superficial F-factor, h_w equals the weir height, Sc_v equals the vapour-phase Schmidt number and L_F is the liquid flow rate of width of flow path on the tray. The method is described in detail elsewhere [158].

Chan and Fair (1984) modified the AIChE model focussing only on sieve trays [159]. They achieved an improvement of the model fit with an average absolute standard deviation of 6.3 % in comparison to 22.9% of the AIChE approach. Based on the efficiency database and Higbie's penetration theory (1935) [216], they derived a correlation for the vapour volumetric mass transfer coefficient $k_V'a$.

$$k'_V = 2\left(\frac{D_V w_s}{\pi * h_f * \varepsilon}\right)^{0.5} \tag{3.24a}$$

$$k_V' a_i = \frac{D_V^{0.5}(1030f - 867f^2)}{h_L^{0.5}} \tag{3.24b}$$

Where f ($=w_s/w_{sfl}$) is the fractional approach to flood defined as the ratio of vapour velocity through the active, or bubbling area w_s to equivalent velocity at flooding w_{sfl}. The volumetric mass transfer coefficient for the liquid $k_L'a_i$ is taken from the relationship of Foss and Gerster (1956) [217] which is restated in the AIChE approach.

$$k_L' a_i = 1.97 * 10^4 D_L^{0.5}(0.403F + 0.17) \tag{3.25}$$

The mass transfer coefficients are linked with the phase transfer units by the following relationship

$$N_V = k_V' a_i t_V \tag{3.26a}$$

$$N_L = k_L' a_i t_L \tag{3.26b}$$

The calculation procedure of t_L and t_V can be found elsewhere [159]. According to Chen and Chuang (1993) the Chan/Fair model overpredicts the efficiency for liquid-phase controlled systems [218]. They developed a new semi-empirical model for determining the number of mass transfer units, hence tray efficiency for distillation interfacial area and mass transfer coefficients were calculated separately; the former based on Levich theory [219] the latter based on the penetration theory.

$$k_V' t_V \propto \left(D_V t_V^{'}\right)^{0.5} \tag{3.27a}$$

$$k_L' t_L \propto \left(\frac{M_V V}{M_L L}\right)\left(D_L t_L^{'}\right)^{0.5} \tag{3.27b}$$

$$a \approx \frac{1}{\mu^{0.1}\left(\frac{A_h}{A_b}\right)^{0.14}}\left(\frac{\rho_L F^2}{\sigma^2}\right)^{\frac{1}{3}} \tag{3.28}$$

Combining the new equations for the vapour- and liquid-phase mass transfer, the number overall vapour-phase mass transfer units becomes

$$N_{OV} = \frac{C_1 \dfrac{1}{\mu^{0.1}\left(\frac{A_H}{A_A}\right)^{0.14}}\left(\frac{\rho_L F^2}{\sigma^2}\right)^{\frac{1}{3}}\left(D_V t_V^{'}\right)^{0.5}}{1+\lambda\dfrac{C_1}{C_2}\left(\dfrac{D_V \rho_V}{D_L \rho_L}\right)\left(\dfrac{M_L L}{M_V V}\right)} \tag{3.29}$$

The constants C_1 and C_2 were determined by fitting the number of overall vapour-phase mass transfer units N_{OV} to the experimental data[24] as a function of the slope of the equilibrium line m. The values for C_1 and C_2 were 11 and 14, respectively. The rigorous model description can be found elsewhere [218].

Prado and Fair (1990) proposed a model for the prediction of tray efficiency based on fundamental considerations of sieve tray hydraulics[25] combined with a diffusional mechanism [166]. Experiments with an air-water system, conducted in a rectangular sieve tray with several tray geometries, supported the development of the model. The dispersion above the tray is divided into three zones. The zone closest to the tray (hole activity zone) corresponds to the activity at the holes (jetting or bubbling). The middle section (bulk froth zone) is composed of gas bubbles dispersed in the liquid, while the top zone (spray zone) is gas continuous, with liquid drops and ligaments

[24] Free of weeping and entrainment conditions.
[25] Namely the froth regime.

dispersed throughout. Tray hole activity is classified as: jetting, bubbling, and small bubbling. The zones are illustrated in Figure 3.7.

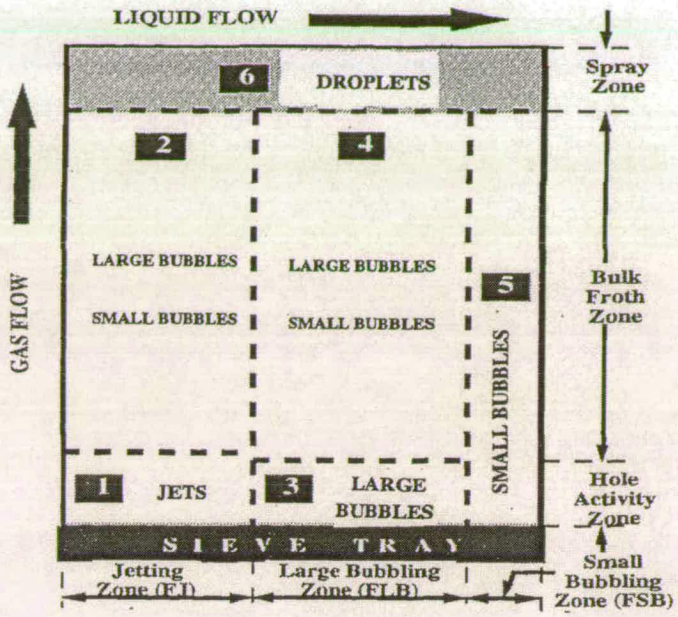

Figure 3.7: Schematic representation of the location of the mass transfer zones. (Source: Prado and Fair 1990 [166])

The final model describes the efficiency E_L for the total liquid resistance for the tray

$$E_L = FJ\left[1 - e^{-N_{LFJ}}\right] + FLB\left[1 - e^{-N_{LFLB}}\right] + FSB\left[1 - e^{-N_{LS}}\right] \tag{3.30}$$

Where FJ, FSB and FLB are the fraction of holes jetting, the fraction of holes producing small and large bubbles, respectively. N_{LFJ} and N_{LFLB} are the number of transfer units for the zones 1 & 2 and 3 & 4, respectively. Mass transfer units in the liquid phase N_V are obtained by using an equation that transforms the previously calculated N_L. A rigorous model description involving the calculations of the transfer units in each zone can be found elsewhere [166]. Their model also relies on parameters, derived from experimental data, which will change from system type to system type.

Garcia and Fair (2000) improved the aforementioned mechanistic model and expanded it for the use in aqueous and hydrocarbon systems [167]. They validated their model by comparison with a tailor-made database. Predicted efficiencies were

within -+ 25% of the measured efficiencies. The final efficiency equations for the liquid and vapour phase are given below.

$$E_L = FJ * \left(1 - e^{-N_{LFJ}}\right) + FLB * \left(1 - e^{-N_{LFLB}}\right) + FSB * \left(1 - e^{-N_{LFSB}}\right) \qquad (3.31a)$$

$$E_V = FJ * \left(1 - e^{-N_{VFJ}}\right) + FLB * \left(1 - e^{-N_{VFLB}}\right) + FSB * \left(1 - e^{-N_{VFSB}}\right) \qquad (3.31b)$$

The model introduces newly modified parameters namely diffusion coefficients, jet height, Sauter mean bubble diameter at formation, rise velocity for small bubbles, bubble size distribution and the fraction of small bubbles in the froth. A detailed treatise of the model description can be found in Garcia's dissertation (2000) [220].

3.2 Distillation modelling of heat integration

After the assessment of stage models containing heat transfer, featured in Chapter 2, we decided to choose Krishnamurthy and Taylor's approach (1985) [161]. Their non-equilibrium model is the most rigorous model available, and it offers the option of modifying heat loads transferred to the stage. Additionally, although not designed for it, the model allows the calculation of tray efficiencies. The following lines explain the model in detail and its possible application in diabatic distillation focussing on binary systems.

The model deviates from MESH (Material balances, equations of phase Equilibrium, Summation equations and Heat balance) equations for each phase (v, l), which allows to predict the separation quality on the stage. Computations of stage efficiencies are entirely avoided. Several factors lead to the model inventor's decision to leave any efficiency computations out

- Stage Efficiency models are means of connection between pure equilibrium models and the reality.
- There are a lot of stage efficiency definitions around and no valid convention available.
- Stage efficiency models can hardly deal with multicomponent mixtures due to interactions in these sorts of liquids.

- Mass transfer coefficients are constant on any stage.

According to Krishnamurthy's thoughts, it is much better to develop a model, which is closer to the reality, which means a pure non-equilibrium model. The following assumptions were made for this model

- The interface is at thermodynamic equilibrium.
- The stage is a mechanical equilibrium $\left(P_j^V = P_j^L = P_j\right)$.
- The system is in steady state.

Figure 3.8 visualises the model of a single stage in a distillation column.

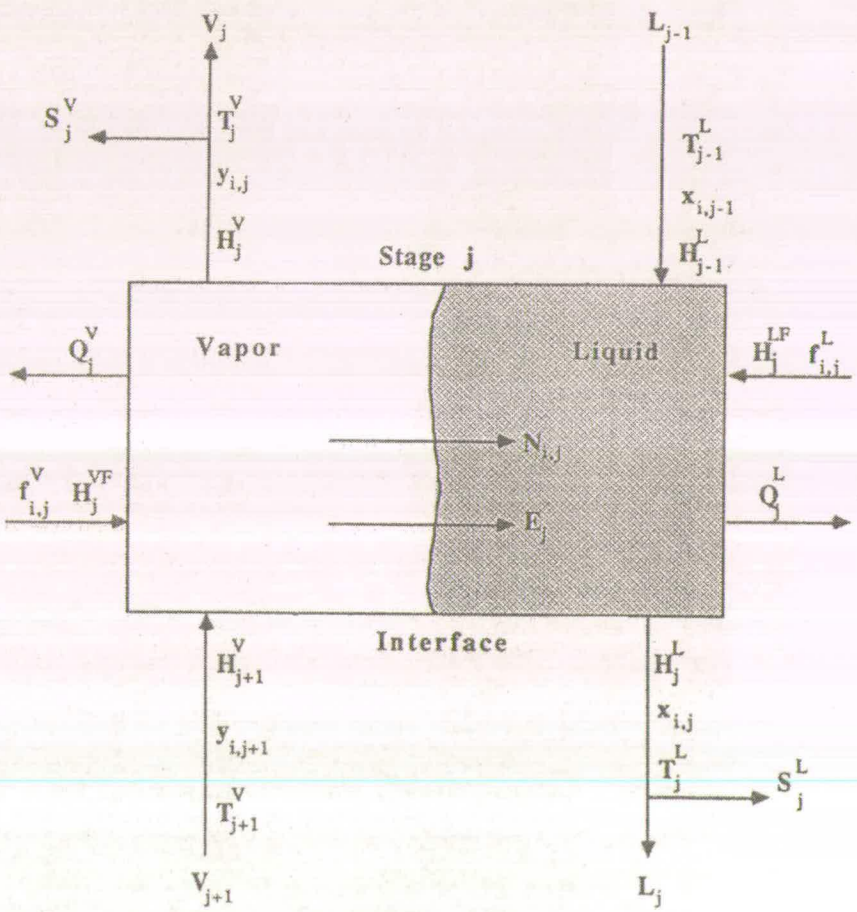

Figure 3.8: Schematic representation of a nonequilibrium stage.
(Source: Krishnamurthy & Taylor 1985 [161])

3.2.1 Model equations

3.2.1.1 Conservation relations

Mass balance

$$M_{ij} = \left(1 + r_j^V\right) v_{ij} + \left(1 + r_j^l\right) l_{ij} - v_{i,j+1} - l_{i'j-1} - f_{ij} = 0 \tag{3.32}$$

$$r_j^v = \frac{S_{Vj}}{V_j} \tag{3.33a}$$

$$r_j^L = \frac{S_{Lj}}{L_j} \tag{3.33b}$$

Energy balance

$$E_j = \left(1 + r_j^V\right) V_j H_j^V - V_{j+1} H_{j+1}^V + \left(1 + r_j^l\right) L_j H_j^L - L_{j-1} H_{j-1}^L + Q_{ij} - F_j H_j^F = 0 \tag{3.34}$$

In the equilibrium stage calculations, the equations above are solved with the requirement that the vapour and liquid streams leaving stage j are in complete thermal, mechanical, and chemical equilibrium. In the development of a non-equilibrium stage model, these equations are not useful as they stand. Instead, the stage balances are split into two parts, one for each phase. For the vapour phase, the component mass balance is

$$M_{ij}^L = \left(1 + r_j^V\right) v_{ij} - v_{i,j+1} - f_{ij}^V + N_{ij}^V = 0 \tag{3.34a}$$

and for the liquid phase

$$M_{ij}^L = \left(1 + r_j^L\right) l_{ij} - l_{i,j+1} - f_{ij}^L + N_{ij}^L = 0 \tag{3.34b}$$

The last terms in the two equations above represent the net loss or gain of species i due to interphase transport. Formally, we may write

$$N_{ij}^V = \int N_{ij}^V da_j \qquad N_{ij}^L = \int N_{ij}^L da_j \tag{3.35}$$

where N_{ij} is the molar flux species i at a particular point in the two-phase dispersion, and da_j represents the small amount of interfacial area through which that flux passes. They adopt the convention that transfers from the vapour phase to the liquid phase are positive. Hence

$$M_{ij}^I \equiv N_{ij}^V - N_{ij}^L = 0 \tag{3.36}$$

The equation above is a statement of the assumption that there is no accumulation of mass at the interface. The same conversion can be made with the energy equations.

Energy balance for the vapour phase

$$E_j^V = (1+r_j^V)V_j H_j^V - V_{j+1}H_{j+1}^V + Q_j^V - F_j^V H_j^{VF} + \varepsilon_j^V = 0 \qquad (3.37b)$$

Energy balance for the liquid phase

$$E_j^L = (1+r_j^L)L_j H_j^L - L_{j-1}H_{j-1}^L + Q_j^L - F_j^V H_j^{LF} + \varepsilon_j^L = 0 \qquad (3.37b)$$

Here ε_j represents the net loss or gain of energy due to interphase transport. This term may be defined by

$$\varepsilon_{ij}^V = \int e_{ij}^V da_j \qquad (3.38a)$$

$$\varepsilon_{ij}^L = \int e_{ij}^L da_j \qquad (3.38b)$$

where e_j is the energy flux at some particular point in the dispersion. An energy balance around the interface yields

$$E_j^I = \varepsilon_j^V - \varepsilon_j^L = 0 \qquad (3.38c)$$

3.2.1.2 Transport relations

Many factors such as chemical potential, temperature, concentration, the physical properties of the fluids, system geometry and hydrodynamics, and the mass transfer rates themselves influence the actual rates that are achieved (Sherwood *et al.* 1975) [221]. Current practice is to lump the effects of most of these variables into mass transfer coefficients and write

$$N_i^V = k_i^V (y_i^V - y_i^I) \qquad N_i^L = k_i^L (x_i^I - x_i^L) \qquad (3.39)$$

Rate equations of this form are consistent with the material balance equations for the interface region only when all the k_i^V have the same value and all the k_i^L are equal (but not necessarily to k_i^V). Under these circumstances the component efficiencies would be equal on any stage j (they may, of course, vary from one stage to another)

Krishna (1979) offered more rigorous treatment of mass transfer in multicomponent systems by using *rate equations* [222]

$$N_i^V = \sum_{k=1}^{c-1} k_{ik}^V (y_k^V - y_k^I) + y_i^V N_t^V \qquad i = 1,2 \ldots c\text{-}1 \qquad (3.40a)$$

$$N_i^L = \sum_{k=1}^{c-1} k_{ik}^L \left(x_k^I - x_k^L\right) + x_i^L N_t^L \qquad \text{i = 1,2 ... c-1} \tag{3.40b}$$

where k_{ik}^V, k_{ik}^L are the multicomponent mass transfer coefficients. These flux equations can be expressed as implicit and nonlinear relations of the general functional form

$$N_i^V = N_i^V\left(k_{ik}^V, y_k^I, y_k^V, N_k^V, k = 1,2....c-1\right) \qquad \text{i = 1,2....c-1} \tag{3.41a}$$

$$N_i^L = N_i^L\left(k_{ik}^L, x_k^I, x_k^L, N_k^L, k = 1,2....c-1\right) \qquad \text{i = 1,2....c-1} \tag{3.41b}$$

It should be recognised that only c-1 of each of the equations above can be written down. The flux of component c is determined from the first c-1 fluxes and from the energy transfer equation as shown below. The local energy flux, e, is made up of a conductive heat flux and a convective contribution due to the transport of enthalpy by interphase transport (Bird *et al.* 1960) [223]

$$e^V = q^V + \sum_{i=1}^{c} N_i^V \overline{H_i^V} \tag{3.42a}$$

$$e^L = q^L + \sum_{i=1}^{c} N_i^L \overline{H_i^L} \tag{3.42b}$$

$$q^V = h^V\left(T^V - T^I\right) \tag{3.43a}$$

$$q^L = h^L\left(T^I - T^L\right) \tag{3.43b}$$

where h^V and h^L are the heat transfer coefficients, which depend, amongst other things, on the mass transfer rates themselves. The local energy fluxes can be expressed in their implicit and nonlinear relations by

$$e^V = e^V\left(h^V, T^V, T^I, N_k^V\right) \tag{3.44a}$$

$$e^L = e^L\left(h^L, T^L, T^I, N_k^L\right) \tag{3.44b}$$

The calculation of the mass and energy transfer rates $N(tot)_{ij}$ and ε_j requires the integration of the point flux relations over some model flow path. This is what is done in the efficiency models, but with a different result in mind. The integration is explained in detail in Krishnamurthy's paper [161]. The results are given below.

$$N(tot)_{ij}^{V} = N_{ij}^{V} a_j \equiv N(tot)_{ij}^{V}(k_{ij}^{V} a_j, y_{kj}^{\ I}, \overline{y}_{kj}^{V}, \overline{T}_j^{V}, T_j^{V}, N(tot)_{kj}^{V} \quad \text{k = 1,2...c)} \tag{3.45a}$$

$$N(tot)_{ij}^{L} = N_{ij}^{L} a_j \equiv N(tot)_{ij}^{L}(k_{ij}^{L} a_j, x_{kj}^{\ I}, \overline{x}_{kj}^{V}, \overline{T}_j^{L}, T_j^{L}, N(tot)_{kj}^{L} \quad \text{k = 1,2...c)} \tag{3.45b}$$

$$\varepsilon_j^{V} = e_j^{V} a_j \equiv \varepsilon_j^{V}(h_j^{V} a_j, \overline{T}_j^{V}, T_j^{I}, \overline{y}_k^{V} N(tot)_{kj}^{V}) \tag{3.46a}$$

$$\varepsilon_j^{L} = e_j^{L} a_j \equiv \varepsilon_j^{L}(h_j^{L} a_j, \overline{T}_j^{L}, T_j^{I}, \overline{x}_k^{L} N(tot)_{kj}^{L}) \tag{3.46b}$$

Several bulk temperatures and compositions appear in the equations above. The best way to deal with these variables is computing an average value for each of those.

3.2.1.3 Interface model

The usual equations of phase equilibrium relate mole fractions on each side of the interface are given by

$$Q_{ij}^{I} = K_{ij} x_{ij}^{I} - y_{ij}^{I} = 0 \tag{3.47}$$

$$S_j^{V} = \sum_{i=1}^{c} y_{ij}^{I} - 1 = 0 \qquad S_j^{L} = \sum_{i=1}^{c} x_{ij}^{I} - 1 = 0 \tag{3.48}$$

where $K_{ij} = \left(x_{ij}^{I}, y_{ij}^{I}, T_j^{I}, P_j\right)$ are the equilibrium ratios defined in the usual way.

3.2.2 Variables and functions for a single non-equilibrium stage

Given the state of all feed streams, the flow rate of all side streams, heat loads, and pressures on the stage, there is total of 6*c*+5 unknown quantities for each stage *j*. To permit the calculation of the unknowns 6*c*+5 appropriate and independent equations must exist. The unknown quantities and equations are listed in Table 3.1.

unknown quantities	equations
component vapour flow rate	vapour component material balance
component liquid flow rate	liquid component material balance
vapour temperature	interface component material balance
liquid temperature	vapour phase energy balance
interface temperature	liquid phase energy balance
vapour composition at the interface	interface energy balance
liquid composition at the interface	interface equilibrium relations
vapour mass transfer rates	summation equations
liquid mass transfer rates	vapour phase mass transfer rate equations
vapour energy transfer rates	liquid phase mass transfer rate equations
liquid energy transfer rates	energy transfer rate equations

Table 3.1: Unknown quantities and equations.

The non-linearity in these equations stem from the presence of the K values and enthalpies, as well as the mass and energy transfer rate terms. A reduction in this rather large number of equations and unknowns can be obtained by eliminating certain equations that are simple linear combinations of variables. Recognising there is really only one set of c strictly independent transfer rates, the $N(tot)_{ij} (= N(tot)_{ij}^{V} = N(tot)_{ij}^{L})$ say, we can eliminate the $N(tot)_{ij}^{V}$ from Eq. 3.45a and $N(tot)_{ij}^{L}$ from Eq. 3.45b using the balance equations

$$R_{ij}^{V} = N(tot)_{ij} - N(tot)_{ij}^{V}(k_{ij}^{V} a_j, y_{kj}^{I}, \bar{y}_{kj}^{V}, \bar{T}_j^{V}, T_j^{V}, N(tot)_{kj}^{V} \text{ k = 1,2...c}) = 0 \quad (3.49a)$$

$$\text{i + 1,2 ..... c-1}$$

$$R_{ij}^{L} = N(tot)_{ij} - N(tot)_{ij}^{L}(k_{ij}^{L} a_j, x_{kj}^{I}, \bar{x}_{kj}^{V}, \bar{T}_j^{L}, T_j^{L}, N(tot)_{kj}^{L} \text{ k = 1,2...c}) = 0 \quad (3.49b)$$

$$\text{i + 1,2 ..... c-1}$$

The energy transfer rate equations are substituted into the energy balance to give

$$E_j^V = \varepsilon_j^V(h_j^V a_j, \bar{T}_j^V, T_j^I, \bar{y}_k^V N(tot)_{kj}^V - \varepsilon_j^L(h_j^L a_j, \bar{T}_j^L, T_j^I, \bar{x}_k^L N(tot)_{kj}^L = 0 \qquad (3.50)$$

Note that only c mass transfer rates N_{ij} appear in the three equations above; the transfer rates N_{ij}^L (or N_{ij}^V), E_j^L, E_j^V are removed from the list from the set of independent functions. Two more variables x_{cj}^I and x_{cj}^I can easily eliminated from the set of variables. They can be obtained directly from the summation equations (S_j^V, S_j^L), which therefore, are dropped from the list of independent equations.

The final set of $5c + 1$ independent variables per stage is ordered in a vector (X_j) and the $5c + 1$ corresponding independent equations in a vector (Z). The vector components are given in Table 3.2. The resulting system was called MERQ equations[26].

Variable vector (X)	Equation vector (Z)
C component vapour flows	C vapour mass balance functions
C component liquid flows	C liquid mass balance functions
C – 1 vapour phase compositions	C – 1 vapour rate relation functions
C – 1 liquid phase compositions	C – 1 liquid rate relation functions
C interphase mass transfer rates	C interphase equilibrium relations
1 vapour phase temperature	1 vapour phase energy balance function
1 liquid phase temperature	1 liquid phase energy balance function
1 interface temperature	1 interface energy balance function

Table 3.2: (X) and (Z) vector components.

This equation system can further be simplified in special cases (i.e. single-phase control, vapour phase-controlled distillation at total reflux). The procedure is explained elsewhere [161].

[26] Material balances, Energy balances, Rate equations and Equilibrium relations

3.2.3 Solving the MERQ equations

Krishna and Taylor tested various solving methods listed below:

- Tearing methods.
- Newton's method.
- Hybrid Method.

Detailed information about these approaches can be found in their paper [161]. Newton's method has proved the most successful algorithm. Newton's method can be expressed

$$[J_k](X_{k+1} - X_k) = - (Z(X_k)) \tag{3.51}$$

where (Z) = (Z(X)) denotes any collection of equations, nonlinear in (X), the collection of variables, with the solution (Z) = 0. $[J_k]$ represents the Jacobian matrix with the elements

$$J_{ij} = \frac{\delta Zi}{\delta Xi} \tag{3.52}$$

3.2.4 Set of variables required and corresponding equations for the modeling of a non-equilibrium stage containing a binary mixture

According to Krishnamurthy's and Taylor's paper 5c + 1 variables will be needed for a general stage model approach [161]. In the case of a binary mixture the set contains 11 variables. The same number of corresponding equations allows us to solve the system with several algorithms (e.g. Newton's Method using the Jacobian matrix). The system is simplified because all the matrixes are of a c-1 dimension type. Therefore the matrixes turn into single lined equations resulting in a set of 11 main equations. The defined variables are listed in Table 3.3 and the equations in Table 3.4.

Component 1 vapour flow v_1
Component 2 vapour flow v_2
Component 1 liquid flow l_1
Component 2 liquid flow l_2
Component 1 vapour interface composition y^I_1
Component 1 liquid interface composition x^I_1
Component 1 interface mass transfer rate N_1
Component 2 interface mass transfer rate N_2
Vapour phase temperature T^v
Liquid phase temperature T^l
Interface temperature T^I

Table 3.3: List of required variables for a binary mixture stage model.

Component 1 vapour mass balance M^v_1	(eqn. 3.34a)
Component 2 vapour mass balance M^v_2	(eqn. 3.34a)
Component 1 liquid mass balance M^l_1	(eqn. 3.34b)
Component 2 liquid mass balance M^l_2	(eqn. 3.34b)
Component 1 vapour rate relation R^v_1	(eqn. 3.49a)
Component 1 liquid rate relation R^l_1	(eqn. 3.49b)
Component 1 interface equilibrium function Q^I_1	(eqn. 3.47)
Component 2 interface equilibrium function Q^I_2	(eqn. 3.47)
Vapour phase energy balance E^v	(eqn. 3.37a)
Liquid phase energy balance E^l	(eqn. 3.37b)
Interface energy balance E^I	(eqn. 3.50)

Table 3.4: List of corresponding equations for a binary mixture stage model.

For a binary mixture eqn. 3.49 can be expressed as

$$R_j^V = N(tot)_j - k_j^V a_j(\bar{y}_j^V - y_j^I) - N(tot)_j^V(\bar{y}_j^V) = 0 \tag{3.53a}$$

$$R_j^L = N(tot)_j - k_j^L a_j(x_j^I - \bar{x}_j^L) - N(tot)_j^L(\bar{x}_j^L) = 0 \tag{3.53b}$$

Likewise, the energy rate equations for each phase and the interphase energy balance can be expressed as

$$\varepsilon^V = h^V a \frac{\in^V}{e^{\in^V - 1}}\left(T^V - T^I) + \sum_{i=1}^{2} N_i \bar{H}_i^V\right) \tag{3.54a}$$

$$\varepsilon^L = h^L a\left(T^I - T^{\bar{L}}\right) + \sum_{i=1}^{2} N_i \bar{H}_i^L \tag{3.54b}$$

$$E_j^I = h_j^V a_j \frac{\varepsilon^V}{e^{\varepsilon_j^V} - 1}\left(\bar{T}_j^V - T_J^I\right) - h_j^L a_j\left(T^I - \bar{T}^I\right) + \sum_{i=1}^{2} \mathrm{N}_{ij}\left(\bar{H}_{ij}^v - \bar{H}_{ij}^L\right) \tag{3.54c}$$

where $\in^V$ and is defined by

$$\in^v = \sum_{i=1}^{2} \frac{\mathrm{N}_i Cp_i^v}{h^v a} \tag{3.55}$$

Various constants and properties have to be calculated by sub-equation systems (i.e. K values at the temperature and composition of the interface; enthalpies of the vapour and liquid stream entering and leaving the stage; partial molar enthalpies of the bulk vapour and liquid phases; heat and mass transfer coefficients). The calculation of the last two entries involves the evaluation of several other physical and transport properties of the bulk vapour and liquid: Diffusion coefficients, viscosity, density, heat capacity and thermal conductivity. All properties of the pure components ought to be calculated separately by appropriate software (ASPEN plus). If no data are available, predictive methods for mixtures collected by Reid are recommended. Finding an appropriate treatment for the mass transfer coefficients seems to be the most difficult task. After a consultation with Prof. Taylor it appears that the calculation of the product of mass transfer coefficient and the interfacial area are more feasible.

3.2.5 Determination of $k^v a$, $k^l a$, $h^v a$ and $h^l a$ respectively

By modifying eqn. 3.18, the vapour mass transfer coefficient-interfacial area product can be obtained

$$k_V a = \frac{(0.776 + 4.567 h_w - 0.2377F + 87.319 L_F)V}{\sqrt{\frac{\mu_m}{\rho_m D_V}}} \tag{3.56}$$

The product of the liquid mass transfer coefficient-interfacial area can be obtained from eqn. 3.25. Alternately, mass transfer coefficients combined with the liquid residence time for both phases can be calculated by eqn. 3.27a & 3.27b respectively. Additionally, the interfacial area can be computed by eqn. 3.28. As a first approach, heat transfer coefficients for the vapour phase can be calculated by using the Chilton-Colburn analogy.

$$h^V = k^V \overline{C}_p^V Le^{2/3} \tag{3.57}$$

It is estimated that the heat transfer coefficient for the liquid phase needs to be 1000 times larger than h^V in order to keep the liquid saturated. It ought to be mentioned that composition profiles predicted by Krishnamurthy and Taylor's model (1985b) were virtually independent of the numerical values of the heat transfer coefficients [162]. Additional models can be found in Lockett's textbook [36].

3.2.6 Derivation and comparison of $k_l a$ and $k_v a$ values

For a future programming approach, it is useful to know which equations to select for obtaining reasonable simulation results. The calculation of mass transfer coefficients (k) and interfacial areas (a) is inevitable in flux-based distillation models. This part presents specific values, converted for our system and gives a comparison and assessment of the values obtained.

As mentioned in the section addressing tray efficiency, point efficiencies are linked with transfer units featured in eqn. 3.22 & 3.23. The sum of reciprocal values gives the number of overall vapour-phase transfer units. Assuming plug flow in the vapour phase N_{OV} is defined as the following

$$N_{OV} = \int dN_{OV} = \int_{y_{n-1}}^{y_n} \frac{dy}{y^* - y} \tag{3.58a}$$

and

$$N_{OV} = \int_0^{h_f} \frac{K_{OV} a}{V'} dh = \frac{K_{OV} a h_f}{V'} \tag{3.58b}$$

The number of vapour-phase transfer units N_V is obtained when there is no liquid phase resistance, so that $K_{OV} = k_V$ and

$$N_V = \frac{k_V a h_f}{V'} = k_V' a' t_V \tag{3.59}$$

The number of liquid-phase transfer units is obtained when there is no vapour phase resistance

$$N_L = \frac{k_L a h_f}{m V'} = \frac{k_L' a' t_V}{m} \frac{\rho_L'}{\rho_V'} \tag{3.60}$$

The equations are solved for the product of $k_L a$ and $k_V a$ respectively. With the assumption of plug flow in the horizontal flow direction and no vertical liquid mixing, an alternative liquid-phase transfer unit can be defined.

$$N_L' = \int dN_L' = \int_{x_{n+1}}^{x_n} \frac{dx}{x_i - x} \tag{3.61a}$$

and

$$N_L' = \int_0^Z \frac{k_L a h_f W dz'}{L} = \frac{k_L a h_f W Z}{L} = k_L' \bar{a} t_L \tag{3.61b}$$

Database

For the derivation of the values desired, some column characteristics and physical properties for an equimolar methanol-water mixture had to be specified. They are given in Table 3.5. The gas-phase diffusion coefficient was calculated with the approach of Chapman and Enskog, which is described in Reid, Prausnitz and Pauling (1987) [224]. Liquid diffusion coefficients were extracted from the Landolt Boernstein compilation (1969) [225]. Physical properties of the pure components

were obtained by empirical correlation given in Yaws (1999) [226]. The calculations of various physical properties for mixtures are based on the suggestions found in Reid *et al.* [224]. The calculations of the tray characteristics are based on approaches found in Lockett [36].

Physical property of an equimolar MeOH-H_20 mixture/ tray characteristics	**Values given in appropriate units**
Weir length W	0.116 m
Liquid flow rate L	2.4E-4 kmol/s
Weir height h_W	0.005 m
Liquid hold-up fraction α (1-ε)	0.38
Vapour hold-up fraction ε	0.62
Liquid density ρ_L	874 kg/m^3
Vapour density ρ_V	0.89 kg/m^3
Liquid residence time t_L	6.48 s
Vapour residence time t_V	3.2E-3 s
Vapour Sherwood number Sc_V	0.34
Liquid Sherwood number Sc_L	520
Superficial vapour velocity w_V	0.52 m/s
Surface tension σ	2.59E-2 kg/s
Bubble rise velocity w_b	0.15 m/s
Vapour viscosity μ_V	1.11E-5 Pas
Liquid viscosity μ_L	6.69E-4 Pas
Vapour flow rate V	2.4E-4 kmol/s
Fractional tree area of the tray	0.04
Hole diameter d_H	0.004 m
Clear liquid height h_{cl}	4.72E-3 m
Column diameter d	0.15 m
Flooding vapour velocity u_s,	2.86 m/s
Fractional approach to flooding FF	0.18
Average relative volatility α	4
Slope of equilibrium line m	0.64
Stripping factor λ	0.64
Liquid diffusion coefficient D_L	1.47E-9 m^2/s
Vapour diffusion coefficient D_V	3.65E-5 m^2/s

Table 3.5: Physical properties of an equimolar methanol-water mixture and tray characteristics.

The models compared are given in Table 3.6. More details of those models can be found in the literature (Lockett 1984) [36].

AIChE (1958) [158]
Harris (1965) [227]
Asano&Fujita (1966) [228]
Jeromin (1969) [229]
Chan and Fair (1984) [160]
Sherwood (1975) [221]
Stichlmair (1978) [230 & 231]

Table 3.6: Models for the derivation of $k_l a$ and $k_V a$ respectively.

We were mainly interested in obtaining $k_L a$ and $k_V a$ values in the appropriate units. Many of the approaches deliver values that have to be converted first, because they differ in their units. The most frequently used conversion equations are given below.

$$k_v a = k_v' \rho_V' a' \varepsilon \tag{3.62}$$

$$k_L a = k_L' \rho_L' \overline{a} \varepsilon \tag{3.63}$$

$$N_L = \frac{N_L'}{\lambda} \tag{3.64}$$

The results obtained from the models are illustrated in Tables 3.7 & 3.8 and in the Figures 3.9 and 3.10 respectively. The unit of the $k_l a/k_v a$ values is kmol/s m^3. For our purposes, these are multiplied by the appropriate froth volume.

	AIChE	Chan & Fair	Harris	Asano & Fujita	Jeromin	Stichlmair
N_L'	1.79	1.79	1.55	33.15	1.68	4.14
N_L	2.80	2.80	2.43	51.81	2.63	6.48
N_V	1.18	0.44	0.59	1.91	1.90	0.32

Table 3.7: Number of transfer units per plate in the liquid and the vapour phase respectively.

	AIChE	Harris	Asano & Fujita	Jeromin	Chan and Fair	Stichlmair	Sherwood
k'_va'	368.90	186.27	601.40	596.01	139	100.75	368.90
k'_La'	0.28	0.24	5.12	0.26	0.28	0.64	1.37
k_va	8.15	4.11	13.28	13.16	3.08	3.59	8.15
k_La	6.00	5.20	111.00	5.61	6.00	22.36	47.86

Table 3.8: Values of k_la and k_va respectively.

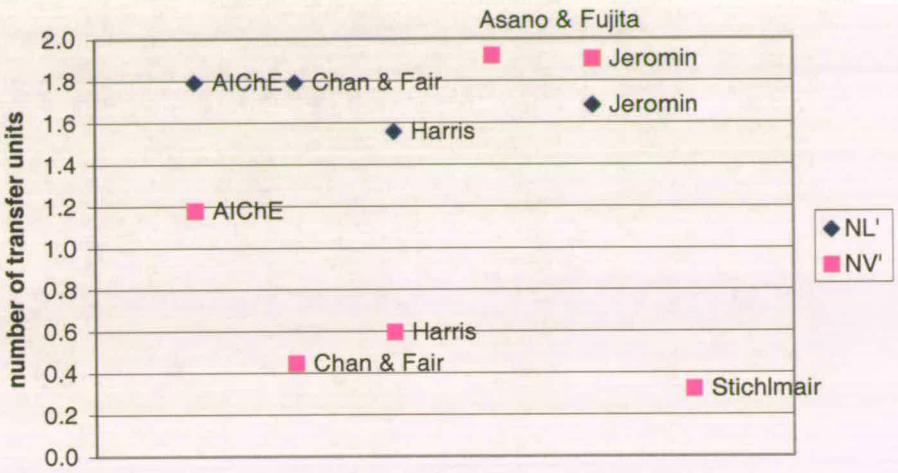

Figure 3.9: N'_L and N_V comparison.[27]

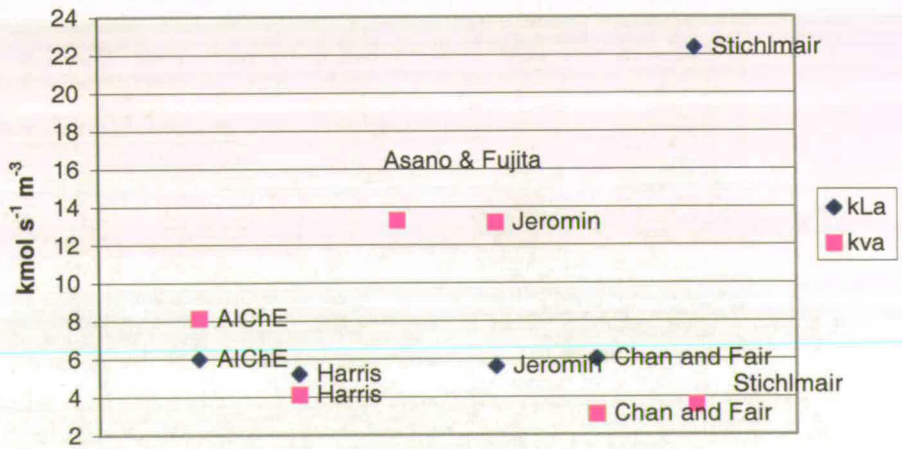

Figure 3.10: k_La and k_va value comparison.

[27] The x-axes in Figures 3.8 & 3.9 do not have units. They are a means for organising the correlations of several authors properly

Result evaluation

The results obtained by various models are the basis for the development of a rate based mass transfer model. An analysis of the values can be made in terms of the statistical significance. Apart from a few outliers (Asano & Fujita and Sherwood's k_La values) the results appear relatively consistent. The k_La values scatter less than the k_va values. The quality of these values is debatable. The nature of all the models used for the calculations is purely empirical. They take physical properties like surface tension or viscosity into account and they also involve tray characteristics like the weir height or the weir length. The only significant difference between the approaches is the fact, that Stichlmair's approach calculates k and a values separately. A similar approach, much simpler than Stichlmair's approach, has been developed by Zuiderweg [171]. Empirical approaches suffer from the fact that their validity is doubtful if they are used for the prediction of systems, on which they are not based. Plenty of discussions have been held in the past about the influence and magnitude of surface tension and viscosity on the number of transfer units. A satisfying solution has not been found yet. The usefulness of these values will be proven in direct comparison of modelling results with experimental data.

The N_L and N_V could be used for the derivation of Murphree point and Murphree tray efficiencies.

3.3 Heat transfer coefficients on sieve trays

For successful simulations and reliable design methods in diabatic distillations, a knowledge of heat transfer coefficients is crucial. As mentioned in Chapter 2, overall heat transfer coefficients were obtained for packed columns. They were calculated by analysing experimental data comprising temperature profiles and heat transfer areas. The general equation is given below.

$$U = \frac{\dot{Q}}{A\Delta T_{LM}} \tag{3.65}$$

The heat transfer occurring in the concentric diabatic column system can be regarded as a combination of film condensation and film evaporation on a vertical wall. The heat transfer is dominated by the two convection-based mechanisms on both sides of

the wall of the rectifying section. The conductive heat transfer contribution is generally neglected for engineering computations that consider overall heat transfer coefficients. Depending on the film flow regime, appropriate equations can be selected for the calculation of convection heat transfer coefficients. For instance, McAdams (1954) derived an equation for the calculation of heat transfer coefficients in condensation, valid for laminar film flow [232]. Additionally, Kirkbride (1934) proposed a correlation for film condensation on a vertical plate after the onset of turbulence [233]. Both correlations were obtained from experimental data. Yue and Weber (1973) proposed a correlation for film boiling [234]. Many other correlations may be obtained from heat transfer textbooks such as Ozisik (1985) [235] or Collier (1994) [236], for instance.

We entered new shores when it came down to heat transfer on sieve trays. First of all, it was difficult to find any relevant literature. This can be explained by the novelty of the project. Sieve trays are not usually used as "heat exchangers". The design of our diabatic sieve tray is described in Chapter 4. Similarities can be drawn to pool boiling or forced convection related experiments respectively; although the degree of turbulence is much higher on a sieve tray before any boiling occurs.

3.3.1 Pool boiling

Depending on the temperature difference between the surface and the liquid, 3 types of boiling can be distinguished. These are:

- Interface evaporation.
- Nucleate boiling.
- Film boiling.

The boiling regimes and their related temperature differences and heat transfer coefficients are given in Figure 3.11[28].

[28] The curve is representative for a pure component liquid.

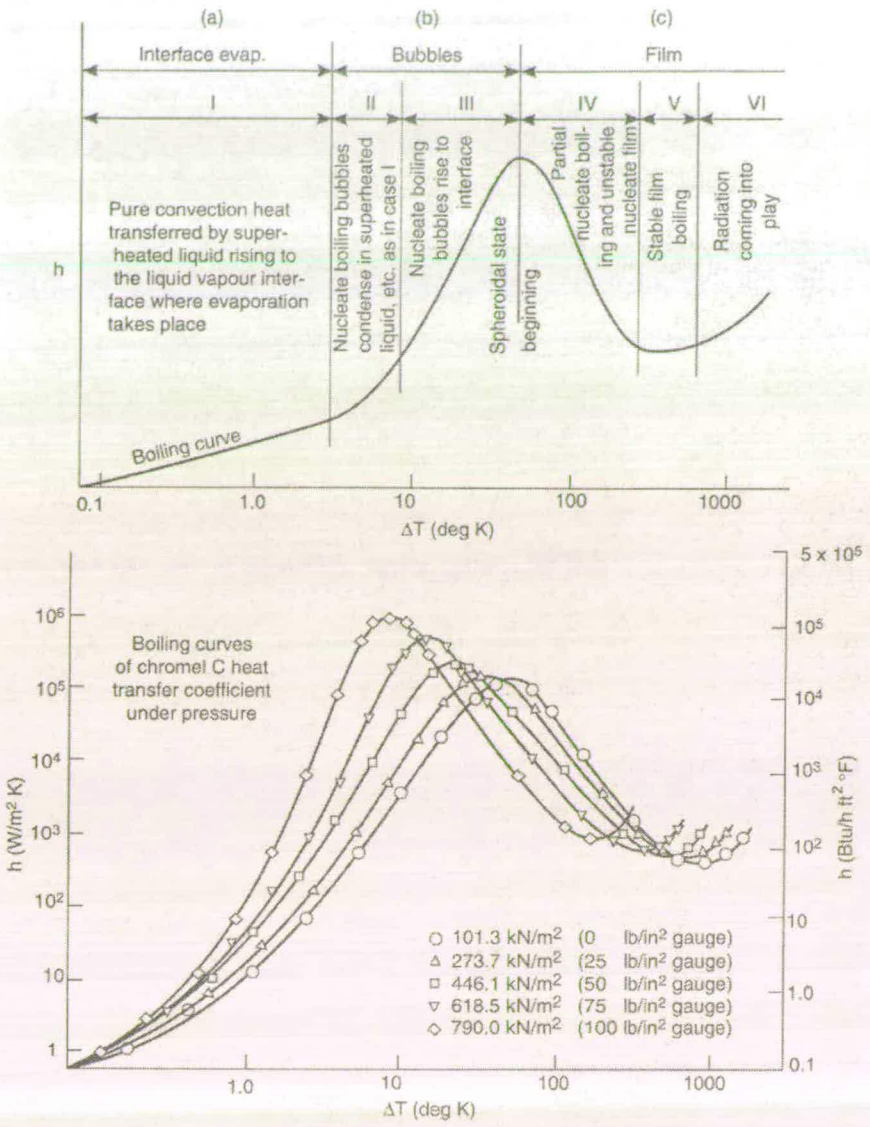

Figure 3.11: Heat transfer results of boiling water.

(Source: Farber and Scorah (1948) [237]

In interface evaporation, the bubbles of vapour formed on the heated surface move to the vapour-liquid interface by natural convection and exert very little agitation in the liquid. At higher values of ΔT, the bubbles form more rapidly and form more centres of nucleation. Under these conditions the bubbles exert an appreciable agitation in the liquid and the heat transfer coefficients rise rapidly. With a sufficiently high value of ΔT, the bubbles are formed so rapidly that they cannot get away from the hot surface, and therefore form a blanket over the surface A maximum heat flux can be found at transition between nucleate and film boiling.

Evaporation in pool boiling has been thoroughly investigated for decades. Major contributions have been made by Jakob (1936) [238], Rohsenow (1951) [239], Forster (1954) [240] and Westerwater (1956) [241]. Out of a plethora of derivations for nucleate boiling, Rohsenow's approach (1952) [242] is an example.

$$\frac{c_{pl}\Delta T}{\lambda \Pr_l^n} = C_{sl}\left[\frac{q}{\mu_l \lambda}\sqrt{\frac{\sigma^*}{g(\rho_l - \rho_v)}}\right]^{\frac{1}{3}} \tag{3.66}$$

In the empirical eqn 3.66 the exponent n and the coefficient C_{sl} are the two parameters to fit the correlation for the liquid-surface combination. C_{sl} varies from 0.0050 – 0.0154 depending on the surface material, surface structure and the covering liquid. The value for n should be taken as 1 for water and 1.7 for all other liquids investigated by Rohsenow.

The pool boiling curves for binary mixtures considerably differ from the curves for pure components. The principal differences are shown diagrammatically in Figure 3.12. Firstly, the onset of boiling is delayed to higher wall superheats, as a result of the temperature gradients set up in the pool to accommodate the corresponding gradients in liquid composition. Heat transfer coefficients are sharply reduced. The critical heat flux may be increased or reduced depending on the extent of the contribution from convection in the pool. The minimum heat flux and the corresponding wall superheat are increased. Finally, heat transfer rates in the film boiling region are somewhat higher.

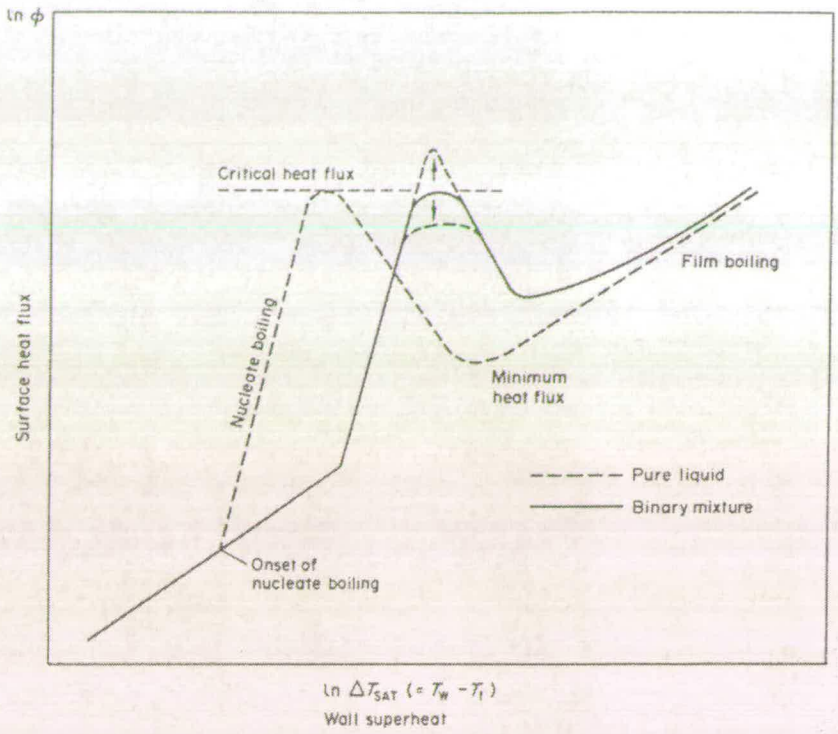

Figure 3.12: Principal changes to pool boiling curve for binary mixtures.
(Source: Collier & Thome 1994 [236])

Some of the most prominent derivations for heat transfer coefficients in binary mixtures are based on the "ideal value" approach (h_{ideal}), in which the heat transfer coefficients of the pure components (h_A & h_B) are combined in relation to the liquid composition.

$$h_{ideal} = h_A(1 - x_B) + h_B x_B \tag{3.67}$$

Those ideal values are then corrected by using appropriate correlations such as Thome and Shakir's derivation (1987) [243].

$$\frac{h_{real}}{h_{ideal}} = \left[1 + \frac{h_{ideal}}{\phi} \Delta\theta_{bp} \left(1 - e^{\frac{-B_0 \phi}{\rho_l \lambda k'_l}} \right) \right]^{-1} \tag{3.68}$$

The method can be used for the prediction of heat transfer coefficients in plain tubes and low finned tubes (Bajorek *et al.* 1991 [244], and is suitable for multi-component

mixtures[29]. The standard deviation is 15%. Recommended values for the scaling factor B_0 and the liquid mass transfer coefficient β_f can be found elsewhere [236].

3.3.2 Forced convective boiling

The heat transfer mechanisms are described in a different way, if a liquid, which is about to boil, flows through channels or ducts. The regions of heat transfer for convective boiling are given in Figure 3.13.

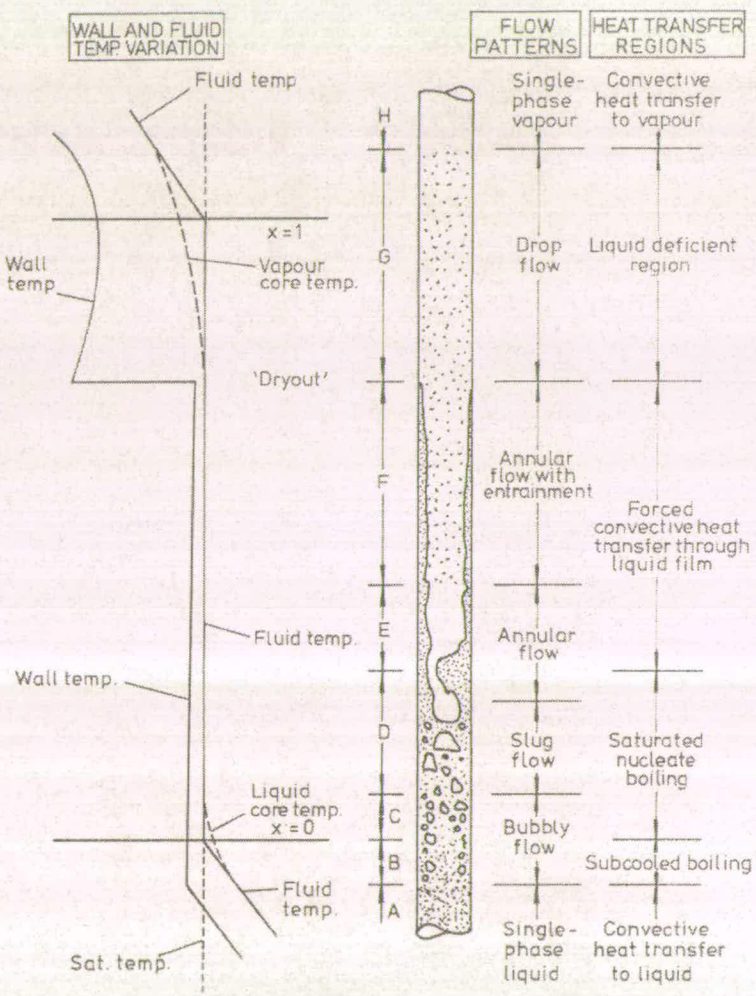

Figure 3.13: Regions of heat transfer in convective boiling.

(Source: Collier & Thome 1994 [236])

[29] 2 –4 components.

The two most important regions are the saturated nucleate boiling region (C & D), in which nucleate boiling occurs at the wall; and the two-phase region (E & F), in which nucleate boiling at the wall is absent and annular flow dominates. Derivations for pure components dominate and binary mixtures are treated in the same way as we dealt with pool boiling mixtures. Though in this case, the quality of the fluid is taken into account.

Research data for forced convective boiling of multi-component mixtures is even more limited than in the case of pool boiling. Most of the work published deals with binary refrigerant mixtures (Signal *et al.* (1983) [245], Ross *et al.* (1987) [246], Hihara et al (1989) [247]). Thome (1989) investigated the links between pool boiling mixture correlations and flow boiling [248]. He proved that eqn 3.68 can accurately model the mixture effect on the nucleate boiling contribution to flow boiling. Heat transfer coefficients for binary mixtures in the two-phase region do not increase much (< factor 2). This is illustrated by eqn 3.69

$$\frac{h_{mc}}{h_{pure}} = \left(\frac{1}{1-\alpha} \right)^{0.8} \tag{3.69}$$

where α is the volume average gas fraction and h_{mc}/h_{pure} are the heat transfer coefficients for the binary mixture and the pure component. A detailed explanation of this phenomenon can be found elsewhere [236].

3.3.3 Calculation of h_i and $h_{p\text{-}f}$

Neither pool boiling nor forced convective boiling derivations can be applied in our case. Nevertheless, the theory of pool boiling and its temperature relations are helpful for the development of general approaches. Our diabatic sieve tray can be considered as a sandwich plate made of Dural with heat transfer medium flowing through a serpentine duct system. A vertical cross-section is given in Figure 3.14.

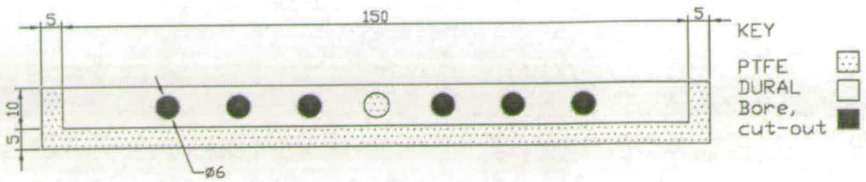

Figure 3.14: Vertical cross-section of the diabatic sieve tray.

In the case of transferring heat to the plate, heat travels from the heat transfer medium to the plate by convective heat transfer mechanism. Afterwards, heat crosses the Dural plate by means of conduction. Eventually, heat is transferred from the plate surface to the froth by convective heat transfer mechanism. An overall heat transfer coefficient (htc) U_p is defined by

$$\frac{1}{U_p} = \frac{A_P}{h_i A_D} + \frac{A_P t}{A_D k} + \frac{1}{h_{p-f}} \tag{3.70}$$

where A_D is the heat-transferring area of the channel in the heat transfer plate and t is the average thickness of metal separating these surfaces. The high thermal conductivity of the material used, Dural, implies that the whole heat transfer surface is isothermal. Although only a minor contributor to the U_p and mostly neglected in engineering applications, the t/k term is taken into account in our calculations.

The overall htc U_p, based on the heat-transferring plate surface area, can be computed by taking the heat flux $\dot{Q}$, the heat transferring area of the plate surface A_p and the logarithmic temperature difference ΔT_{lm} between the heat transfer medium and the froth temperature into account.

$$U_p = \frac{\dot{Q}}{A_p \Delta T_{lm}} \tag{3.71}$$

With the backing of experimental data (U_p values), we can define general correlations for h_{p-f}.

Two cases can be distinguished:

a) in the cooling mode, turbulence induced by the vapour flow through the sieve tray is the predominant factor in heat transfer and $h_{p\text{-}f}$ is assumed to be correlated with the vapour velocity V:

$$h_{p\text{-}f,c} = k_1 V^m \tag{3.72}$$

b) in the heating mode, we anticipate that the plate-to-froth temperature difference gives rise to augmentation of nucleate boiling, such that

$$h_{p\text{-}f,h} = k_2(T_p - T_f)^n \tag{3.73}$$

However, a part of the plate surface may be insulated by vapour, in which case the nucleate boiling regime will apply only to a fraction of the surface, and the remaining surface heat transfer will be affected by vapour velocity, analogously to the cooling mode

$$h_{p\text{-}f,h} = xk_2(T_p\text{-}T_f)^n + (1\text{-}x)k_1 V^m \tag{3.74}$$

where x is the fraction of the free area of the plate on which nucleate boiling takes place; (1-x) is the fraction (close to the holes) over which heat transfer is predominantly metal-to-vapour (convective) and V is the vapour velocity through the holes of the sieve tray. k_1 & k_2 represent constants in those two approaches.

In order to separate the values of $h_{p\text{-}f}$ from the other heat transfer resistances contributing to the overall htc U_p, we need to know the tubeside htcs. In our experiment this is pipe flow in the transition region ($2000 < Re < 10000$) with some entrance effects[30]. For the computation of film heat transfer coefficient h_i various approaches exist. All approaches are based on dimensionless parameters (St, Nu, Re, Pr) of forced convection and the friction factor f. The parameter definitions are given below.

$$St\,\mathrm{Pr}^{\frac{2}{3}} = \frac{f}{8} \tag{3.75}$$

where St is defined as

$$St = \frac{Nu}{\mathrm{Re}\,\mathrm{Pr}} \tag{3.76}$$

---

[30] Additional information of the plate can be obtained in Chapter 4.

By substitution of f into eqn 3.75

$$f = 0.184\,\mathrm{Re}^{-0.2} \qquad \text{valid for } 2*10^4 < \mathrm{Re} < 3*10^5 \tag{3.77}$$

one obtains the Colburn equation for smooth pipes.

$$Nu = 0.023\,\mathrm{Re}^{0.8}\,\mathrm{Pr}^{\frac{1}{3}} \tag{3.78}$$

In the case of smaller Re, f needs to be adapted

$$f = 0.316\,\mathrm{Re}^{-0.25} \qquad \text{valid for } 2*10^3 < \mathrm{Re} < 2*10^4 \tag{3.79}$$

resulting in

$$Nu = 0.0395\,\mathrm{Re}^{0.75}\,\mathrm{Pr}^{\frac{1}{3}} \tag{3.80}$$

Both equations for f are simple but approximate expressions. A more accurate equation for f had been developed by Nikuradse (1932) [249]

$$f = (1.82\log_{10}\mathrm{Re} - 1.64)^{-2} \tag{3.81}$$

leading to

$$Nu = \frac{\left((1.82\log_{10}\mathrm{Re}) - 1.64\right)^{-2}}{8}\,\mathrm{Pr}^{\frac{1}{3}}\,\mathrm{Re} \tag{3.82}$$

For entry regions in which turbulent flow is not fully developed, two equations are recommended [235].

$$Nu = 0.036\,\mathrm{Re}^{0.8}\,\mathrm{Pr}^{\frac{1}{3}}\left(\frac{D}{L_p}\right)^{0.055} \tag{3.83}$$

and

$$Nu = \left(\frac{\left(\frac{f}{8}\right)(\mathrm{Re}-1000)\mathrm{Pr}}{1+12.7\left(\frac{f}{8}\right)^{0.5}\left(\mathrm{Pr}^{\frac{2}{3}}-1\right)}\right)\left[1+\left(\frac{D}{L_p}\right)^{\frac{2}{3}}\right] \tag{3.84}$$

h_i values can be calculated by using

$$h_i = \frac{Nu * k}{D} \tag{3.85}$$

We decided to use the derivation of eqn. 3.83.The temperature dependent physical properties k, C_p and μ of distilled water, which served as heat transfer medium (HEM) inside the ducts were calculated with the following equations

$$\mu = \frac{10^{-10.2158+\frac{1.29*10^3}{T}+1.7710^{-2}*T-1.2610^{-5}*T^2}}{1000} \tag{3.86}$$

$$k = -2.758*10^{-1} + 4.612*10^{-3}*T - 5.5391*10^{-6}*T^2 \tag{3.87}$$

$$C_P = 4.182 + 0.00043(T - 327.15) \tag{3.88}$$

Alternatively to the aforementioned approach, $h_{p\text{-}f}$ can be computed from the heat flux relations. In this case the plate temperature T_p needed may be estimated from the heat flux equations

$$Fc_p(T_{in} - T_{out}) = h_i 6\pi DL(T_{HEM} - T_p')_{lm} \tag{3.89}$$

$$Fc_p(T_{in} - T_{out}) = kA_p \frac{T_p' - T_p}{t} \tag{3.90}$$

$$Fc_p(T_{in} - T_{out}) = h_{p-f} A_p (T_p - T_f) \tag{3.91}$$

where T_p' is temperature of channel surface; T_p of the plate surface. $h_{p\text{-}f}$ can be obtained by substituting eqn 3.89 & 3.90 into eqn 3.91. Additionally, the aforementioned set of equations can be used for the prediction of U_p.

3.4 Conclusion

Although various tray efficiency definitions exist, it had been decided to go for the simplest approach, namely Murphree tray efficiency. This decision is based on the grounds that Murphree tray efficiency needs fewer parameters in comparison to the other definitions with the exception of the Hausen efficiency. Furthermore, it comes close to a standardised approach in terms of data available, far superior to the Hausen definition. For obtaining Murphree tray efficiency-relevant data, one needs to measure vapour compositions below and above a tray and the liquid stream composition leaving a particular tray. Accurate and reproducible sampling will be

crucial in the series of experiments. The design of appropriate sampling devices and the analysis of the samples obtained are addressed in the following Chapter.

Predictive models are mostly of empirical or semi-empirical nature. Most of them are rather inappropriate for modelling diabatic distillation. Nevertheless, they contribute valuable equations for the determinations of parameters like $k_l a$ and $k_v a$ for more appropriate models. The most suitable model available for diabatic distillation seems to be Krishnamurthy and Taylor's nonequilibrium model. Their rigorous model is demanding; but it can be applied to multicomponent mixtures. The model does not involve any sub-matrices for binary systems. The set of equations and sub-equations required are presented in this Chapter. A complete simulation would be time consuming and was regarded as worthy of a separate project.

As shown in Chapter 2, heat transfer coefficients determine the performance of a diabatic distillation column. A model approach for the prediction of such coefficients has been developed in consideration of the importance of the knowledge of heat transfer coefficients in diabatic distillation. The model allows the prediction of overall and plate-to-froth heat transfer coefficients of a diabatic sieve tray. It relies on experimentally obtained plate temperature and heat flux data. The heat transfer from the medium to the plate is subject to well-established theories considering conductive heat transfer in ducts. The model will be validated with experimental data. The design of a diabatic sieve tray, which can deliver/remove sufficient heat to/from the plate is addressed in Chapter 4.

The proposed diabatic sieve tray serves two functions. First of all, it performs heat transfer operations that lead to changes in Murphree tray efficiency, which can be monitored. Secondly, the plate is a system for obtaining temperature profiles and heat fluxes on one hand, and on the other hand, measuring overall- and plate-to-froth heat transfer coefficients. The plate cannot be used for the application in a commercial column due its relative large tray thickness, which lead to unacceptable pressure drop in such a column.

Chapter 4

Analytical Methods, Experimental Rig Design & Experimental Plan

This Chapter describes the development of analytical methods and the design of a suitable experimental rig for our proposed research project. It starts with the adaptation of a method for the quantitative analysis of a binary mixture. The analytical method is verified by calibration of liquid and vapour samples, including accuracy analysis using standard deviation. The second part focuses on the design of the distillation column; and more particularly, on the design of the heat transfer plate. Criteria for the binary mixture selection and design restrictions are stated. This is followed by development and implementation of liquid and vapour sampling systems respectively. The Chapter concludes with the development of a plan of experiments, which includes the assessment of relevant parameters.

4.1 Analytical methods

Scope

To determine the Murphree tray efficiency, it is essential to analyse several liquid and vapour compositions. These data are needed *inter alia* for the calculation of vapour liquid equilibrium data. A literature survey revealed several approaches to the determination of Murphree tray efficiencies in previous research projects. Lockett (1983) [250] used density measurement, Stevens (1989) [181] relied on a Mettler D18 water analyser, Abu Bakr (1993) [182] analysed the samples with an Abbe

refractometer, Xu (1995) [186] applied a VIS spectrometer and Lopez (1999) [192] used gas chromatography (GC). Amongst all those methods, GC is subject to the fewest restrictions. Different from the aforementioned approaches, there is no need to maintain a particular temperature for the measurement. Additionally, GC can analyse samples in the liquid and gaseous states online.

Accurate analysis of the samples is paramount in terms of the impact on Murphree tray efficiencies. Due to the nature of the experiments, several error sources ought to be minimised to achieve reasonable results. Too large deviations in the sample analysis can falsify the efficiency values obtained. An example is given in Figure 2.1. If the sample analysis method is flawed it will cause havoc (in combination with sampling errors) in the efficiency values and the whole procedure is in vain.

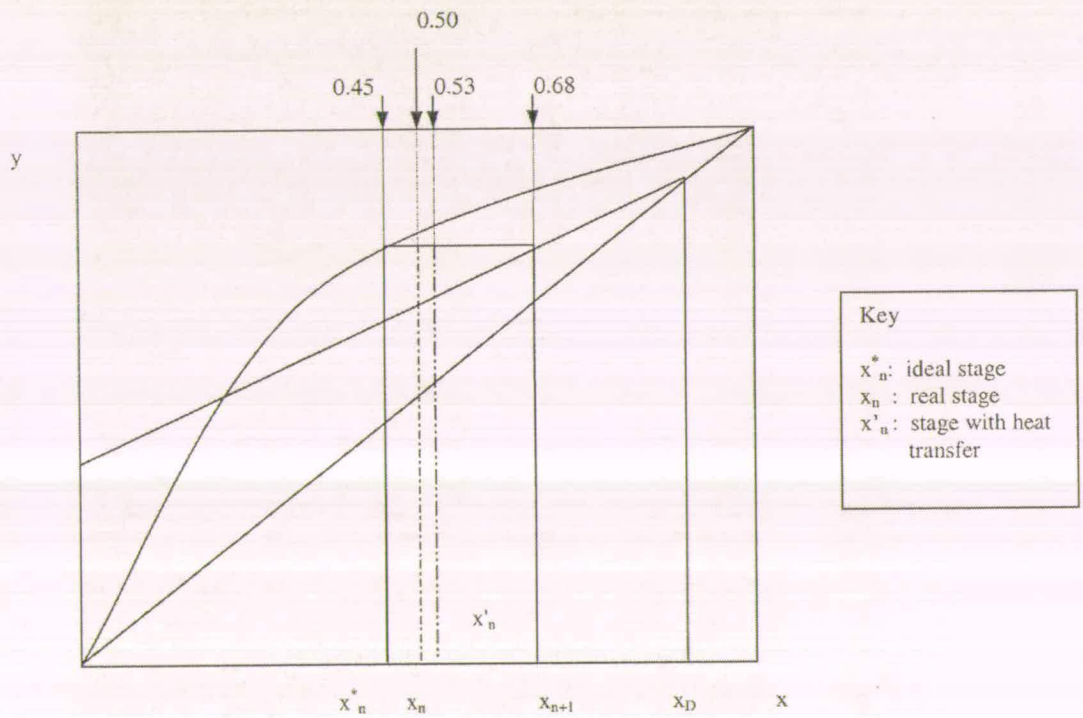

Figure 4.1: McCabe-Thiele diagram showing the influence of the sensitivity of the analysis on E_{ML}.

4.1.1 GC method

A gas chromatography method was applied for the analysis of the chosen binary mixture (MeOH-H_2O)[31]. The instruments used for the analytical method are listed in Table 4.1.

Analysis instruments used
PE GC Series 8700
PE HPLC pump Series 10
PE LC-100 Laboratory computing integrator

Table.4.1: Analysis instruments.

The PE GC Series 8700, displayed in Figure 4.2 is equipped with two Valco valves, which control the injection volume of the continuously flowing liquid and vapour sample streams respectively. A hot wire detector (HWD) enables the detection of H_2O in the samples. Focus was set on a quick and reproducible method with a satisfying accuracy in terms of the standard deviation. A typical chromatogram is given in Figure 4.3. The first peak is H_2O followed by the MeOH peak.

[31] The binary mixture selection will be thoroughly explained in section 4.2.

Figure 4.2: PE GC 8700.

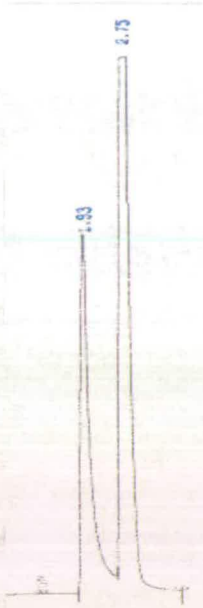

Figure 4.3: Chromatogram of the MeOH -H_20 mixture.

In order to avoid any dependency on internal or external standard caused by changes in the injection volumes, the area ratios of the MeOH-H_2O mixtures have been compared. The relevant method data are given in Table 4.2.

Column	Hayesep R 100/120
Carrier gas / flow rate	Helium / 35 ml/min
Injector temperature[32]	58°C
Oven temperature	150°C
Detector temperature	180°C
Detector type	HWD; medium sensitivity
Integration time	1 min – 4 min
Sample flow rate	3 ml/min
Sample injection volume	0.1µl

Table 4.2: Relevant method data.

[32] The low injector temperature appears rather unusual. It has to be said that experiments with higher injector temperatures led to evaporation in the sample valve and in this case no MeOH peak or no peaks at all could be detected. Samples with a high MeOH content were particularly affected.

4.1.2 Liquid sample calibration

In order to obtain a linear correlation for the samples, several calibration mixtures were produced. The composition of the mixtures is given in Table 4.3. MeOH HPLC grade (99.9 GC area %) and H_2O HPLC grade were used for the creation of the calibration mixtures. Both chemicals are distributed by ALDRICH.

Moles MeOH	Moles H_2O	Mole fraction MeOH	Weight fraction MeOH
4.5	10.5	0.30	0.43
6.0	9.0	0.40	0.54
8.0	8.0	0.50	0.64
9.2	6.0	0.60	0.73
10.5	4.5	0.70	0.81
12.0	3.0	0.80	0.88

Table 4.3: Calibration mixtures for GC.

The reproducibility was tested by calculating the standard deviation from injections of the same composition. Each sample mixture was injected at least 5 times. The bottles were changed in a sequence of raising MeOH concentration. It was evident that at least 5 min of continuous pumping was necessary to flush the piping properly.

4.1.2.1 Results

Overall 44 samples have been analysed. The relevant runs are listed in Tables D1 & D2 in the Appendix. In order to validate the method, and assess its accuracy, the standard deviations of the area and height ratios were calculated. The results for peak areas and peak heights are given in Tables 4.4 & 4.5.

MeOH content	Area ratio	Relative standard deviation in %
30 mol % MeOH	1.174	0.788
40 mol % MeOH	0.725	0.453
50 mol % MeOH	0.474	0.090
60.4 mol % MeOH	0.306	0.261
70 mol % MeOH	0.166	0.542
80 mol % MeOH	0.095	0.678

Table 4.4: Standard deviation of peak area ratios.

MeOH content	Height ratio	Relative standard deviation in %
30 mol % MeOH	1.034	0.984
40 mol % MeOH	0.661	1.561
50 mol % MeOH	0.445	0.465
60.4 mol % MeOH	0.305	1.059
70 mol % MeOH	0.160	2.672
80 mol % MeOH	0.081	1.578

Table 4.5: Standard deviation of peak height ratios.

The next step contained the search for a linear dependency of area and height ratios. The data obtained were plotted against mole ratio, which resulted in a linear relationship. The results are represented in Figures 4.4 & 4.5.

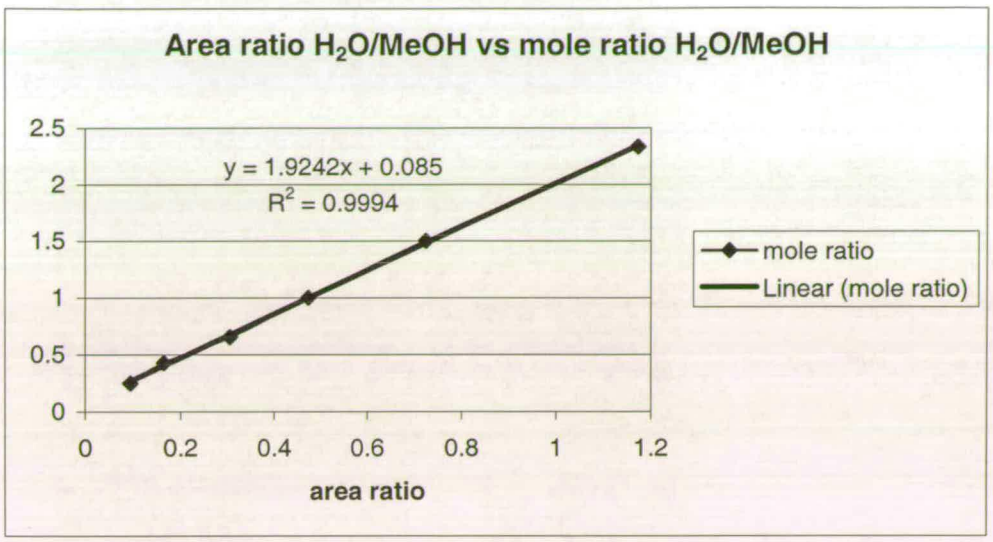

Figure 4.4: Peak area ratio plotted against mole ratio.

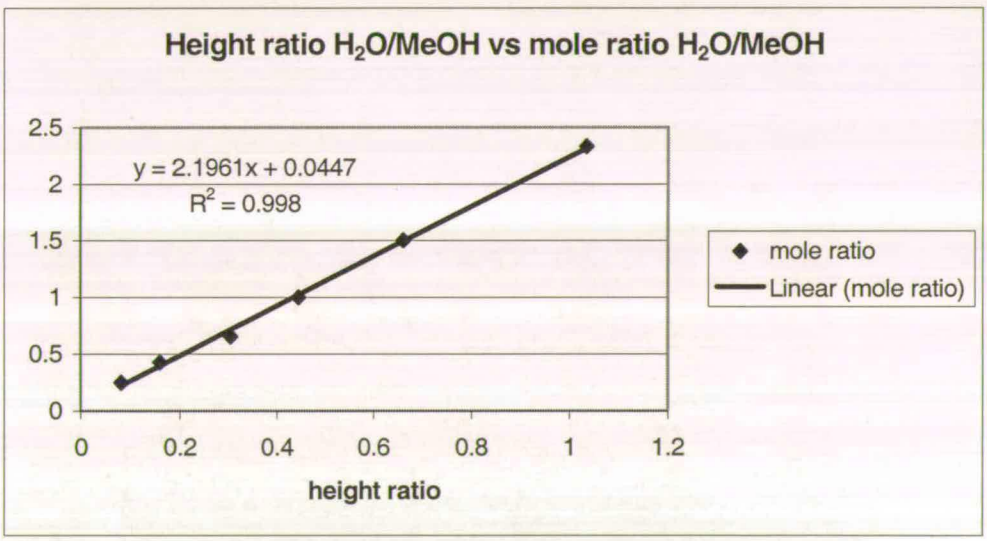

Figure 4.5: Peak height ratio plotted against mole ratio.

Due to the relatively good reproducibility of the total areas we attempted to introduce a normalised method with response factor (RF) determination for H_2O and MeOH respectively. The purpose of RFs is the compensation of the different signal intensity of each component. Taking the RF properly into account, it ought to be possible to

obtain results in terms of sample quantification straight from the integrator. The definition of response factors is given below.

$$\text{Relative response factor of component}_i = \frac{Amt_i * Area_{standard}}{Area_i * Amt_{standard}} \quad (4.1)$$

This approach is only useful if one obtains constant RFs. This proved not to be the case in our sample range. This problem is considered in the discussion.

4.1.3 Vapour sample calibration

4.1.3.1 Equipment used

Figure 4.6 shows the glass apparatus, which was used for the make up of the vapour samples. The mixture make up is based on calculated volumes. Appropriately chosen micro-syringes minimised the experimental error (Hamilton syringes 10 μl & 100μl shown in Figure 4.7) caused by the liquid injection.

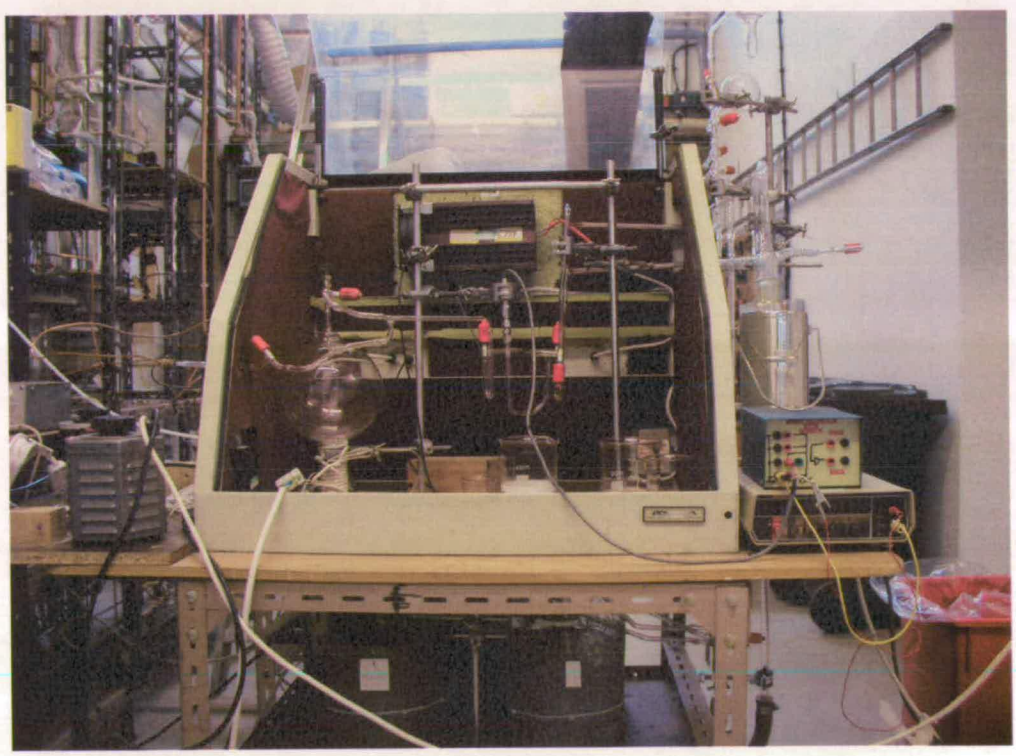

Figure 4.6: Glass apparatus for vapour sample make up.

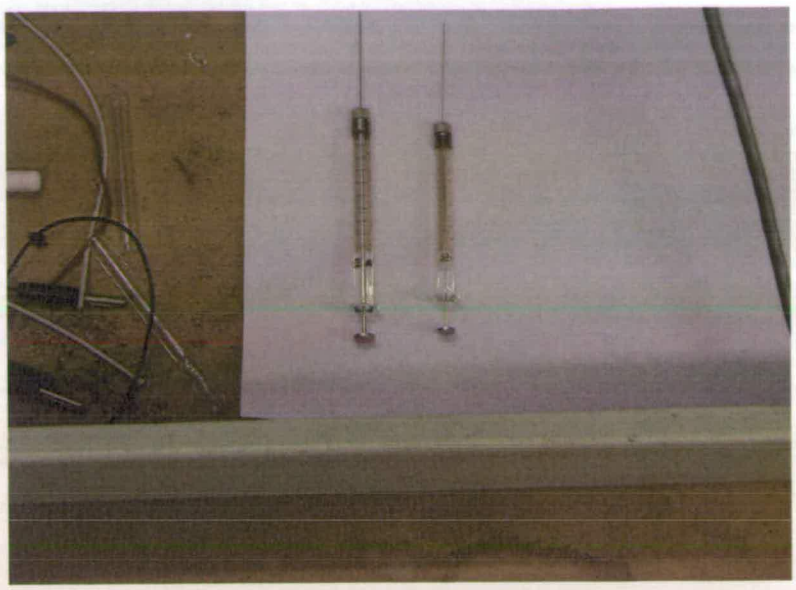

Figure 4.7: Hamilton micro syringes.

The same gas chromatography method mentioned in section 4.1.1 was applied for the calibration of the liquid samples. The instruments used for the analytical method were the same as described in Table 4.1.

4.1.3.2 Calibration make up

Object of the calibration was to demonstrate the application of existing linear relationship (valid for the liquid samples) onto the vapour samples. Furthermore the reproducibility of the results obtained from the vapour samples had to be proven. Problems like condensation occurring in the ducts had to be avoided. Condensation was avoided by calculating the saturation pressure of MeOH and H_2O at 20°C. The next step included the application of a safety factor lowering the dew point concentration to 50 % of the saturated values. The calculations based on Antoine are given below.

$$\log_{10} P = A + \frac{B}{T} + C \log_{10} T + DT + ET^2 \qquad (4.2)$$

Values for the constants are given in Table 4.6 .

	MeOH	H_2O
A	45.6171	29.8605
B	-3.2447E3	-3.1522E3
C	-1.3988E1	-7.3037
D	6.6365E-3	2.4247E-9
E	-1.0507E-13	1.8090E-6

Table 4.6: Antoine constants for MeOH and H_2O. (Source: Yaws 1999 [226])

One obtains 129 mbar vapour pressure for MeOH and 23 mbar for H_2O. By dividing the values by 2 and applying the vapour pressures on a 2 l glass flask one ends up with the same values as above in ml. The calculation of the number of moles was performed by using the ideal gas law. The relevant injection volumes were calculated by using the molar volumes of the chemicals at 20°C stated in Table 4.7.

	Molar liquid volume in cm^3/mol, 20°C
MeOH	40.70
H2O	18.07

Table 4.7: Molar liquid volumes at 20°C. (Source: Perry 1984 [251])

Table 4.8 shows the calibration mixtures used for the sample quantification. The same principles as in section 4.1.2 have been applied.

mMoles MeOH	mMoles H_2O	Mole fraction MeOH	Mole ratio H_2O/MeOH
1.220	1.107	0.526	0.901
2.457	1.107	0.689	0.450
3.685	1.107	0.768	0.300
4.913	1.107	0.816	0.225

Table 4.8: Calibration mixtures for GC.

The mixing took place in the glass flask (Figure 4.8). The vapour sample make up was performed in 5 steps:

1. Evacuation of the glass apparatus for about 5 min; control of the vacuum by a transducer (Figure 4.9).
2. Flushing of the apparatus with Helium until ambient pressure was established.
3. Injection of MeOH and H_2O through a septum into the 2 l flask.
4. Establishment of a slight Helium overpressure (about 100 mbar).
5. Mixing of the components by thermal convection (heating tape wrapped around a heating finger at the bottom of the glass flask. This takes about 20-30 min for achieving equilibrium.

Figure 4.8: Glass flask with heating tape.

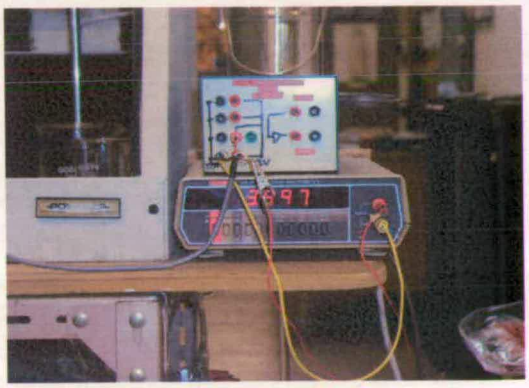

Figure 4.9: Transducer for vacuum control.

The pressure equivalent of the transducer are given in Table 4.9.

Transducer reading	Pressure in mbar
0.900	20
3.895	1013
4.242	1128

Table 4.9: Transducer readings.

By means of overpressure, the samples were flushed into the GC line. One sample make up was sufficient for 1 injection. Due to the long time for a simple run injections of the same compositions were reduced to 2-3 injections. The reproducibility was tested by calculating the standard deviation from injections of the same composition. Each sample mixture was injected at least twice.

4.1.3.3 Results

Overall 25 samples have been analysed. The relevant runs are listed in Appendix D. An accuracy assessment was performed by calculating the standard deviation of the area ratios. The results are given in Table 4.10.

MeOH content	Area ratio	relative standard deviation in %
52.6 mol % MeOH	0.432	0.211
68.9 mol % MeOH	0.217	0.082
76.8 mol % MeOH	0.140	0.025
81.6 mol % MeOH	0.109	0.010

Table 4.10: Standard deviation of peak area ratios.

The plot of the data obtained against mole ratio created the same linear relationship as in the liquid sample correlation. The results are represented in Figures 4.10 & 4.11[33].

[33] Figure 4.11 shows the difference in results by using different integral methods. Nevertheless, the linearity is not influenced.

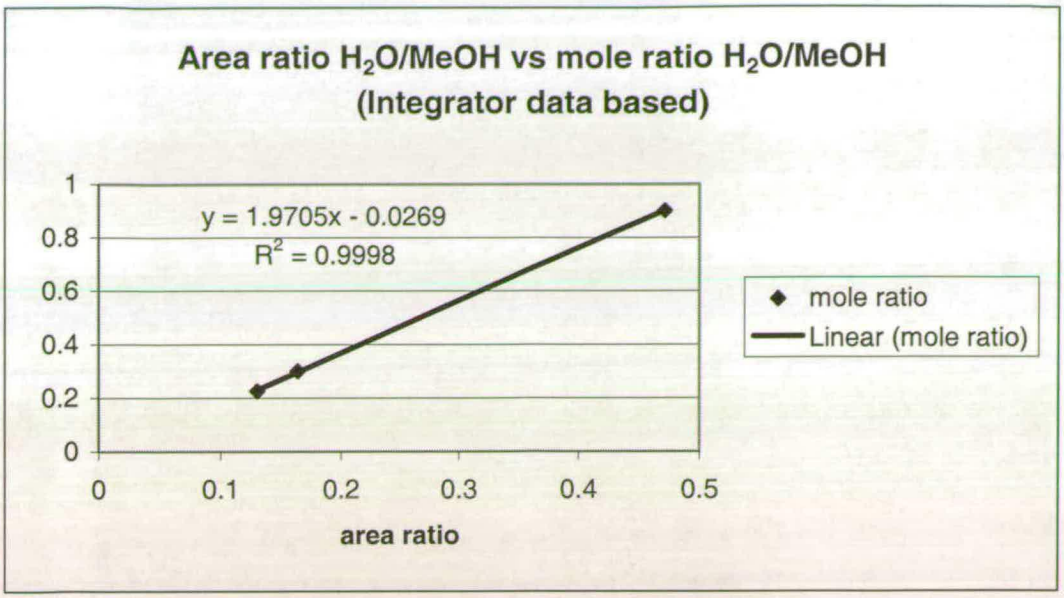

Figure 4.10: Peak area ratio plotted against mole ratio; based on integrator data.

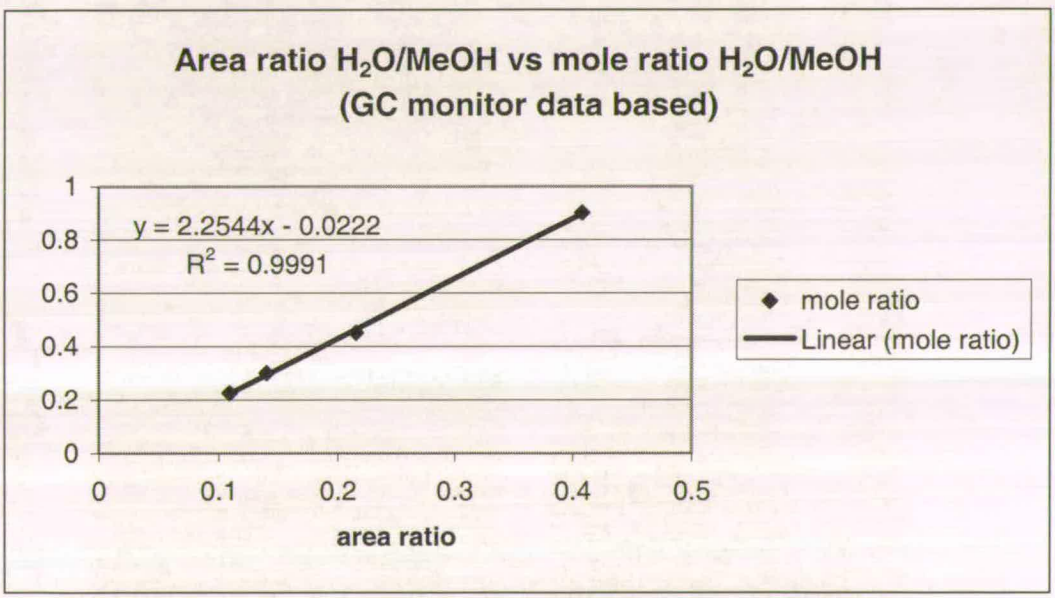

Figure 4.11: Peak area ratio plotted against mole ratio; based on screen data.

4.1.4 Discussion

It has been shown that an analysis of our binary mixture via GC is feasible. The biggest problem was caused by the water peak. Its tailing shape made the integration of the peak less reproducible than the MeOH peak that followed it. This was expected. In order to obtain a proper separation of the two peaks, isothermal

programs were tested at temperatures ranging from 110-160 °C. The lower temperature limit caused a broadening of the water peak; therefore peak recognition problems appeared. The higher temperature limit caused an overlay of the two peaks. Temperature ramps could not solve the water peak tailing either. The best and most suitable chromatograms were obtained with an isothermal program maintaining the temperature at 150°C. This temperature programme led to a satisfactory resolution and it also delivered an appropriate run time of 4 min that doesn't restrict online sampling much. The minimum flushing time of the tubing system is approximately 5 min.

The standard deviation test demonstrated the superiority of the area ratio over the height ratio method. Both ratios are similar in their values but the average relative standard deviation for the height ratio ($\approx$ 1.4%) is approximately 3 times higher than the deviation for the area ratio ($\approx$ 0.5%). The main problem in both cases was caused by the reproducibility of the water peak. Assuming an almost identical injection volume for the same samples, it could be illustrated that the water areas and heights scatter more than the values for MeOH. The deviation slightly increased with the reduction of the water content. The analysis of the liquid samples withdrawn from the column features the injection of two consecutive samples from the same sample point.

Several plots were produced for finding a linear relation related to the area ratio obtained. Plotting area ratios against mole ratios lead to success. The result from the statistical residue analysis was more than sufficient ($R^2 > 99.9\%$).

In the beginning of the trial runs the injector temperature caused some problems. A rule of thumb in GC mentions the need of a higher injector temperature in comparison with the oven temperature. This secures a complete evaporation of the sample; hence a proper separation on the column can be achieved. Following this rule, evaporation resulted in the valve chamber; particularly in samples with a high MeOH content. The consequence was the injection of an insufficient sample amount; therefore no MeOH peak (or in the worst case no peak at all) appeared. Lowering the injection temperature below the boiling point of MeOH solved this problem. (This measure also counteracts the evaporation effect from the column, which obviously

has a higher operating temperature than the boiling point of water). Due to the small valve chamber size (0.1 ml injection volume) a complete evaporation occurs right at the entrance of the column. The results obtained by this rather unconventional approach showed no contradictions. An alternative would have been the increase of the sample flow rate, serving as a coolant for the injector block. This is not particularly desirable due to an increase of the liquid amount withdrawn from the plate (disturbance of the plate hydraulics in the worst case).

Alternative methods to the area ratio approach would be the normalisation of the method or the use of internal or external standards. None of the aforementioned methods are suitable for our purposes. Due to the online character of the method, no sample preparation is needed; therefore no standard can be added to the samples unless it already exists in the mixture. This is not recommendable due to the creation of a ternary mixture. Furthermore, a specific concentration could not be maintained on the heat exchanger tray by altering the operating conditions. The normalisation approach also failed in our case because the response factors changed over the concentration range considered. RFs could be quite useful if the samples were diluted.

It has been shown that the analysis of the vapour samples follows the same linear function as for the liquid samples. The slight deviation of the linear functions is probably result of experimental errors, and can be neglected. Due to its larger concentration range, the function of the liquid samples will be used for the analysis of the vapour and liquid samples. In comparison to the liquid sample calibration, the vapour sample calibration was more labour- and time-intensive. The preparation for a single vapour sample calibration run took about 45-60 min. Most of this time was needed for the proper mixing of the MeOH and the water in the glass flask. The successful reproducibility of the same samples proved the proper mixing in the glass flask.

Potential problems like condensation inside the copper ducts could be avoided by using 50% saturated vapour samples at room temperature (20°C). In the experiments, the dilution of the saturated vapour with N_2 (factor 4-5) in the column experiments created an environment equalling saturated vapour at 40°C. Heated copper lines

(heating tape) maintained a temperature above the dew point (50°C). Test runs with the vapour sampler proved the vulnerability of the gas valve to flooding. Any condensate ought to be removed by flushing the sample system with N_2 before any samples are taken from the column.

4.1.5 Conclusion

An analytical online method for the binary MeOH-H_2O system was established satisfactorily. The method is GC based and independent of the injection volume, due to the comparison of the areas of the two peaks. Relative standard deviations and linearity tests have also been performed. Linearity exists between the area ratio and the mole ratio. The results obtained scatter 0.5% (absolute value) in average. In order to generate reliable results; it is necessary to flush the piping system for a minimum time period.

Individually made up vapour samples of various concentrations were analysed by the GC method, that had been developed for the liquid sample calibration. The same linear function as for the liquid samples could be found for the vapour samples. Relative standard deviations were slightly better than in the case of the liquid samples. The linear function obtained from the liquid samples was used for the analysis of the experimental data.

4.2 Apparatus design

4.2.1 General design

The focus for the experimental work has been set on a sieve plate, which is capable of adding to or removing heat from the plate surface. The column design is subject to limitations in terms of the reboiler performance. The best available reboiler was an electrical one with a performance of 9 kW that could be expanded to 16 kW. A steam-driven reboiler was considered as a possible alternative. The design procedure is to a certain degree dependent on the properties of the binary mixture used. Hence a decision in terms of an appropriate binary mixture had to be made first. After a first selection the following list was obtained:

- Acetone-water.
- Benzene-toluene.
- Ethanol-water.
- Methanol-water.

Although ethanol-water mixtures are popular in chemical engineering applications, it is not possible to use them in the UK due to strict legislation in terms of alcohol handling. The next test contained a heat of mixing examination of the remaining mixtures. The data were obtained from the Christiansen's heat of mixing handbook (1982) [252]. The result is given in Figure 4.12.

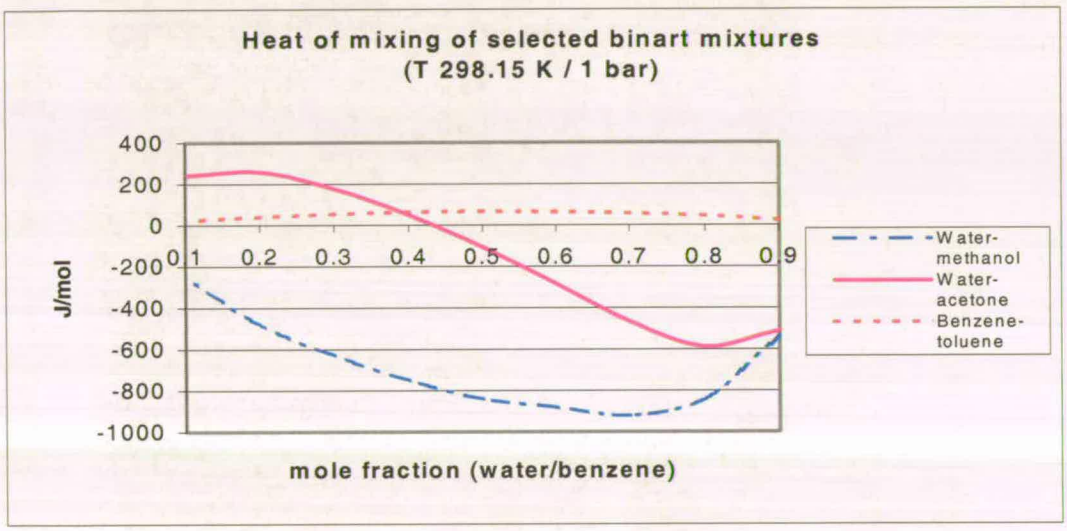

Figure 4.12: Heat of mixing of selected binary mixtures

According to the graph, the benzene-toluene mixture was the obvious first choice. Hardly any heat of mixture appears over the whole range and hence it would have influenced the system least. But firstly, benzene-toluene mixtures are highly flammable and secondly, benzene is on the list of carcinogenic substances. The other mixtures contain either ranges of low heat of mixtures or low gradients respectively. An appropriate range could be found between 0.4 and 0.6 mol/mol water. Due to its smaller change in terms of heat of mixture methanol-water was the preferred binary system. Therefore the methanol-water system (0.5 mol/mol water) was chosen for the experiments. The relevant system properties are given in Table 4.11.

Properties	Methanol	Water	Equimolar mixture (methanol-water)
Boiling point at 1 bar	338.15K[a]	373.15K[a]	332.95 K[a]
Surface tension	22.7 dyn/cm	66.5 dyn/cm	18.85 dyn/cm
Critical temperature	512.60K	647.37K	-
Critical pressure	81.0 bar	47.0 bar	-
Molecular weight	32 kg/kmol	18 kg/kmol	25 kg/kmol
Density gas	-	-	1.37 kg/m^3
Density liquid	791 kg/m^3	983 kg/m^3	864 kg/m^3
Heat of vaporisation	35278 kJ/kmol	41275 kJ/kmol	35390 kJ/kmol

Table 4.11: Useful properties for the column design, boiling points.
(Source: Thomas and McAllister 1957 and Yaws 1999 [253 & 226])

The following equations have been used for the calculation of the properties.

Heat of vapourisation

$$\lambda = A\left(1-\frac{T}{T_c}\right)^n \qquad \text{(modified Wilson approach, Yaws, (1999) [226])} \qquad (4.3)$$

A methanol: 49.244 A water: 52.053

n methanol: 0.481 n water: 0.321

To facilitate the calculations, it was assumed that the heats of vaporisation are additive and no mixing effects were taken into account. More precise approaches can be found elsewhere (Reid 1987) [224].

Surface tension of pure substances

$$\sigma = A\left(1-\frac{T}{T_c}\right)^n \qquad \text{(Yaws, (1999)) [226]} \qquad (4.4)$$

Surface tension of binary mixtures

The calculation is a complicated matter. A quite difficult but nevertheless reliable approach has been developed by Tamura *et al.* (1955) [254]. It's only valid for binary mixtures. Other approaches dealing with surface tension in mixtures can be found elsewhere (Reid, (1987)) [224].

$$\sigma_m^{\frac{1}{4}} = \psi_w^{\sigma}\sigma_w^{\frac{1}{4}} + \psi_o^{\sigma}\sigma_o^{\frac{1}{4}} \qquad (4.5)$$

$$\psi_w^{\sigma} = \frac{x_w^{\sigma}V_w}{V^o} \qquad (4.6a) \qquad \psi_o^{\sigma} = \frac{x_o^{\sigma}V_o}{V^o} \qquad (4.6b)$$

(4.7)

$$C = \log\frac{\left(\psi_w^{\sigma}\right)^q}{\psi_o^{\sigma}} \qquad (4.8)$$

$$C = B + W \qquad (4.9)$$

$$W = 0.441\frac{q}{T}\left(\frac{\sigma_o V_0^{\frac{2}{3}}}{q} - \sigma_w V_w^{\frac{2}{3}}\right) \qquad (4.10)$$

$$\psi_w = \frac{x_w V_w}{x_w V_w + x_o V_o} \qquad (4.11a) \qquad \psi_o = \frac{x_o V_o}{x_w V_w + x_o V_o} \qquad (4.11b)$$

where σ_m, σ_w, σ_o = surface tension of the mixture, of pure water and pure organic component
V_w, V_o = molar volume of pure water and pure organic component
x_w, x_o = bulk mole fraction of pure water and pure organic component
T = temperature, K
q = number of carbon atoms, 1
ψ , ψ^{σ} = volume fraction in the bulk liquid and in the surface phase

The design went through several attempts before an appropriate solution could be found. The basis for the first attempt was the column profile at UMIST. The relevant data are given in Table 4.12.

Column diameter	590 mm
Weir length	457 mm (77.5% of d)
Liquid flow path length	374 mm (63.4% of d)
Cross section area	0.273 m^2
Active area (bubbling area)	0.200 m^2
Hole diameter	4.8 mm
Total hole area	0.0185 m^2
Downcomer area	0.034 m^2
Hole pitch triangular	12.7 mm
Exit weir height	50 mm
Inlet weir height	25 mm
Tray thickness	3 mm
Fractional free area/ hole area/bubbling area	0.0925

Table 4.12: Tray dimensions UMIST column. (Source: Lockett 1983[250])

Because column fabrication costs are lower in customary sizes, the first attempt aimed for a 150 mm diameter column. Hence a downscale factor of 3.9 (related to column diameter) was obtained. The adjusted dimensions, as far as they could be calculated, are given in Table 4.13.

Column diameter	150 mm
Weir length	116 mm (77.5% of d)
Liquid flow path length	95 mm (63.4% of d)
Cross section area	0.0177 m^2
Active area (bubbling area)	0.0129 m^2
Hole diameter	? mm
Total hole area	0.0012 m^2
Downcomer area	0.0022 m^2
Hole pitch triangular	? mm
Exit weir height	? mm
Inlet weir height	? mm
Tray thickness	? mm
Fractional free area/ hole area/bubbling area	0.0925

Table 4.13: Downscaled tray dimensions[34]

For the appropriate column diameter determination two approaches have been used. The first approach is based on the correlation factor k_V (Sounders and Brown (1934), stated in Billet (1973) [255]. The correlation factor is defined as

$$k_V = \sqrt{\frac{4d_T * g}{3c_W}} \tag{4.12}$$

and is dependent on the tray construction, the tray spacing, hydraulic conditions, and the mixture properties (particularly the surface tension). It has to be determined experimentally and is usually given by the tray manufacturers. k_V can also be estimated for the most important tray types with the help of empirical correlations.

[34] Parameters with a question mark ought to be determined in a different way.

The appropriate correlation to calculate the correlation factor for sieve trays at the upper loading boundary is given below:

$$k_V = 0.0045 \frac{\sqrt{\Delta z}}{\sqrt[5]{d_h}} \tag{4.13}$$

To avoid entrainment, the tray spacing (Δz) was maximised (600 mm) and for the first attempt a hole diameter (d_h) of 4.8 mm was set. With these numbers k_V becomes 8.054E-2. With k_V the maximal loading factor can be calculated

$$F_{\max} = k_V \sqrt{\rho_l - \rho_v} \tag{4.14}$$

In our case F_{max} is equivalent to $2.36\sqrt{Pa}$. The next step contains the calculation of the gas velocity in the free column cross section. This is defined by

$$w_{sfl} = \frac{F_{\max}}{\sqrt{\rho_v}} \tag{4.15}$$

The ideal gas velocity for distillation columns equals 0.7-0.8 * w_{sfl}. We chose the lower value due to our reboiler performance limit. The ideal gas velocity becomes 1.41 m/s. With the help of the simple relations

$$A_b = \frac{V}{w_s} \tag{4.16}$$

$$A_c = \frac{A_b}{1 - 0.6\left(\frac{W}{d}\right)^{3.36}} \tag{4.17}$$

$$d = \sqrt{\frac{4A_c}{\pi}} \tag{4.18}$$

we obtained a diameter (d) of 9.2 cm, obviously not enough for our needs.[35]

The second approach is independent of the correlation factor, and was developed by Stichlmair (1971) [256]. His approach is given below:

---

[35] W/d equals 0.775 according to the UMIST template.

$$F_{max} = 2.5 * \left[\left(\frac{A_h}{A_b} \right)^2 * \sigma_l * (\rho_l - \rho_v) * 9.81 \right]^{0.25} \tag{4.19}$$

$$F = 0.7 * F_{max} \tag{4.20}$$

$$w_s = \frac{F}{\sqrt{\rho_v}} \tag{4.21}$$

$$A_b = \frac{V}{w_s} \tag{4.22}$$

$$A = \frac{A_b}{1 - 0.6 * \left(\frac{W}{d} \right)^{3.36}} \tag{4.23}$$

$$d = \sqrt{\frac{4 * A}{\pi}} \tag{4.24}$$

A column diameter of 8.6 cm was obtained by this approach, not enough either. So there was a need to take measures in terms of enlarge the column diameter. Several factors can increase the column diameter

- A higher reboiler performance.
- A reduction of the gas velocity with the side effect of leaving the ideal operating range.

Increasing the reboiler performance was not the means of our first choice. We rather preferred to examine the other end of the loading. First and foremost we calculated the minimum velocity in the holes obtained from the compilation of Sattler (1995) [257]

$$w_h = \frac{10}{\sqrt{\rho_v}} \tag{4.25}$$

This yielded to a minimal hole velocity of 8.54 m/s. The recommended velocity ought to be 1.8 times higher, so one computed 15.38 m/s as a recommended hole velocity. With a fractional free area of 9.25% the gas velocity in the free column cross section becomes 1.44 m/s, a value, which we have already calculated earlier by

Sounders and Brown's approach. The reboiler can generate a maximal vapour stream of 2.53E-2 m^3/s. For a 150 mm diameter column one obtains a gas velocity of 0.36 m/s. This corresponds to 3.89 m/s in the holes, far below the allowed minimal gas velocity. The only way to obtain a sufficient gas velocity in the holes with a given gas stream is reducing the fractional free area. With a fractional free area of 4.0 % the gas velocity in the holes becomes 8.96 m/s.

Due to design reasons a hole number of about 42 is desirable. This equals 7 rows with 6 holes per row. The size of the hole diameter can be calculated by

$$d_{hole} = \sqrt{\frac{A_h 4}{42 * \pi}} \tag{4.26}$$

One yields a hole diameter of 4mm. The hole pitch for 60 degree pitch perforations, calculated by

$$p = \sqrt{\frac{\pi * d_{hole}^2 A_b}{2\sqrt{3} A_h}} \tag{4.27}$$

corresponds to 19 mm. The tray and parts of the column dimensions are given in Table 4.14.[36]

Active area (bubbling area)	0.0129 m^2
Hole diameter	4.0 mm
Total hole area	0.000516 m^2
Downcomer area	0.00238 m^2
Hole pitch triangular	19 mm
Exit weir height	13 mm
Tray thickness	? mm
Tray spacing	600 mm
Fractional free area hole area/bubbling area	0.04

Table 4.14: ***Tray and column dimensions based on a 9.6 kW reboiler.***

[36] The reboiler was upgraded to 16 kW in the development of the experiments

The determination of the tray thickness is discussed elsewhere due to the special structure of the modified tray.

4.2.1.1 Rig description

Figure 4.13 features an outline of the complete rig. Blue lines display heat exchanger medium cycles. An enlarged version and a more detailed rig flow sheet can be found in Appendix E. A detailed description of the various rig components is given below. A photograph of the complete rig is given in Figure 4.14.

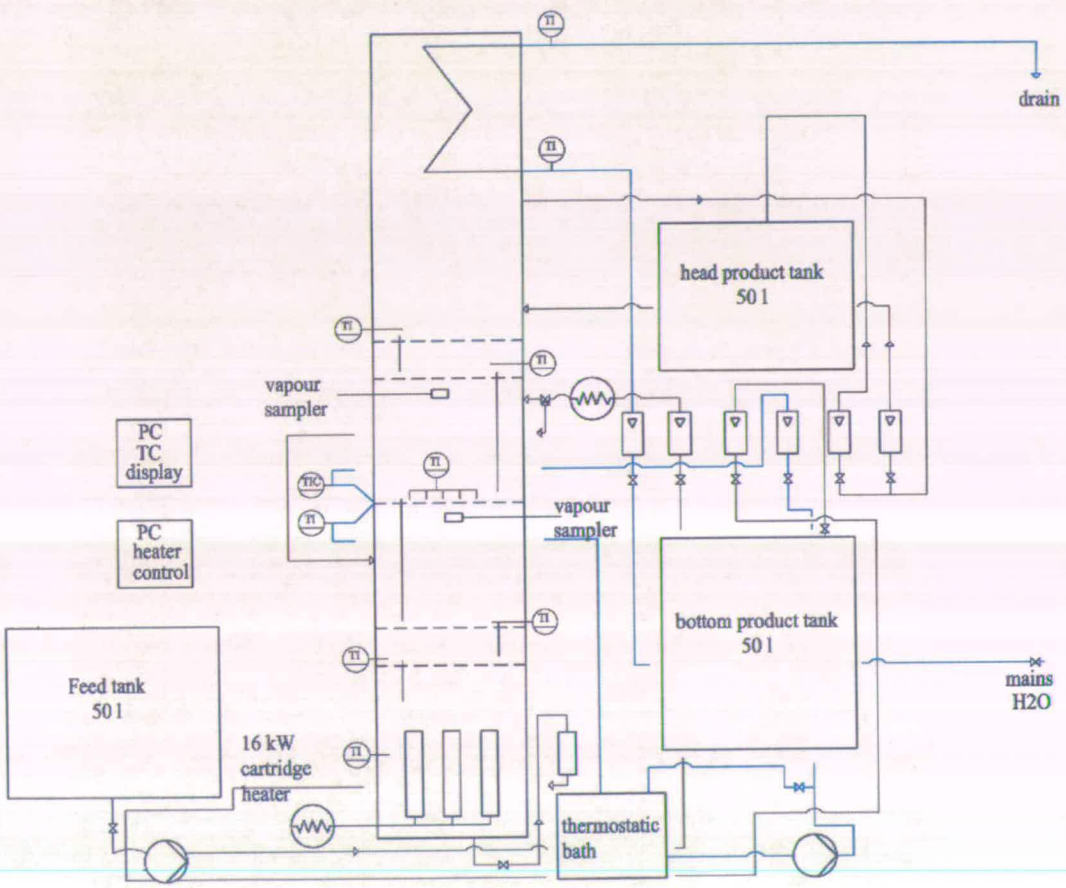

Figure 4.13: Schematic diagram of the experimental rig.

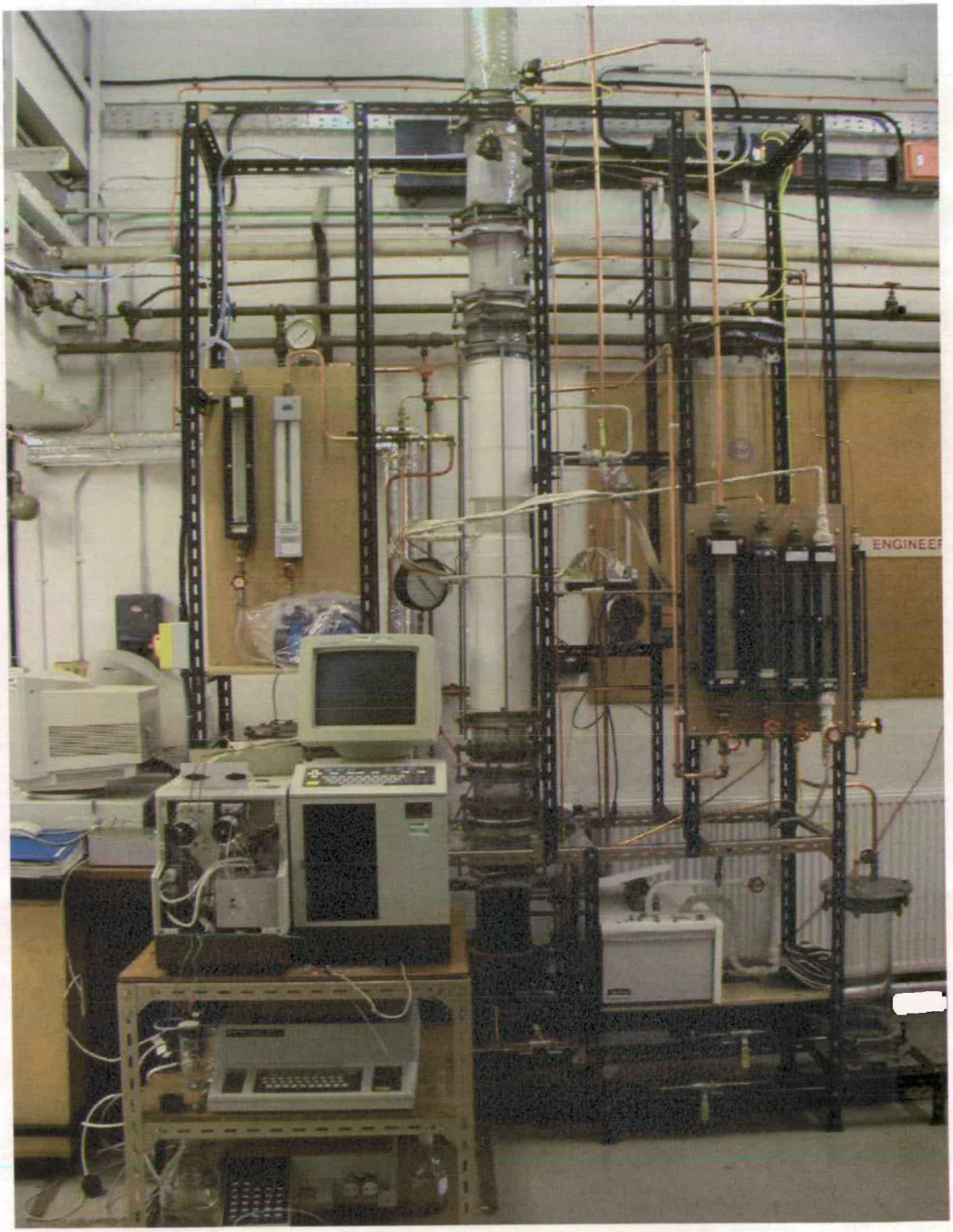

Figure 4.14: Snap shot of the experimental rig.

4.2.1.2 Column

The column consists 5 sieve trays with a diameter of 150 mm. 4 plates are standard adiabatic sieve trays, shielding the diabatic plate uniformly from above and below. The tray spacing varies from plate to plate. The tray positioning is given in Figure 4.15. The uneven tray spacing was caused by avoiding entrainment around the vapour samplers (tray spacing = 550 mm) and the lack of height available for the shielding plate (tray spacing = 150 mm) to copy the tray spacing between the adiabatic plate. The diabatic section is created by reducing heat loss and specifically directing the heat transfer by using PTFE adjacent to the heat transfer plate.

Figure 4.15: Tray spacing.

Figure 4.16: PTFE insulation of the heat transfer plate.

PTFE tubing with a wall thickness of 25 mm and a length of about 500 mm demarcated the diabatic section from the rest of the column (Figure 4.16). Each plate has a single sample port for manual sample withdrawal.

Feed is supplied at one of two ports. They enter the column above or below the heat transfer tray respectively. The feed is preheated by a 1 kW cartridge heater (Figure 4.17). The cartridge heater is continuously adjustable to cope with different feed rates and compositions. A metering pump delivers a flow rate of 25 l/h. A reboiler is made up of 6 cartridge heaters; 4 with a performance of 2500 W each and 2 with a performance of 3000 W each, provides a main vapour flow rate of 43.2 m^3/h. A sketch of a cartridge heater can be found in the Appendix.

Figure 4.17: Feed-preheater.

A glass condenser produces the reflux for the adiabatic part of the column. The condenser dimensions are given in Figure 4.18 and Table 4.15 respectively. Water with a maximum flow rate of 1.23 m^3/h serves as coolant in the condenser.

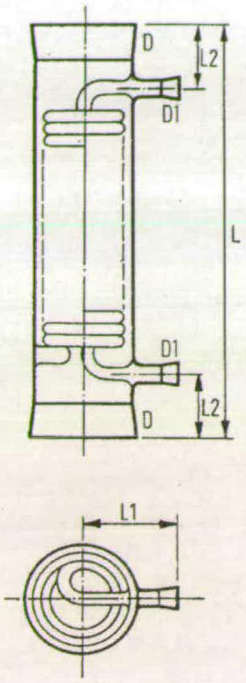

D	150 mm
D1	25 mm
L	600 mm
L1	150 mm
L2	100 mm
Condenser area	1 m^2

Table 4.15: Condenser data (Source QVF).

Figure 4.18: Condenser sketch.

4.2.1.3 Feed and product vessels

A 50 l cylindrical glass vessel serves as feed tank. Two 50 l cylindrical glass tanks collect the bottom and head products respectively. The feed leaves the tank by means of gravity and flows into a metering pump. The metering pump delivers the feed into the column. The separated products are collected in the feed tank after a run. The head product tank can be emptied by means of gravity. The bottom product tank is discharged by means of compressed air. Over pressure built up caused by compressed air is avoided by orifice plates in the vent lines.

4.2.1.4 Flow-, level control, temperature indication

In order to avoid any drainage of the cartridge heater, a level controller (overflow), including a diode switch interrupts the energy supply to the heaters. The feed flow rate is adjusted by the pump setting and displayed on a rotameter. The reflux and bottom product flow is controlled by two rotameters. The bottom product withdrawal

is established by a passive controller (overflow). The rotameters are set up on two control panels; one each for the liquid flow of the column and the gas flow (N_2 & N_2 + vapour) for the vapour sampling system respectively (Figures 4.19 & 4.20). A comprehensive rotameter description concerning sizes and reading maxima is given in Appendix E .

Figure 4.19: Rotameter panel for liquid flows.

Figure 4.20: Rotameter panel for vapour sampling flow.

Thermocouples (type K) on each plate, in the reboiler, at the inlet and outlet of the heat transfer plate, at the condenser coolant inlet and outlet, in the vapour stream leading to the GC and at feed ports, indicate temperature throughout the rig. The thermocouples are connected to two thermocouple readers (PICO TC 08) and displayed on a computer screen. The TC 08 is shown in Figure 4.21 and the displayed thermocouples are given in Table 4.16. The five thermocouples across the centre line of the heat transfer plate have been calibrated and the calibration function has been implemented to establish a better uniformity of the measurement devices. Hence a more precise temperature profile across the plate can be obtained (+/- 0.5°C). The calibration was accomplished with a thermostatic bath and a high precision thermometer. An example of a calibration plot is given in Appendix D.

Figure 4.21: PICO TC08 thermocouple reader.

Thermocouple location	
Plate 1	Heat exchanger medium inlet
Plate 2	Heat exchanger medium outlet
Plate 4	Heat exchanger plate point 1
Plate 5	Heat exchanger plate point 2
Condenser inlet	Heat exchanger plate point 3
Condenser outlet	Heat exchanger plate point 4
Feed port 1	Heat exchanger plate point 5
Feed port 2	reboiler

Table 4.16: Thermocouple location.

4.2.1.5 Pump systems

Various pumps drive several flows or driving forces. The pumps and their functions are listed in Table 4.17.

Kind of pump	Function
2 head metering pump	Feed supply; bottom product withdrawal[37]
Centrifugal pump	Heat transfer medium pump
HPLC pump	Liquid sample withdrawal
Peristaltic pump	Vapour sample driving force

Table 4.17: Rig pumps and their functions.

4.2.1.6 Health and safety

Before an experimental rig could be operated at Edinburgh University a "Research Apparatus Safety Assessment" form had to be completed in the first place. The safety assessment features comprehensive operating instruction for the experimental rig[38]. The document can be found in the Appendix.

4.2.2 Heat transferring sieve tray

A 150 mm diameter sieve tray, preferable made of Dural, was designed to fulfil the following tasks:

- Ability of adding or removing heat in the magnitude of 1 kW.
- Point efficiency measurement (liquid sampling across the tray).
- Measurement of the clear liquid height (manometer integration).
- Observation of the bubble forming and bubble flow respectively (use of a high-speed camera).

---

[37] Bottom product was pumped from the overflow collector to the bottoms tank.

[38] Particular attention was paid to the safe operation of the reboiler. It will be switched off in the case of either: 1. Drainage of the cartridge heaters (diode level controller)
2. Current flow too high

Adding heat in the magnitude of 1 kW did not represent a big problem. It can be achieved by means of electricity, for instance. Cooling, on the other hand is another matter. The solution involves a serpentine tube system within the plate, which contains coolant (preferably water). The thickness of the tubes not only defines the inner heat transfer area, it also influences the thickness of the tray. The heat transfer calculations are based on the equations below

$$\dot{Q} = m * c_p * \Delta T \tag{4.28}$$

$$\dot{Q} = A * U_p * \Delta T \tag{4.29}$$

$$U_i = \frac{1}{\frac{1A_p}{h_i A_i} + \frac{A_p t}{A_m k} + \frac{1}{h_o}} = \frac{1}{A_p R} \tag{4.30}$$

Heat transfer coefficient correlations are thoroughly discussed in Chapter 3.

The core of the rig is an especially designed sieve tray capable of adding heat to, or withdrawing heat from the plate. The centre of the plate is made of Dural embedded in PTFE. Relevant data are given in Table 4.18. Pictures and sketches of the plate can be found in several Figures (4.22, 4.23 & 4.24).

Diameter	150 mm
Liquid flow path length	95 mm
Cross section area	0.0177 m^2
Active area	0.0129 m^2
Downcomer area	0.00238 m^2
Weir length	116 mm
Weir height	50 mm
Gap between downcomer and weir	25 mm
Tray thickness	15 mm
Hole diameter	4 mm
Total hole area	0.000516 m^2
Fractional free area/ hole area / bubbling area	0.04

Table 4.18: Tray data.

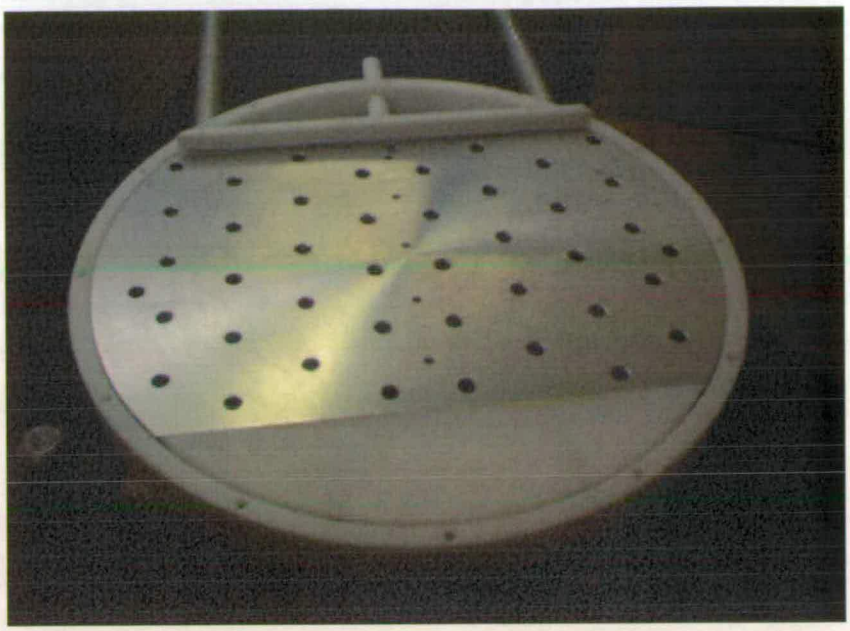

Figure 4.22*:* Heat transfer plate.

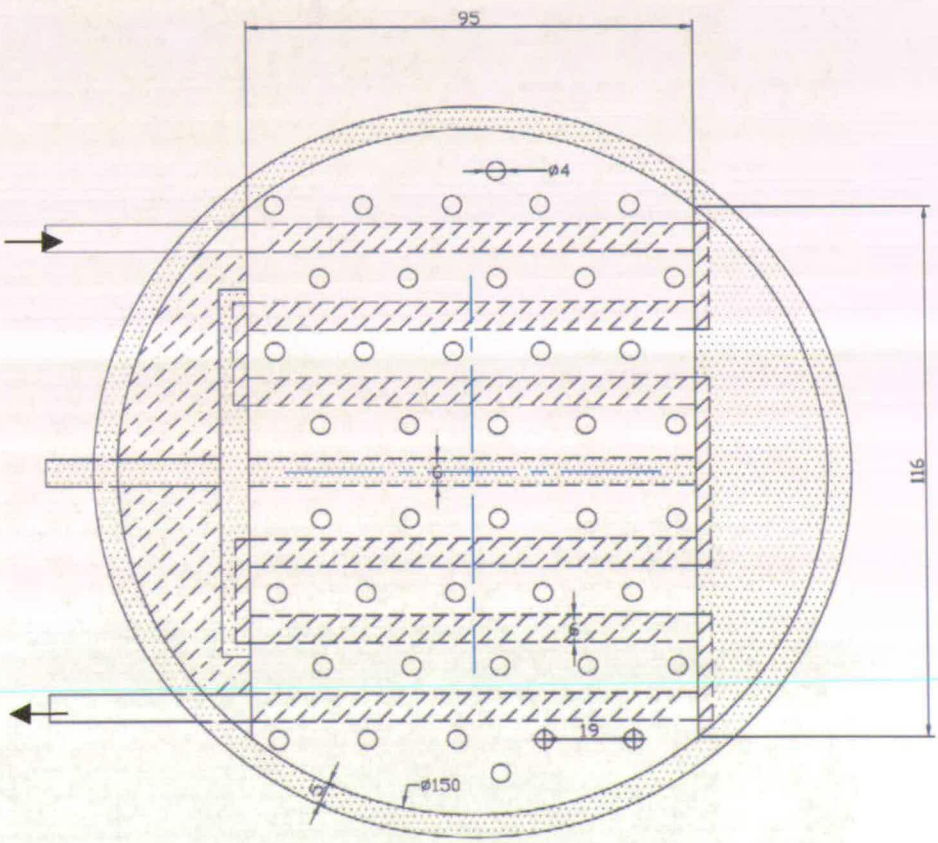

Figure 4.23: Sketch of the heat transfer plate.

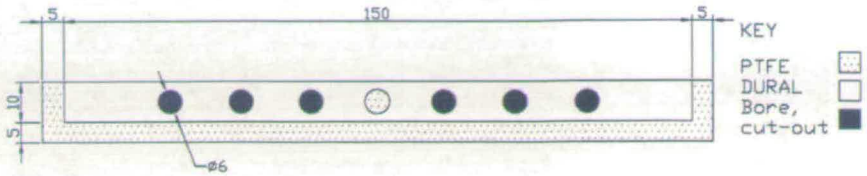

Figure 4.24: Vertical cross-section of the heat transferring plate; dimensions in mm.

Water, serving as heat transfer medium enters the serpentine ducts. The heat transfer rate is determined by the measurement of the medium flow rate and the temperature difference at the entrance and exit. The inlet water temperature is kept constant by means of a thermostatic bath for heat addition and by means of a cooling coil embedded in the thermostatic bath for heat withdrawal respectively.

4.2.3 Liquid and vapour sample systems

According to the Murphree tray efficiency theory described in Chapter 3, several mean liquid and vapour concentrations (x, y) of streams exiting the plate are needed. Locations of the liquid and vapour sampling systems are given in Figure 4.25. It is assumed that the vapour entering the vapour sampler (see Figure 4.26 & 4.27) is completely mixed and equals the mean vapour concentration.

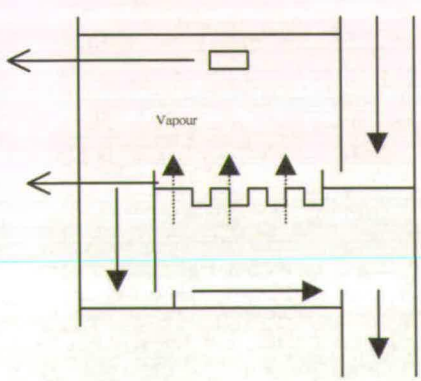

Figure 4.25: Sampler positions in the column.

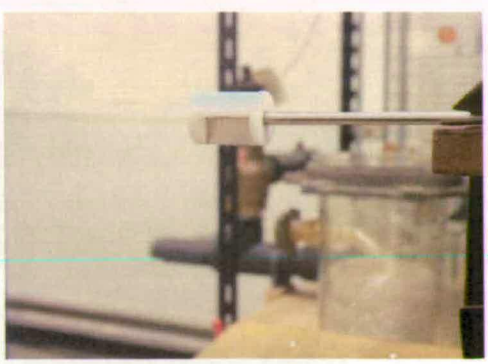

Figure 4.26: Vapour sampler.

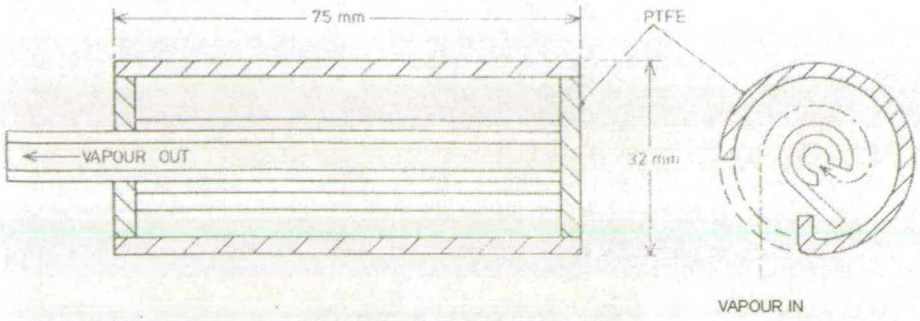

Figure 4.27: Cross section of the centrifugal vapour sampler; dimensions not to scale. (Source: Kastaneck 1974 [153])

The vapour sampler separates any traces of liquid by centrifugal force. Calculations of minimum entrainment drop sizes can be found in Perry's chemical engineering handbook (1984) [251], Coulson (1999) [24 & 258] and others [259 & 260]. Vapour samples were withdrawn by suction. A membrane pump provided the vacuum. A sketch of the complete vapour sampling system is given in Figure 4.28.

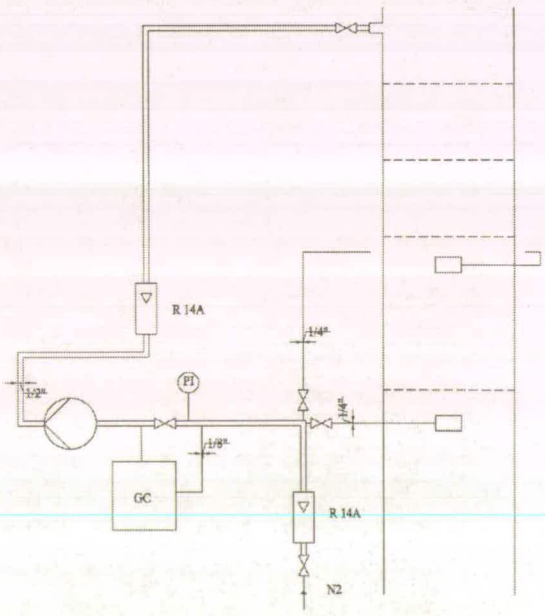

Figure 4.28: Embedded vapour sampling system.

The liquid concentration of the liquid leaving the tray can be obtained from withdrawing samples close to the weir using a mulitport sampler shown in Figure

4.29. Additionally, this pivotable device allows the determination of the liquid concentration profile across the plate.

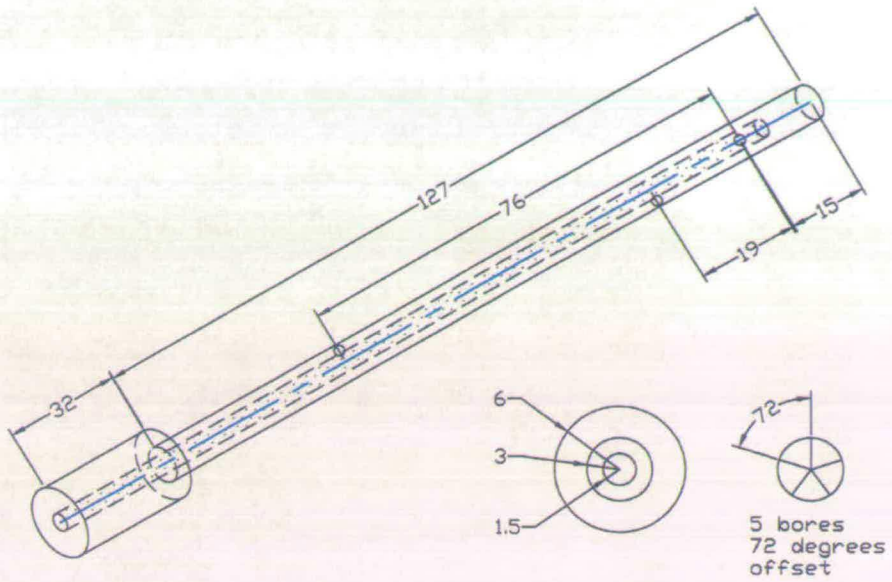

Figure 4.29: Sketch of the pivotable multi-port liquid sampler.

Due to unsatisfactory control system of the first sampling system, a better one had to be designed. The idea was to establish a stable vapour / N_2 ratio independent of the valve settings or gas velocities. This can be obtained by applying pressure drop along capillary tubing. The calculations are based on the fluid dynamics equations applicable in ducts [251 & 261].

The flow pattern across ducts significantly influences the pressures drop caused. The calculation of the Reynolds number (Re) as an indicator for the flow pattern is essential in the first place. With an assumed mass flow (G), an appropriate duct diameter (d) and the viscosity values (μ) obtained from the literature Re can be computed [261].

$$\mathrm{Re} = \frac{4G}{\pi \mu d} \tag{4.31}$$

According to Re achieved the flow pattern is determined using Table 4.19.

Re	Flow pattern
< 2000	laminar
> 2000 < 3000	transition region
> 3000	turbulent

Table 4.19: ***Flow pattern in ducts.***

(Source: Coulson % Richardson (1999) [261])

The transition region ought to be avoided. This can be achieved by either altering the mass flow or the diameter of the duct [261]. In the case of a turbulent flow the pressure drop is a function of the shear stress on the duct surface R, the fluid density ρ, and the fluid velocity w in the duct.

$$\Phi = \frac{R}{\rho w^2} \tag{4.32}$$

The determination of R can be rather laborious. A number of expressions have been proposed for calculating Φ. Blasius (1913) [262] derived the following equation for smooth pipes from considerations of velocity profiles.

$$\Phi = 0.0396\,\mathrm{Re}^{-0.25} \qquad \text{(valid for } 2500 < \mathrm{Re} < 10000\text{)} \tag{4.33}$$

The length of a duct can be calculated for a given pressure drop

$$l = \frac{\Delta p d}{4\Phi\rho u^2} \tag{4.34}$$

Various sub-equations were used for the computation of the variables in equation 4.34.

$$w = \frac{V}{A} \tag{4.35}$$

$$G = nM \tag{4.36}$$

$$n = \frac{V}{v} \tag{4.37}$$

$$v = \frac{RT}{p} \tag{4.38}$$

In the case of laminar flow the duct length is defined by equation 4.39.

$$l = \frac{\pi \Delta p r^4}{8V\mu} \tag{4.39}$$

For a desired pressure drop of 10 kPa across the capillary tubes and the parameters given in Table 5 capillary tube lengths of 300 mm for the vapour samplers and 290 mm for the N_2 were obtained. A dilution factor of 4 was taken into account

For a desired pressure drop of 10 kPa across the capillary tubes and the parameters given in Table 4 capillary tube lengths of 300 mm for the vapour samplers and 290 mm for the N_2 were obtained. A dilution factor of 4 was taken into account.

Vapour flow rate	0.21 l/s
N_2 flow rate	0.84 l/s
Capillary tubing diameter for the vapour	1.96 mm
Capillary tubing diameter for N_2	3.20 mm
Pressure drop across the capillary tubing	10 kPa
Length of the vapour capillary tubing	300 mm
Length of the N_2 capillary tubing	290 mm

Table 4.20: Parameters for the determination of the capillary tubing length.

About 1 % of the diluted flow is diverted through the GC tubing. This is obtained by creating a pressure drop in the main line by an orifice plate, which equals the pressure drop in the GC tubing. The pressure drop in the GC tubing was computed with the equations aforementioned (laminar flow regime). The diameter of the orifice plate was obtained by solving equation 4.40 for A_O.

$$G = cA_O\rho_v \sqrt{\frac{2\Delta p}{\rho_v\left(1-\frac{A_O^2}{A_r^2}\right)}} \tag{4.40}$$

The value of 0.65 for the discharge coefficient (c) was obtained from charts [262]. A sketch of the modified vapour sampling system is given in Figure 4.30.

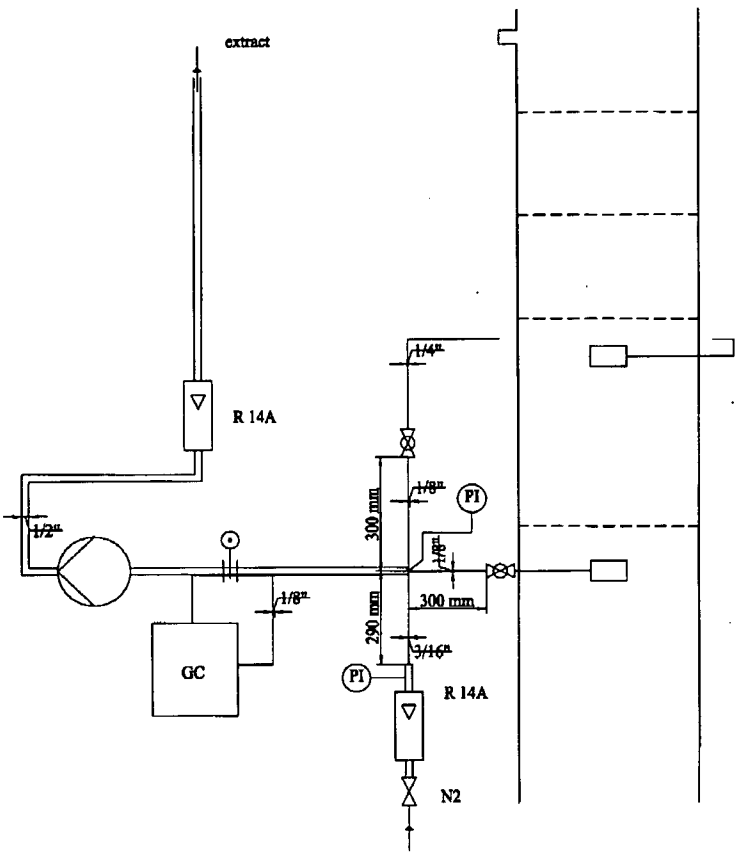

Figure 4.30: Modified vapour sampling system.

4.2.4 Discussion

The set up of the experimental rig proved to be a time consuming task that took about 3 – 4 months to be finished. A test run period of about one month was also performed. The results from the various test runs led to continuous modifications and corrections. The first test runs aiming for the detection of leaks revealed a structural weakness of the PTFE. Particularly affected was the PTFE ring sitting underneath the heat transfer plate. Due to thermal expansion and contraction of the PTFE the heat transfer plate was pushed into the PTFE tube, opening a gap on the heat transfer medium inlet side. The sinking worsened from run to run, eventually leading to a deformation of the Dural tubing (inlet and outlet for the heat exchanger medium) of the heat exchanger medium. The fact that the PTFE sections were made from different off-cuts, and the rather small diameter of the PTFE ring wrapping the heat transfer plate, intensified the problem. Two options were considered for solving the problem:

- Reducing the weight coming from the upper half of the column (glass sections, reflux divider, condenser).
- Insertion of a hard material between the 2 PTFE sections.
- Enlargement of the PTFE ring for better weight distribution.

The former point was not considered as being recommendable because a reduction of the weight would also reduce the impermeability of other sections of the column. Therefore the column was dismantled down to the heat exchanger plate, the outer PTFE ring was enlarged and a Dural ring was inserted in the PTFE section below. The Dural ring not only has a lower coefficient of expansion it also helps to distribute the weight more evenly.

The test runs also revealed an inconvenient operating regime of the column due to large heat losses. In the early design stages of the project one had to rely on existing devices. Therefore existing cartridge heaters were used for reboiler construction leading to a operating regime dangerously close to the weeping regime. Heat losses were not taken into account at this stage. Even with the insulation arrangements the reboiler performance was insufficient to overcome the weeping regime. While the column was equipped with lagging, stronger cartridge heaters were ordered, boosting the reboiler performance from 9.6 kW to 16 kW. This shifted the operating field of the column into a safe zone with reserves available. The lagging procedure proved to be rather tricky due to the number of pipelines entering and leaving the column perpendicularly. Another problem was the need for a visual control of the plates' hydraulic performance. The aforementioned reasons led to the rejection of the simple use of insulation cylinder jackets due to the inability to cover the column properly. Cutting windows into the jackets was also unsuitable due to the fibre glass fill (health and safety). The solution came in form of the application of several insulation materials listed below:

- Insulation cylinder jackets for the reboiler.
- Insulation foam for the bulk of the column.
- Radiator reflectors and textured fortaglas webbing for the PFFE section.

- Removable cut outs in the foam to provide a visual control of most of the plates.

Another problem encountered was the reflux tubing. The head product leaves the column by gravity and flows through two rotameters, which regulate the reflux. The rotameters are at the bottom of the reflux tubing. The liquid rises from the rotameters and enters the column at a point 30 cm below the exit. On the first runs, the head product was accumulated in the reflux divider underneath the glass condenser. This was caused by a counter pressure in the inlet tubing. The height difference between the inlet and outlet points proved to be insufficient. The problem was solved by the addition of two valves, which prevented vapour from entering the inlet tubing in the first place and offered an option of removing any gas accumulation by suction. Further runs did not feature this problem anymore.

The modification of the vapour sampling system proved to be unavoidable. three sample withdrawal runs were performed; all unsuccessful. Each run led to flooding of the entire system. Water condensate even reached the rotameter after the peristaltic pump. The main problem was the overload of the GC column and the adjacent tubing system. The water had to be driven out by dismantling the system and flushing it with compressed air and Helium, all-in-all a cumbersome and fairly time-consuming operation. The first suspicion was focused on condensate accumulation in the vapour sampling tubing before the valves. Due to the positioning of one of the vapour samplers, condensate could enter the system by gravity after opening the particular valve. This problem was solved by flushing this part of the tubing with N_2 first, driving the condensate back into the column. A succeeding run applying this approach also failed, the flooding was just less severe. It seemed that the valves were not sensitive enough to regulate the vapour flow coming from the samplers. The simple two-way valves were substituted with needle valves. Furthermore, to achieve evenly constant dilution of the vapour sample flow, independent of the vapour flow rates, a regulation system based on pressure drop across capillary tubes was applied.

4.2.5 Conclusion

A rig was designed capable of measuring various heat transfer coefficient (U, $h_{p-f,}$) and the determination of Murphree tray efficiencies by analysing vapour and liquid samples. Additionally, the temperature profile along the column and across the heat transfer plate were monitored. The rig was capable of delivering heat to and removing heat from a specifically designed diabatic sieve tray. The rig design allowed the investigation of the impact of key variables influencing tray efficiency and heat transfer respectively.

4.3 Experimental Plan

As was shown in the previous Chapters, heat transfer in distillation columns affects vapour and liquid flow rates. Thus, the influence of varying vapour and liquid flow rates on E_{MV} ought to be investigated. The study should also show the difference between stream manipulation on the plate and by the reboiler; therefore, the HEM flow rate was also taken as key variable. Additionally, changes in vapour load and HEM flow rate were the key parameters for approving /disapproving our h_{f-p} model proposals. The HEM flow rate determined the heat flux transferred to or removed from the plate and the ΔT between the plate surface and the froth. Physical properties like viscosity and surface tension were not chosen as variables to be investigated because, according to previously reported tray efficiency studies, they do not influence E_{MV}[39] significantly on a single plate [157, 175 &195]. This could be expanded to our five-plate system. Equimolar methanol-water mixtures were chosen as experimental fluid, which provide detectable composition changes between two plates. The composition was changed to 0.3 water and 0.7 methanol (mole fraction) because the equimolar mixture was more vulnerable to evaporation in the storage vessels and more expensive to maintain (due to the methanol loss). The key variables and their boundaries are listed below.

[39] The concentration change across the plate is to small to cause drastic changes in physical properties

- Vapour flow rate: controlled by the 16.0 kW reboiler. The reboiler load could be lowered down to 11.2 kW before weeping started.
- HEM flow rate: with water as HEM the flow rate was stepwise increased from 18 – 78 kg/h.
- Liquid flow rate: controlled by the reflux ratio. Runs were performed under total reflux; additionally, the reflux ratio was stepwise altered from 1 – 7.

Chapter 5

Results and Discussion

This Chapter presents the results and interpolations of experimental data, which are discussed simultaneously. It starts with the calculation of overall heat transfer coefficients in the bench-scale plant of Maruzen (Japan), based on their reported experimental temperature profiles. Additionally, the number of theoretical stages in this column is calculated and compared with an adiabatic column with equivalent external reflux and achieving the same separation quality.

Next, temperature and temperature-related composition profiles across our experimental column are presented. Those plots give information about the time needed for reaching steady state and the influence of heat transfer on the column temperature/composition profile. This is followed by Figures showing experimental overall heat transfer and plate-to-froth heat transfer coefficients respectively, determined in both cooling and heating modes. These values are used to test our heat transfer models.

The Chapter closes with the presentation of Murphree tray efficiency results, obtained from cooling and heating runs. Those efficiencies are compared with Murphree tray efficiencies from adiabatic runs, produced in the same column.

5.1 Preliminary calculations

The intention of this calculation was the evaluation of an average overall heat transfer coefficient in the packed bench-scale column and the familiarisation with the curved operating line concept.

5.1.1 Heat and mass balances for a experimental HIDiC

By using the available data of the plant in Japan (taken from sample control room screens), which can be found in Appendix C, the heat and mass balance for the binary mixture toluene-benzene was calculated. The balances were carried out for the whole system, and also for the rectification column and the stripping column separately. The overall mass balance and heat balance for the rectifying section are given in Tables 5.1 & 5.2. The agreement of the overall mass balances was not really satisfying; it became even worse by taking the component mass balance into account. These mass accumulations in the balance indicate a system that has not yet reached steady state. The mass flows were used to calculate the heat balance according to eqn 5.1. The calculation of the heat capacities is given in Appendix C.

$$\dot{Q} = N_{tot} * c_p * \Delta T + N_{tot} * \lambda \qquad (5.1)$$

	Stream in kmol/h
Overhead product	0.719
Bottom product	1.653
Feed	2.797

Table 5.1: Overall mass balance.

	Mass flux in kmol/h	Energy consumption in kJ/h
Condensing vapour	3.7	117660
Reflux heating	0.1	-330
Vapour cooling	0.8	1840
Condensate cooling	(3.7)	3100
Sum	4.6	122270

Table 5.2: Heat balance for the rectifying section.

5.1.2 Overall heat transfer coefficient

A temperature profile of the two sections was created on the basis of the temperature readings from the screen shot, given in Figure 5.1. The overall heat transfer coefficient was calculated by applying logarithmic temperature differences and taking the geometry and the dimensions of the cascaded column – illustrated in Figure 5.2 - into account.

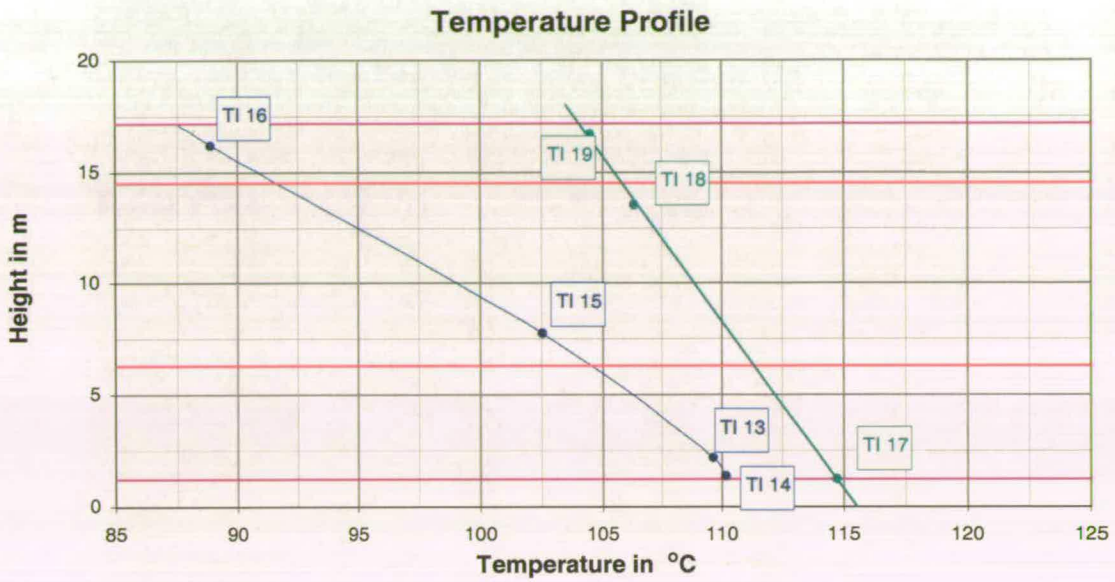

Figure 5.1 Measured temperature profile for stripping and rectifying section.

The overall heat transfer coefficient U can be calculated by eqn. 5.3. The related numbers can be found in Table 5.3. U was assumed constant for every section. Figure 5.2 shows the geometry of the column sections.[40]

$$U = \frac{\dot{Q}_{transferred}}{A\Delta T_{LM}} = \frac{\dot{Q}_{transferred}}{A_1\Delta T_{LM1} + A_2\Delta T_{LM2} + A_3\Delta T_{LM3}} \tag{5.3}$$

A_1 in m^2	A_2 in m^2	A_3 in m^2	Δ_{TLM1} in K	Δ_{TLM2} in K	Δ_{TLM3} in K	$\dot{Q}$ kW
0.75	4.25	2.27	13.78	9.49	5.34	34

Table 5.3: Heat transfer area segments and ΔT_{LM} for experimental HIDiC.

[40] Black areas indicate adiabatic zones.

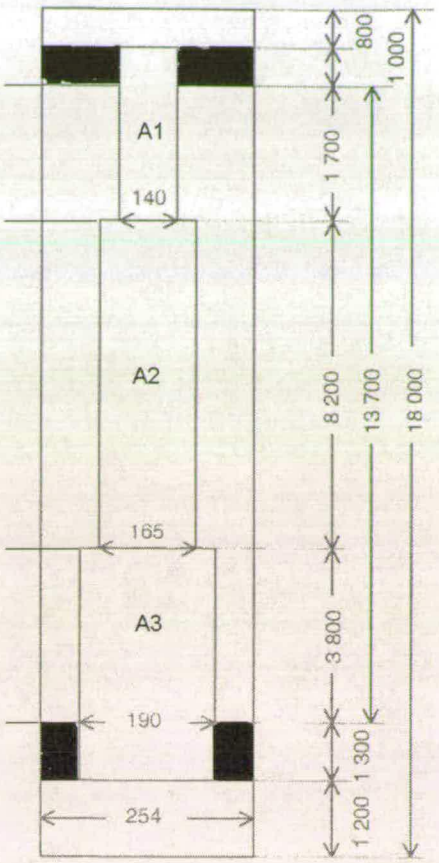

Figure 5.2: Geometry of the HIDiC in Maruzen, Japan. Dimensions are given in mm.

This gave a U of around 530 W/m^{2}K, which is an acceptable value for such a system (Sattler 1995) [257] and it coincides with the experimental U values for a concentric column, measured by Nakaiwa and Noda [123 & 137].

It was assumed that U remained constant along the length of the column, maintained by a uniform liquid film on the column walls. The major disadvantage is the lack of sufficient temperature data from the column. 3 thermocouples in each section for a 16 m column are insufficient, and the temperature profile so indicated appears arbitrary. Consequently, the real overall heat transfer coefficient might differ from the calculated value.

5.1.3 Number of theoretical plates

The bench-scale column in Maruzen separates an equimolar feed (x_F = 0.555) of benzene-toluene into an overhead product (x_F = 0.999 benzene) and bottoms (x_B = 0.004 benzene). The number of theoretical stages and the related height equivalent of a theoretical stage (HETS) for this separation were obtained by stage-by-stage calculation, taking the component compositions at the exits of the column as boundaries. The computation is based on a modified McCabe-Thiele method, presented by Nakanishi *et al.* [122]. The model is illustrated in Figure 5.3.

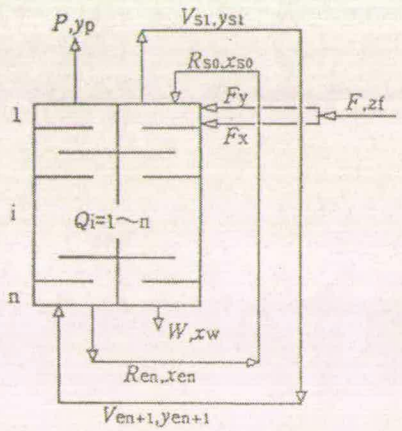

Figure 5.3: Scheme of the HIDiC model

As outlined in Chapter 2, diabatic distillation operates with varying liquid and vapour rates, thus creating curved operating lines. This is taken into account by eqn. 5.4 & 5.5. for the rectifying section

$$y_{r(i+1)} = \frac{r_r x_{r(i)}}{r_{r(1)} + 1} + \frac{y_p}{r_{r(i)} + 1} \tag{5.4}$$

$$r_{r(i)} = \frac{R_{r(i)}}{P} \tag{5.5}$$

where $r_{r(i)}$ and $R_{r(i)}$ are liquid reflux and liquid flow rate on plate i. $R_{r(i)}$ can be calculated by adding the condensate – caused by heat removal from plate i – to the liquid flow rate from the plate above ($R_{r\,(i-1)}$)

$$R_{r(i)} = R_{r(i-1)} + \frac{\dot{Q}_i}{\lambda} \tag{5.6}$$

where $\dot{Q}_{(i)}$ can be calculated by

$$\dot{Q} = AU\Delta T_{LM} \tag{5.7}$$

liquid equilibrium compositions were calculated by using Raoult's law

$$y_{(i)} = \frac{\alpha x_{(i)}}{(\alpha - 1)x_{(i)} + 1} \tag{5.8}$$

An Excel worksheet performed the calculations. A few simplifications were applied. First, the 3 different diameters were replaced with an area-average column diameter of 0.169 m. Second, an average logarithmic temperature difference of 10.6 deg C was used along the whole column. The spreadsheet requires a guess of the height of a theoretical stage. The convergence criterion is achieved if the column height and the total heat transferred are matched. The spreadsheet can be found in the Appendix. 18 stages for the rectifying section (HETS 0.75m) and 17 stages for the stripping section (HETS 0.8m) were obtained. It is impossible to achieve the same separation using an adiabatic column with a reflux ratio of 0.15. The separation quality can be achieved by using an adibatic column with 35 stages and a reflux ratio, which is larger than 1.5. It has to be mentioned that the modified McCabe-Thiele method not only leads

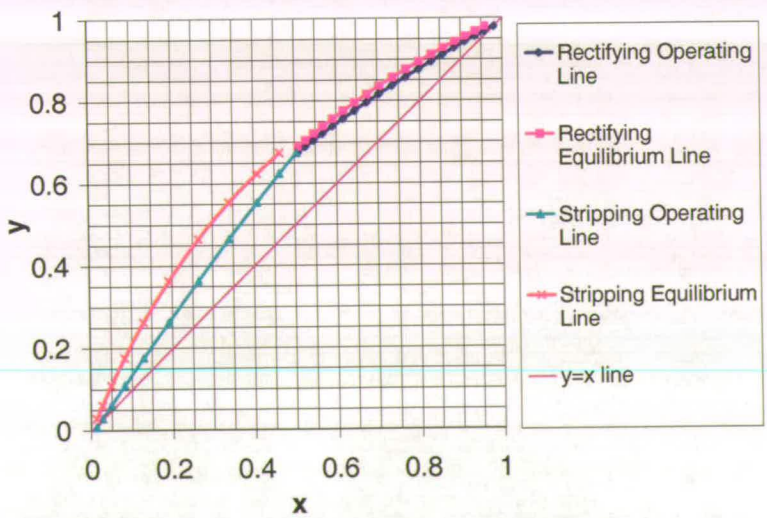

Figure 5.4: xy diagram for a HIDiC.

(Source: Easton 2001 [263])

to a curved operating line, but also to "interrupted" stages due to the pressure difference between the two sections. This is illustrated in Figure 5.4.

The modified Mc Cabe Thiele method delivers reasonable results. The method can be improved by using a detailed temperature profile obtained from a temperature versus stage plot for both columns. Additionally a sub-routine could incorporate the geometry of the HIDiC. Numerical iterations have been conducted by Beggs (2002) and Caldwell (2003), taking those points into account [264 & 265].

5.2 Column and heat transfer plate temperature profiles

In the period from May 2003 to April 2004 a total of 81 experiments have been conducted in the experimental 150 mm diameter column. The experiments included adiabatic, cooling and heating runs under total reflux and product withdrawal conditions. A list of all runs can be found in Appendix B. The early runs were conducted with water, serving as test runs for the apparatus and simultaneously producing the first heat transfer coefficient results. The complete temperature monitoring produced valuable data in terms of steady state conditions and composition profiles.

5.2.1 Steady state operation

In order to achieve reproducible results, steady state conditions for operation are paramount. Temperature profile monitoring allows identification of such states. The temperature profile for two adiabatic runs under total reflux is given in Figures 5.5 & 5.6.

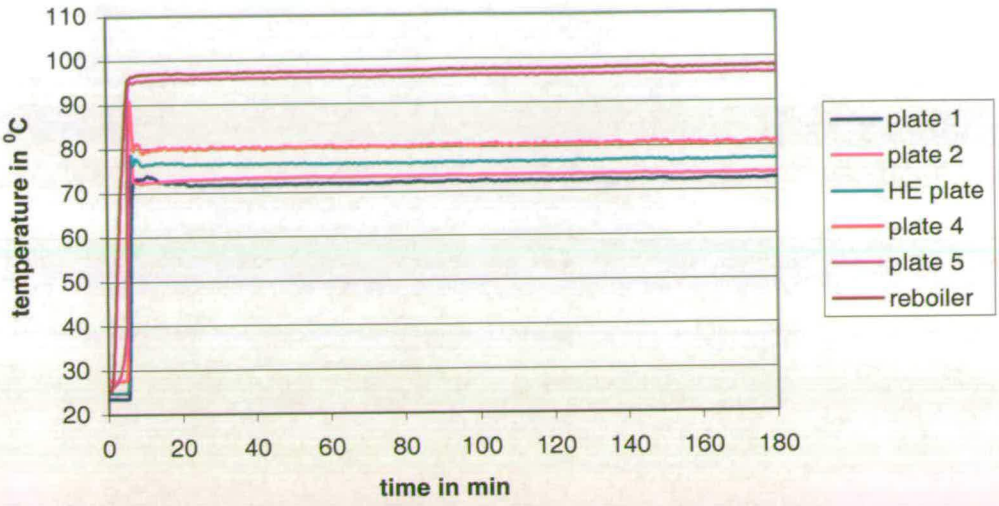

Figure 5.5: Column temperature profile with a reboiler load of 11.2 kW, total reflux; run performed on 10.02.2004.

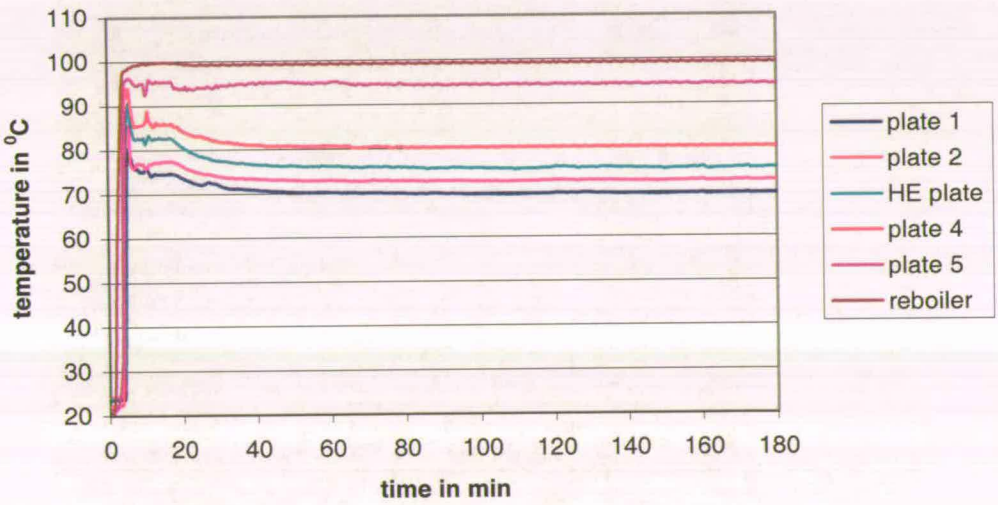

Figure 5.6: Column temperature profile with a reboiler load of 14.4 kW, total reflux; run performed on 22.01.2004.

Steady state is reached after 90 min. A further 30 min were added to be on the safe site concerning sampling. Long time experiments[41], such as in Rivero's experiments with over 8 hours' operation time before sampling [63], were infeasible due to the

[41] Experiments conducted over a period of 6 hours plus

manual control of the column. The rig had to be under ceaseless supervision. Figures 5.5 & 5.6 show that larger temperature differences between the plates, causing bigger concentration gradients along the column, are linked with higher reboiler loads. The same plots were produced for product withdrawal runs. Figures 5.7 & 5.8 show temperature profiles for reflux ratios 1 and 4.

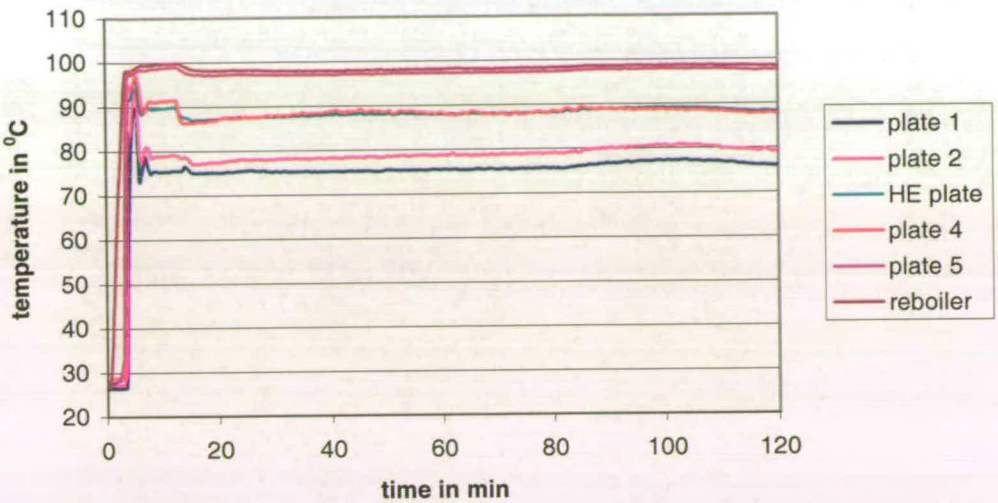

Figure 5.7: Column temperature profile with a reboiler load of 16 kW, feed rate 19 kg/h, reflux ratio: 1.0; run performed on 02.04.2004.

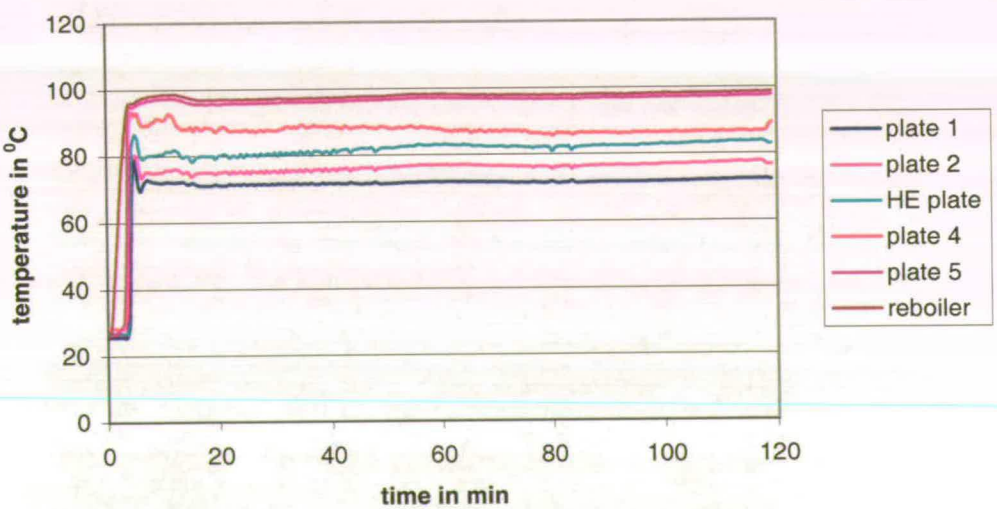

Figure 5.8: Column temperature profile with a reboiler load of 16 kW, feed rate 19 kg/h. reflux ratio: 4.0; run performed on 16.04.2004.

Pseudo steady state was reached within 30–60 min, depending on the reflux ratio. At higher reflux ratios, the achievement of pseudo steady state was longer. Samples were withdrawn after 1h of operation. The wavy pattern in Figure 5.7 is caused by concentration gradients in the feed. It has to be said that there were not many options left due to the fact that the feed rate allowed only a feeding time of about 2 hours. The last point to be controlled was the margin of concentration/temperature change caused by the active heat transfer medium circulating in the heat transfer plate. Figures 5.9 & 5.10 illustrate this for heating and cooling runs respectively.

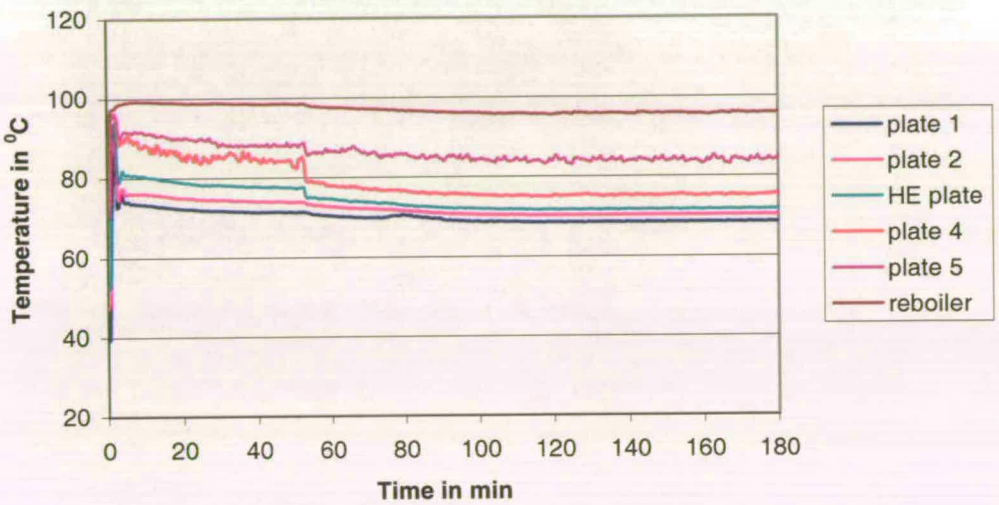

Figure 5.9: Influence of cooling on steady state, total reflux run, 13.6 kW; run performed on 16.01.2004.

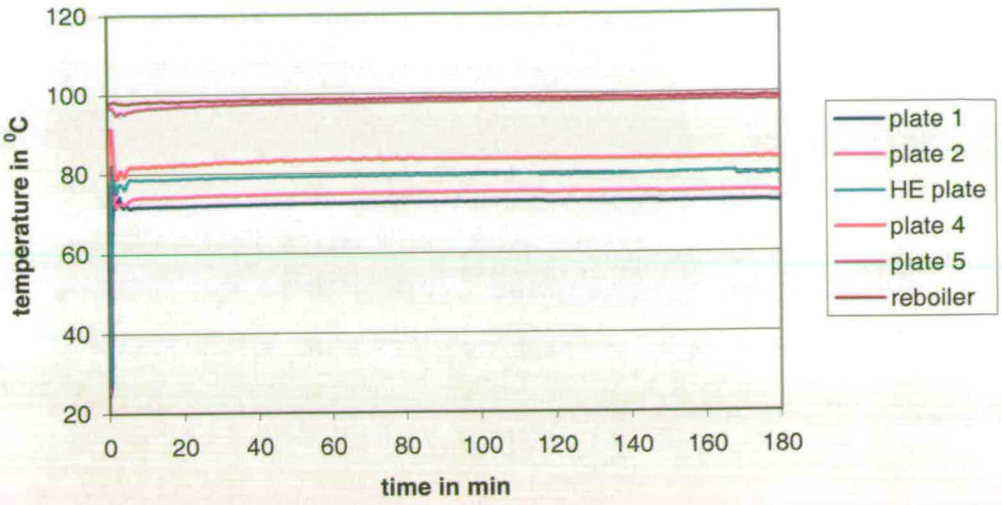

Figure 5.10: Influence of heating on steady state, total reflux run, 12.8 kW; run performed on 11.02.2004.

Similar to the adiabatic runs, steady state is reached in about 90 min. The temperature change is more significant in the case of cooling. One can observe a shift downward, almost parallel to the adiabatic profile. The heating mode in Figure 5.10 shows only a small temperature rise at the beginning of the run (a simultaneous temperature rise on the plates 2 –4 is notable), since less energy is transferred in comparison to the cooling mode. This point will be addressed in the heat transfer coefficient section.

5.2.2 Liquid concentration profiles across the heat transfer plate and the column

The heat transfer plate is equipped with 5 sampling points evenly distributed across the centre line of the column (see also Figure 4.23). Additionally, 5 thermocouples are placed straight above those sampling points, permitting temperature monitoring at those points. The sampling across the plate generates information about the concentration distribution of the liquid on the plate for adiabatic and diabatic runs. Figures 5.11-5.13 show the concentration profiles obtained from different modes.

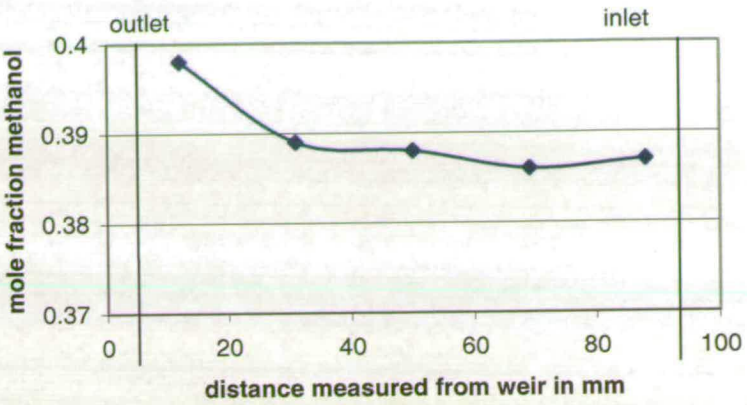

Figure 5.11: Liquid Concentration profile of an adiabatic run; 14.4 kW reboiler load.

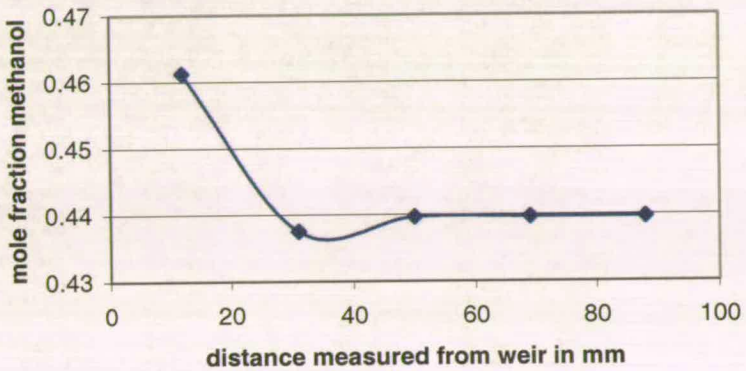

Figure 5.12: Liquid Concentration profile of a heating run; 14.4 kW reboiler load.

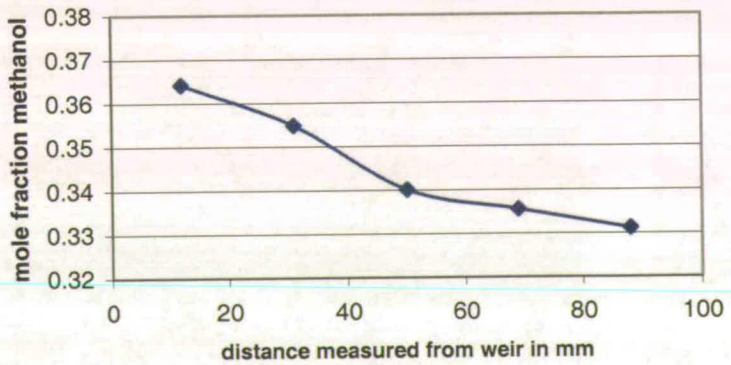

Figure 5.13: Liquid concentration profile of a cooling run; 14.4 kW reboiler load.

The heating mode and the adiabatic run show uniform concentration across the plate, with the exception of the sample point closest to the weir. One notices a sharp concentration rise at this location. This is caused by vapour bypassing over/beside the weir (vapour from the plate below entered the downcomer and pored into the liquid on the tray by flowing over the weir and through the sealant of the PTFE weir and the glass) due to the structural weakness of the PTFE weir and downcomer; thus creating additional vapour liquid contact at this point. Another picture is drawn in the cooling mode. The profile is roughly uniform as far as the centre of the plate, followed by a rise in concentration. It is assumed that the backmixing from the "weir vapour" is stronger due to less turbulent conditions on the plate. This hypothesis might be tested by tracer experiments. However, such experiments ought to be planned and conducted carefully. The plate can be considered as a system with uniform concentration, with the exception of the weir (outlet) region. Consequently, to get samples undisturbed by vapour entrainment, we withdrew liquid samples from the second sample point from the weir.

Another point to be addressed is the comparability of measured liquid concentration profiles[42] and the derived from temperature profiles. By taking the ambient pressure into account, the liquid concentrations were calculated from the temperatures on the plate using the Wilson VLE model. The heat transfer tray with its sample ports was used to compare the two profiles. The results of such a comparison are given in Table 5.4 including deviations between those two compositions.

	Adiabatic run	Heating run	Cooling run
MeOH concentration measured in mole %	20.9	45.7	13.9
MeOH concentration from temperature in mole %	21.4	46.1	15.3
Relative deviation[43] in %	2	1	10

Table 5.4: Comparison of measured and calculated methanol concentrations.

[42] The samples were withdrawn from the sampler second closest to the weir.
[43] Deviation from measured concentration.

The results suggest that the temperatures obtained from adiabatic and heating modes can be used for concentration calculations in a straightforward manner; but caution is demanded in the cooling mode by the conversion of temperature profiles from the heat transfer plate. Measured and calculated methanol concentrations can deviate up to 10% in the case of total reflux. This over-prediction of the calculated values can be explained by having slightly sub-cooled liquid on the plate. The observed deviation corresponds to sub-cooling of roughly 0.8 deg C. Nevertheless, the temperature profile across the column can be used for the visualisation of concentration profiles, taking a correction for the heat exchanger plate in the cooling mode into account. Such profiles are given in Figures 5.14 & 5.15.

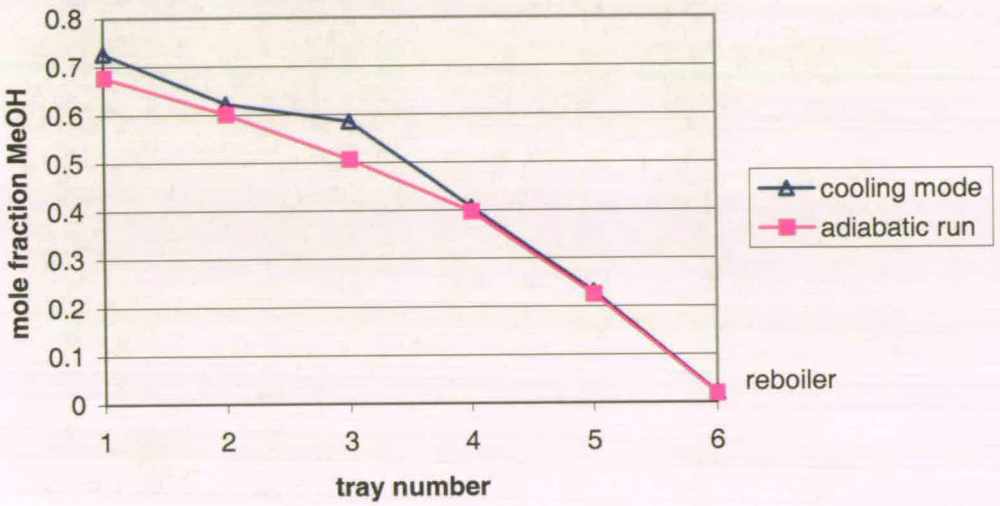

Figure 5.14: Comparison between adiabatic and cooling mode run composition profiles; 12.8 kW reboiler load.

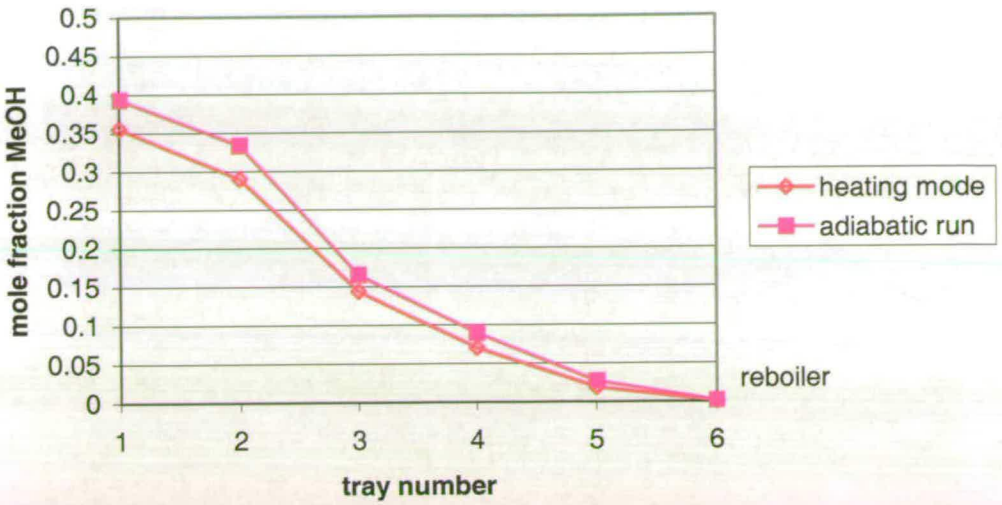

Figure 5.15: Comparison between adiabatic and heating mode run composition profiles; 12.8 kW reboiler load.

The Figures reveal an abrupt change in composition at the heat transfer plate (plate number 3). It is larger for the cooling mode due to a larger amount of heat transferred (800 W in cooling mode vs. 370 W in heating mode). However, the heat transferred to the plate inflicts a temperature shift down the whole column. Heat removed from the plate creates a deviation on the heat transfer plate and on the plate above, but not on the plates underneath. This could be an indication of sub-cooled liquid on the plate. Product withdrawal might influence this pattern, which was obtained under total reflux. This is illustrated for two reflux ratios (1 & 3) in Figures 5.16 & 5.17.

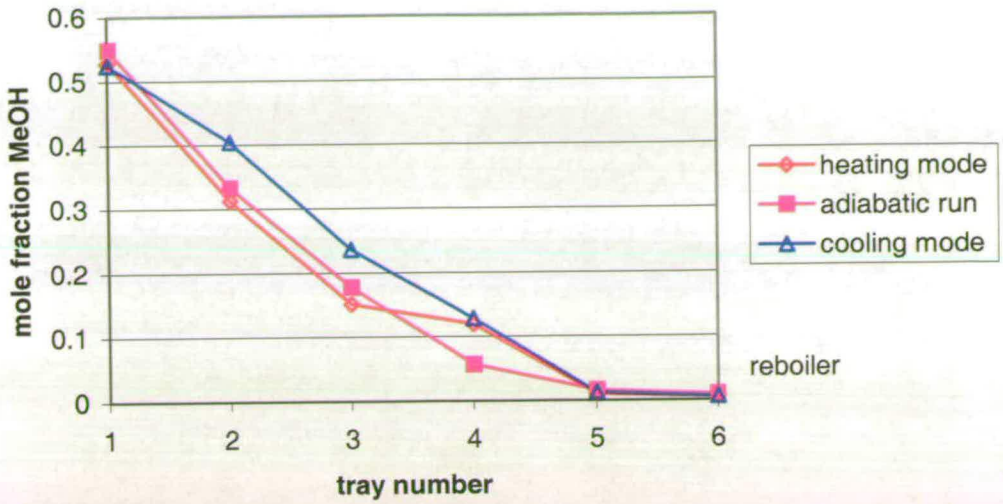

Figure 5.16: Comparison between adiabatic and diabatic run composition profiles; 16 kW reboiler load, reflux ratio 3.

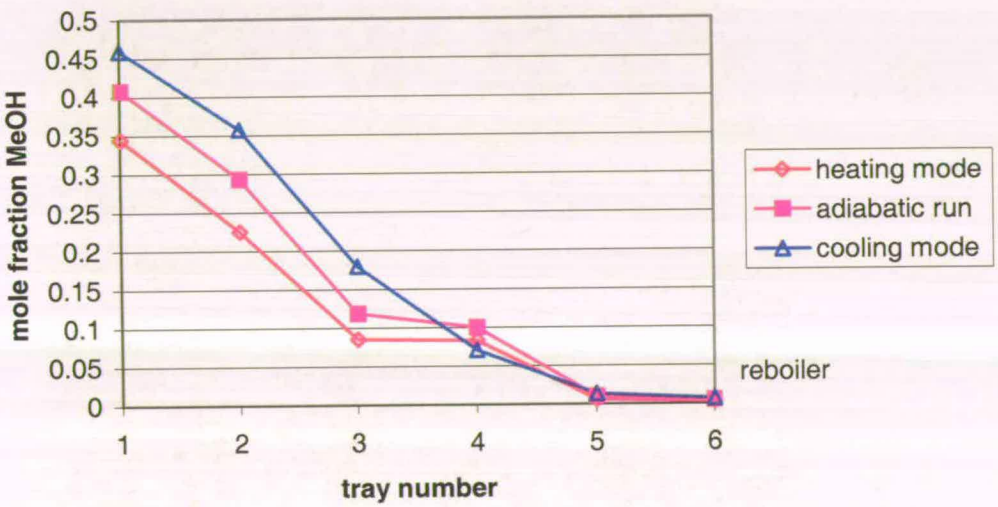

Figure 5.17: Comparison between adiabatic and diabatic run composition profiles; 16 kW reboiler load, reflux ratio 1.

The reboiler load of 16 kW was chosen to maximise the separation between the plates concerning the vapour flow, therefore compensating for the diminishing effect of reduced reflux on composition profiles by product withdrawal. It is noticed that smaller reflux ratios lead to carry-over of the heat transfer effects to adjacent plates.

This is mainly the result of reduced residence time of the fluid in the column. There is less time to balance the effects like in the case of total reflux.

5.3 Heat transfer coefficients on sieve trays

All diabatic experiments simultaneously produced heat transfer data. Preliminary experiments were conducted with distilled water for the commissioning of the experimental rig, which also delivered the first heat transfer data available. Although dependent on geometry, overall heat transfer coefficients (U_p), based on the plate surface area, are the most accessible; hence they are treated first.

5.3.1 Overall heat transfer coefficients

Experimental U_p values were obtained by using the measured heat flux, heat transfer medium (HEM) inlet/outlet temperatures, and the froth temperature in eqn. 3.71. The water-only system was only investigated briefly. With two different HEM flow rates (48.0 & 73.8 kg/h) the values varied between 2.4 and 2.6 kW/m^2 K.

The methanol-water system was subject to a detailed series of experiments. U values were compared between heating and cooling modes with different HEM flow rates. Table 5.5 shows the influence of the HEM flow rate on U.

HEM flow rate in kg/h	U for cooling mode in kW/m^{2}K	U for heating mode in kW/m^{2}K
19.8	2.2	1.6
28.8	2.6	1.9
48.0	3.4	2.7
67.8	3.9	3.1
85.8	4.3	3.7

Table 5.5: U values for various HEM flow rates; 15 kW reboiler load.

The measured results spread about +/- 4%, which is acceptable for engineering applications. The U values rise with increasing HEM flow rates, which appears

logical since there will be higher heat transfer effect inside the duct, due to higher turbulence. U appears somewhat higher in the cooling mode than in the heating mode. The flow rate of 85.8 kg/h marked the upper limit for our experimental heat transfer plate. Under these conditions, a maximum of 50 kW/m^2 in the heating mode, and 110 kW/m^2 in the cooling mode could be transferred or removed from the plate (Exceeding this flow rate led to leakage of HEM into the system[44]).

The experimental U were compared with calculated values, based on eqn. 3.70, 3.83 & 3.85. The results are in good agreement as can be seen in Figure 5.18. (This is not surprising, because both approaches use the same temperature data, but slightly differently. Even if either of the two coefficients (h_i, $h_{p\text{-}f}$) in eqn 3.70 is miss-predicted, the equation will balance this effect by misspredicting the other.)

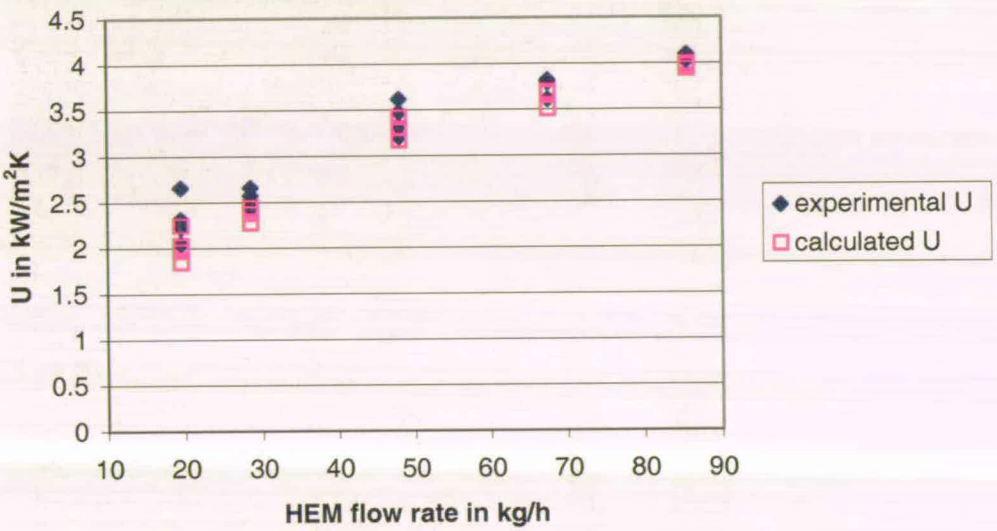

Figure 5.18: Comparison of experimental and computed[45] U values; cooling mode, 15 kW reboiler load.

The significance in the determination of U lies not in development of accurate prediction methods. It is the revelation of boundaries of feasibility related to a particular geometry. They are also a useful tool for economic optimisation in the

[44] This was evaluated during test runs by pumping HEM through the plate with no liquid inside the column.
[45] The spread of the computed values is caused by the different heat fluxes of the data set used.

design of adiabatic columns. This point will be picked up later on. It is important to understand the contributions to U and where they come from. A simple tool such as a plot of 1/U vs. Re_i^{-1} resolves the question whether the plate-to-fluid film coefficient $h_{p\text{-}f}$ is constant for different flow rates of HEM. If all of the variation in U can be accounted for by variations in h_i, then this plot should be approximately a straight line. The data are plotted in Figures 5.19 & 5.20. Since the variation in U cannot, on the evidence of these plots, be wholly accounted for by the variation in h_i, it is probable that $h_{p\text{-}f}$ is not constant in this series of experiments.

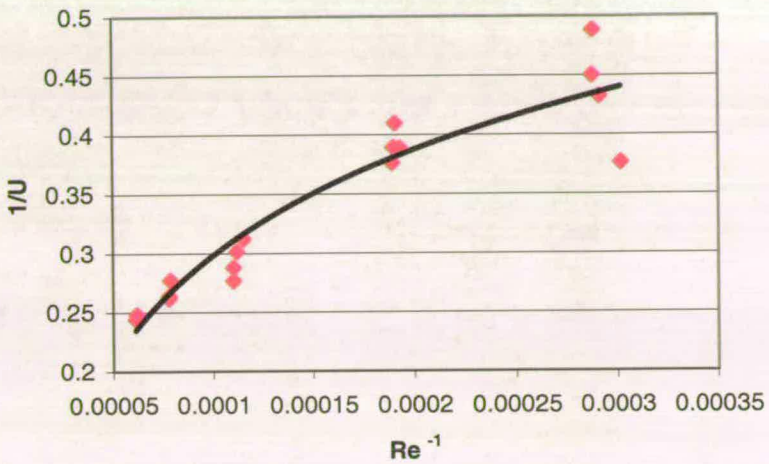

Figure 5.19: Plot 1/U vs Re^{-1} for methanol/water; 15kW; heating mode.

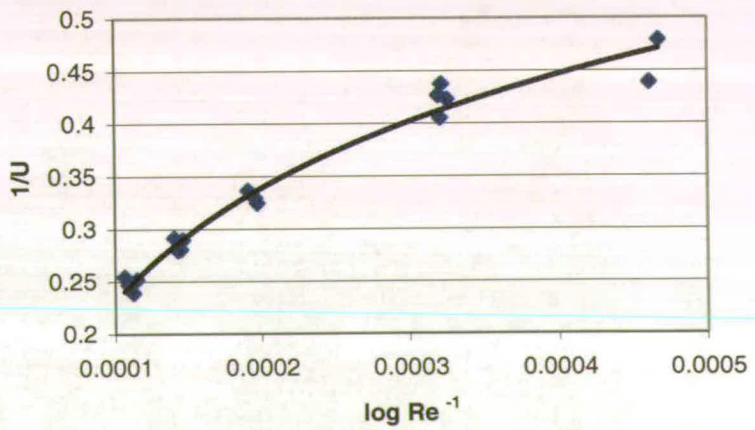

Figure 5.20: Plot 1/U vs Re^{-1} for methanol/water; 15kW; cooling mode.

The results from the Figures above require a more detailed analysis of the film heat transfer coefficient h_i and the plate-to-fluid heat transfer coefficient h_{p-f}. The next sub-Chapter is dedicated to this task.

5.3.2 Plate-to-fluid heat transfer coefficients

The predicted values of h_{p-f} presented here are based on the recommendations made in Chapter 3, which are compared with measured values of h_{p-f}. Furthermore, h_{p-f} are related to the heat transfer models proposed in Chapter 3. A final consideration is given to the influence of reflux ratio on h_{p-f}, a parameter that has not been considered in the heat transfer models.

5.3.2.1 Prediction of h_{p-f}

Calculated h_i values were used to determine h_{p-f}. Table 5.6 shows that in the heating mode,h_i and h_{p-f} are of comparable significance for the overall heat transfer coefficient. Additionally, h_{p-f} increases as the HEM flow rate (and the rate of on-tray boiling) increases. The reboiler load was kept constant in this series of experiments.

HEM flow rate kg/h	h_i kW/m^{2}K	h_{p-f} kW/m^{2}K	U kW/m^{2}K
28.8	3.5	4.7	1.8
48.0	5.1	6.8	2.6
67.8	6.5	7.4	3.1
85.8	7.8	8.0	3.6

Table 5.6: h_i and h_{p-f} values for heating runs; 15 kW reboiler load.

A completely different situation was encountered in the cooling mode in which it was shown that, since h_{p-f} values were usually 2 – 10 times larger than h_i values, h_i is dominant in the overall heat transfer coefficients. Furthermore, the h_{p-f} values remained roughly constant with increased HEM flow rates. (However, the theoretical h_{p-f} values calculated for the cooling runs are not shown, since they are obtained from an inferred value of T_p; and we believe that these calculated T_p values are not

representative due to uncertainties in h_i in the lower transition region, leading to unrealistically high values of h_{p-f}). A plot of predicted h_{p-f} values of the cooling mode can be found in Appendix B. Values for h_i based on Re < 5000 caused an overprediction by a factor of 3. Higher values of Re still caused an overprediction by factor 1.2 –1.7.

We were able to obtain experimental h_{p-f} values by using a built-in thermocouple to measure T_p within the Dural plate and computing the coefficients using eqn. 3.91. Table 3 shows experimental h_{p-f} values acquired.

	heating	cooling
HEM flow rate kg/h	h_{p-f} kW/m^{2}K	h_{p-f} kW/m^{2}K
19.8	3.1	11.3
28.8	3.8	10.8
48.0	7.2	11.0
67.8	8.7	10.8
85.8	10.3	12.6

Table 5.7: Experimental h_{p-f} values for heating and cooling runs respectively: 15 kW reboiler load.

The experimental h_{p-f} values were compared with the previously predicted values. As stated before, the h_{p-f} values so calculated in the cooling mode were unrealistically large. This could be an effect of (entrance effects etc.) mispredicting h_i in the transition region, entrance effects etc. Therefore it seems that our proposed h_i equation is not wholly appropriate for the transition region. (An alternative approach, demanding additional data, would be to determine h_i values from the experimental h_{p-f} values, then search for a more appropriate h_i correlation for this region of Re.)

The prediction of h_{p-f} values in the heating mode was more successful. This is illustrated in Figure 5.21. The h_i - based correlations appear to over-predict h_{p-f} in the low Re region and under-predict h_{p-f} in the high Re region respectively. Nevertheless, the method gives constant results and is useful for engineering purposes.

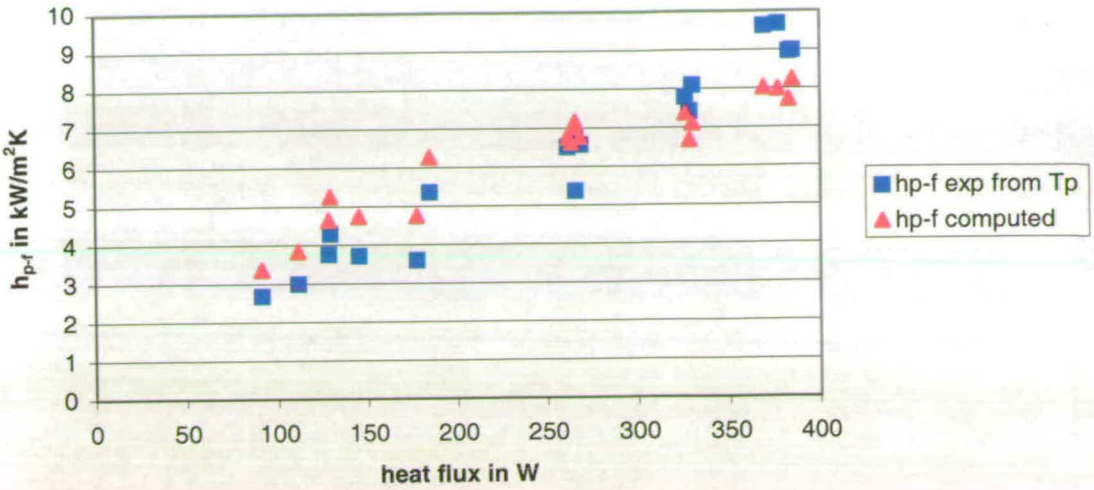

Figure 5.21 Experimental and computed h_{p-f} values vs. heat flux transferred; heating mode; 15 kW.

5.3.2.2 Test of heat transfer models for h_{p-f}

In order to verify or disprove our heat transfer models, we need to determine values for the powers n & m in eqn 3.72 & 3.73. This can be achieved by logarithmic plots. Those plots of h_{p-f} vs (T_p-T_f) (heating)[46] and h_{p-f} vs V (cooling)[47] are displayed in Figure 5.22 & 5.23. In Figure 5.22; although the data are scattered, they are indicative of a nucleate boiling mechanism, with $h_{p-f} \alpha (T_p-T_f)^{0.9}$.

[46] Based on h_{p-f} in W.
[47] Based on h_{p-f} in kW.

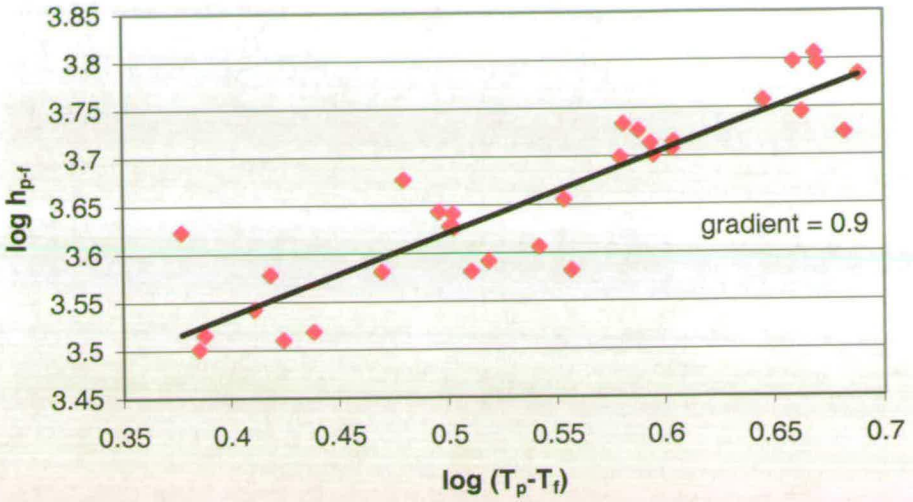

Figure 5.22: Log h_{p-f} vs log (T_p-T_f); heating mode; MeOH-H_2O; 15 kW.

Figure 5.23 suggests that, in experiments in which the value of h_i was kept constant by applying a constant HEM flow rate, h_{p-f} is substantially independent of V. This in turn indicates that, in the already-turbulent froth regime on the heat transfer plate, h_{p-f} is not influenced by V. The spread of data within a the same reboiler load did not exceed +/- 3%. Consequently, no further efforts were put into unscrambling eqn. 3.74.

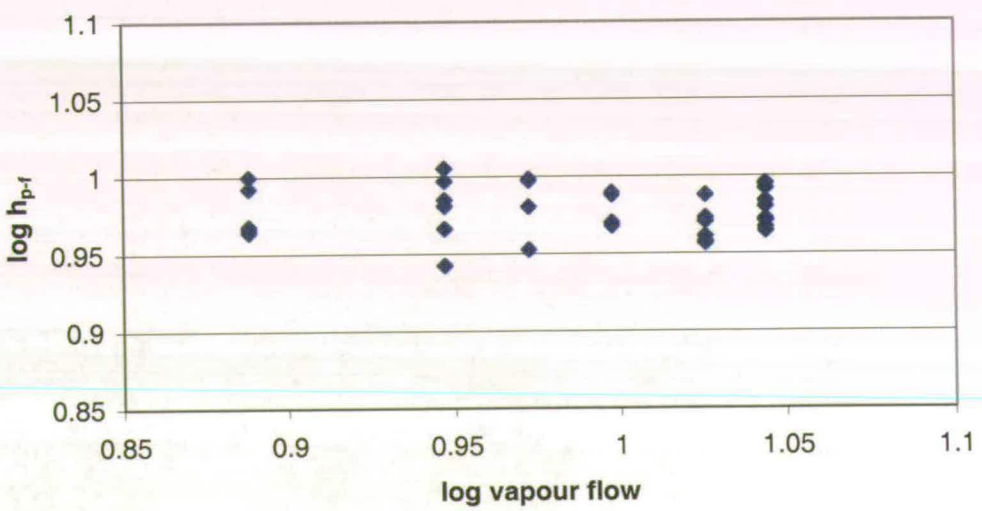

Figure 5.23: Log h_{p-f} vs. log vapour flow (l/s); cooling mode; MeOH-H_2O; 15 kW.

5.3.2.3 Influence of reflux ratio on h_{p-f}

The heat transfer models previously developed considered the impact of vapour load and heat flux. The last parameter to be treated; as outlined in Chapter 4, is the impact of the reflux ratio[48] on h_{p-f}. This was examined by a series of product withdrawal runs. Heat flux and reboiler load were kept constant. Figures 5.24 & 5.25 display the influence of the liquid load (varied by altering the reflux ratio) on h_{p-f}. The feed rate (19 kg/h) and the heat fluxes were kept constant. h_{p-f} increases with an increasing liquid load as shown in Figure 5.24. This can be related to an increase of liquid-phase turbulence with the increasing liquid flow caused by the higher reflux ratios. Visual evidence of the increased turbulence is an accompanying increase of the froth height on the heat exchanger plate.

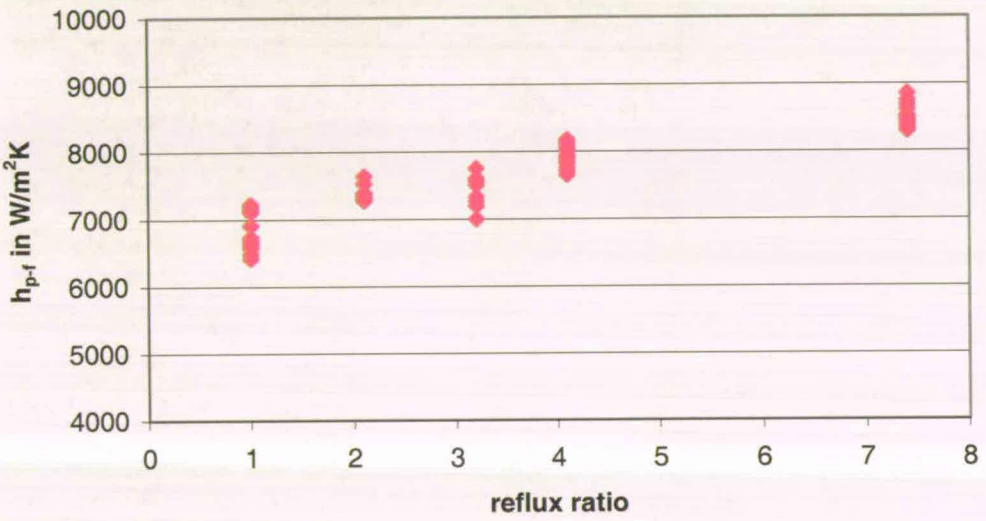

Figure 5.24: h_{p-f} vs. reflux ratio; heating mode (heat flux:31 kW/m^2).

A different situation is encountered in the cooling mode, displayed in Figure 5.25. Initially, the h_{p-f} values fall with increasing reflux ratio, then remain roughly constant for R > 4. This pattern ought to be verified by additional experiments, in order to exclude the possibility that h_{p-f} is actually affected by the reflux ratio. A definitive answer could be obtained by conducting more extensive heat transfer research

[48] Liquid flow across the plate.

carried out by recording temperature distribution (horizontally & vertically) with an infrared camera).

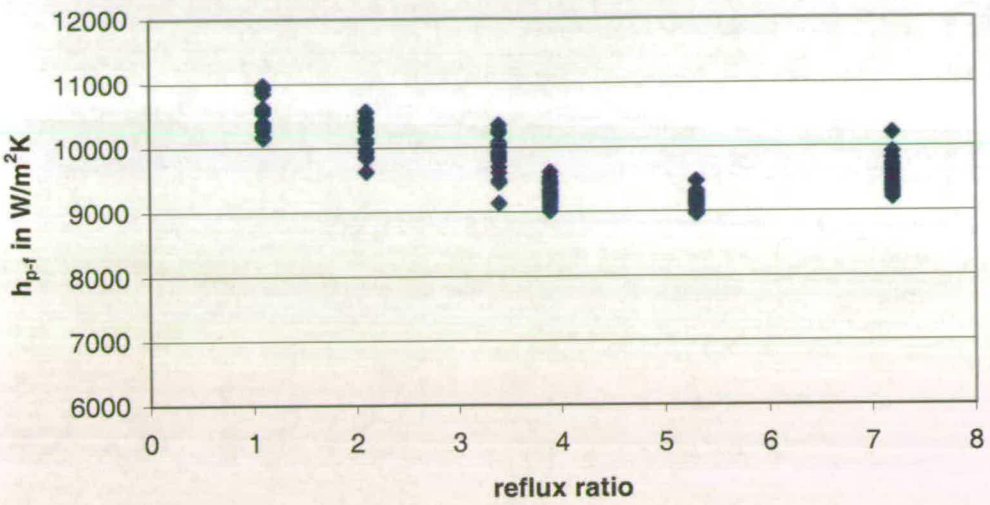

Figure 5.25: h_{p-f} vs. reflux ratio; cooling mode (heat flux: 100 kW/m^2).

Although the data recording procedure for monitoring heat transfer coefficients was fairly simple (measurement of liquid flow rates in calibrated rotameters and temperature profiles with thermocouples) some problems were encountered. First of all, some data scattering was caused by fluctuations of the pump driving the HEM. Although those fluctuations were recorded instantly by the computer–linked thermocouples, this was not the case for the monitoring manually-set rotameters. Therefore, discrepancies were created by combining those two sets of data in the calculation heat transfer coefficients. Additionally, those fluctuations could lead to disturbance of the fluid dynamics, hampering the maintenance of steady state.

The heat transfer coefficients obtained (U & h_{p-f}) look promising. With U 4 – 8 times larger than in Nakaiwa's experimental HIDiC [136], this could help to compensate for the reduced heat transfer area in a diabatic trayed column in comparison to the packed column approach. They could be implemented in simulations of diabatic distillation columns using the proposed or similar tray designs. Nonetheless, two points ought to be mentioned. First, deviations between the composition profiles derived from temperature profiles and measured compositions in the cooling mode, and constant h_{p-f} in the cooling mode, raise the suspicion that sub-cooling of liquid

(at least partly) takes place. This would not coincide with the purpose of condensing vapour on the plate. Sub-cooling is likely, because the liquid-vapour ratio at the plate surface is in favour of the liquid due to the fact that bubble growth is still in progress and bubble detachment has not yet occurred at this very place. The problem could be reduced or even eliminated, by reducing the temperature difference between the plate and the fluid by reducing the heat load removed from the plate (the HEM flow rate difference could be adapted to match the maximum heat load in the heating mode, for instance). Second, the design and placement of our heat exchanger plate does not maximise the amount of vapour condensed. An ideal "condenser" ought to be in contact with pure vapour. Therefore, a logical placement would be out of the froth, in the spacing between two plates. Due to the nature of our plate, which works simultaneously as heat exchanger and sieve tray, this approach is impractical. How the overall heat transfer coefficient will be affected in such "ideally positioned" condensers are another matter.

A final consideration ought to be given to the temperature distribution on the heat transfer plate. Although the claim of uniform temperature distribution (horizontally and vertically) is reasonable; proof of this assumption would be welcome. This might be achieved by conducting experiments with a modified heat transfer plate (equipped with thermocouples in different positions) or by simulating the temperature distribution with appropriate heat transfer software. We believe that the temperature is uniform between the heat transfer ducts, but this might not be the case at the periphery of the plate. If this were so, then our thermocouple measuring the plate temperature would deliver unrepresentative temperatures.

5.3.3 Conclusion

Heat fluxes up to 50 kW/m^2 were transferred to the plate. In the cooling mode, heat fluxes up to 110 kW/m^2 could be removed from the plate. It was shown that the overall heat transfer coefficient (U) is mainly controlled by the vapour load (and thus the degree of turbulence on the plate) and by the internal film coefficient h_i of the heat transfer medium (HEM) and to a lesser degree by the liquid load. The impact of h_i on U was stronger in the cooling mode since h_p-values were 2-10 larger than the

corresponding h_i values. Influenced by the aforementioned variables, U varied from 2.2 - 4.0 kW/m^2K. Furthermore, at comparable HEM flow rates (and thus h_i values), U is slightly higher in the cooling mode than in the heating mode.

Geometry-independent plate-to-fluid heat transfer coefficients (h_{p-f}) were monitored in the heating and cooling mode respectively. Measured values of h_{p-f} ranged from 3 – 9 kW/m^2 K, depending on the temperature difference between the plate and fluid, and 9 – 11 kW/m^2 K for the cooling mode, which remained unaffected by the vapour flow. An approach was attempted to predict h_{p-f} and relate this to simple heat transfer models. While the prediction method failed to produce satisfying results for the cooling mode, it was capable of producing satisfactory predictions for the heating mode. Furthermore, it was found that $h_{p-f} \alpha (T_p-T_f)^{0.9}$, which appears to confirm our proposal that the mechanism is that of enforced nucleate boiling.

5.4 Tray efficiencies

Adiabatic distillation leads to change of conditions on sieve trays. Inevitably, tray efficiencies will be affected thereby. The influence of three key parameters (heat flux, vapour load and liquid load) was investigated. Of particular interest was the impact of the heat flux, which directly manipulates the other two parameters. The results obtained from diabatic runs were compared with adiabatic runs, which served as benchmarks.

5.4.1 Influence of vapour load on tray efficiency

We first investigated the change in Murphree tray efficiencies resulting from changes in the vapour flow rate. The vapour rate effect was visualised by the change of the froth height. The heat transfer rates were kept constant for the heating mode (28 kW/m^2) and for the cooling mode (85 kW/m^2) respectively. All experiments in this set were conducted under total reflux.

As expected, Murphree efficiency increased with increasing vapour flow rate. The Murphree tray efficiency results are shown in Figure 5.26. In the heating mode, an

efficiency gain of approximately 7% could be achieved across the range of vapour flow rates. In the cooling mode there was an efficiency reduction, becoming more pronounced in comparison to the adiabatic efficiencies (3% - 18%) with increasing vapour load. This can be explained by the extremely low efficiencies obtained at low vapour flow rates, at which the bubble regime dominates. In the froth regime, obtained at higher vapour rates, the efficiency is more strongly influenced by vapour flow rate.

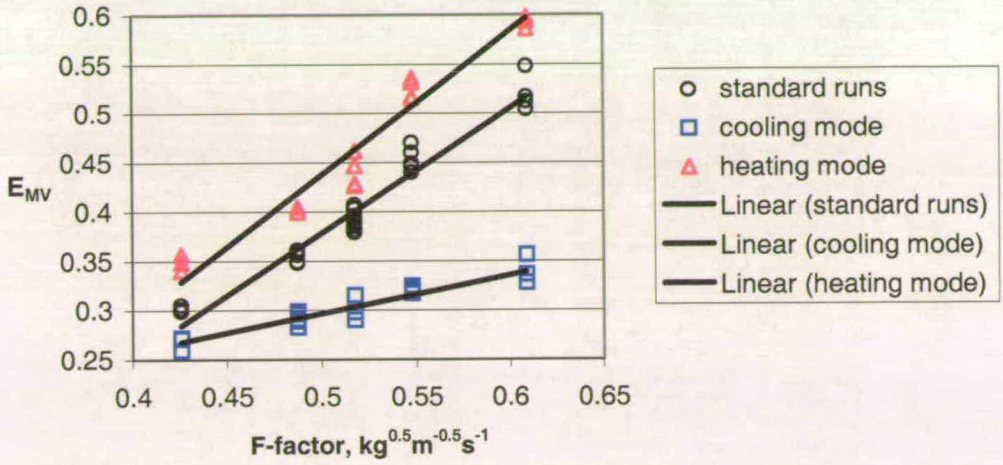

Figure 5.26: E_{MV} vs. F-factor.

These efficiencies might appear low in comparison to values reported in the literature [157, 178, 193 & 195]. This is principally because even the maximum reboiler load was not enough to create an optimal operating zone in the vapour space between the trays. The column diameter was too large for the reboiler available, and thus produced vapour flows too low for "ideal conditions". On the other hand, we made sure – by reducing the fractional free area on the trays – that the vapour flow was sufficiently high in the holes. Working with existing material and insisting on the 150 mm column diameter (we had hopes to detect any significant concentration changes across a 150 mm tray) was a compromise, which led to suboptimal tray efficiencies. Higher efficiencies could be achieved by either using a more powerful reboiler or blocking off parts of the column, hence effectively reducing the column diameter.

5.4.2 Influence of direct heat transfer on tray efficiency

Further experiments examined the effects on efficiency of the heat transferred to or removed from the tray, when the vapour load was maintained constant. As in the set of experiments aforementioned, the runs were performed under total reflux. The results are shown in Figures 5.27 & 5.28. The difference between the two heat loads can be explained by taking the different ΔT_{LM}s of the heat transfer medium and the fluid on the plate into account (20 - 25 deg C for the cooling mode and 5 - 8 deg C in the heating mode). Although a higher heat load can be transferred by applying a higher ΔT_{LM}, high ΔT_{LM}s may only be achieved in heat integrated distillation at the expense of work of compression. The temperature difference between the plate and the fluid was 5 – 10 deg C for the cooling mode and 2.5 – 3.5 deg C for the heating mode, depending on the heat flux. The rather big difference between the plate and the fluid bolster the suspicion that liquid on the tray is sub-cooled. Furthermore, the experiments showed that direct heat integration has a bigger impact on tray efficiency than the equivalent change in reboiler heat load, since the effect of the latter may be attenuated by heat losses along the column.

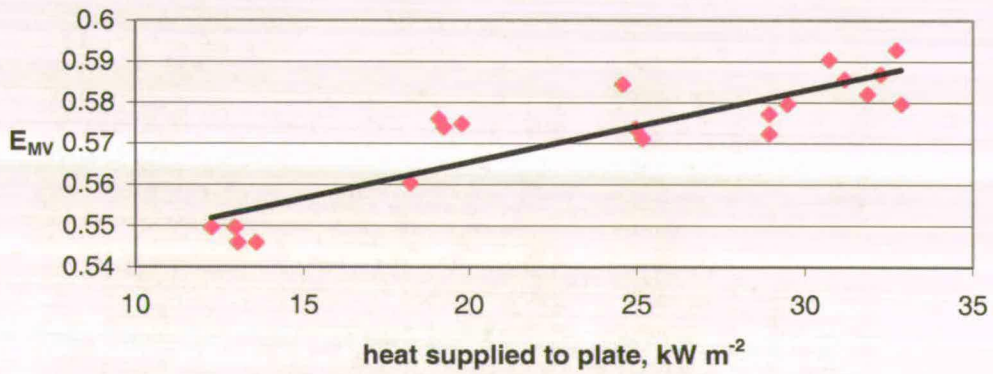

Figure 5.27: E_{MV} vs. heat load transferred; cooling mode; constant vapour load (0.48 kg s^{-1} m^{-2}).

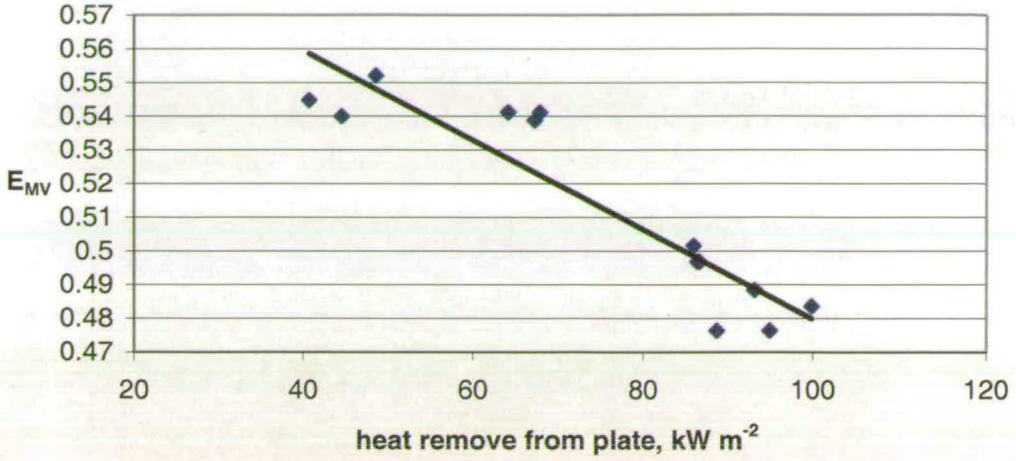

Figure 5.28: E_{MV} vs. heat load transferred; cooling mode; constant vapour load (0.48 kg s^{-1} m^{-2}).

Again, as previously mentioned, the upper limit of vapour flow in our column, restricted by the reboiler performance, may have restricted the maximum separation performance of the sieve trays. Each change in heat transfer led to a considerable change in the efficiency.

5.4.3 Influence of reflux ratio on tray efficiency

This set of experiments, designed to determine change of heat transfer coefficients also produced tray efficiency data. The experiments investigated the effects on efficiency of the reflux ratio (R) for each mode, when the on-tray heat flux and the boil-up rate was maintained constant. The apparatus was run with maximum reboiler load (16 kW) to counter the effect on separation of introducing a feed to the column. The feed rate was kept constant at 19 kg/h. An adiabatic run served as a reference. The results are given in Figures 5.29 – 5.31.

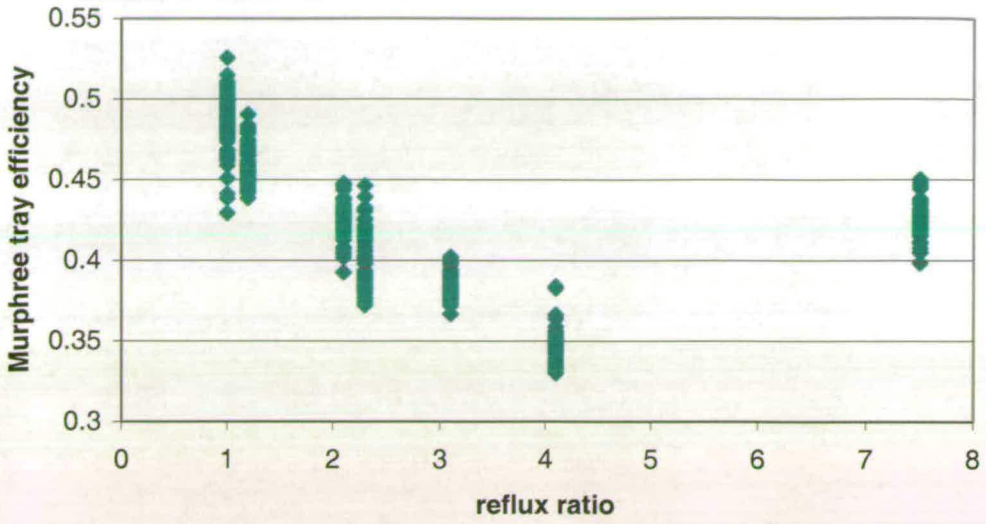

Figure 5.29: Murphree tray efficiency vs. reflux ratio[47]; adiabatic runs.

An initial drop in the efficiency as r increases, followed by a recovery, can be observed in all three cases. This phenomenon could be explained by the shorter contact time of the vapour-liquid mixture caused by higher liquid loads. This effect is compensated as total reflux is approached, increasing the height of liquid on the tray and thus increasing residence time of the liquid on the tray again (a rigorous tracer experiment sequence leading to residence time plots could clarify this matter). Additionally, higher reflux ratio created larger mass transfer areas.

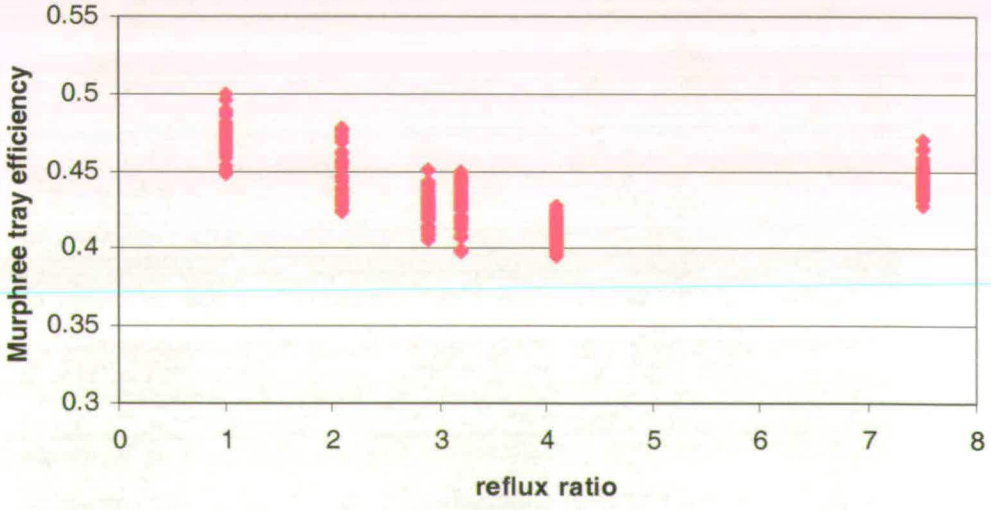

Figure 5.30:Murphree tray efficiency vs. reflux ratio[47]; heating mode (heat flux: 31 kW/m^2).

The efficiency drop is less distinct in the heating mode as shown in Figure 5.30. The increased froth height might have a compensating effect. Froth heights in the glass section were measured by scale. Froth heights increased by 20% for heating mode runs and dropped by 10-15% in the cooling mode. Froth height tables for runs with different reflux ratios can be found in Appendix C. The froth height was not only influenced by the heat flux transferred or removed from the plate, but also by the temperature on the plate. Lower temperatures (higher methanol concentrations) caused higher froth heights. This can be linked to the lower surface tension obtained in methanol-richer systems.

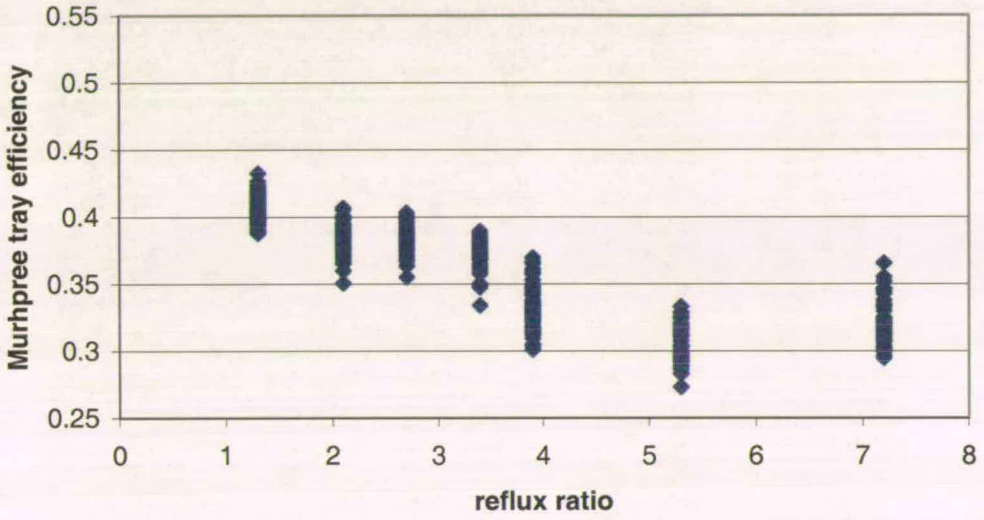

Figure 5.31: Murphree tray efficiency vs. reflux ratio[49]; cooling mode (heat flux:100 kW/m^2).

The measured efficiencies at particular reflux ratios show substantial scatter. The average deviation with a particular reflux ratio (r) group was -/+ 5%. Additional experiments covering the gap between r 4 and r 8 would clarify the observed trends. Going beyond r = 8 might be theoretically interesting (but in practice difficult to achieve with our rotameter-based reflux ratio controller. A much more accurate controller would be needed for such experiments).

[49] Boil-up rate was kept constant (V constant); only the liquid varied.

The last set of experiments produced the largest set of tray-efficiency related data. This was definitely linked with the experience gained during the period over which the experiments had been conducted. The practised routine of operation allowed us to look at other aspects, which had not been considered quantitatively due to trouble shooting. The biggest reason for concern was the sampling procedure. The liquid sampling and the analysis delivered consistent results. With a cycle time of 5 min, it was clear that the wealth of tray efficiency data would not be as impressive as the temperature data. The inability to measure vapour and liquid samples simultaneously reduced the numbers of samples further. However, the major problem was the interruptions caused by flooding the vapour sampling system. Not only did they lead to delays in terms of vapour sampling, they also – in some cases – produced disturbance in the following samples from residual liquid droplets somewhere in the sample loop. The system purge was always laborious and time-consuming. The latter factor proved to be particularly fatal in product withdrawal runs. Only careful and meticulous valve handling, gained by growing experience, could overcome the problem of flooding the sample lines. More sensitive valves and additional equipment are probably necessary for better vapour sample stream control and monitoring. Still, vapour sampling remains troublesome and ought to be avoided. An alternative would be the use of liquid concentrations only for the calculation of Murphree tray efficiencies. This approach replaces y_n with x_{n+1} and y_{n-1} with x_n respectively. Of course, this is only valid for systems under total reflux, where the liquid flow rate (L) equals the vapour flow rate (V). Strictly speaking, it is only applicable to adiabatic distillation, because any diabatic manipulation will inevitably lead to changes in L and V. Another alternative would be total condensation of the vapour samples as recommended by Kastanek (1967) [153]. On the other hand, this would sacrifice the online analysis capability of the existing system.

5.4.4 Conclusion

A 150 mm diameter distillation column with a diabatic section has been used with MeOH / water system to generate Murphree tray efficiencies (E_{MV}) on a single, heat transferring sieve tray. Heat flux, vapour load and reflux ratio were varied in order to

investigate the impact of these variables on E_{MV}. The transfer of approximately 40 kW m^{-2} led to an E_{MV} increase of 7% regardless of the vapour flow rate. Heat removal of approximately 90 kW m^{-2} caused a efficiency drop of 3 – 18%, the efficiency difference between adiabatic and cooling mode steadily rising with the vapour load. The efficiency change is associated with a froth height change, which alters the mass transfer area available. Variations in heat flux in both modes led to a larger E_{MV} change than an equivalent alteration of the reboiler load.

The E_{MV} data obtained here may be used in the modelling of diabatic distillation columns. The decrease of E_{MV} in the cooling mode occurring in the rectifying section, and the increase of E_{MV} in the heating mode occurring in the stripping section mark this kind of diabatic distillation as ideal for the separation of high purity bottom products. The sacrifice of stages in the rectifying system is irrelevant in such a system and outweighed by the increased tray efficiency in the stripping section. In general, a trayed diabatic distillation system can be successfully applied where the application of heat pumps is favourable.

5.5 Suggested Heat transfer plate improvements

Although the heat transferring plate was able to produce satisfactory results in terms of obtaining heat transfer coefficients and Murphree tray efficiency values under diabatic conditions, its performance was limited due to some material restrictions:

The HEM flow rate was limited to 85.8 kg/h. Exceeding this flow rate led to water leakage into the system, affecting the composition of the test mixture. (The weak spot was the contact area between the Dural and the PTFE of the plate: additional sealant, to withstand the fluid pressure, is recommended. However the material properties of PTFE make it impossible that anything could be attached to its surface, so this can only be achieved by replacing the PTFE adjacent to the Dural)

The weirs made of PTFE proved to be inadequate. The weirs began to distort under the influence of the process fluid temperature; leading to lower liquid levels on the trays. Replacing the PTFE weirs with Dural ones could solve this problem (as long as the weir is separated from the Dural plate by some kind of sealant in order not to affect the heat flux from the tray).

Chapter 6

Conclusions and Recommendations for Future Work

6.1 Conclusions

1. A literature survey was conducted that considered heat integration in distillation columns. In particular, direct heat integration established between a high pressure rectifying section and a stripping section in packed columns (the HIDiC concept) was reviewed. The survey revealed a paucity of experimental studies, especially in the application of such a concept in trayed towers.

2. A novel heat transfer (diabatic) sieve tray was designed and implemented in a 150 mm diabatic column. The plate either transferred heat to or removed heat from the plate surface. The adjacent surroundings were insulated with PTFE, thus ensuring that all heat transfer occurred at the plate surface. Distilled water was used as heat transfer medium (HEM) in the diabatic sieve tray at flow rates up to 85.8 kg/h.

3. A system for online quantitative analysis of liquid and vapour samples was developed, and the resulting gas chromatography (GC) method calibrated with methanol-water mixtures. Samples could be analysed with a relative standard deviation of 0.5%. The vapour samples were withdrawn isokinetically, and premature condensation was prevented and by using heated sample lines and by dilution with N_2.

4. The experimental plate was operated in diabatic mode as reference, and in cooling and heating modes respectively. Runs were performed under total reflux and at various reflux ratios. Temperature monitoring across the heat transfer plate and along the column was used to identify start-up periods and steady state. The temperature profile was used to predict the composition profile. These profiles were compared with liquid samples from the heat transfer plate. Concentration profiles from adiabatic and heating runs were in good agreement with the measured profile. The results from the cooling mode deviated to a certain degree, indicating sub-cooling on the plate.

5. Heat fluxes up to 50 kW/m^2 were transferred to the plate. In the cooling mode, heat fluxes up to 110 kW/m^2 could be removed from the plate. It was shown that the overall heat transfer coefficient (U) is mainly controlled by the vapour load (and thus the degree of turbulence on the plate) and by the internal film coefficient h_i of the heat transfer medium (HEM) and to a lesser degree by the liquid load. The impact of h_i on U was stronger in the cooling mode since h_p-values were 2-10 larger than the corresponding h_i values. Influenced by the aforementioned variables, U varied from 2.2 - 4.0 kW/m^2K. Furthermore, at comparable HEM flow rates (and thus h_i values), U is slightly higher in the cooling mode than in the heating mode. The U values obtained for our sieve tray system were 4 to 8 times larger than through-the-wall values of U reported for packed column systems [123 & 137].

6. Geometry-independent plate-to-fluid heat transfer coefficients (h_{p-f}) were monitored in the heating and cooling modes. In the heating mode, h_{p-f} measured ranged from 3 – 9 kW/m^2 K, depending on the temperature difference between the plate and fluid, and in the cooling mode from 9 – 11 kW/m^2 K, which remained unaffected by the vapour flow. h_{p-f} also increases with higher liquid loads in the heating mode, whilst it remained constant in the cooling mode. The constant h_{p-f} in the cooling mode suggested that liquid on the plate was being sub-cooled.

7. An approach was attempted to predict $h_{p\text{-}f}$ and relate them to simple heat transfer models. While our simple model failed to produce good correlation in the cooling mode, it predicted htc in the heating mode well. It was found that for heating, $h_{p\text{-}f} \alpha (T_p\text{-}T_f)^{0.9}$, which was in accordance with our proposed nucleate boiling mechanism.

8. The heat transfer plate section was operated with a methanol-water system to generate Murphree tray efficiencies (E_{MV}). Heat flux, vapour load and reflux ratio were varied in order to investigate the impact of these variables on E_{MV}. Heating at approximately 40 kW m^{-2} led to an E_{MV} increase of 7% regardless of the vapour flow rate. Heat removal at approximately 90 kW m^{-2} caused an efficiency decrease of 3 - 18%, the difference in efficiency between adiabatic and cooling runs increasing with the vapour load. The efficiency change was accompanied by a froth height change, which altered the mass transfer area available. Variations in both modes led to a larger E_{MV} change than an equivalent alteration of the reboiler load, since the effect of the latter may be attenuated by heat losses along the column. Runs, in which product was withdrawn produced an initial drop in the efficiency as r increased, followed by a recovery, which can be observed in both adiabatic and diabatic runs. The measured values of E_{MV} were somewhat lower than those reported [157, 178, 193 & 195], because of the upper limit of our vapour flow rates.

9. The effect of heat transfer on E_{MV} evaluated in this experimental study (in combination with the experimental htc), may be used in the modelling of diabatic distillation columns. The decrease of E_{MV} in the cooling mode occurring in the rectifying section, and the increase of E_{MV} in the heating mode occurring in the stripping section mark this kind of diabatic distillation as ideal for the separation of high purity bottom products. The sacrifice of stages in the rectifying system is irrelevant in such a system and outweighed by the increased tray efficiency in the stripping section. In general, a trayed diabatic distillation system can be successfully applied where the application of heat pumps is favourable.

10. Krishnamurthy and Taylor's nonequilibrium stage model (1985) [161] was adapted for the use in diabatic distillation. A set of equations for modelling a binary mixture is presented. The model is the most rigorous approach taking heat exchange into account and is applicable to multicomponent mixtures.

6.2 Recommendations for future work

The consolidated findings of this study led to the following recommendations, which can be divided into three fields.

- Fundamental research
- Design improvements
- Expansion of the system

6.2.1 Fundamental research

Additional experiments are recommended for investigating sub-cooling on the heat transfer tray. Lowering the temperature difference between the plate and the liquid could lead to a different behaviour of $h_{p\text{-}f}$ in the cooling mode. A lower temperature difference can readily be achieved by reducing the heat removal from the plate.

To gaining a better understanding of the fluid dynamics on a diabatic plate, knowledge of froth structure, bubble size development and bubble distribution are essential. This could be performed in a tooled-up version of our experimental rig. Precise measurement techniques will be paramount in such a project. This demands for monitoring with high tech equipment such as high-speed cameras, video and infra red cameras, which will give rise to high project costs. On the other hand, such an experimental rig could be a rich source of valuable data for validating simulation approaches.

The uniformity of temperature distribution on the plate has not yet been completely investigated. A tooled-up heat transfer plate with thermocouples at various locations on and in the plate could be used for such a project. Those experiments could be

linked with tracer experiments, which investigate the residence time of liquid on the tray. The highly turbulent regime on the plate might complicate the tracer monitoring.

Although the 150 mm diameter plate had a uniform composition profile, efforts could be put into a composition profile study of commercial trays under diabatic conditions. The nonavailability of such large columns for research necessitates the application of simulations, using of computational fluid dynamics (CFD).

6.2.2 Design improvements

Other heat exchanger systems ought to be tested for establishing diabatic conditions on sieve trays. Heating or cooling coils, such as used by Rivero (1993) [63], are a good starting point. Recent Meng. student projects have been targeting the determination of overall heat transfer coefficients of copper coils in cooling and heating modes (2004) [148]. One should consider the placement of such coils carefully. For heating tasks, they should be submerged in the froth. On the other hand, it might be worth trying to conduct experiments with cooling coils right underneath the plates, therefore ensuring that only vapour will be condensed and no liquid becomes sub-cooled. However, this coil arrangement may lower U values though. Olujic *et al.* (2004) have chosen an alternative approach by implementing heating panels in their pilot plant column [149].

Diabatic distillation features changing vapour and liquid streams across the column length. Sieve trays are usually designed to operate optimally in a particular regime. Instead of using sieve trays with different fractional free areas, lift trays (proposed by Noda in 2003 [191]) could be used for dealing with this problem. A lift tray cannot be used for our heat exchanger plate design, but coils could be applied above or below instead. Pritchard has already directed research efforts into this direction.

6.2.3 Expansion of the system

The single heat transfer plate system (after the design improvements) can be applied to the whole system; hence creating a completely diabatic column. Other heat transfer mediums than water can be used as HEM. The use of binary refrigerants, proposed by Pritchard in 2004 [146], seems to be most promising for establishing a constant temperature glide across the plates of a diabatic column. Suitable binary mixtures, chosen from Watson's work (2004) [147], could be used in an experimental study, which investigates the heat transfer performance and temperature profile of various HEMs.

Wherever diabatic distillation will lead and whatever approach is taken, there is always a compromise between the heat exchanger area and the temperature difference between the HEM and the tray fluid, which affects the capital and operating costs respectively. This is illustrated in Figure 6.3. The engineer's task is to find the economic optimum. A key parameter is U. Maximising the product of U and the ratio of heat exchanger area and bubbling area ($U^*(A_{he}/A_p)$) will lead to cost effective solutions and should be the main concern of the optimisation process after a particular design has been chosen.

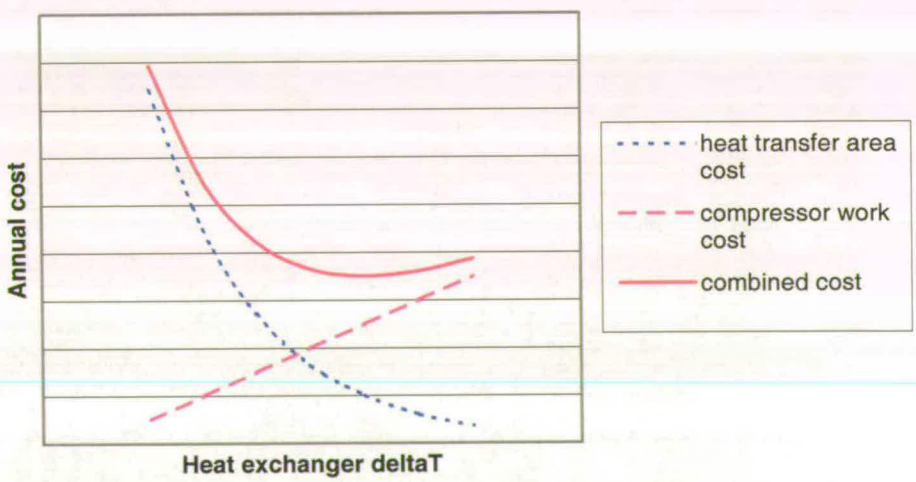

Figure 6.1: Trade-off between the investment/operating cost and ΔT between HEM and the process fluid

Bibliography

[1] J. L. Humphrey and G. E. Keller. *Separation process technology,* McGraw-Hill, New York, 1997.

[2] R. J. Forbes. *A short history of the art of distillation.* E. J. Brill, Leiden, 1948.

[3] G. E. Keller. Separations: new directions for an old field. *AIChE Monograph Series*, No. 17, 83, 1987.

[4] G. G. Haselden and P. N. Snowden. *Practical distillation – a post experience course.* University of Leeds, 1981.

[5] S. R. M. Ellis and A. P. Boyes. Research and development in distillation – some aspects of future. *T. I. Chem. Eng-Lond.,* 52: 202, 1974.

[6] F. E. Rush. *I. Chem. E. Symp. Ser.,* 56: 411, 1979.

[7] F. J. Zuiderweg. *Chem. Engr. Centenary Supplement*: 44, Dec 1988.

[8] J. R. Fair. *Chem. Proc.,* Sept.: 23, 1990.

[9] T. J. Mix, J. S. Dweck, M. Weinberg and R. C. Armstrong. Energy-conservation in Distillation. *Chem. Eng. Prog.,* 74 (4): 49-55, 1978.

[10] J. D. Seader and E. J. Henley. *Separation process principles.* John Wiley and Sons, New York, 1998.

[11] R. F. Strigle. *Random packings and packed towers: design and applications.* 2nd edn, Gulf, 1994.

[12] R. Billet. *Packed towers.* VCH, Weinheim, 1995.

[13] R. J. Hengstebeck. Simplified method for solving multicomponent distillation problems. *Trans. Am. Inst. Chem. Eng.,* 42: 309, 1946.

[14] A. Kremser. *Natl. Petroleum News.* 22 (21): 43-49, 1930.

[15] M. Souders and G. G. Brown. *Ind. Eng. Chem.,* 24: 519-522, 1932.

[16] G. Horton and W. B. Franklin. *Ind. Eng. Chem.,* 32: 1384-1388, 1940.

[17] W. C. Edminster. *Ind. Eng. Chem.*, 35: 837-839, 1943.

[18] M. R. Fenske., *Ing. Eng. Chem.*, 24: 482-485, 1932.

[19] A. J. V. Underwood. *Trans. Inst. Chem. Eng.,* 10: 112-158, 1932.

[20] E. R. Gilliland. *Ind. Eng. Chem.,* 32: 1101-1106, 1940.

[21] J. H. Erbar and R. N. Maddox. Latest score: reflux vs. trays. *Pet. Ref.,* 40 (May): 183, 1961.

[22] C. J. King. *Separation processes.* 2nd edn., McGraw-Hill, New York, 1980.

[23] H. Z. Kister. *Distillation design,* McGraw-Hill, New York, 1992.

[24] J. M. Coulson and J. F. Richardson. *Chemical Engineering*, Vol 6, Butterworth & Heinemann, Oxford, 6th edn., 1999.

[25] J. Stichlmayr, J. R. Fair and J. L. Bravo. *Chem. Eng. Prog,* 85 (1): 63-69 1989.

[26] M. F. Doherty and J. D. Perkins. *Chem. Eng. Sci.,* 33: 281-301, 1978.

[27] J. Stichlmair. "Distillation and rectification" in *Ullmann's Encyclopedia of Industrial Chemistry,* 5th edn., VCH, Weinheim, Vol. B3: 4-1 to 4-94, 1988.

[28] L. R. Partin. *Chem. Eng. Progress,* 89 (1): 43-48, 1993.

[29] R. J. Hengstebeck. *Distillation: principles and design procedures,* Reinhold, 1961.

[30] R. W. Ellerbe. "Batch distillation" in *Handbook of separation processes for chemical engineers,* P. A. Schweitzer (ed), McGraw-Hill, New York, 1979.

[31] R. Billet. *Distillation Engineering,* Heydon, 1979.

[32] R. Zanetti. Distillation: a technology in crisis. *Chem. Eng.,* 104 (June): 1997.

[33] BP, *2002 in review.* http://www.bp.com/liveassets/bp_internet/globalbp/STAGING/global_assets/downloads/T/T_pri_cons.pdf

[34] BP, *2002 in review.* http://www.bp.com/liveassets/bp_internet/globalbp/STAGING/global_assets/downloads/T/Table_of_refinery_capacities_pdf.

[35] B. F. Smith. *Design of equilibrium stage processes,* McGraw-Hill, New York, 1963.

[36] M. J. Lockett. *Distillation tray fundamentals.* Cambridge University Press, London, 1986.

[37] R. Billet. *Die industrielle Destillation.* VCH, Weinheim, 1973.

[38] F. J. Zuiderweg. Distillation – science and business. *The Chem. Eng.,* (Sept): 404, 1973.

[39] Le Goff, Institute National Polytetechnique de Lorraine, Nancy, France http://www.ensic.inpl-nancy.fr/ENSIC/LSGC/gb/esve.htm, accessed in 2002.

[40] M. Gouy. Sur l'energie utilisable. *J. Phys.*, (Paris) 8: 501, 1889.

[41] A. Stodola. *Steam and gas turbines.* McGraw-Hill, New York, 1910.

[42] G. Darrieus. The rational definition of steam turbine efficiencies. *Engineering*, London, 283, 1930.

[43] J. H. Keenan. *Thermodynamics.* Chapter XVII, MIT Press, Cambridge, Massachusetts, USA, 1941.

[44] D. C. Freshwater. Thermal economy in distillation. *Trans. Instn. Chem. Engrs.,* 29: 149-159, 1951.

[45] K. G. Denbigh. The second-law efficiency of chemical processes. *Chem. Eng. Sci.,* 6 (1): 1-9, 1956.

[46] Z. Rant. Exergie ein neues Wort fuer "technische Arbeitsfaehigkeit". *Forsch. Ingenieurwes.,* 22: 36, 1956.

[47] Z. Fonyo, Thermodynamic analysis of rectification. 1. Reversible model of rectification. *Int. Chem. Eng.*, 14 (1): 18-27, 1974.

[48] J. R. Flower. *T. I. Chem. Eng-Lond.*, 42: 249, 1964.

[49] T. A. Brzustowski and P. J. Golem. Second-law analysis of energy processes part I: exergy – an introduction. *Trans. CSME,* 4 (4): 209-218, 1976-77.

[50] A. Bejan. A study of entropy generation in fundamental convective heat transfer. *J. Heat Transfer.* 101: 718-725, 1979.

[51] A. Bejan. Second-law analysis in heat transfer and thermal design. *Advances in Heat Transfer Volume 15* (ed J. P. Harnett & T. F Irvine Jr.), Academic Press, New York: 1-58, 1982.

[52] J. H. Keenan. Availability and irreversibility in thermodynamics. *Br. J. Appl. Phys.*, 2: 183, 1951.

[53] R. Clausius. *"Die mechanische Waermetheorie"*. Braunschweig, Germany, 1887.

[54] G. Darrieus. L'evolution des centrales thermiques et la notion d'energie utilisable. *Sci. Ind. (Paris),* 15: 206, 1931.

[55] S. Ray and S. P. Sengputa. Irreversibility analysis of a sieve tray in a distillation column. *Int. J. Heat Mass transfer,* 39 (7): 1535-1542, 1996.

[56] P. Le Goff, T. Cachot and R. Rivero. Exergy analysis of distillation processes. *Chem. Eng. Tech.*, 19, (6): 478-485, 1996.

[57] B. Andresen and P. Salamon. Optimal distillation calculated by thermodynamic geometry. *Entropie,* 224/225: 4-10, 2000.

[58] F. Weinhold. Metric geometry of equilibrium thermodynamics. *J. Chem. Phys.*, 63: 2479, 1975.

[59] F. Weinhold. Geometrical aspects of equilibrium thermodynamics. In: *Theoretical chemistry, advances and perspectives. Vol 3* (ed. D. Henderson, H. Eyring), Academic Press, New York, 1978.

[60] P. Salamon, B. Andresen, P. Gait and R. S. Berry. The significance of Weinhold's length. *J. Chem. Phys.*, 73: 1001, 5407E, 1980.

[61] M. Schaller, K. H. Hoffmann, G. Siragusa, P. Salamon and B. Andresen. Nummerically optimized performance of diabatic distillation column. *Comp. Chem. Eng.*, 25: 1537-1548, 2001.

[62] J. S. Rowlinson. *Liquids and liquid mixtures.* Plenum Press, New York, 1969.

[63] R. Rivero. *L'analyse d'exergie: Application à la distillation diabatique et aux pompes à chaleur à Absorption.* PhD thesis, Institute National Polytetechnique de Lorraine, Nancy, France, 1993.

[64] R. Rivero. Application of the exergy concept in the petroleum refining and petrochemical industry. *Energy Conversion and Management,* 43: 1199-1220, 2002.

[65] R. Rivero. *Optimización de las Instalatiociones Existentes en la Refinería de Tula, Hidalgo, Utilizando el Método de Exergia.* Report Final de Proyecto E-2277, Tomos I a IX. Mexico,Grupo de Exergia, Inst. Mex. Del Petróleo: 713, 1988.

[66] R. Rivero. Tridimensional exergy diagram. In: J. Szargut, Z. Kolenda, G. Tsatsarotis, A. Ziebik, editors. *Energy Systems and Ecology, Volume 1.* Polish Ministry of National Education and American Society of Mechanical Engineers, Cracow: 305-312, 1993

[67] T. Gundersen and L. Naess. The synthesis of cost optimal heat-exchanger networks – an industrial review of the state of the art. *Comp. and Chem. Eng.,* 12 (6): 503-530, 1988.

[68] F. Huang and R. V. Elshout. Optimizing the heat recovery of crude units. *Chem. Engng. Prog.,* 72: 68-74, 1976.

[69] T. Umeda, J. Itho and K. Shiroko. Heat exchange system synthesis. *Chem. Engng. Prog.,* 74: 70-76, 1978.

[70] B. Linnhoff *et al. User guide on process integration for efficient use of energy.* IChemE, London, 1982

[71] E. Rev and Z. Fonyo. Diverse pinch concept for heat exchange network synthesis: the case of different heat transfer conditions. *Chem. Engng. Sci.,* 46 (7): 1623-1634, 1991.

[72] L. T. Biegler, I. E. Grossmann and A. W. Westerberg. *Systematical methods of chemical process design.* Prentice Hall International, London, 1997.

[73] G. Sobočan and P. Glavič. A simple synthesis method for studying thermally integrated distillation sequences. *Can. J. Chem. Eng.,* 78: 908-916, 2000.

[74] F. B. Petlyuk, V. M. Platonov and D. M. Slavinsk. Thermodynamically optimal method for separating multicomponent mixtures. *Int. Chem. Eng.,* 5 (3): 555-561. 1965.

[75] H, Becker, S. Godorr, H. Kreis and J. Vaughan. Partitioned distillation columns – Why, when and how. *Chem. Eng.,* 108 (1): 68-74, 2001.

[76] C. Triantafyllou and R. Smith. The design and optimisation of thermally coupled distillation columns. *Chem. Eng. Res. Des.*, 70 (2): 118-132. 1992.

[77] W. J. Stupin and F. J. Lockhart. Distillation practices – thermally coupled distillation – case history. *Chemical Engineering Progress,* 68 (10): 71, 1972.

[78] D. W. Tedder and D. F. Rudd. Parametric studies in industrial distillation 1-3. *AIChE Journal,* 24 (2): 303-334, 1978.

[79] Y. H. Kim. Rigorous design of extended fully thermally coupled distillation columns. *Chem. Engng. J.,* 89: 89-99, 2002.

[80] Y. H. Kim, D. W. Choi and K. S. Hwang. Industrial application of an extended fully thermally coupled distillation column to BTX separation in a naphta reforming plant. *Korean J. Chem. Eng.,* 20 (4): 755-761, 2003.

[81] A. Jimenez, N. Ramirez, A. Castro and S. Hernandez. Design and energy performance of alternative schemes to the Petlyuk distillation system. *Chem. Eng. Res. Des.*, 81 (A5): 518-524. 2003.

[82] M. A. Schultz, D. G. Stewart, J. M. Harris, S. T. Harris, S. T. Rosenblum, M. S. Shakur and D. E. O'Brien. Reduce costs with dividing-wall columns. *Cepmagazine, 2002. http://www.cepmagazine.org/pdf/050264.pdf.*

[83] K. Muralikrishna, V. K. P. Madhavan and S. S. Shah. Development of dividing wall distillation column design space for a specific separation. *Trans. IChemE.*, 80: 155-166, 2002.

[84] I. J. Halvorsen and S. Skogestad. Integrated column designs for minimum energy and entropy requirements in multicomponent distillation. Unpublished paper 2001. http://www.nt.ntu.no/user/skoge/publications/2001/halvorsen_reno/.

[85] K. Stephan. Absorption heat pumps and working pair development in Europe until 1974. *Paper presented at the Berlin meeting of the ad hoc group on new absorption working pairs*, Berlin, 14-16 April 1982.

[86] F. Merkel and F. Bosnjakovic. *Diagramme und Tabellen zur Berechnung der Absorptions-Kaeltemaschinee.* Springer, Berlin, 1929.

[87] Z. Fonyo and P. Mizsey. Economic applications of heat pumps in integrated distillation systems. *Heat Recov. Syst. CHP,* 14 (3): 249-263, 1994.

[88] J. R. Flower and R. Jackson. Energy requirements in the separation of mixtures by distillation. *Trans IChemE,* 42: T249-T258, 1964.

[89] F. Ziegler and P. Riesch. Absorption cycles: a review with regard to energy efficiency, *Heat Recov. Syst. CHP*, 13 (2): 147-159, 1993.

[90] Z. Fonyo, R. Kurrat, D. W. T. Rippin and I Meszaros. Comparative analysis of various heat pump schemes applied to C_4 splitters. *Computers chem. Engng.*, 19 (suppl.): S1-S6, 1995.

[91] F. Moser and H. Schnitzer. *Heat pumps in industry.* Elsevier, Oxford, 1985.

[92] G. Alefeld and R. Rademacher. *Heat conversion systems.* CRP Press, London, 1994.

[93] A. Rojey. "Heat pump operating with fluid mixture" in *New ways to save energy,* D. Reidel Publishing Company, Boston, 1980.

[94] C. L. Pritchard and R. E. Low. A self-regulating heat pump to utilize wind and wave energy resources. *Energy sources,* 12: 15-24, 1990.

[95] S. M. Sami and M. A. Comeau. Experimental study of the dynamic behavior of nonazeotropic binary-mixtures in heat pumps. *Heat recovery systems & CHP.* 11 (6): 505-515, 1991.

[96] W. Keuther. Otimierung der Ethan-Ethylen Trennung bei der Ethylenerzeugung. *Linde Ber.*, 33: 22, 1973.

[97] H. Schulze-Trautmann. Energieeinsparung bei der Propylen-Propan Trennung, *Redoel Koehle,* 29 (9): 403, 1976.

[98] G. P. Quadri. Use heat pumps for p-p-splitter. *Hydrocarbon Proc.,* 60 (2): 119-126, 1981.

[99] S. Finelt. Better C3 distillation pressure. *Hydrocarbon Proc.,* 58 (2): 95-98, 1979.

[100] Z. Fonyo and N. Benkö. Comparison of various heat pump assisted distillation configurations. *Trans IChemE,* 76: 348-360, 1998.

[101] R. E. Fitzmorris and R. S. H. Mah. Improving distillation column design using thermodynamic availability analysis. *AIChE J.,* 26 (2): 265-273, 1980.

[102] N. L. Franklin and M. B. Wilkinson. Reversibility in the separation of multicomponent mixtures. *Trans IChemE,* 60 (5): 276-282, 1982.

[103] J. Koehler, P. Aguirre and E. Blass. Minimum reflux calculations for nonideal mixtures using the reversible distillation model. *Chem. Engng. Science.* 46 (12): 3007-3012, 1991.

[104] D. Pradubsripetch, Y. Naka and Z. Fan. Analysis of heat demand and supply in multicomponent distillation systems. *J. Chem. Eng. Japan,* 27 (2): 188-193, 1994.

[105] E. Sauar, R. Rivero, S. Kjelstrup and K. M. Lien. Diabatic column optimization compared to isoforce columns. *Energy Conversion and Management,* 38 (15-17): 1777-1783, 1997.

[106] R. Rivero. Exergy simulation and optimization of adiabatic and diabatic binary distillation. *Energy*, 26 (6): 561-593, 2001.

[107] M. Schaller, K. H. Hoffmann, R. Rivero, B. Andresen and P. Salamon. The influence of heat transfer irreveribilities on the optimal performance of diabatic distillation columns. *Journal of Non-equilibrium Thermodynamics*, 27 (3): 257-269, 2002.

[108] K. de Koeijer and R. Rivero. Entropy production and exergy loss in experimental distillation columns. *Chem. Eng. Sci.,* 58 (8): 1587-1597, 2003.

[109] R. Rivero, M. Garcia and J. Urquiza. Simulation, exergy analysis and application of diabatic distillation to a tertiary amyl methyl ether production unit of a crude oil refinery. *Energy,* 29 (3): 467-489, 2004.

[110] R. Agrawal, Z. T. Fidkowski and J. G. Xu. Prefractionation to reduce energy consumption in distillation without changing utility temperatures. *AIChE J.,* 42 (8): 2118-2127, 1996.

[111] R. Agrawal and Z. T. Fidkowski. On the use of intermediate reboilers in the rectifying section and condensers in the stripping section of a distillation system. Ind. Engng. Chem. Res., 35 (8): 2801-2807, 1996.

[112] R. Agrawal and D. M. Herron. Intermediate reboiler and condenser arrangement for binary distillation. *AIChE J.,* 44 (6): 1316-1324, 1998.

[113] R. Agrawal and D. M. Herron. Efficient use of an intermediate reboiler or condenser in binary distillation. *AIChE J.,* 44 (6): 1303-1315, 1998.

[114] R. Agrawal and Z. T. Fidkowski. Thermodynamically efficient systems for ternary distillation. *Ind. Engng. Chem. Res.*, 38 (5): 2065-2074, 1999.

[115] A. Gunther. New distillation approach. *Chem. Eng.*, 140: 140-141, 1974.

[116] R. S. H. Mah, J. J. Nicholas JR. and R. B. Wodnik. Distillation with secondary reflux and vaporisation: a comparative evaluation. AIChE J., 23 (5): 651-658, 1977.

[117] T. Glenchur and R. Govind. Study on a contious heat integrated distillation column. *Sep. Sci. Technol.*, 22 (12): 2323-2338, 1987.

[118] J. F. Boston, S. L. Sullivan. *Can. J. Chem. Eng.*, 50: 663, 1972.

[119] T. Takamatsu, V. Lueorasitsakul and M. Nakaiwa. Modelling and design method for internal heat-integrated packed distillation. *J. Chem. Eng. Japan,* 21: 595-601, 1988.

[120] T. Takamatsu. Heat integrated distillation columns. *Private report*, 1994.

[121] T. Takamatsu, M. Nakaiwa and T. Nakanishi. *Kagaku Kogaku Ronbunshu*, 22: 985, 1996.

[122] T. Nakanishi, K. Aso, H. Noda, M. Nakaiwa and T. Takamatsu. On development of a new distillation column for energy saving. 1. On design of an ideal heat integrated distillation column (HIDiC). *in Asia-Pacific conference on sustainable energy and environmental technology,* G.Q. Lu, P. F. Green (ed.), Singapore: 313-320, 1996.

[123] H. Noda, K. Aso, N. Kobayasi, M. Nakaiwa and T. Takamatsu. On development of a new distillation column for energy saving. 2. A fundamental experimental research on mass & heat transfer in HIDiC. *in Asia-Pacific conference on sustainable energy and environmental technology,* G.Q. Lu, P. F. Green (ed.), Singapore: 321-326, 1996.

[124] K. Huang, M. Nakaiwa, T. Akiya and M. Owa. Dynamics of heat integrated distillation columns. *J. Chem. Eng. Japan,* 29 (4): 656-661, 1996.

[125] K. Huang, M. Nakaiwa and T, Akiya. A numerical consideration on dynamic modelling and control of ideal heat integrated distillation columns. *J. Chem. Eng. Japan,* 29 (2): 344-351, 1996.

[126] K. Huang, M. Nakaiwa, T. Akiya and M. Owa. Performance evaluation of ideal heat integrated distillation columns. *J. Chem. Eng. Japan,* 30 (1): 108-115, 1997.

[127] K. Huang, M. Nakaiwa, M. Owa, T. Akiya, K. Aso and T. Takamatsu. Determining appropriate configuration of ideal heat integrated distillation columns (HIDiC). *J. Chem. Eng. Japan,* 30 (3): 575-579, 1997.

[128] M. Nakaiwa, K. Huang, M. Owa, T. Akiya, T. Nakane, M. Sato and T. Takamatsu. Energy savings in heat integrated distillation. *Energy,* 22 (6): 621-625, 1997.

[129] M. Nakaiwa, K. Huang, M. Owa, T. Akiya and T. Nakane. Operating an ideal heat integrated distillation column with different control algorithms. *Computers chem. Engng.*, 22 (suppl.): 389-393, 1998.

[130] K. Huang, M. Nakaiwa, M. Owa, T. Akiya, T. Nakane, M. Sato and T. Takamatsu. Identification and internal model control of an ideal heat integrated distillation column. *J. Chem. Eng. Japan,* 31 (1): 159-164, 1998.

[131] M. Nakaiwa, K. Huang, M. Owa, T. Akiya, T. Nakane, M. Sato and T. Takamatsu. Potential energy savings in heat-integrated distillation column. *Applied Thermal Engineering,* 18: 1077-1087, 1998.

[132] K. Huang, D. Zhan, M. Nakaiwa, T. Nakane and T. Takamatsu. Modelling and analysis of internal heat integrated distillation columns. *Chinese J. of Chem. Eng.*, 7 (1): 67-76, 1999.

[133] K. Huang, J. Qian, M. Nakaiwa, T. Nakane and T. Takamatsu. Assessment of control configurations for a general heat integrated distillation column. *Chinese J. of Chem. Eng.*, 8 (4): 339-346, 2000.

[134] K. Huang, M. Nakaiwa, K. Naito, A. Endo, M. Owa, T. Akiya, T. Nakane, M. Sato and T. Takamatsu. On the start-up of ideal heat integrated distillation columns (HIDiC).

[135] M. Nakaiwa, K. Huang, K. Naito, A. Endo, M. Owo, T. Akiya, T. Nakane and T. Takamatsu. A new configuration of heat integrated distillation columns (HIDiC). *Comput. Chem. Eng.*, 24: 239-245, 2000.

[136] K. Naito, M. Nakaiwa, K. Huang, A. Endo, K. Aso, T. Nakanashi, T. Nakamura, H. Noda and T. Takamatsu. Operation of a bench-scale ideal heat integrated distillation column (HIDiC): an experimental study. *Comput. Chem. Eng.*, 24: 495-499, 2000.

[137] H. Noda, T. Takamatsu, K. Aso, T. Nakanishi, K. Yoshida, M. Nakaiwa, T. Mukaida and N. Kuratani. Development on a coaxial heat integrated distillation column (HIDiC). *Korean J. Chem. Eng.*, 17 (5): 593-596 2000.

[138] M. Nakaiwa, K. Huang. A. Endo, T. Ohmori, T. Akiya and T. Takamatsu. Internally heat-integrated distillation columns: A review. *Chem. Engng Res. Des.*, 81 (A1): 162-177, 2003.

[139] M. B. Niang, T. Cachot and P. Le Goff. *Proceedings of second law analysis workshop*. 333-338, 1995.

[140] P. Rivera-Ortega, M. Picon-Nunez, E. Torres-Reyes and A. Gallegos-Munoz. Thermal integration of heat pumping systems in distillation columns. *Applied Thermal Eng.*, 19, 819-829 1999.

[141] X. G. Liu, J. X.Qian. Modelling, control, and optimisation of ideal thermally coupled distillation columns. *Chem. Eng. Technol.*, 23: 235-241, 2000.

[142] C. Pritchard, S. Beggs, M. Kaeser and M. Nakaiwa. *Sixth International Conference on Greenhouse Gas Control Technologies*, Kyoto, Japan, 2002.

[143] P. J. Jansens, F. Fakhri, J. de Graauw and Ž. Olujić. Energy saving potential of heat integrated distillation column. *AIChE Spring National Meeting,* Houston: 1-6, 2001.

[144] M. Nakaiwa, K. Huang, T. Endo, T. Ohmori, T. Akiya, T. Takamatsu, S. Beggs and C. Pritchard. Contributing to reduction of CO2 emissions through development of heat-integrated distillation column. *Sixth International Conference on Greenhouse Gas Control Technologies*, Kyoto, Japan, 2002.

[145] S. Beggs. Meng. project report, University of Edinburgh, 2002.

[146] C. L. Pritchard, T. Caldwell and W. Morton. Retrofitting internal heat integration to a distillation column. *Paper presented at ECOS 2004 in Guanajuato,* Mexico, 2004.

[147] K. Watson. *Meng. project report*, University of Edinburgh, 2004

[148] J. Cameron and N. Mottram. *Meng. project report*, University of Edinburgh, 2004.

[149] Z. Olujic, F. Fakhri, J. de Graauw and P. J. Jansens. Internal heat integration – the key to an energy-conserving distillation column. J. Chem. Technol. Biotechnol., 78: 241-248, 2003.

[150] Z. Olujic, F. Fakhri, J. de Graauw and P. J. Jansens, *Heat panels in heat integrated distillation columns.* Group meeting at Delft University, February 2004.

[151] Z. Olujic, L. Sun, A. de Rijke, P. J. Jansens. Conceptual design of an energy efficient propylene splitter. *Paper presented at ECOS 2004 in Guanajuato,* Mexico, 2004.

[152] G. Standart and F. Kaštánek. Studies on distillation: VIII: The effect on carryover on plate efficiency. *Separation Science*, 1 (1): 27-39, 1966.

[153] F. Kaštánek and G. Standart. Studies on Distillation: XX. Efficiency of selected types of large distillation trays at total reflux. *Separation Science*, 2 (4): 439-486, 1967.

[154] S. Bakowski. *Brit. Chem. Eng.*, 8: 384, 1963.

[155] A. G. Kasatkin, Ju. I. Dytnerskij, D. G. Piterskirch and Chla Mauung. *Chim. Promy.*, 4: 279,1963.

[156] N. A. Kočergin. *Research report875-57L* (in Russian), Lisičansk Laboratory of GIAP, Severodoneck, Russia, 1960.

[157] M. J. Lockett and I. S. Ahmed. Tray and point efficiencies from a 0.6 metre diameter distillation column. *Chem. Eng. Res. Des.*, 61: 110-118, 1983.

[158] *AIChE bubble tray design manual.* American Institute of Chemical Engineers, New York, 1958.

[159] H. Chan and J. R. Fair. Prediction of point efficiencies on sieve trays. 1. Binary systems. *Ind. Eng. Chem. Proc. Des. Dev.*, 23 (4): 814-819, 1984.

[160] H. Chan and J. R. Fair. Prediction of point efficiencies on sieve trays. 2. Multicomponent systems. *Ind. Eng. Chem. Proc. Des. Dev.*, 23 (4): 820-827, 1984.

[161] R. Krishnamurthy and R. Taylor. A nonequilibrium stage model of multicomponent separation processes. Part I: model description and method of solution. *AIChE J.*, 31(3): 449-456, 1985.

[162] R. Krishnamurthy and R. Taylor. A nonequilibrium stage model of multicomponent separation processes. Part II: Comparison with experiment. *AIChE J.*, 31(3): 456-466, 1985.

[163] R. Taylor, H. A. Kooijman and J–S. Hung. A second generation nonequilibrium model for computer simulation of multicomponent separation processes. *Comput. Chem. Engng.*, 18 (3): 205-217, 1994.

[164] N. P. Mueller, H. Segura. An overall rate-based stage model for cross flow distillation columns. *Chem. Eng. Sci.*, 55: 2515-2528, 2000.

[165] T. Plaka, M. R. Ehsani and W. J. Korchinski. Determination of individual phase transfer units, N_G and N_L, for a 0.6 m diameter distillation column sieve plate: methylcyclohexane-toluene system. *Chem. Eng. Res. Des.*, 67: 316-328, 1989.

[166] M. Prado and J. R. Fair. Fundamental model for the prediction of sieve tray efficiency. *Ind. Eng. Chem. Res.*, 29: 1031-1042, 1990.

[167] J. A. Garcia and J. R. Fair. A fundamental model for the prediction of distillation sieve tray efficiency. 1. Database development. *Ind. Eng. Chem. Res.*, 39: 1809-1817, 2000.

[168] J. A. Garcia and J. R. Fair. A fundamental model for the prediction of distillation sieve tray efficiency. 2. Model development and validation. *Ind. Eng. Chem. Res.*, 39: 1818-1825, 2000.

[169] G. X. Chen and K. T. Chuang. Prediction of point efficiency for sieve trays in distillation. *Ind. Eng. Chem. Res.*, 32: 701-708, 1993.

[170] G. X. Chen and K. T. Chuang. Determining the number of gas-phase and liquid-phase transfer units from point efficiencies in distillation. *Ind. Eng. Chem. Res.*, 33: 907-913, 1994.

[171] F. J. Zuiderweg. Sieve trays, a view of the state of the art. *Chem. Eng. Sci.*, 37: 1441, 1982.

[172] M. M. Dribika and M. W. Biddulph. Scaling-up distillation efficiencies. *AIChE J.*, 32 (9): 1864, 1986.

[173] M. J. Lockett and T. Plaka. Effect of non-uniform bubbles in the froth on the correlation and prediction of point efficiencies. *Chem. Eng. Res. Des.*, 61: 119, 1983.

[174] G. X. Chen and K. T. Chuang. Liquid-phase resistance to mass transfer on distillation trays. *Ind. Eng. Chem. Res.*, 34: 3078-3082, 1995.

[175] W. J. Korchinsky, M. R. Ehsani and T. Placka. Sieve plate point efficiencies: 0.6 m diameter column. *Trans IChemE,* 72: 465-471, 1994.

[176] J. Stichlmair. Dimensionierung des Gas/Fluessigkeit Kontaktapparates Bodenkolonne. *Chem. Ing. Tech.,* 50: 281-284 & 383-387, 1978.

[177] W. J. Korchinski. Liquid mixing in distillation trays: simultaneous measurement of the diffusion coefficient and point efficiency. *Trans IChemE,* 72: 472-478, 1994.

[178] Z. P. Xu, A. Afacan and K. T. Chuang. Prediction of packed sieve tray efficiency in distillation. Trans *IChemE,* 74: 893-900, 1996.

[179] D. L. Bennet, D. A. Watson and M. A. Wiescinki. New correlation for sieve tray point efficiency, entrainment, and section efficiency. *AIChE J.,* 43 (6), 1611-1626, 1997.

[180] B. M. Jaćimović. Entrainment effect on tray efficiency. *Chem. Eng. Sci.,* 55: 3941-3949, 2000.

[181] R. Stevens and I. A. Furzer. Incipient three phase distillation: experimental tray composition profiles. *AIChE J.*, 35 (7), 1199-1202, 1989.

[182] A. Bakr and S. H. Salem. Efficiency of distillation columns containing packed sieve trays. *Sep. Sci. Technol.*, 28 (13&14): 2255-2272, 1993.

[183] A. A. Sidyagin and O. S. Chekov. Influence of gas by-passing on the efficiency of mass transfer in tray contact devices. *Russian Chem. Ind.*, 26 (4): 247-251, 1994.

[184] Z. Minqing and Y. Guocong. Simulation of two dimensional liquid phase flow on a distillation tray. *Chin. J. Chem. Eng.,* 2 (2): 63-71, 1994.

[185] R. Krishna and J. M. van Baten. Modelling sieve tray hydraulics using computational fluid dynamics. *Chem. Eng. Res. Des.,* 81 (A1): 27-38, 2003.

[186] Z. P. Xu, A. Afacan and K. T. Chuang. Liquid mixing on packed sieve trays. *Trans IChemE,* 73: 406-412, 1995.

[187] D. A. Spagnolo and K. T. Chang. Improving sieve tray performance with knitted mesh packing. *Ind. Eng. Chem. Processes Des. Dev.,* 23: 561-565.

[188] E. F. Wijn. The effect of downcomer layout pattern on tray efficiency. *Chem. Eng. J.,* 63:167-180, 1996.

[189] R. Billet. A contribution to the evaluation of mass transfer trays. *Chem. Eng. Technol.*, 20: 221-229, 1997.

[190] Stahl Apparate- und Geraetebau GmbH, 68519 Viernheim. *Short report on Dualflow trays from ACHEMA*, Germany, 1994.

[191] H. Noda. *Lift tray.* GPAT. NO. 2227280, 2003. http://ho.kce.co.jp/english/lifttrayeng.htm

[192] F. Lopez and F. Castells. Influence of tray geometry on scaling up distillation efficiency from laboratory data. *Ind. Eng. Chem. Res.,* 38 (7) 2747-2753, 1999.

[193] P. E. M. Gouvêa, T. M. K. Ravangani and A. F. R. Pereira. Parastillation columns as an alternative to conventional and vacuum distillation. *Latin American Applied Research,* 30: 365-371, 2000.

[194] C. Heucke. Vorteile von parallelen Stroemen bei Rektifikation, Absorption und Extraktion. *Chemie Ingenieur Technik,* 59 (2): 107-111 (1987).

[195] N. S. Yang, K. T. Chuang, A. Afacan, M. R. Resetarits and M. J. Binkley. Improving the efficiency and capacity of methanol-water distillation trays. *Ind. Eng. Chem. Res.,* 42: 6601-6606, 2003.

[196] S. R. Syeda. *Froth structure and mass transfer on distillation trays.* PhD Thesis, University of Alberta, Edmonton, Alberta, Canada, 2003.

[197] S. R. M. Ellis and M. W. Bidduph. The effect of surface tension on characteristics on the plate efficiency. *Trans. Inst. Chem. Eng., 45 (6): T223,* 1967.

[198] P. L. T. Brian, J. E. Vivian and S. T. Mayer. Cellular convection in desorbing surface tension lowering solutes from water. *Ind. Eng. Chem. Fundam.,* 10 (1): 75, 1971.

[199] D. A. Spagnolo, E. L. Plaice, H. J. Neuburg and K. T. Chuang. Heat transfer modelling on sieve trays. *Ca. J. Chem. Eng.,* 66: 367-376, 1988.

[200] M. R. Galley, A. R. Bancroft. *Canadian heavy water production – 1970-1980.* Atomic Energy of Canada Limited, report AECL-7429, 1981.

[201] I. N. Björn, U. Grén and F. Svensson. Simulation and experimental study of intermediate heat exchange in a sieve tray distillation column. In *11^{th} European Symposium on Computer aided Process Engineering,* R. Gani, S. B. Jørgensen (editors), Elsevier Science: 105-110, 2001.

[202] E. V. Murphree. Rectifying column calculations with particular reference to N component mixtures. *Ind. Engng. Chem.*, 17 (7): 747, 1926.

[203] W. K. Jr. Lewis. Rectification of binary mixtures. *Ind. Eng. Chem.,* 28 (1): 399, 1936.

[204] A. S. Foss, J. A. Gerster and R. L. Pigford. Effect of liquid mixing on the performance of bubble trays. *AIChE J.,* 4 (2): 231-239, 1958.

[205] T. J. Gilbert. Liquid mixing on bubble-cap and sieve plates. *Chem. Eng. Sci., 10: 243, 1959.*

[206] P. E. Barker and M. F. Self. The evaluation of liquid mixing effects on a sieve plate using unsteady and steady state tracer techniques. *Chem. Eng. Sci.*, 17: 541-553, 1962.

[207] D. Shore and G. G. Haselden. Liquid mixing on distillation plates and its effect on plate efficiency. *IChemE Symp. Ser.,* No. 32, 2: 54-62, 1969.

[208] K. T. Yu, J. Huang, J. L. Li and H. H. Song. Two dimensional flow and Eddy diffusion on a sieve tray. *Chem. Eng. Sci.,* 45 (9): 2901-2906, 1990.

[209] D. L. Bennet and H. J. Grimm. Eddy diffusivity for distillation sieve trays. *AIChE J.,* 37 (4): 589-596, 1991.

[210] H. Hausen. A definition of exchange efficiency of rectifying plates for binary and ternary mixtures. *Chem.-Ing.-Tech.* 25: 595, 1953.

[211] C. D. Holland. *Multicomponent distillation*. Prentice-Hall, Englewood Cliffs, New Jersey, 1963

[212] G. Standart. Studies on distillation-V. *Chem. Eng. Sci.*, 20, 611- (1965)

[213] H. G. Drickhammer and J. R. Bradford. Overall plate efficiency of commercial hydrocarbon fractionation column as a function of viscosity. *Trans AIChE,* 39: 319, 1943.

[214] H. E. O'Connell. Plate efficiency of fractionating columns and absorbers. *Trans. AIChE,* 42: 741, 1946.

[215] S. A. MacFarland, P. M. Sigmund and M. Van Winkle. Predict Distillation efficiency. *Hydrocarbon Proc.*, 7: 111, 1972.

[216] R. Higbie. The rate of absorbtion of a pure gas in a still liquid during short periods of exposure. *Trans. AIChE,* 31: 365, 1935.

[217] A. S. Foss, J. A. Gerster, and R. L. Pigford. Effect of liquid mixing on the performance of bubble trays. *AIChE J.*, 4 (2): 231-239, 1958.

[218] G. X. Chen and K. T. Chuang. Prediction of point efficiency for sieve trays in distillation. *Ind. Eng. Chem. Res.*, 32: 701-708, 1993.

[219] V. G. Levich. *Physichemical Hydrodynamics*. Prentice Hall, Englewood Cliffs, New York: 464, 1962.

[220] J. A. Garcia. *Fundamental model for the prediction of distillation sieve tray efficiency: hydrocarbon and aqueous systems.* PhD thesis, University of Texas at Austin, 1999.

[221] T. K. Sherwood, R. L. Pigford and C. R. Wilke. *Mass transfer.* McGraw-Hill, New York: 148, 1975.

[222] R. Krishna and G. L. Standart. Mass and energy transfer in multicomponent systems. *Chem. Eng. Commun.*, 3: 201, 1979.

[223] R. B. Bird. W. E. Stewart and E. N. Lightfoot. *Transport phenomena,* Wiley, New York: 566, 1960.

[224] R. C. Reid, J. M. Prausnitz and B. E. Poling. The properties of gases & liquids. McGraw Hill, New York, 4th edition, 1987.

[225] *Landolt-Boernstein, Eigenschaften der Materie und ihrer Aggregatszustaende,* Vol 2, Springer Verlag, Berlin, 6th edition, 1969.

[226] C. L. Yaws. *Chemical properties handbook.* McGraw-Hill, New York, 1999.

[227] I. J. Harris. Optimum design of sieve trays. *Brit. Chem. Eng.*, 10 (6): 377, 1965.

[228] K. Asano and S. Fujita. Vapour and liquid phase mass transfer coefficients in tray towers. *Kagaku Kogatu,* 4: 330 & 369, 1966.

[229] L. Jeromin, H. Holik and H. Knapp. Efficiency calculation method for sieve-plate columns of air separation plants, *Inst. Chem. Engrs. Symp. Series,* No 32: 5-45, 1969.

[230] J. Stichlmair. *Bodenkolonne.* VCH, Weinheim, 1978.

[231] J. Stichlmair and A. Mersmann, Dimensioning plate columns for absorption and rectification. *Int. Chem. Engng.* 18 (2): 223-. 1978.

[232] W. H. McAdams, *Heat transmission,* McGraw-Hill, New York, 3rd edition, 1954.

[233] C. C. Kirkbride, Heat transfer by condensing vapours, *Trans. AIChE,* 30: 170-186, 1934.

[234] P. L. Yue and M. E. Weber. Film boiling of saturated binary mixtures. *Int. J. heat mass transfer,* 16: 1877-1887, 1973.

[235] M. N. Oezişik. *Heat transfer, a basic approach.* McGraw Hill, New York, international edition, 1985.

[236] J. G. Collier and J. R. Thome, *Convective boiling and condensation,* Oxford science publications, Oxford, 3rd edition, 1994.

[237] E. A. Farber and R. L. Scorah, Heat transfer to boiling water under pressure, *Trans. Am. Soc. Mec. Eng.,* 70: 369, 1948.

[238] M. Jackob. Heat transfer in evaporation and condensation. *Mech. Eng.,* 58: 643 & 729, 1936.

[239] W. M. Rohsenow and J. A. Clark., A study of the mechanism of boiling heat transfer. *Trans. Am Soc. Mech. Eng.,* 73: 609, 1951.

[240] H. K. Forster. On the conduction of heat into a growing vapour bubble. *J. Appl. Phys.*, 25: 1067, 1954.

[241] J. W. Westwater. In *Advances in chemical engineering.* (Eds. T. B. Drew and J. W. Hooper), Academic Press, New York, 1956.

[242] W. M. Rohsenow. A method of correlation heat transfer data for surface boiling liquids. *Trans. ASME,* 74: 969-975, 1952.

[243] J. R. Thome and S. Shakir. A new correlation for nucleate pool boiling of aqueous mixtures. *AIChE Symp. Ser.,* 83 (257): 46-51, 1987.

[244] S. M. Bajorek, J. R. Lloyd and J. R. Thome. Prediction methods of boiling of pure and multicomponent fluids on a low finned tube. *Fouling and enhancement interactions,* ASME HTD 164: 101-108, 1991.

[245] L. C. Signal, C. P. Sharma and H. K. Varma. Experimental heat transfer coefficient for binary refrigerant mixtures of R13 and R12. *ASHRAE Trans,* 2747: 165-188, 1983.

[246] H. Ross, R. Radermacher, M. di Marzo and D. Didion. Horizontal flow boiling of pure and mixed refrigerants. *Int. J. Heat Mass Transfer.* 30: 979-992, 1987.

[247] E. Hihara, K. Tanida and T. Saito. Forced convective boiling experiments of binary mixture. *JSME Int. J.* Series II, 32(1): 98-106, 1989.

[248] J. R. Thome. Prediction of the mixture effect on boiling in vertical thermosyphon reboilers. *Heat Transfer Eng.*, 10 (2): 29-38.

[249] J. Nikuradse, *Forsch. Arb. Ing. Wes.*, no. 346, 1932.

[250] M. J. Lockett and I. S. Ahmed. Tray and point efficiencies from a 0.6 metre diameter distillation column. *Chem Eng Res*, 61: 110-118, 1983.

[251] R. H. Perry and D. Green. *Perry's chemical engineers' handbook.* McGraw-Hill, New York, 6th international edition, 1984.

[252] J. J. Christiansen, H. W. Hanks and R. M. Izatt. *Handbook of heats of mixing.* John Wiley & Sons, New York, 1982.

[253] K. T. Thomas and R. A. McAllistar. Densities of liquid-acetone-water solutions up to their normal boiling points. AIChE J., 3: 161-164, 1957.

[254] M. Tamura, M. Kurata and H. Odani. Practical method for estimating surface tensions of solutions. *Bull. Chem. Soc. Japan.* 28: 83-88, 1955.

[255] R. Billet. *Die industrielle Destillation.* VCH, Weinheim, 1973.

[256] J. Stichlmair. Distillation and Rectification. *Ullmann's encyclopaedia of industrial chemistry.* Vol. 3, VCH, Weinheim, 5th ed., 1988.

[257] K. Sattler. *Thermische Trennverfahren.* VCH, Weinheim, 2nd ed., 1995.

[258] J. M. Coulson and J. F. Richardson. *Chemical Engineering. Vol 2,* Butterworth & Heinemann, Oxford, 6th ed., 1999.

[259] W. H. Koch and W. Licht. New design apporach boosts cyclone efficiency. *Chem. Eng.*, 7: 80-88, 1977.

[260] S. Constantinescu. Sizing gas cyclones. *Chemical Engineering,* 20: 97-100, 1984.

[261] J. M. Coulson and J. F. Richardson. *Chemical Engineering. Vol 1,* Butterworth & Heinemann, Oxford, 6th ed., 1999.

[262] H. Blasius. Das Aehnlichkeitsgesetz bei Reibungsvorgaengen in Fluessigkeiten. Forsch. *Ver. Deut. Ing.*, 131, 1913.

[263] G. Easton. *Meng project report*, University of Edinburgh, 2001.

[264] S. Beggs. *Meng project report*, University of Edinburgh, 2002.

[265] T. Caldwell. *Meng project report*, University of Edinburgh, 2003.

Glossary

The Glossary features explanations of frequently appearing acronyms and describes the meaning of certain key words. The key word content reflects the viewpoint of the author in context with this thesis. Other authors may have different descriptions for the key words mentioned.

Acronyms

AHP	Absorption heat pump
AHPDE	Double stage absorption heat pump
AHPSP	Single stage absorption heat pump; parallel operation
AHPSS	Single stage absorption heat pump; sequential operation
COP	Coefficient of performance
ECF	Energy cost factor
ETD	Equal thermodynamic distance
FTCDC	Fully thermally coupled distillation column
HEM	Heat transfer medium
htc	Heat transfer coefficient
MHP	Mechanical heat pump
MHPBF	Bottom flash mechanical heat pump

MHPCC	Closed cycle mechanical heat pump
MHPVR	Vapour recompression mechanical heat pump
PER	Primary energy ratio

Key words

Adiabatic	Greek: "not to pass through", occurring without loss or gain of heat.
Adiabatic distillation column	A "standard" distillation column with a reboiler delivering heat to the system and a condenser withdrawing heat from it. No other heat crosses the system boundaries (column).
Diabatic	Greek: "to pass through"; involving a transfer of heat.
Diabatic distillation column	Any distillation column using heat integration concepts.
HIDiC	Heat integrated distillation column. A diabatic distillation column variant developed by Japanese engineers. The HIDiC variant separates the stripping and the rectifying section and rearranges them concentrically. The rectifying section works under higher pressure and delivers heat to the surrounding stripping section. The concept was applied to packed distillation systems.

Reversible distillation	A distillation with no entropy generation. A diabatic distillation with an infinite number of intermediate heat exchangers; heat transfer occurs at an infinitesimal temperature difference.

Appendix A

Nomenclature

The following symbols have been commonly used without explanation in the body of the text and as such are here defined for reference.

A	heat transfer area in eqn 3.70	$[m^2]$
A_O	cross-sectional area of the orifice (eqn 4.40)	$[m^2]$
A_b	active or tray bubbling area	$[m^2]$
A_c	cross-sectional area of the column (eqn 4.17)	$[m^2]$
A_d	hole area on sieve tray (eqn 4.19)	$[m^2]$
A_D	heat transfer area of the channel in the heat transfer plate (eqn 3.70)	$[m^2]$
A_i	inside surface area (tube system) (eqn 4.30)	$[m^2]$
A_p	heat transfer area of the plate surface (eqn 3.70)	$[m^2]$
A_r	cross-sectional area of the tubing system (eqn 4.40)	$[m^2]$
a	interfacial area per unit volume of two phase dispersion	$[m^2/m^3$
a'	interfacial area per unit volume of vapour (eqn 3.59)	$[m^2/m^3$
$\overline{a}$	interfacial area per unit volume of liquid (eqn 3.61b)	$[m^2/m^3$
C_p	heat capacity	[kJ/mol K]
c_{pl}	specific heat of saturated liquid (eqn 3.66)	[KJ/kg k]
c_e	unit cost of electricity (eqn 2.14)	[£/unit]
c_s	unit cost of steam (eqn 2.14)	[£/unit]
c_w	resistance coefficient (eqn. 4.12)	[-]
D	exergy loss or anergy (eqn 2.4)	[kJ]
D	diffusivity	$[m^2/s]$
D	tube diameter (eqn 3.83 & 3.89)	[m]
d	column or plate diameter	[m]
De	Eddy diffusivity for liquid mixing	$[m^2/s]$
d_h	sieve hole diameter (eqn 4.13)	[mm]

d_T	liquid droplet diameter (eqn 4.12)	[m]
E	energy balance function (eqn 3.34 & 3.50)	[kW]
E_{ML}	Murphree liquid tray efficiency defined in eqn 3.1b	[-]
E_{MV}	Murphree liquid tray efficiency defined in eqn 3.2a	[-]
E_O	overall column efficiency	[-]
E_{OH}	heat transfer efficiency defined in eqn 2.18	[-]
E_{OV}	Murphree point efficiency defined in eqn 3.5	[-]
E_S	Standart efficiency defined in eqn 3.14 & 3.15	[-]
Δe_c	exergy loss in a conventional column (eqn 2.15)	[kJ]
Δe_h	exergy loss in HIDiC (eqn 2.16)	[kJ]
e	energy flux	[kW/ m^2]
Ex	exergy	[kJ]
F	F-Factor defined in eqn 1.2	[$kg^{0.5}/m^{0.5}s$]
F	feed rate (eqn 2.5)	[kg or kmol/s]
f	comonent feed rate (eqn 3.32)	[kmol/s]
f	friction factor (eqn 3.79)	[-]
H	enthalpy	[kJ]
H_0	enthalpy referred to environment state	[kJ]
h	heat transfer coefficient	[kW/m^2 K]
h_{ideal}	heat transfer coefficient of an ideal binary mixture (eqn 3.67)	[kW/m^2 K]
h_L	clear liquid height	[m]
h_{mc}	multicomponent heat transfer coefficient	[kW/m^2 K]
h_w	weir height	[m]
G	mass flow rate (eqn 4.31)	[kg/s]
g	gravitational acceleration	[m^2/s]
K	equilibrium ratio (eqn 3.47)	[-]
K_{OV}	overall mass transfer coefficient based on vapour (eqn 3.58b)	[kmol/m^2s]
k'	molar transfer coefficient (eqn. 2.20)	[m/s]
k	mass transfer coefficient (eqn 3.39)	[kmol/m^2 s]
k	thermal conductivity (eqn 3.85)	[kW/m K]
k_v	Sounders correlation factor (eqn 4.12)	[-]
L	liquid flow rate	[kg or kmol/s]

L	length of a single pipe in the heat exchanger plate (eqn 3.89)	[m]
l	component liquid flow (eqn 3.32)	[kmol/s]
l	tube length (vapour sampling system (eqn 4.34)	[m]
L_F	liquid flow rate per unit width of flow path on tray (eqn 3.18)	[m^2/s]
L_p	pipe length (eqn 3.83)	[m]
L_T	liquid path on tray (eqn 3.7)	[m]
Le	Lewis number ($\kappa/\rho*D*C_p$)	[-]
M	molecular weight of the vapour- and liquid phase (eqn 3.27b, 3.29 & 4.36)	[kg/kmol]
M	mass balance function (eqn 3.32)	[-]
m	slope of the binary equilibrium line	[-]
N	number of stages (eqn 3.1)	[-]
N(tot)	total interface mass transfer rate	[kmol/s]
N	total molar flux	[kmol/m^2 s]
N_L	number of liquid phase transfer units (eqn 3.21)	[-]
N_{OV}	number of overall vapour phase transfer units (eqn 3.22)	[-]
N_V	number of vapour phase transfer units (eqn 3.18)	[-]
n	molar flow (eqn 4.37)	[kmol/s]
Nu	Nusselt number (3.78)	[-]
P	pressure	[Pa]
P	vapour distillate flow rate (eqn 2.15 & 2.16)	[kmol/s]
P	distillate flow rate at the top of the column (eqn 5.5)	[kmol/s]
p	hole pitch (eqn 4.27)	[m]
Pr	Prandl number ($c_{pl}*\mu_l/k_l$)	[-]
Q	heat (eqn 2.1)	[kJ]
Q	heat removal from vapour or liquid phase (eqn 3.37)	[kW]
Q^I	interface equilibrium function (eqn 3.47)	[-]
$\dot{Q}$	total heat transfer rate (eqn 3.65)	[kW]
q	parameter in the q-line (eqn 2.15)	[-]
q	boiling heat flux (eqn 3.66)	[kW/m^2]
R	Gas constant (eqn 2.5 & 2.9)	[kJ/kg K]
R	reflux rate	[Kmol/s]

R	rate relation function (eqn 3.49)	[-]
R	total thermal resistance from inside to outside flow (eqn 4.30)	[K/W]
R	shear stress at pipe wall	[N/m^2]
r	reflux ratio (R/P)	[-]
r	reflux ratio at the bottom of the rectifying section (eqn 2.15)	[-]
r	ratio of side stream to interstage flow (eqn 3.32)	[-]
r	tube radius (eqn 4.39)	[m]
Re	Reynolds number ($4*L/\pi d\mu$)	[-]
S	entropy	[kJ/K]
S	side stream flow rate (eqn 3.33)	[kmol/s]
S	summation function (eqn 3.48)	[-]
S_0	entropy referred to environment state	[kJ/K]
Sc	vapour-phase Schmidt number ($\mu_v/\rho_v D_v$) (eqn 318)	[-]
St	Stokes number (eqn 3.76)	[-]
T	temperature	[K]
T_0	temperature of the environment	[K]
T_C	condensing temperature (eqn 2.11)	[K]
T_C	critical temperature of pure component (eqn 4.3)	[K]
T_E	evaporating temperature (eqn 2.11)	[K]
T_p	plate surface temperature (eqn 3.90)	[K]
T_p'	channel surface temperature (eqn 3.90)	[K]
T_{rect}	temperature in the rectifying section (eqn 2.16)	[K]
t_L	mean residence time of liquid in dispersion (eqn 3.7)	[s]
W	work (eqn 2.1)	[kJ]
W	weir length (eqn 3.61b)	[m]
w	vapour velocity in the column	[m/s]
w_b	bubble rise velocity	[m/s]
w_h	vapour velocity in the sieve tray holes (eqn 4.25)	[m/s]
w_s	superficial vapour velocity based on A_b	[m/s]
w_{sfl}	superficial vapour velocity at flooding based on A_b	[m/s]
V	vapour flow rate (eqn 3.32)	[kg or kmol/s]
V'	vapour flow rate per unit bubbling area (eqn 3.58b)	[$kmol/m^2s$]

V	vapour flow rate in the column (eqn 4.16)	[m^3/s]
V	molar volume (eqn 4.6)	[cm^3/mol]
v	component vapour flow (eqn 3.32)	[kmol/s]
ν	molar volume of vapour (eqn 4.38)	[m^3/mol]
x	liquid mole fraction	[-]
y	vapour mole fraction	[-]
U	internal energy (eqn 2.6)	[kJ]
U	overall heat transfer coefficient	[kW/m^2 K]
Z	Liquid flow path length	[m]
Δz	tray spacing (eqn 4.13)	(mm)

Greek

α	relative volatility (eqn 1.1)	[-]
α	liquid holdup fraction (Table 3.5)	[-]
β_0	scaling factor	[-]
γ	activity coefficient	[-]
Δ	difference between two properties	[-]
ε	effectiveness (eqn 2.7)	[-]
ε	volume of vapour per unit of two phase dispersion (vapour holdup fraction) (eqn 3.24)	[-]
ε	total interphase energy transfer rate (eqn 3.38, 346 & 354)	[J/s]
η	efficiency (defined in eqn 2.1 & 2.2)	[-]
θ	Carnot temperature (defined in eqn. 2.9b)	[-]
θ	boiling point range (eqn 3.68)	[K]
κ	thermal conductivity	[kW/m K]
λ	stripping factor (defined in eqn 3.4)	[-]
λ	latent heat	[kJ/kmol]
μ	viscosity	[Pa s]
ρ	density	[kg/m^3]
ρ'	density (eqn 3.60)	[$kmol/m^3$]
σ	surface tension	[N/m]
σ^*	surface tension of liquid-vapour interface	[N/m]
Φ	pressure drop function (eqn 4.32)	[-]

ϕ	surface heat flux (eqn 3.68)	[kW/m^2]
ψ	volume fraction of component in the bulk liquid (eqn 4.11)	[-]
ψ^{σ}	volume fraction of component in the surface liquid (eqn 4.6)	[-]

Sub- and Superscripts

-	average of physical properties
b	bubbling area
c	condenser
chem	chemical
D	distillate
F	feed
F	fluid (on the plate)
I	Interface
irrev	irreversible
i	component
j	stage number
LM	logarithmic
l	liquid
n	tray
0	environment
p	plate
p-f	plate-to-fluid
r	reboiler
rev	reversible
sep	separation
v	vapour

Appendix B

Results

Appendix B features the results of the study. Most of the data obtained has been stored as electronic files, accessible on the attached CD. Table B3 features an index of all runs performed including relevant data such as: a/diabatic mode, reboiler performance, etc. Sample calculations explain how the results for htc and E_{MV} were computed. Finally, Table B4 features measured froth heights of product withdrawal runs.

Sample calculation for obtaining heat transfer coefficients

Overall heat transfer coefficient U_p (plate side)

The Pico logger TC 08 monitored the inlet T_{in} (43.2°C) and outlet T_{out} (58.7°C) temperatures of the HEM. The first step comprised the calculation of the mean average temperature T_m (50.7°C). Additionally, the temperature difference ΔT (-15.0 degC) between the in and outlet was calculated as a parameter needed for the computation of the amount of heat Q transferred. Q is given by

$$Q = F^*C_p^*\Delta T_{HEM}$$

where F is the HEM flow rate (1.3E-2 kg/s). The average heat capacity C_p (4.181 kJ/K kg) of water was calculated for T_m (50.7°C) using eqn. 3.88.

$$C_P = 4.182 + 0.00043(T - 327.15)$$

The temperature in K is used in this empirical correlation. The HEM flow rate F was transformed into a flow/s (0.013 kg/s), which led to a value of Q of –815 W. U was calculated by eqn. 3.71.

$$U_p = \frac{Q}{A_p \Delta T_{lm}}$$

With the given fluid temperature T_f (71.9°C) the logarithmic temperature difference ΔT_{lm} (20.0 degC) was calculated. A U value of 3160W/m^2 K was obtained for our plate (A_p = 0.0129 m^2). Alternatively, U could be predicted by using eqn. 3.70.

$$\frac{1}{U_p} = \frac{A_P}{h_i A_D} + \frac{A_P t}{A_D k} + \frac{1}{h_{p-f}}$$

Computation of h_i

The film heat transfer coefficient was needed for our correlation that predicted $h^{p\text{-}f}$. h_i is based on several dimensionless parameters. The Reynolds number was calculated first by using

$$\mathrm{Re} = \frac{4F}{\pi D \mu}$$

The viscosity μ (5.45E-4 Ns/m^2) of the HEM was calculated at T_m with the empirical correlation given in eqn. 3.86 (T in K).

$$\mu = \frac{10^{-10.2158 + \frac{1.29*10^3}{T} + 1.7710^{-2}*T - 1.2610^{-5}*T^2}}{1000}$$

Taking the duct diameter D (0.006m) into account, one obtained Re = 5190. h_i was extracted from the Nusselt number, which was calculated with eqn. 3.80.

$$Nu = 0.0395\,\mathrm{Re}^{0.75}\,\mathrm{Pr}^{\frac{1}{3}}$$

The Prandl number Pr (3.58) was computed by using

$$\mathrm{Pr} = \frac{C_p \mu}{k}$$

with the thermal conductivity κ (0.637 W/mK), computed from the empirical correlation given in eqn.3.87 (T in K).

$$k = -2.758*10^{-1} + 4.612*10^{-3}*T - 5.5391*10^{-6}*T^2$$

This gave a Nu = 36.67 that was used in eqn. 3.85 for obtaining h_i = 4690 W/m^{2}K.

$$h_i = \frac{Nu * k}{D}$$

Prediction of $h_{p\text{-}f}$

Before a thermocouple was installed in the Dural of the heat exchanger plate, we calculated the temperature of the plate surface for the prediction of $h_{p\text{-}f}$, which was derives from the heat flux balances given in eqn. 3.89 – 3.91.

$$Fc_p(T_{in} - T_{out}) = h_i 6\pi DL(T_{HEM} - T_p')_{lm}$$

$$Fc_p(T_{in} - T_{out}) = kA_p \frac{T_p' - T_p}{t}$$

$$Fc_p(T_{in} - T_{out}) = h_{p-f} A_p (T_p - T_f)$$

The eqn. were solved for the three unknowns: T_p' (temperature of channel surface: 67.2°C), T_p (plate surface: 68.0°C) and $h_{p\text{-}f}$ (plate-to-fluid htc: 16300 Wm^2K). Those values were obtained with a thermal conductivity k of the Dural of 174 W/m K, a Dural thickness t of 0.002m. and a duct length L of 0.095m. The other parameters were taken from the example mentioned above (F = 1.3E-2 kg/s, C_p = 4.181 kJ/K kg, T_{in}–T_{out} = -15.0 K, T_{HEM} = 50.7°C, T_f = 71.9°C, A_p = 0.0129m^2, h_i = 4690 W/m^2K). The calculation was simplified by replacing $(T_{HEM} - T_p')_{lm}$ with $\Delta(T_{HEM} - T_p')_{arithmetic}$.

Calculation of $h_{p\text{-}f}$

The insertion of the thermocouple in the Dural of the heat transfer plate allowed the experimental determination of by using the heat flux balance given in eqn 3.91.

$$Fc_p(T_{in} - T_{out}) = h_{p-f} A_p (T_p - T_f)$$

With the following parameters (F = 1.3E-2 kg/h, C_p = 4.181 kJ/K kg, T_{in}–T_{out} = -17.9 K, T_p = 65.8°C, T_f = 73.7°C) a $h_{p\text{-}f}$ of 9840 W/m^2K was obtained.

Sample calculation for obtaining Murphree tray efficiencies

The definition of the vapour phase Murhpree tray efficiency is given in eqn. 3.2a.

$$E_{MV} = \frac{\bar{y}_n - \bar{y}_{n-1}}{y_n^* - \bar{y}_{n-1}}$$

The gas chromatograph (GC) produced area values of the integrated peaks. The results for the GC data transformations are given in Table A.1.

	Area H_2O	Area MeOH	Area ratio H_2O/MeOH	Mole ratio H_2O/MeOH	Mole fraction H_2O
Liquid sample	6547004	2778623	2.356	4.618	0.822
Vapour sample top	2470328	3963333	0.623	1.284	0.562
Vapour sample bottom	492200	246448	1.997	3.92	0.797

TableB.1: GC data transformations

The peak areas obtained ratio was transformed into mole ratio by using the function derived from the calibration runs, given in Figure 4.3

Mole ratio = 1.9242*Area Ratio+0.085

This was followed by the computation of the mole fraction of water from

$$Mole\ fraction = \frac{Mole\ ratio}{Mole\ ratio + 1}$$

The corresponding mole fraction of methanol were obtained from the simple correlation $x_{MeOH} = 1\text{-}x_{H20}$. Table B.2 shows the mole fractions of the two vapour samples and the liquid sample. The vapour composition y* in equilibrium with the liquid sample was obtained by applying the Wilson VLE model.

sample	Mole fraction MeOH
y_n	0.437
y_{n-1}	0.203
x_n	0.178
y^*_n	0.560

Table B.2:Methanol mole fraction values for E_{MV} calculations

With the values from Table B2 the computation of the Murphree vapour tray efficiency was straightforward.

$$\frac{0.437 - 0.203}{0.560 - 0.203} = 0.655$$

Table B.3 is an index of all the runs performed. This is followed by tables which feature examples of the prediction of $h_{p\text{-}f}$. Detailed information can be found in the CD attached to the thesis. The tray efficiency values are given as result table on the CD.

Date of run	Mode	Reboiler load in kW	Reflux ratio
31.05.03	Cooling	9.6	total reflux
02.06.03[50]	Cooling	15.0	total reflux
04.06.03	Adiabatic	15.0	total reflux
05.06.03	Heating	15.0	total reflux
09.06.03	Cooling	10.0	total reflux
10.06.03	Cooling	15.0	total reflux
11.06.03	Heating	15.0	total reflux
14.07.03	Heating	15.0	total reflux
14.07.03	Cooling	15.0	total reflux
20.08.03	Adiabatic	15.0	total reflux

Table B.3: Index of conducted runs

[50] no PICO logger data available for this run

Date of run	Mode	Reboiler load in kW	Reflux ratio
22.08.03	Adiabatic	15.0	total reflux
24.08.03	Adiabatic	13.5	total reflux
25.08.03	Adiabatic	13.5	total reflux
25.08.03	Cooling	13.5	total reflux
26.08.03	Cooling	12.0	total reflux
26.03.03	Cooling	10.5	total reflux
27.08.03	Adiabatic	12.8	total reflux
27.08.03	Cooling	12.8	total reflux
28.08.03	Adiabatic	13.5	15[51]
29.08.03	Adiabatic	14.4	15[51]
09.10.03	Adiabatic	14.4	total reflux
10.10.03	Adiabatic	14.4	total reflux
13.10.03	Adiabatic	14.4	total reflux
15.10.03	Adiabatic	14.4	total reflux
16.10.03	Adiabatic	14.4	total reflux
16.10.03	Adiabatic	14.4	total reflux
17.10.03	Adiabatic	14.4	total reflux
07.01.04	Cooling run	16.0	total reflux
08.01.04	Adiabatic	14.4	total reflux
08.01.04	Cooling run	14.4	total reflux
09.01.04	Adiabatic	13.6	total reflux
09.01.04	Cooling run	13.6	total reflux
13.01.04	Cooling run	12.8	total reflux

TableB.3: Index of conducted runs.

[51] test run for product withdrawal

Date of run	Mode	Reboiler load in kW	Reflux ratio
14.01.04	Adiabatic	12.8	total reflux
14.01.04	Cooling run	12.8	total reflux
15.01.04	Adiabatic	11.2	total reflux
15.01.04	Cooling run	11.2	total reflux
16.01.04	Cooling run	13.6	total reflux
19.01.04	Heating run	13.6	total reflux
20.01.04	Heating	13.6	total reflux
22.01.04	Adiabatic	14.4	total reflux
22.01.04	Heating	14.4	total reflux
23.01.04	Adiabatic	14.4	total reflux
02.02.04	Adiabatic	16.0	total reflux
03.02.04	Heating	16.0	total reflux
04.02.04	Adiabatic	16.0	total reflux
04.02.04	Heating	16.0	total reflux
05.02.04	Adiabatic	12.8	total reflux
06.02.04	Heating	12.8	total reflux
09.02.04	Heating	11.2	total reflux
10.02.04	Adiabatic	11.2	total reflux
10.02.04	Adiabatic	12.8	total reflux
11.02.04	Heating	12.8	total reflux
12.02.04	Adiabatic	13.6	total reflux
12.02.04	Adiabatic	14.4	total reflux
13.02.04	Heating	14.4	total reflux
16.02.04	Adiabatic	16.0	6.5

Table B.3: Index of conducted runs.

Date of run	Mode	Reboiler load in kW	Reflux ratio
23.03.04	Adiabatic	16.0	7.0
23.03.04	Cooling	16.0	5.3
24.03.04	Heating	16.0	7.6
25.03.04	Cooling	16.0	3.6
26.03.04	Cooling	16.0	4.2
29.03.04	Cooling	16.0	2.7
29.03.04	Cooling	16.0	3.0
30.03.04	Heating	16.0	3.2
30.03.04	Cooling	16.0	2.1
31.03.04	Adiabatic	16.0	2.1
01.04.04	Adiabatic	16.0	3.2
01.04.04	Heating	16.0	2.2
02.04.04	Adiabatic	16.0	1.0
05.04.04	Adiabatic	16.0	1.2
06.04.04	Adiabatic	16.0	1.0
06.04.04	Heating	16.0	1.1
08.040.4	Cooling	16.0	1.1
15.04.04	Adiabatic	16.0	3.1
16.04.04	Cooling	16.0	6.8
16.04.04	Adiabatic	16.0	4.1
18.04.04	Cooling	16.0	1.3
19.04.04	Heating	16.0	4.0
19.04.04	Heating	16.0	2.1

Table B.3: index of conducted runs

Table of predicted $h_{p\text{-}f}$/ U and experimental $h_{f\,p}$ for total reflux runs

F kg/min	T_m ^0C	T_f ^0C	h_i W/m^2 K	Q W	$T_{p'}$ ^0C	T_p ^0C	$h_{p\text{-}fcalc}$ W/m^2 K	U W/m^2 K	Re -	$T_{p\,cexp}$ ^0C	$h_{p\text{-}f\,cexp}$ W/m^2 K	date of run -
1.13	35.7	93.1	5298	-1766	66.7	68.3	5533	2381	5.51E+03	-	-	31.05.2003
1.13	42.6	93.3	5695	-1631	69.2	70.7	5591	2486	6.30E+03	-	-	Water run
1.13	52.9	94.0	6287	-1378	73.3	74.5	5478	2590	7.59E+03	-	-	
0.80	57.9	94.5	5002	-1147	79.3	80.3	6259	2425	5.86E+03	-	-	
0.80	61.1	95.1	5139	-1026	79.7	80.6	5483	2333	6.16E+03	-	-	
0.80	66.9	96.0	5385	-933	83.1	83.9	5968	2481	6.73E+03	-	-	
1.13	36.5	87.6	5342	-1929	70.1	71.8	9484	2917	5.59E+03	-	-	02.06.2003
1.13	42.0	88.4	5660	-1727	70.4	71.9	8144	2878	6.23E+03	-	-	Water run
1.13	46.6	88.8	5923	-1616	71.9	73.4	8142	2958	6.78E+03	-	-	
1.13	52.0	91.6	6234	-1430	73.3	74.6	6525	2790	7.47E+03	-	-	
0.80	57.5	93.6	4985	-1188	79.7	80.8	7195	2548	5.82E+03	-	-	
0.80	61.2	93.4	5143	-1137	81.8	82.8	8335	2732	6.17E+03	-	-	
0.80	63.3	93.7	5233	-1074	82.4	83.4	8078	2734	6.38E+03	-	-	
0.80	64.8	93.5	5295	-1020	82.7	83.6	8019	2747	6.52E+03	-	-	
1.13	84.5	72.4	8012	628	77.2	76.7	11451	4004	1.20E+04	-	-	05.06.2003
1.13	85.2	72.8	8050	644	77.8	77.2	11294	3996	1.21E+04	-	-	
1.13	85.6	73.9	8066	667	77.9	77.3	15401	4418	1.21E+04	-	-	
1.13	85.8	74.5	8079	646	78.4	77.8	14996	4388	1.22E+04	-	-	
1.13	86.7	74.6	8125	597	79.9	79.3	9782	3808	1.23E+04	-	-	
0.80	87.5	75.4	6215	415	81.3	80.9	5870	2659	8.83E+03	-	-	
1.13	48.9	70.9	6057	-915	63.0	63.8	9953	3213	7.07E+03	-	-	06.06.2003
1.13	49.4	70.7	6085	-905	63.2	64.0	10517	3279	7.13E+03	-	-	
1.13	49.6	71.2	6100	-930	63.8	64.7	11003	3330	7.17E+03	-	-	
1.13	49.6	71.2	6098	-921	63.7	64.5	10625	3294	7.16E+03	-	-	
1.13	49.6	71.3	6096	-907	63.4	64.2	9927	3223	7.16E+03	-	-	

Table of predicted $h_{p\text{-}f}$/ U and experimental $h_{f\,p}$ for total reflux runs

F kg/min	T_m ^0C	T_f ^0C	h_i W/m^2 K	Q W	$T_{p'}$ ^0C	T_p ^0C	$h_{p\text{-}fcalc}$ W/m^2 K	U W/m^2 K	Re -	$T_{p\,cexp}$ ^0C	$h_{p\text{-}f\,cexp}$ W/m^2 K	date of run -
0.80	50.7	71.9	4691	-832	67.2	68.0	16335	3032	5.19E+03	-	-	06.06.2003
0.80	50.7	71.7	4691	-770	66.0	66.7	11895	2836	5.19E+03	-	-	
0.80	50.3	71.9	4672	-794	66.1	66.8	12110	2840	5.16E+03	-	-	
0.80	50.6	72.3	4684	-813	66.7	67.4	12943	2889	5.18E+03	-	-	
0.48	51.6	69.9	3117	-503	66.6	67.1	13877	2128	3.13E+03	-	-	09.06.2003
0.48	51.0	70.0	3098	-503	66.1	66.5	11155	2042	3.10E+03	-	-	
0.48	50.7	70.1	3090	-522	66.4	66.9	12640	2082	3.08E+03	-	-	
0.48	50.6	70.1	3088	-528	66.5	67.0	13425	2102	3.08E+03	-	-	
0.48	51.3	70.3	3108	-511	66.6	67.0	12351	2084	3.12E+03	-	-	
1.43	48.2	69.6	7271	-999	61.0	61.9	10030	3605	8.85E+03	-	-	
1.43	48.5	69.8	7293	-955	60.7	61.6	9037	3474	8.90E+03	-	-	
1.43	51.1	70.2	7469	-885	62.1	62.9	9367	3570	9.31E+03	-	-	
1.43	50.6	69.9	7434	-888	61.7	62.5	9265	3546	9.23E+03	-	-	
1.43	47.8	70.3	7245	-993	60.6	61.5	8760	3419	8.79E+03	-	-	
0.48	51.6	72.7	3118	-596	69.4	70.0	16858	2188	3.13E+03	-	-	10.06.2003
0.48	51.2	73.0	3106	-603	69.3	69.8	14787	2143	3.11E+03	-	-	
0.48	51.4	73.1	3111	-642	70.6	71.2	26181	2290	3.12E+03	-	-	
0.48	50.6	72.9	3088	-635	69.8	70.3	19146	2205	3.08E+03	-	-	
0.80	49.4	73.0	4632	-900	67.5	68.3	14881	2950	5.07E+03	-	-	
0.80	49.7	73.0	4648	-878	67.3	68.1	13737	2909	5.11E+03	-	-	
0.80	51.2	73.0	4713	-804	67.1	67.8	12029	2853	5.24E+03	-	-	
0.80	50.4	73.3	4678	-851	67.3	68.1	12785	2878	5.17E+03	-	-	
1.13	47.0	72.3	5949	-1096	64.1	65.1	11890	3350	6.84E+03	-	-	
1.13	47.6	73.1	5980	-1142	65.3	66.3	13118	3453	6.91E+03	-	-	
1.13	48.4	73.0	6027	-1107	65.4	66.4	13065	3468	7.01E+03	-	-	
1.13	49.4	73.1	6085	-1020	65.0	65.9	11058	3330	7.14E+03	-	-	

Table of predicted $h_{p\text{-}f}$/ U and experimental $h_{f\,p}$ for total reflux runs

F kg/min	T_m ^0C	T_f ^0C	h_i W/m^2 K	Q W	$T_{p'}$ ^0C	T_p ^0C	$h_{p\text{-}fcalc}$ W/m^2 K	U W/m^2 K	Re -	$T_{p\,cexp}$ ^0C	$h_{p\text{-}f\,cexp}$ W/m^2 K	date of run -
1.43	51.7	73.4	7510	-1079	65.0	66.0	11313	3834	9.40E+03	-	-	10.06.2003
1.43	50.4	73.5	7422	-1181	65.2	66.2	12607	3942	9.20E+03	-	-	
1.43	48.6	73.4	7297	-1308	65.3	66.4	14560	4068	8.91E+03	-	-	
1.43	47.3	73.4	7210	-1307	64.2	65.4	12624	3871	8.72E+03	-	-	
0.33	52.3	74.6	2316	-575	75.5	76.0	-32093	2001	2.17E+03	-	-	
0.33	51.6	74.7	2300	-558	74.2	74.7	1350854	1868	2.14E+03	-	-	
0.33	81.1	77.2	2901	113	77.5	77.4	50652	2241	3.32E+03	-	-	11.06.2003
0.33	83.9	77.8	2956	160	78.9	78.7	13331	2025	3.43E+03	-	-	
0.33	84.8	77.7	2973	170	79.5	79.4	7907	1842	3.47E+03	-	-	
0.33	84.9	78.6	2975	162	79.9	79.7	10751	1964	3.48E+03	-	-	
0.48	86.5	79.1	4070	228	81.3	81.1	8781	2373	5.18E+03	-	-	
0.48	87.5	79.5	4097	237	82.1	81.9	7395	2268	5.24E+03	-	-	
0.48	87.9	79.8	4107	249	82.3	82.1	8557	2371	5.27E+03	-	-	
0.48	88.2	80.1	4113	256	82.4	82.1	9472	2439	5.28E+03	-	-	
0.80	89.9	80.9	6308	396	84.0	83.7	11046	3408	9.08E+03	-	-	
0.80	89.8	81.0	6306	378	84.2	83.9	9884	3288	9.07E+03	-	-	
0.80	88.6	81.1	6259	306	84.0	83.8	8886	3155	8.94E+03	-	-	
0.80	86.1	80.8	6161	323	81.2	80.9	234116	4723	8.68E+03	-	-	
1.13	90.4	81.6	8314	421	85.7	85.3	8599	3659	1.28E+04	-	-	
1.13	90.6	81.7	8322	424	85.8	85.5	8741	3687	1.29E+04	-	-	
1.13	89.8	81.5	8280	374	85.6	85.2	7769	3493	1.27E+04	-	-	
1.43	89.5	82.0	9985	385	85.9	85.5	8354	3960	1.61E+04	-	-	
1.43	90.1	82.1	10024	406	86.3	86.0	8157	3922	1.62E+04	-	-	
1.43	90.8	82.5	10066	428	86.8	86.4	8395	3985	1.63E+04	-	-	
0.33	47.7	74.9	2217	-679	76.2	76.8	-27628	1931	2.00E+03	76.9	-26589	14.07.2003 I
0.33	51.0	74.3	2289	-580	74.6	75.2	-51347	1932	2.12E+03	69.4	9258	
0.33	50.1	74.5	2269	-602	74.8	75.3	-57478	1907	2.09E+03	69.7	9744	

Table of predicted $h_{p\text{-}f}$ / U and experimental $h_{f\,p}$ for total reflux runs

F kg/min	T_m ^0C	T_f ^0C	h_i W/m^2 K	Q W	$T_{p'}$ ^0C	T_p ^0C	$h_{p\text{-}fcalc}$ W/m^2 K	U W/m^2 K	Re -	$T_{p\,cexp}$ ^0C	$h_{p\text{-}f\,cexp}$ W/m^2 K	date of run -
0.33	50.9	74.9	2286	-622	76.3	76.8	-25233	2008	2.12E+03	70.4	10740	14.07.2003 I
0.33	52.0	75.4	2308	-584	75.5	76.0	-70087	1929	2.16E+03	70.6	9410	
0.48	51.6	75.0	3117	-709	72.8	73.4	34850	2345	3.13E+03	68.9	8951	
0.48	51.5	75.2	3114	-737	73.5	74.2	54392	2401	3.13E+03	69.1	9317	
0.48	51.3	75.1	3109	-727	73.1	73.8	41667	2365	3.12E+03	69.5	10039	
0.48	51.3	75.7	3107	-754	73.8	74.5	48799	2384	3.11E+03	70.2	10622	
0.80	49.6	75.3	4642	-1029	70.2	71.1	19101	3091	5.09E+03	67.3	9920	
0.80	52.6	75.6	4771	-970	71.5	72.4	22908	3248	5.36E+03	67.7	9519	
0.80	54.2	76.1	4844	-925	72.0	72.8	22094	3271	5.52E+03	68.6	9523	
0.80	54.5	76.3	4856	-916	72.1	72.9	20966	3252	5.54E+03	68.2	8806	
1.13	51.3	75.8	6197	-1203	69.4	70.5	17363	3789	7.38E+03	65.3	8844	
1.13	50.8	76.2	6165	-1220	69.2	70.3	15980	3705	7.31E+03	66.1	9377	
1.13	49.9	75.9	6115	-1239	68.8	69.9	15985	3683	7.20E+03	66.8	10533	
1.43	49.1	75.7	7330	-1435	67.3	68.6	15598	4158	8.99E+03	65.2	10638	
1.43	49.1	75.7	7333	-1469	67.7	69.1	17044	4256	8.99E+03	66.4	12168	
1.43	49.0	75.8	7324	-1459	67.5	68.8	16192	4197	8.97E+03	66.1	11698	
1.43	48.9	75.8	7317	-1455	67.4	68.7	15775	4166	8.96E+03	63.9	9456	
1.43	48.9	75.7	7317	-1481	67.7	69.0	17291	4264	8.96E+03	67.0	13228	
0.33	84.4	79.1	2965	91	81.5	81.4	2991	1330	3.45E+03	81.7	2679	14.07.2003 II
0.33	85.2	79.1	2980	111	81.7	81.6	3362	1403	3.49E+03	81.9	2995	
0.33	85.7	79.3	2989	129	81.7	81.5	4404	1559	3.51E+03	81.6	4287	
0.33	86.0	79.4	2996	128	82.1	81.9	3958	1502	3.52E+03	82.1	3757	
0.48	87.3	80.0	4090	185	83.1	82.9	5019	1979	5.23E+03	82.7	5363	
0.48	87.7	80.1	4102	177	83.7	83.5	3990	1799	5.26E+03	83.9	3600	
0.48	87.0	80.8	4084	145	83.7	83.6	3981	1793	5.21E+03	83.8	3718	
0.80	88.9	81.0	6270	264	85.0	84.7	5408	2571	8.97E+03	84.1	6591	
0.80	89.0	81.2	6275	266	85.1	84.8	5668	2629	8.99E+03	85.0	5366	
0.80	89.2	81.2	6284	269	85.3	85.0	5506	2596	9.01E+03	84.4	6569	

Table of predicted $h_{p\text{-}f}$ / U and experimental $h_{f\,p}$ for total reflux runs

F kg/min	T_m ^0C	T_f ^0C	h_i W/m^2 K	Q W	$T_{p'}$ ^0C	T_p ^0C	$h_{p\text{-}fcalc}$ W/m^2 K	U W/m^2 K	Re -	$T_{p\,cexp}$ ^0C	$h_{p\text{-}f\,cexp}$ W/m^2 K	date of run -
0.80	89.4	81.6	6290	261	85.5	85.3	5490	2593	9.03E+03	84.7	6504	14.07.2003 II
0.80	89.4	81.7	6290	266	85.5	85.2	5764	2653	9.03E+03	84.7	6756	
1.13	90.4	82.1	8314	330	86.7	86.4	5933	3072	1.28E+04	85.3	8090	
1.13	90.4	82.3	8311	326	86.7	86.4	6115	3119	1.28E+04	85.6	7796	
1.13	90.5	82.0	8318	328	86.8	86.6	5629	2989	1.29E+04	85.5	7418	
1.43	91.0	82.8	10078	377	87.5	87.2	6726	3566	1.64E+04	85.8	9674	
1.43	91.0	83.0	10076	369	87.5	87.2	6754	3574	1.64E+04	86.0	9628	
1.43	91.0	82.5	10076	383	87.4	87.1	6533	3511	1.64E+04	85.8	8966	
1.43	91.0	82.8	10078	385	87.4	87.1	6901	3615	1.64E+04	86.1	8986	
0.48	46.6	73.0	2211	-808	80.6	81.3	-7554	2363	2.87E+03	68.8	14905	25.08.2003
0.48	45.9	73.1	2196	-735	77.1	77.7	-12173	2096	2.83E+03	65.8	7874	
0.48	47.5	73.4	2229	-669	75.4	76.0	-19884	1997	2.91E+03	67.9	9546	
0.80	48.9	73.6	3431	-1130	79.6	80.6	-12445	3544	5.03E+03	68.3	16554	
0.80	47.4	73.0	3381	-910	72.5	73.3	-297304	2745	4.90E+03	65.6	9538	
0.80	47.2	73.3	3376	-879	71.5	72.3	63412	2604	4.88E+03	64.5	7702	
1.13	46.6	73.5	4407	-1087	69.5	70.5	28132	3119	6.79E+03	64.5	9340	
1.13	46.5	73.2	4402	-1095	69.6	70.6	32382	3162	6.77E+03	64.1	9321	
1.13	46.5	73.7	4402	-1105	69.8	70.8	29583	3133	6.77E+03	64.5	9289	
1.13	45.9	73.3	4379	-1066	68.6	69.6	21987	3010	6.71E+03	64.8	9759	
1.13	46.0	73.6	4383	-1095	69.3	70.3	25166	3065	6.72E+03	64.9	9726	
0.48	48.6	72.0	2254	-600	73.4	73.9	-24438	1983	2.97E+03	66.0	7785	26.08.2003 I
0.48	49.6	72.2	2275	-594	73.9	74.4	-20547	2034	3.02E+03	66.6	8277	
0.48	49.5	72.7	2274	-597	74.0	74.5	-25310	1995	3.02E+03	67.7	9317	
0.80	47.8	72.1	3395	-819	70.3	71.0	55986	2603	4.94E+03	65.2	9144	
0.80	47.4	72.7	3381	-849	70.7	71.5	55080	2591	4.90E+03	65.9	9660	
0.80	46.9	72.3	3364	-861	70.7	71.5	76667	2614	4.85E+03	65.1	9230	
1.13	45.9	72.9	4379	-1055	68.4	69.3	23029	3028	6.71E+03	64.8	10125	

Table of predicted $h_{p\text{-}f}$/ U and experimental $h_{f\,p}$ for total reflux runs

F kg/min	T_m ^0C	T_f ^0C	h_i W/m^2 K	Q W	$T_{p'}$ ^0C	T_p ^0C	$h_{p\text{-}fcalc}$ W/m^2 K	U W/m^2 K	Re -	$T_{p\,cexp}$ ^0C	$h_{p\text{-}f\,cexp}$ W/m^2 K	date of run -
1.13	45.8	72.5	4374	-1027	67.7	68.6	20281	2973	6.70E+03	63.4	8759	26.08.2003 I
1.13	45.9	72.3	4379	-1032	67.9	68.8	22834	3025	6.71E+03	64.0	9660	
1.13	46.1	72.5	4385	-1025	67.8	68.8	21317	3001	6.73E+03	64.2	9571	
1.13	46.0	72.6	4381	-1033	67.9	68.8	21390	3000	6.71E+03	63.9	9254	
1.13	46.2	72.9	4389	-1073	68.9	69.9	27501	3101	6.74E+03	64.5	9934	
1.43	45.6	72.9	5272	-1202	66.8	67.9	18562	3399	8.44E+03	63.5	9921	
1.43	45.8	72.9	5281	-1189	66.7	67.8	18112	3388	8.47E+03	64.1	10569	
1.43	46.1	72.5	5296	-1197	67.1	68.1	21180	3490	8.51E+03	63.5	10229	
0.48	46.0	72.8	2198	-706	75.9	76.5	-14736	2037	2.84E+03	67.3	9873	26.08.2003 II
0.48	45.9	73.6	2196	-719	76.4	77.0	-16104	2011	2.83E+03	68.4	10757	
0.48	45.9	73.7	2197	-734	77.0	77.7	-14298	2044	2.83E+03	68.7	11268	
0.80	44.0	73.7	3269	-997	72.3	73.2	158580	2590	4.60E+03	65.5	9386	
0.80	44.5	73.7	3287	-999	72.8	73.7	-16046146	2647	4.65E+03	65.8	9838	
0.80	45.2	73.6	3309	-973	72.6	73.4	405502	2647	4.71E+03	66.0	9940	
1.13	45.2	73.6	4347	-1136	69.5	70.5	28895	3092	6.62E+03	64.1	9289	
1.13	45.5	74.0	4361	-1098	68.9	69.9	21111	2983	6.66E+03	64.7	9208	
1.13	46.0	74.1	4383	-1117	69.8	70.8	25771	3074	6.72E+03	65.5	10001	
1.13	46.1	74.4	4385	-1115	69.7	70.7	23757	3044	6.73E+03	65.6	9832	
1.13	46.1	74.0	4387	-1113	69.7	70.7	26513	3086	6.73E+03	64.6	9244	
1.43	45.6	73.9	5270	-1248	67.6	68.7	18535	3397	8.44E+03	63.5	9278	
1.43	46.0	74.3	5295	-1255	68.1	69.2	19343	3436	8.51E+03	64.3	9800	
1.43	46.2	73.7	5302	-1201	67.2	68.3	17336	3370	8.53E+03	63.7	9346	
1.43	46.5	73.7	5317	-1212	67.7	68.7	19041	3438	8.58E+03	63.9	9585	
0.48	50.3	75.0	2289	-684	78.1	78.7	-14611	2134	3.06E+03	69.6	9707	27.08.2003
0.48	50.5	75.8	2294	-711	79.3	79.9	-13220	2172	3.07E+03	70.3	10070	
0.48	49.8	76.5	2280	-723	79.4	80.0	-16133	2096	3.04E+03	71.0	10173	
0.48	49.6	76.3	2275	-744	80.0	80.7	-13216	2152	3.02E+03	71.1	11111	

Table of predicted $h_{p\text{-}f}$ / U and experimental $h_{f\,p}$ for total reflux runs

F kg/min	T_m ^0C	T_f ^0C	h_i W/m^2 K	Q W	$T_{p'}$ ^0C	T_p ^0C	$h_{p\text{-}fcalc}$ W/m^2 K	U W/m^2 K	Re -	$T_{p\,cexp}$ ^0C	$h_{p\text{-}f\,cexp}$ W/m^2 K	date of run -
0.80	48.5	77.6	3417	-1045	77.0	77.9	-272869	2776	5.00E+03	69.6	10156	
0.80	47.7	76.6	3390	-1035	76.1	77.0	-172739	2771	4.92E+03	69.7	11779	27.08.2003
0.80	48.4	77.2	3414	-1059	77.3	78.2	-82053	2840	4.99E+03	69.6	10814	
1.13	47.9	77.2	4462	-1273	74.4	75.6	62250	3359	6.95E+03	68.5	11452	
1.13	48.1	76.8	4471	-1275	74.6	75.8	94639	3428	6.97E+03	68.4	11808	
1.13	48.4	77.4	4485	-1279	75.0	76.1	76374	3408	7.02E+03	68.6	11228	
1.13	48.5	77.3	4490	-1277	75.0	76.1	86610	3430	7.03E+03	68.5	11323	
1.13	48.5	77.2	4488	-1270	74.8	76.0	76798	3412	7.03E+03	68.0	10628	
1.13	48.6	77.3	4494	-1248	74.5	75.6	56229	3361	7.04E+03	68.2	10652	
1.13	48.8	77.0	4499	-1271	75.0	76.2	116024	3471	7.06E+03	68.2	11210	
1.13	48.8	77.8	4501	-1282	75.3	76.4	75155	3417	7.06E+03	68.8	11068	
1.13	48.9	77.7	4503	-1273	75.2	76.3	69968	3407	7.07E+03	67.9	10037	
1.13	49.0	78.1	4509	-1293	75.7	76.8	78729	3430	7.09E+03	67.5	9475	
1.43	48.2	78.3	5406	-1425	72.7	74.0	25775	3656	8.85E+03	67.2	10018	
1.43	48.6	77.9	5425	-1422	73.0	74.2	30011	3743	8.91E+03	67.3	10442	
1.43	48.8	78.2	5440	-1441	73.5	74.8	32838	3791	8.95E+03	69.0	12106	

Reflux ratio	Mode	Froth height in mm	Date of run
1	Cooling	15	08.04.2004
1	Adiabatic	18	05.04.2004
1	Heating	22	06.04.200
2	Adiabatic	19	01.04.2004
3	Adiabatic	20	15.04.2004
4	Adiabatic	21	16.04.2004
2	Cooling	17	30.03.2004
3	Cooling	17	25.03.2004
4	Cooling	18	26.03.2004
7	Cooling	22	16.04.2004
3	Heating	26	01.04.2004
7	Heating	31	24.03.2004

Table B.4: Froth height of product withdrawal runs

Appendix C

HIDiC Maruzen data

Appendix C features pictures of the control room screen of the Maruzen bench scale HIDiC, which were the basis of the heat transfer and number of theoretical stages calculations given in Chapter 5. Temperature dependant heat capacities and the heat of vaporisation were calculated with the empirical eqn. given below. The constants needed for the computation are given in Table C.1.

$$c_P = A' + BT + CT^2 + DT^3 \qquad \bar{c}_P = \frac{1}{T_2 - T_1}\int_{T1}^{T2} A' + BT + CT^2 + DT^3 dt$$

$$h_{vap} = A''\left(1 - \frac{T}{T_C}\right)^n$$

$$k = \frac{Q}{A * \Delta T_m}$$

$$Q = N_{tot} * c_p * \Delta T + N_{tot} * c_{vap}$$

Constant	benzene	toluene
A'	-31.662	83.703
A''	49.888	50.139
B	1.3043	5.1666E-1
C	-3.6078E-3	-1.4910E-3
D	3.8243E-6	1.9725E-6
N	0.489	0.383
T_C	562.16 K	591.79K

Table C.1: constants for the calculation of C_p and C_{vap}

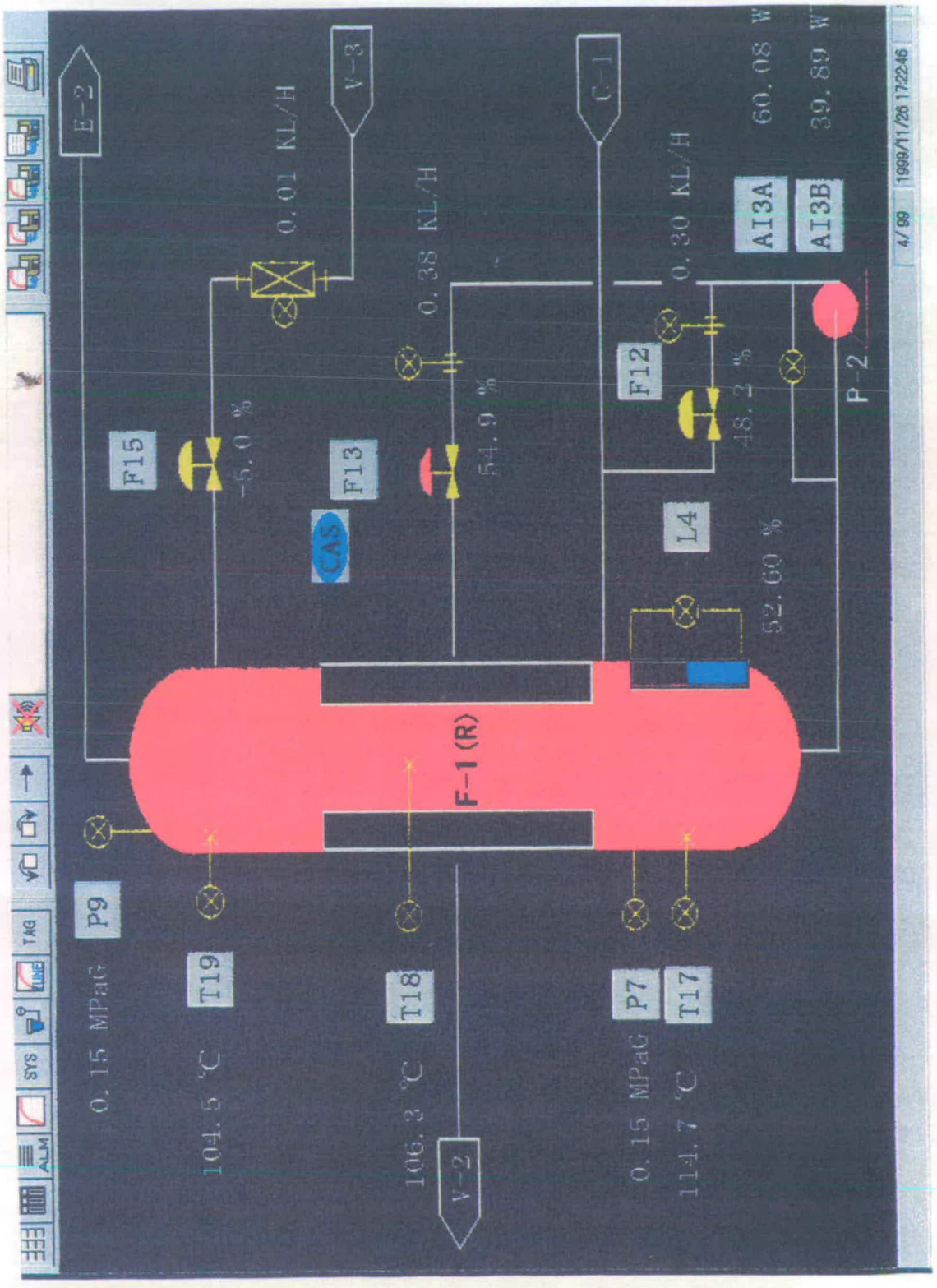

Figure C.1: Picture of the control screen of the rectifying section in Maruzen, Japan.

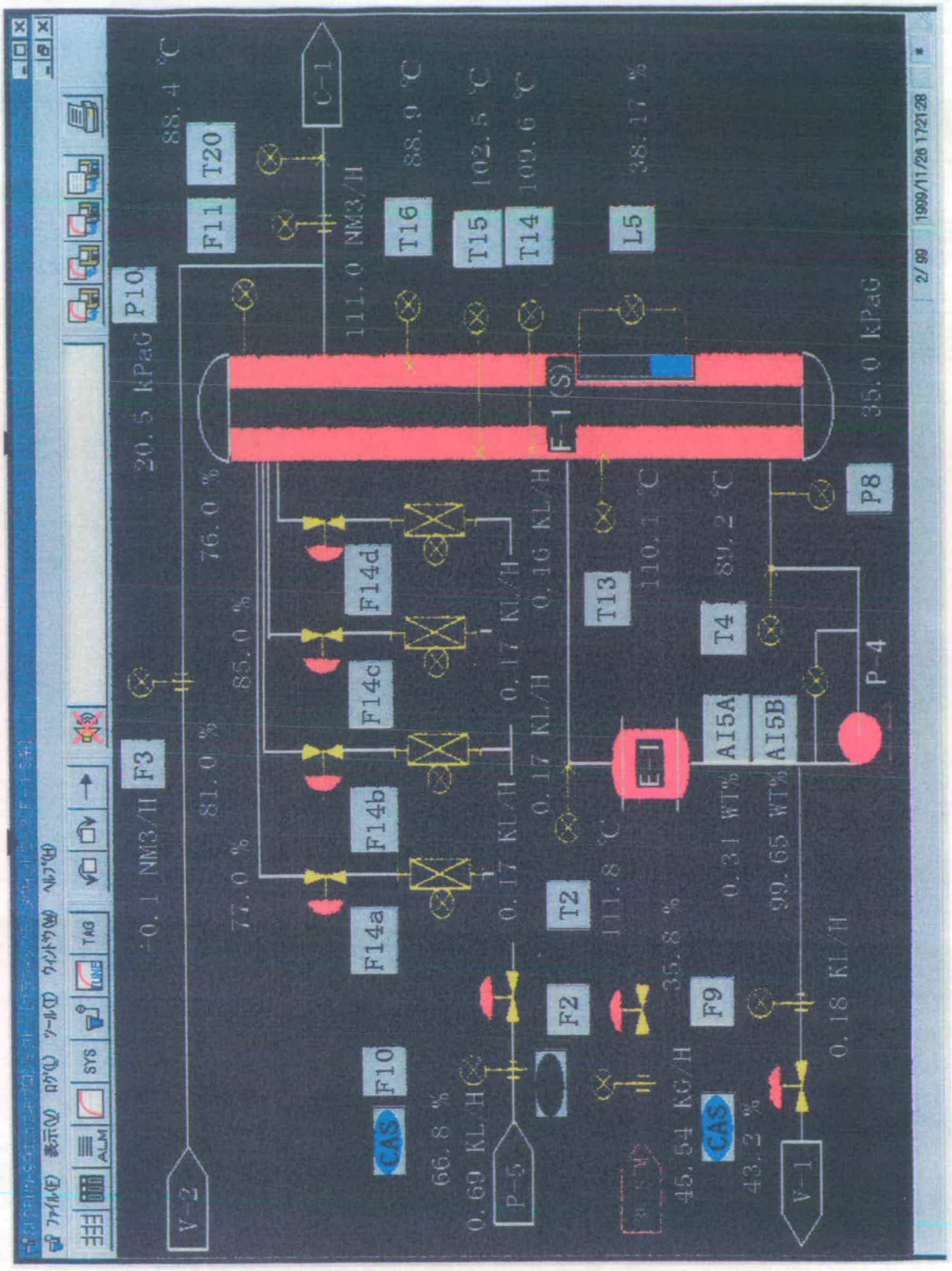

Figure C.2: Picture of the control screen of the stripping section in Maruzen, Japan.

Appendix D

Calibration figures and tables

Appendix D contains tables of the liquid and vapour sampling calibration including different approaches than the area ratio calibration approach, stated in Chapter 4. Furthermore, an example of a thermocouple calibration is given at the end of Appendix D.

Run No	Area H_2O	Area MeOH	Area Ratio	Total Area	Comments
Run 4	4213573	3599791	1.1705049	7813364	30 mol % MeOH
Run 5	4215375	3581093	1.17711967	7796468	30 mol % MeOH
Run 7	3228570	4468795	0.72246993	7697365	40 mol % MeOH
Run 8	3257068	4461260	0.73007805	7718328	40 mol % MeOH
Run 9	3237592	4478527	0.72291448	7716119	40 mol % MeOH
Run 12	2461879	5194800	0.47391218	7656679	50 mol % MeOH
Run 13	2463119	5188112	0.47476211	7651231	50 mol % MeOH
Run 42	1748000	5724030	0.30537925	7472030	60.4 mol % MeOH
Run 43	1749792	5738471	0.30492304	7488263	60.4 mol % MeOH
Run 44	1760862	5736681	0.30694787	7497543	60.4 mol % MeOH
Run 27	1021212	6197932	0.16476657	7219144	70 mol % MeOH
Run 30	1027313	6167706	0.16656322	7195019	70 mol % MeOH
Run 36	625307	6531491	0.09573725	7156798	80 mol % MeOH
Run 38	622808	6594236	0.09444733	7217044	80 mol % MeOH

Table D.1: Runs used for the calibration of the liquid sampling system (area ratio approach).

Run No	Height H_2O	Height MeOH	Height Ratio	Total Height	Comments
Run 4	327.3568	315.3578	1.03804884	642.7146	30 mol % MeOH
Run 5	326.4839	316.7912	1.03059649	643.2751	30 mol % MeOH
Run 7	252.9532	387.961	0.65200677	640.9142	40 mol % MeOH
Run 8	252.1722	385.4166	0.65428474	637.5888	40 mol % MeOH
Run 9	258.9806	382.9012	0.67636403	641.8818	40 mol % MeOH
Run 12	202.2251	452.2724	0.4471312	654.4975	50 mol % MeOH
Run 13	194.0651	438.0807	0.44298939	632.1458	50 mol % MeOH
Run 42	154.9185	499.928	0.30988162	654.8465	60.4 mol % MeOH
Run 43	151.8032	498.5626	0.30448172	650.3658	60.4 mol % MeOH
Run 44	152.178	506.0054	0.30074383	658.1834	60.4 mol % MeOH
Run 27	82.042	528.0844	0.15535774	610.1264	70 mol % MeOH
Run 30	87.7143	535.2136	0.16388653	622.9279	70 mol % MeOH
Run 36	44.6658	558.8587	0.07992324	603.5245	80 mol % MeOH
Run 38	45.9774	557.3929	0.08248652	603.3703	80 mol % MeOH

Table D.2: Runs used for the calibration of the liquid sampling system (area ratio approach).

Run No	Area H_2O	Area MeOH	Area Ratio	comments
Run 3	35.7079	164.3324	0.2173	68.9 mol % MeOH
Run 4	35.5056	164.6311	0.2157	68.9 mol % MeOH
Run 5	35.6155	165.5543	0.2152	68.9 mol % MeOH
Run 7	35.6716	82.1115	0.4344	52.6 mol % MeOH
Run 11	35.6289	82.8196	0.4302	52.6 mol % MeOH
Run 17	35.3153	252.2883	0.1400	76.8 mol % MeOH
Run 18	34.8997	250.1840	0.1395	76.8 mol % MeOH
Run 19	36.4578	333.9800	0.1092	81.6 mol % MeOH
Run 20	36.3259	331.9563	0.1094	81.6 mol % MeOH

Table D.3: Obtained results based on peak area from screen.

Run No	Area H_2O	Area MeOH	Area Ratio	Total Area	comments
Run 13	590178	1251979	0.471	1842157	52.6 mol % MeOH
Run 16	591020	3612364	0.163	4203384	76.8 mol % MeOH
Run 19	631870	4849831	0.130	5481701	81.6 mol % MeOH

Table D.4: Selected liquid runs based on the integrator printout.

Run No	Area H_2O	Area MeOH	Area Ratio	comments
Run 3	35.7079	164.3324	0.2173	68.9 mol % MeOH
Run 4	35.5056	164.6311	0.2157	68.9 mol % MeOH
Run 5	35.6155	165.5543	0.2152	68.9 mol % MeOH
Run 7	35.6716	82.1115	0.4344	52.6 mol % MeOH
Run 11	35.6289	82.8196	0.4302	52.6 mol % MeOH
Run 17	35.3153	252.2883	0.1400	76.8 mol % MeOH
Run 18	34.8997	250.1840	0.1395	76.8 mol % MeOH
Run 19	36.4578	333.9800	0.1092	81.6 mol % MeOH
Run 20	36.3259	331.9563	0.1094	81.6 mol % MeOH

Table D.5: Runs used for the calibration of the vapour sampling system (area ratio approach).

Run No	Area H_2O	Area MeOH	Area Ratio	Total Area	Comments
Run 13	590178	1251979	0.471	1842157	52.6 mol % MeOH
Run 16	591020	3612364	0.163	4203384	76.8 mol % MeOH
Run 19	631870	4849831	0.130	5481701	81.6 mol % MeOH

Table D.6: Selected vapour runs based on the integrator printout.

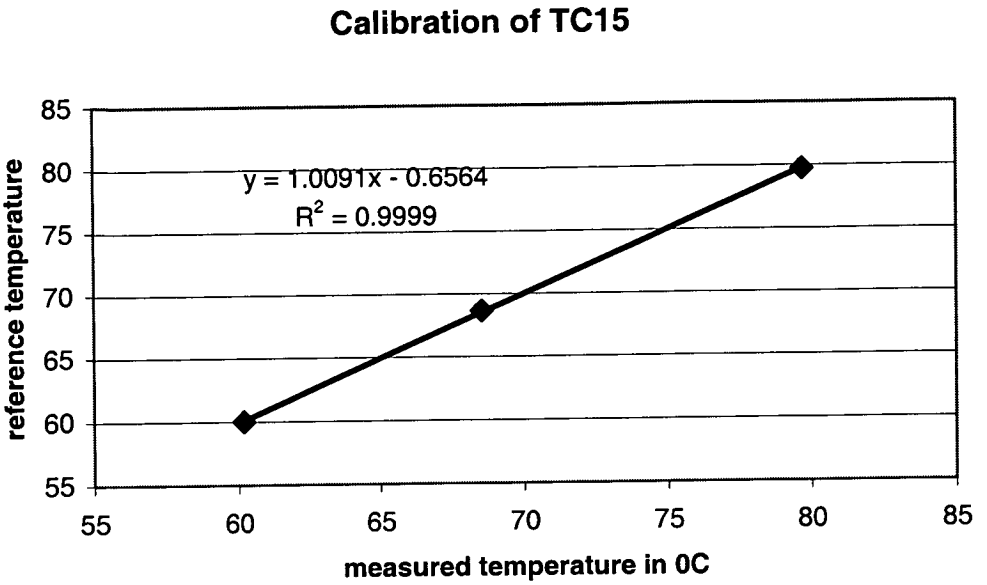

Figure D.1: Calibration plot of a thermocouple

The calibration was performed with all 16 thermocouples used in the rig. The resulting function was programmed into the data logger software.

Appendix E

Rig related information

Appendix E features an operation manual for the experimental rig, including safety information and detailed rig information about the rotameters used. A sketch of the cartridge heaters used in the reboiler is also given.

School of Engineering and Electronics
Research Apparatus Safety Assessment Form

Name of Apparatus:	Diabatic distillation column
Location of Apparatus:	Kenneth Denbigh; ground floor
Supervisor/PI:	Dr. Colin Pritchard
Apparatus Number (if known):	-

Instructions to Research Supervisor or Principal Investigator

This form must be completed if any of the following circumstances applies:

i. If a new apparatus is to be commissioned;

ii. If an existing apparatus, or its operating procedure, has been modified significantly since the last safety assessment;

iii. When the Permit to Operate for this experiment has expired, unless the apparatus has been decommissioned during this time (and a Decommissioning Form filled in). A Permit to Operate will normally be valid for not more than one year, and will expire on 30th September. If no significant changes have been made to the

apparatus since the Safety Assessment was completed it may be updated by attaching a new signature sheet.

Definition of Apparatus

The term "apparatus" refers to the sum of the equipment used to carry out an experiment, including any instruments, whether or not the various components are physically connected to each other. It would normally apply to an assembly of components and instruments used to conduct experimental procedures. Equipment used in accordance with the manufacturer's operating guidelines and not part of an integrated larger assembly would not require this safety assessment.

If in doubt over the need to complete this form please consult the building TSO.

Procedure

The principal Research Worker who is to work on this apparatus, should complete Sections A and B. The research supervisor or principal investigator should then sign Section C and hand the form to the Technical Services Office for your building who will complete section D and issue a Permit to Operate.

Instructions to Research Workers

Before you operate the apparatus you must read this form and sign the declaration contained in section E. You may do this either before or after the Permit to Operate has been issued. In the latter case you should then add your name to the permit to operate.

Section A: The Apparatus

Location of Apparatus: On the ground floor of the Kenneth Denbigh Building; in the laboratory.

Brief description of apparatus (sketch appended)

About 3 meters tall distillation column mostly made of glass. The apparatus involves a gas chromatograph, integrator, an HPLC pump, 3 metering pumps, a diaphragm

pump, a peristaltic pump, 8 rotameters of several sizes and two control PCs. The rig is framed. Dimensions of the frame are given below.

Frame height : 3.00 m

Frame length : 1.82 m

Frame width : 0.52 m

Operating Instructions

List all significant steps. If a set of instructions already exists it may be appended. Reference may be made to a standard procedure, eg as listed in instrument manuals.

Filling of the apparatus

1. Open the bolt on the top flange of the feed tank.
2. Charge the tank with 30 l of MeOH and 13.3 l of distilled water with a hose and a funnel (2 persons needed).
3. Close the feed tank with the bolt.

Ensure that the following valves are closed: 1, 3-16. All the other valves remain open. The apparatus is now ready for operation.

Start-up procedure & operation under total reflux

1. Start computer 1 and open the thermocouple-monitoring program.
2. Turn on mains for the condenser cooling water. Adjust a flow rate of 20 l/min on rotameter 1.
3. Open valve 1 (outlet valve of the feed tank).
4. Open the rotameter 2 for the feed flow control completely.
5. Open valve 2 (feed port selection) to position 1 or 2.
6. Start the metering pump for the feed; adjust a flow rate of 25 l/h (7 cm reading on rotameter 2).
7. Start the feed pre-heater. Increase the power input to incipient boiling. Bubbles appear around the cartridge heater. Note the temperature at TC 17. Reduce the performance of the feed pre-heater slightly without

causing any temperature drop at TC 17. Thus feed enters the column at boiling temperature.

8. Activate the reboiler controller after the reboiler is completely covered with liquid.
9. Open rotameter 8 completely for establishing total reflux. Air might be sucked out of the reflux tubing by opening valve xy and the application of a slight vacuum.
10. As soon as the liquid level in the reboiler exceeds the overflow mark, shut down the feed pump, switch off the feed pre-heater and close rotameter 2. The column operates now under total reflux. Ensure that every plate is covered with liquid (visual inspection).

Operation with product withdrawal

1. Beginning from total reflux conditions, open rotameter 2 completely, start the feed pre-heater and the metering pump for the feed circulation.
2. Open rotameter 3.
3. Open valve 4 (valve at the bottom of the column).
4. Switch on the metering pump for the bottoms withdrawal. Set up a pumping rate of 12.5l/h (4 cm on rotameter scale).
5. Open rotameter 6 and adjust an appropriate ratio between rotameter 5 and 6. This equals the reflux ratio.
6. Adapt the flow rate, to avoid any column flooding, if necessary.

Operation of the heat exchanger plate

1. Switch on the thermostatic bath and the temperature controller.
2. Open valve 5 (bypass valve) and switch on pump 3.
3. Close valve 5 partly and set up an appropriate heat exchanger medium flow rate at rotameter 4.

Sample withdrawal

Liquid sampling

1. Open valve 6 for the re-entry of the liquid samples.
2. Provided that the GC is on since the start-up procedure (see GC manual), activate the HPLC pump and select a flow rate of 3 ml/min (see HPLC pump manual).
3. Select one of the five sample ports by turning the sample tube into the appropriate position.
4. Press the Run button of the GC to start the analysis.

Vapour sampling

1. Activate the heating tapes and control the temperature of TC 17 (> 40°C).
2. Open valve 14 (N_2 cylinder) and adjust a flow rate of 30 l/min on rotameter 7(26.5 cm reading).
3. Open valves 7 and 8.
4. Open rotameter 8 completely.
5. Open valve 3.
6. Switch on the diaphragm pump.
7. Select either vapour sampler 1 or 2 by opening valve 9 or 10 respectively.
8. Press the Run button of the GC to start the analysis.
9. Close the vapour sampling valves after the end of the analysis.
10. Switch off the diaphragm pump.
11. Close valve 14.
12. Turn off the heating tapes.

Control points:

Ensure that the vapour sampling lines are under slight vacuum (- 20 mbar).

Shut-down procedure

1. Switch off the feed pre-heater
2. Switch off the metering pump for the feed.
3. Switch off the reboiler.
4. Switch off the metering pump for the bottom product.
5. Close valve 1 (valve at the bottom of the feed tank).
6. Close rotameter valves 2, 5 and 6.
7. Switch off the centrifugal pump for the heat transfer medium cycle.
8. Switch off the thermostatic bath.

Transfer procedure

1. Close valve 3 (valve at the top of the bottom product tank).
2. Open valve 11 (valve at the bottom of the bottom product tank).
3. Open valve 15 (air supply valve) and displace the bottom product back to the feed tank.
4. Close valve 15.
5. Close valve 11.
6. Open valve 6 (at the bottom of the top product tank) and empty the vessel.
7. Close the valve 6.

Emergency procedure

For discharging the column

In case of a column burst or serious leak open valve 12 at the bottom of the reboiler. This causes a discharge of the column by gravity into a dump tank. The contents of the dump tank can be transferred back into the feed tank by compressed air. Close valve 12 and open valve 13. Open valve 15 (air supply valve) and displace the content of the dump tank back to the feed tank. As soon as the dump tank is empty close valve 13 and valve 15.

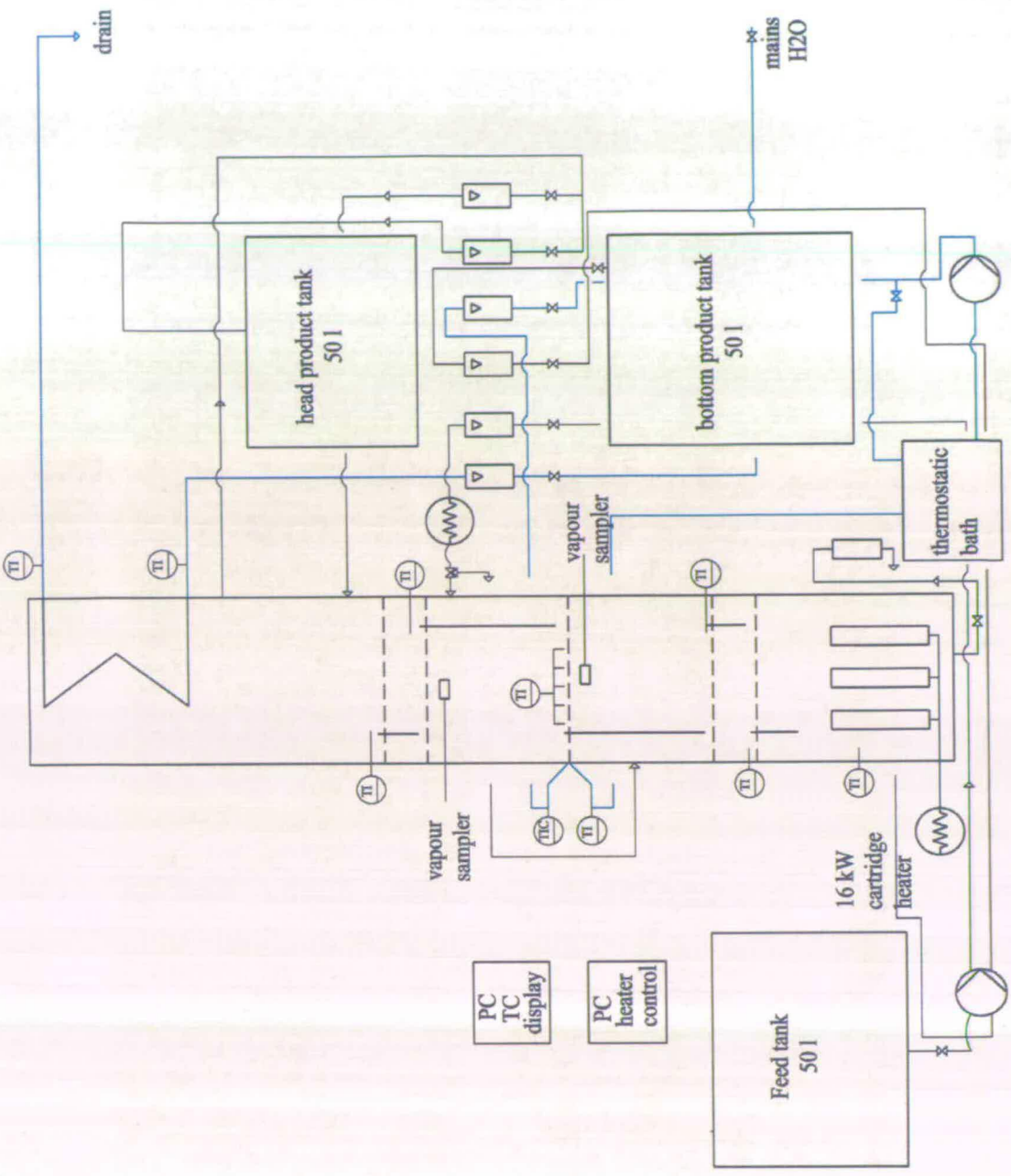

Figure E.1: Schematic diagram of the experimental rig.

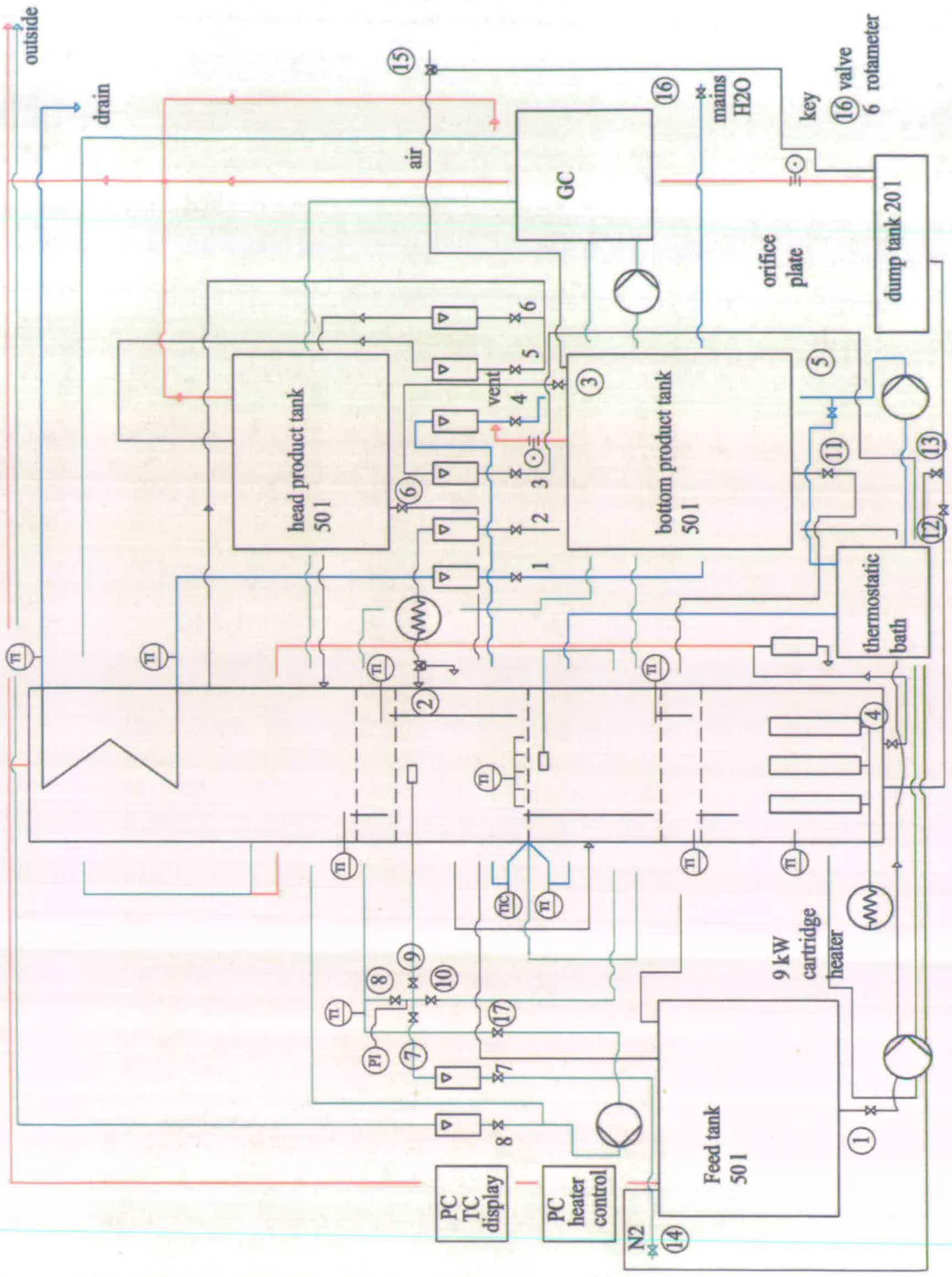

Figure E.2: Sketch of the experimental rig.

Section B: Safety Assessment

Some commonly encountered hazards risks are listed below. Next to each potential hazard, indicate whether this hazard is present in the apparatus in question and describe how this hazard is controlled to minimise risk to workers and others. In each case, where a hazard is identified as being present, those likely to be exposed to the hazard should be listed (in general terms). This list should include any people not directly involved in the experiment but who could be affected by it, for example researchers working on adjacent equipment, occupants of adjoining offices.

Hazards

Chemical/biological

Are chemical/biological hazards present? Yes

MeOH safety form is attached.

Electrical

All electrical equipment must be tested by the workshop as appropriate. Signing this form indicates that you have ensured this has been carried out.

Other Hazards

Pressure vessels

Air is used to transfer contents of dump tank & bottoms tank but pressure built-up is restricted by permanently-opened vent lines (equipped with orifice plates).

Gas cylinders

He, N_2 and compressed air supply, which might leak. Close the cylinder mains to stop the leakage.

Falling cylinders might turn into missiles. Firmly strapped valves and cylinders in vertical position prevent this.

Mechanical (including rotating machinery)

Blockage of metering pump relief valves or closed stop valves, cause overpressure. Pumps must be switched off immediately.

Flammable materials

Flammable methanol vapour concentrations at the top of the column (under the exposure of air) are an ignition source. A flame arrester at the vent exit is necessary.

Temperature

Hot surfaces occurring at the boiler, water bath, feed and hot product tubing are potential sources for burns and have to be insulated with appropriate materials (e.g. foam). The cartridge heaters in the reboiler burn out if they are not covered with liquid. A safety switch (diode switch) controlling the liquid level prevents reboiler damage.

8056

MATERIAL SAFETY DATA SHEET

Section I – Product Information			
Product Name or Identity:	**Veratox ® Fumonisin Dilution Kit, Fumonisin Lab Dilution Kit**		
Manufacturer's Name:	Neogen Corporation	**Emergency Phone No.**	517/372-9200
	620 Lesher Place	**Fax No.:**	517/372-0108
	Lansing, Michigan 48912	**e-mail:**	www.neogen.com
Date Prepared or Revised: 04/14/01			

Section II – Hazardous Ingredients / Identity Information			
Hazardous Components (Specific Chemical Identity: Common Names)	**OSHA PEL** (Permissible Exposure Limits)	**ACGIH TLV** (Threshold Limit Value)	**Toxicity Data LD_{50}**
Methanol (10%)	200 ppm/mg/m^3	250 ppm/mg/m^3 (STEL/C)	ORL-RAT, 5.6 g/kg

Section III – Physical Characteristics	
Boiling Point: 64.7°C (Methanol)	**Specific Gravity (H_2O = 1):** 0.79 g/ml (Methanol)
Vapor Pressure (mm Hg.): 97.7 mm (Methanol)	**Melting Point:** -98°C (Methanol)
Vapor Density (AIR = 1): 1.1 (Methanol)	**Evaporation Rate (Butyl Acetate = 1):** 5.9 (Methanol)
Solubility in Water: Soluble (Methanol)	
Appearance and Odor: Liquid, colorless, faint alcohol odor (Methanol)	

Section IV – Fire and Explosion Hazard Data	
Flash Point (Closed Cup): 11°C (Methanol)	**Flammable Limits:** LEL (Lower Explosive Limit) – 6% (Methanol) UEL (Upper Explosive Limit) – 36% (Methanol)
Extinguishing Media: Suitable extinguishing agents. CO_2, extinguishing powder or water spray.	
Special Fire Fighting Procedures: Fight larger fires with water or alcohol resistant foam. Firefighters should wear protective equipment and self-contained breathing apparatus.	
Unusual Fire and Explosion Hazards: During heating or in case of fire, poisonous gases are produced. Methanol/water mix will burn unless very dilute. Dust may form explosive mixture with air. Vapors may travel a considerable distance to source of ignition and flash back.	

Section V – Reactivity Data			
Stability	Unstable		Conditions to Avoid: Keep away from heat / sparks / flame. Highly flammable. Protect from light and moisture.
	Stable	X	
Incompatibility *(Materials to Avoid)*: May react violently with acids, acid chlorides, acid anhydrides, oxidizing agents, reducing agents, and alkali metals.			
Hazardous Decomposition or Byproducts: Occurs from heat and reaction with materials stated above.			
Hazardous Polymerization	May Occur		**Conditions to Avoid:** Sources of ignition. Incompatible materials.
	Will Not Occur	X	

Section VI – Health Hazard Data			
Route(s) of Entry:	Inhalation? Yes	Skin? Yes	Ingestion? Yes

Health Hazards *(Acute and Chronic)*	Harmful. Methanol may be fatal or cause blindness if swallowed. Harmful if inhaled or absorbed through skin. Irritating effect to skin, respiratory system, and eyes. Cannot be made nonpoisonous.		
Carcinogenicity: NTP? No (National Toxicology Program)		IARC Monographs? Yes, Group 3 (Methanol) (International Agency for Research in Cancer)	OSHA Regulated? No
Signs and Symptoms of Exposure: Vapors may be irritating to skin and mucous membranes. Irritating effect to eye. Symptoms include redness and pain. Overexposure can cause vomiting, convulsion, hypertension, and gastrointestinal cramps.			
Medical Conditions Generally Aggravated by Exposure: May cause eyes, liver, heart, and kidney disease with chronic exposure to Methanol.			
Emergency / First Aid Procedures	Ingestion: If swallowed, seek medical attention immediately.		
	Inhalation: Supply fresh air or oxygen. Seek medical attention immediately. If not breathing, apply artificial respiration. If breathing is difficult, give oxygen.		
	Eye Contact: Rinse opened eye for several minutes under running water. Seek medical attention immediately.		
	Skin Contact: Remove contaminated clothing immediately. Wash with plenty of soap and water for at least 15 minutes. Seek medical attention.		

Section VII – Precautions for Safe Handling and Use
Accidental Release Measures: Wear suitable protective clothing. Flush spill area with water. Wipe up with damp sponge or mop. Shut off ignition sources. Avoid breathing dust.
Waste Disposal Method: Dispose in accordance with all applicable federal, state and local environmental regulations.
Handling and Storing: Keep container tightly closed. Store in a cool, dry, well-ventilated, flammable liquid storage area.
Other Precautions: Prevent formation of dust. Ensure good ventilation / exhaustion at the workplace.

Section VIII – Control Measures		
Respiratory Protection (Specify Type): None required where adequate ventilation conditions exist. If airborne concentration exceeds TLV, a self-contained breathing apparatus is advised.		
Ventilation	Local Exhaust: 50 – 100 CFM	Special
	Mechanical (General): N/A	Other
Protective Gloves: Proper disposable gloves		Eye Protection: Safety goggles
Other Protective Clothing or Equipment: Uniform, lab coat or disposable lab wear.		
Work / Hygienic Practices: Follow the usual precautionary measures for handling chemicals / powder. Keep away from food and beverages. Immediately remove all soiled and contaminated clothing. Avoid contact with eyes, skin and clothing.		

This document is believed to be correct, but does not purport to be all inclusive and shall be used only as a guide. Neogen Corporation shall not be held liable for any damage resulting from handling or from contact with the above product. These suggestions should not be confused with state, municipal or insurance requirements, and constitute NO WARRANTY.

Rotameter Nr	Size	Flow rate range in l/min	Function
1	24	2.5 – 21.0	Condenser controller
2	10x	0.25 – 1.65	Feed flow controller
3	7	0.10 – 1.10	Bottom product indicator
4	10	0.25 – 2.30	Heat transfer medium controller
5	7x	0.10 – 0.90	Head product controller
6	7x	0.10 –0.90	Reflux controller
7	14x	3.0 32.0	N_2 flow controller
8	14	5.0 53.0	N_2 + vapour flow indicator

TableE.1: Description of the rotameters used in the experimental rig.

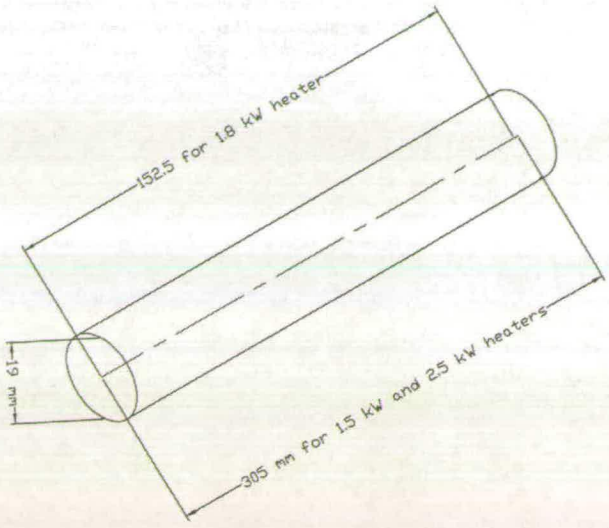

FigureE.3: Sketch of a cartridge heater used in the reboiler

Appendix F

Publications of the author

M. Kaeser and C. L. Pritchard. Heat transfer at the surface of sieve trays. *8th UK National Heat Transfer Conference*, Oxford, September 2003.

M. Kaeser & C. L. Pritchard. The impact of heat transfer on Murphree tray efficiency. *17th International Conference on Efficiency, Costs, Optimisation, Simulation and Environmental Impact of Energy and Process Systems*, Mexico, July 2004.